SCHOOL OF MECHANICAL & SYSTEMS ENGINEERING
NEWCASTLE UNIVERSITY

Operational simulation and an economical modelling study on utilizing waste heat energy in a desalination plant and an absorption chiller

By

Khaled Saeed Al-Zahrani

Dissertation submitted to the
School of Mechanical & Systems Engineering
in partial fulfilment of the requirements for the degree of

Doctor of Philosophy

In
Mechanical Engineering

Approved by:

Dr. Brian Agnew
March 2010

Abstract

It is well established that a large proportion of the global emission of greenhouse gases are produced by electricity power stations and that a power plant typically emits about two thirds of its input energy as waste heat into the atmosphere. As such there is a lot of potential for additional applications that utilize this waste heat energy. Utilizing this waste heat energy in a desalination plant to produce low-cost potable water is the key to overcoming three problems at once, namely the water shortage in arid and semi-arid areas, the continuing increase in oil prices by being more efficient and global warming. In all waste heat recovery or alternative energy systems based on natural phenomena (solar or wind) a major difficulty is decoupling supply from demand as thermal storage is neither efficient nor practical in many cases. A significant difficulty of gas turbine based power generation systems is the derating caused by high ambient temperatures; typically a 1% change in ambient temperature produces a similar reduction in efficiency. Therefore, by also utilizing this waste heat energy in an absorption chiller to pre-cool the gas turbine's compressor inlet-air, the effect of ambient temperature fluctuations on the gas turbine's performance would be eliminated.

The combined cycle described in this study was designed in an attempt to address these issues. A gas turbine based combined heat and power plant was combined further with an absorption refrigeration unit and an MED desalination plant. The absorption unit stabilizes the operation of the gas turbine, reducing the sensitivity to changes in ambient temperature and the desalination plant acts as an energy utilization device that produces a usable product (40,000m^3/day of potable water) that is easily stored and distributed as required. The simulation was performed using IPSEpro on the basis of real data obtained from an existing power plant and commercially available plants. The performance of the sub-plants was investigated using energy and exergy analyses, in design and off-design conditions using real weather data obtained from the Presidency of Meteorology and Environment in Saudi Arabia. Two different desalination technologies and two different coupling techniques were examined in four proposed plants. An optimal plant design was chosen from a comparison between all proposed plants' energy and exergy analysis results. The chosen plant was then optimized and simulated in design and off-design conditions.

The initial results indicated that the simulated combined power plant's carbon footprint was reduced by 36.8% and its energy utilization factor was improved by 30.97%. This approach also stabilized the effect of ambient temperature fluctuations on the gas turbine's performance. After optimization, the carbon footprint was further reduced by 31.17% and the energy utilization factor was further improved by

6.11%. The exergy destroyed through the exhaust stack was reduced by 78% and the proposed plant's overall exergetic efficiency was improved to 49.64%. Furthermore, the desalination plant's concentration factor was reduced by 0.45 and an additional product of a hot water stream at a temperature of 75°C was gained.

An economic study was performed that indicated that the optimized plant is economically viable. As part of this analysis, a number of sensitivity studies defined the minimum selling prices of the plant's products and indicated the influence of fuel price, interest rates, capacity factors and project lifetime on the viability of the plant. The results also indicated that the proposed plant is a good investment, offering competitive energy and potable water prices, in regard to the location indicated by this study.

Declaration

This report is submitted as part of the requirements for a PhD degree at the University of Newcastle and has not been submitted for any other degree at this or any other university. It is solely the work of Khaled Saeed Al-Zahrani. It describes work carried out at the University of Newcastle, which is recorded in its entirety in a project logbook that has been made available for examination.

I am aware of the penalties for plagiarism, fabrication and unacknowledged syndication and declare that this report is free from all of these.

To my family

Acknowledgments

I thank Almighty God for giving me the courage and determination, as well as guidance, in conducting this research study. I extend my utmost gratitude to my supervisor, Dr. Brian Agnew, for his advice and valuable suggestions in regard to this work.

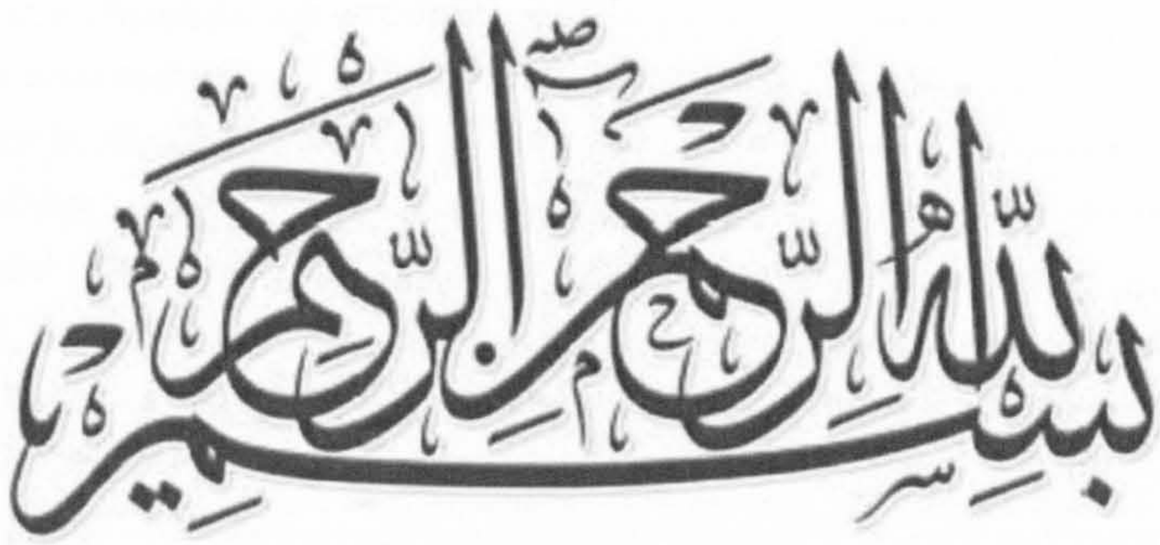
بسم الله الرحمن الرحيم

In the name of Allah
The most gracious and the most merciful

Table of contents

List of Figures

List of Tables

Abbreviations

AC	Absorption chiller
BROAD	Broad Air Conditioning Co., Ltd
C	Compressor
CCPP	Combined cycle power plant
CF	Concentration factor
CFCs	Chlorofluorocarbons
CH_4	Methane
CO_2	Carbon dioxide
ED	Electro-dialysis desalination process
ESDU	Engineering Sciences Data Unit
G	Generator
GOR	Gain output ratio
GT	Gas turbine
HFCs	Hydroflurocarbons
HRSG	Heat recovery steam generation
HT-MED	High temperature multi-effect desalination process
IDE	Israel Desalination Engineering Technologies Ltd
ISO	International Standards Organization
LiBr	Lithium bromide
LT-MED	Low temperature multi-effect desalination process
MDK	The IPSEpro model development kit
MED	Multi-effect distillation desalination process
MF	Make-up feed water
MSF	Multi-stage flash
MVC	Mechanical vapour compression
N_2O	Nitrous oxide
NaREC	New and Renewable Energy Centre
PFCs	Perfluorocarbons
PSE	Process simulation environment
PSExcel	Process simulation MS Excel
RO	Reverse Osmosis
SF_6	Sulphur hexafluoride
SimTech	Simulation technology
ST	Steam turbine
SWCC	Saline water conversion corporation
TVC	Thermal vapour compression
UF	Ultra-filtration
VC	Vapour compression desalination process

Nomenclature

ΔT	Temperature difference	K
C	Heat capacity rate	W/K
C_f	Capacity factor	%
COP	Coefficient of performance	-
Cp	Specific heat	kJ/kg K
C_R	Compression ratio	-
C-Value	Cost per unit $Q/\Delta T$	£/(W/K)
E	Exergy	kW
e	Specific exergy	kJ/kg
EUF	Energy utilization factor	%
Fz	Net money cash flow in year (z)	£
g	Gravity	N
GOR	Gain output ratio	-
h	Enthalpy	kJ/kg
i	Interest rate	%
I_o	Initial capital cost	£
IRR	Internal rate of return	%
L	Load	-
LHV	Low heating value	kJ/kg
w, $\dot{m}$	Mass and mass flow rate	kg/s
M	Molar mass	g/mol
NPV	Net present value	£
NUT	Number of transfer units	-
O&M	Operation and maintenance cost	£
P	Pressure	bar
PBP	Payback period	year
PI	Profitability index	-
PR	Performance ratio	-
$\dot{Q}$	Heat transfer rate	kW
$\bar{R}$	Universal gas constant	J/mol.K
r	Pressure ratio	-
s	Entropy	kJ/K
ShC	Specific heat consumption	kJ/kg
T	Temperature	K
TBT	Top brine temperature	K
UA	Heat transfer area × overall heat transfer coefficient	kW/K
V	Parameter value	-
v	Velocity	m/s
W	Power	kW
x	Molar fraction	-
Z	Altitude	m

Greek Symbols

α	A mount of CO_2/ton of fuel
γ	Specific heat ratio
ε	Effectiveness
η	Efficiency
η_{II}	Exergetic efficiency
Θ	Molar Gibbs function of formation
Ψ	Exergy destruction ratio

Subscripts

App	Approach point
c	refer to cold stream
c,w	Cooling water
COM	Combustion chamber
Cond	Condenser
D	Destruction
Ecn	Economizer
Eva	Evaporator
F	Fuel
gas	Exhaust gas stream
h	refer to hot stream
hw	Hot water
j	Surface conditions
lm	Log mean
max	Maximum
min	Minimum
o	Reference condition
P	Product
pp	Pinch point
Sat	Saturated
SH	Super heater
sol	Solution
T	Turbine
t	Project lifetime
w	Water
z	Number of years

Superscripts

CH	Chemical
KE	Kinetic
PE	Pneumatic
PH	Physical

Chapter 1

Introduction

1.1 Introduction

The water shortage in arid and semi-arid areas has stimulated the research into the desalination process, either to improve the product quality or to reduce its cost through minimizing fuel consumption, using an alternative energy source or improving process efficiency. Several approaches have been developed in the last two decades to achieve this, some of which have suggested that the low temperature multi-effect distillation desalination process (LT-MED) is one of the most efficient ways of resolving most of the above issues. The MED desalination thermal process is both the most efficient and the oldest process, and the one that is driven mainly by thermal energy. Hence, it can utilize a waste heat energy source at temperatures in the range of 70 to 80°C [1], which minimizes its operation cost and reduces the unit product cost.

On the other hand, the significant increase in fossil fuel prices and the environmental restriction on energy production that we have witnessed over the past decade make the power plant the best choice for such an application when compared with other types of processes, for example the chemical complex, refineries, municipal solid waste, the steel industry, etc. This is in addition to its significant contribution to the global warming issue, where it typically emits about two-thirds of its input energy as waste heat into the environment, which increases the need for more efficient, more economic and more environmentally sensitive power plants. One way of minimizing the power plant's CO_2 emission rate and simultaneously improving its thermodynamic performance is by recovering its waste heat energy in another thermal system that can be powered by low-grade heat energy as an MED process for potable water production. Stabilizing the fluctuating ambient temperature by cooling the gas turbine's compressor air-intake using an absorption chiller is another way of improving the power plant's performance, and this has been of interest for more than two decades. However, few attempts have been made to investigate the integration of both methods to improve the power plant: recovering its waste heat energy emitted through the exhaust system and simultaneously cooling the air-intake of the gas turbine's compressor. Furthermore, several techniques have been established to connect the desalination plant to a power plant. None of these techniques utilizes the waste heat energy directly from the exhaust system without it being enhanced through a heat recovery steam generation unit, or being extracted from a steam turbine. Another gap identified by this study is the dilemma of rejected brine by the MED desalination process, which affects the ecological

balance and marine life, either because of its relatively high temperature or its high salinity. Although considerable research has been devoted to resolving this issue, rather less attention has been paid to developing a technique by which this water can be treated in a more economic way that does not increase the unit product cost. Likewise, cooling water that absorbs the plant's unwanted heat energy is usually wasted, which increases the plant's exergy destruction and leads to an inefficient interaction with the environment.

Computational modelling and simulation has become a mainstay in all studies, training and certificating applications. It saves time and money, offers flexibility, enables repeatability and offers control and the ability to push boundaries. Thus, with the limitation in funding an experimental work for this study, this was the perfect method to devise and test the proposed models and investigate their performances in different conditions. The software package used, IPSEpro, was built by SimTech Simulation Technology. It is a set of software modules that create, analyse and utilize models of new or existing process plants throughout their life cycles. Although IPSEpro is an extremely flexible modelling system for calculating heat balances and simulating most industrial processes, for example gas turbines, combined cycles, desalination and refrigeration, it does not support the construction of a model that includes all of these processes. This required further development in the software libraries to allow the construction and simulation of such a model, which was possible with the help of the model development kit (MDK) included in the software package.

1.2 Aims of the Study

Motivated by more than one issue, this study was engaged in the search for solutions to the following issues:

- Increasing the demand and price of electrical power
- Shortage of potable water in arid and semi-arid areas
- Limited resources and increasing prices of fossil fuel
- Urgent need to reduce the effect of greenhouse gases
- Effect of ambient conditions on power plant performance.

Therefore, the aim of this study was to develop technical solutions for these issues by applying a hypothesis that states the following: the main source of plant inefficiency is the source of its improvement. For example, at a typical efficiency of 40% the internal combustion engine wastes 60% of the chemical energy of the input fuel as heat transferred to the cooling system and as hot pressurized gases through the exhaust. Therefore, the main source of car engine inefficiency is the cooling water system and exhaust system; by recovering the heat energy wasted through these two systems the engine can be improved. The improvement can be in reducing system impact on the environment or obtaining an additional product. More precisely, a power plant that consumes 300MW as input energy typically emits about 66% of its input energy as waste heat energy through the exhaust system; recovering this heat energy in another system that can be powered by low-grade heat energy will offer an additional product and reduce its CO_2 emission rate. However, integration of different systems is usually opposed due to lack of knowledge or economic decisions. Therefore, this study was devised to investigate the possibility of integrating different systems with a power plant in order to improve its performance and minimize its impact on the surrounding environment. This investigation will be performed thermodynamically and economically, using real modelling data for all the employed plants collected from power plant sites and other manufacturers, in addition to real weather data.

1.3 Layout of the Thesis

The thesis has been organized into seven chapters and supporting appendices; this introductory chapter outlines the study's aims and motivations while the other chapters are arranged as follows:

- Chapter 2 presents a literature review covering topics related to this study, including the desalination process, water resources in Saudi Arabia, absorption chiller and waste heat energy recovery systems.
- Chapter 3 gives a description of the simulation software package used in this study and introduces the mathematical modelling of the energy and exergy analyses. Moreover, this chapter introduces the real modelling data collected for each employed plant, as well as the weather data for the intended location used in this study.

- Chapter 4 is the base plants modelling chapter and it contains a detailed description of each employed plant (that is, a CC power plant, an MED plant and an absorption chiller), and includes modelling, tests' results and parametric studies.
- Chapter 5 is devoted to presenting the proposed plants' modelling and the results of the tests. After this, an optimization stage with all its modelling and tests results will be presented and discussed. Then the results and an analysis of the parametric studies performed will be presented.
- Chapter 6 presents an economic study that investigates the economic acceptability and profitability of the optimized proposed plant. The performed sensitivity studies, and their analyses and discussions, are then presented at the end of this chapter.
- Chapter 7 concludes the study results and points out the application of the results and gives recommendations for future work.

Chapter 2

Literature Review

2.1 Introduction

Over the past two decades, an extensive amount of research into desalination processes has been undertaken either to improve the product quality or to reduce its cost through minimizing fuel consumption, using alternative energy sources or improving process efficiency. In this chapter, a full literature review will be presented to give an overview of the subject that will be dealt with in the following chapters. The review will start with a brief introduction for the most common desalination technologies, followed by the water resources and desalination technologies in Saudi Arabia. Next, a short review covering the absorption chiller — history, principles and application in cooling gas turbine's compressor air-intake — will be presented. The visibility and availability of waste heat energy and some of the best experiences in waste heat utilization in desalination plants will then be presented. The last topic in this chapter is set to introduce the exergy analysis, present its fundamentals and review some studies that have performed such an analysis to investigate the performance of the power plant, the desalination plant and absorption chillers.

2.2 Desalination

Desalination can be defined as the process that removes the excess salt and other minerals from seawater or brackish water in order to obtain potable water suitable for animal consumption or irrigation and, if most of the salt is removed, for human consumption. The Sun is the oldest and largest desalination plant in the solar system; it has an estimated capacity of $1.2x10^{12}m^3$ per day. It has been operating constantly and totally unattended for at least $3.8x10^9$ years, and has never had any maintenance [2]. Desalination is an old process, known by humans for more than two thousand years. Birkett [3] presented a paper that introduces a brief history of desalination from the Bible to 1940.

2.2.1 Desalination Process Types

Desalination processes can be classified into two main categories: thermal and membrane. Thermal processes are the oldest and most commonly used. They can be classified into two main categories according to the separation method used: evaporation and freezing. The freezing process is not as commonly used as the evaporation process for a number of reasons such as

handling difficulties. In the following section the most common types of desalination processes will be explained briefly. Figure 2-1 summarizes the main desalination process categories.

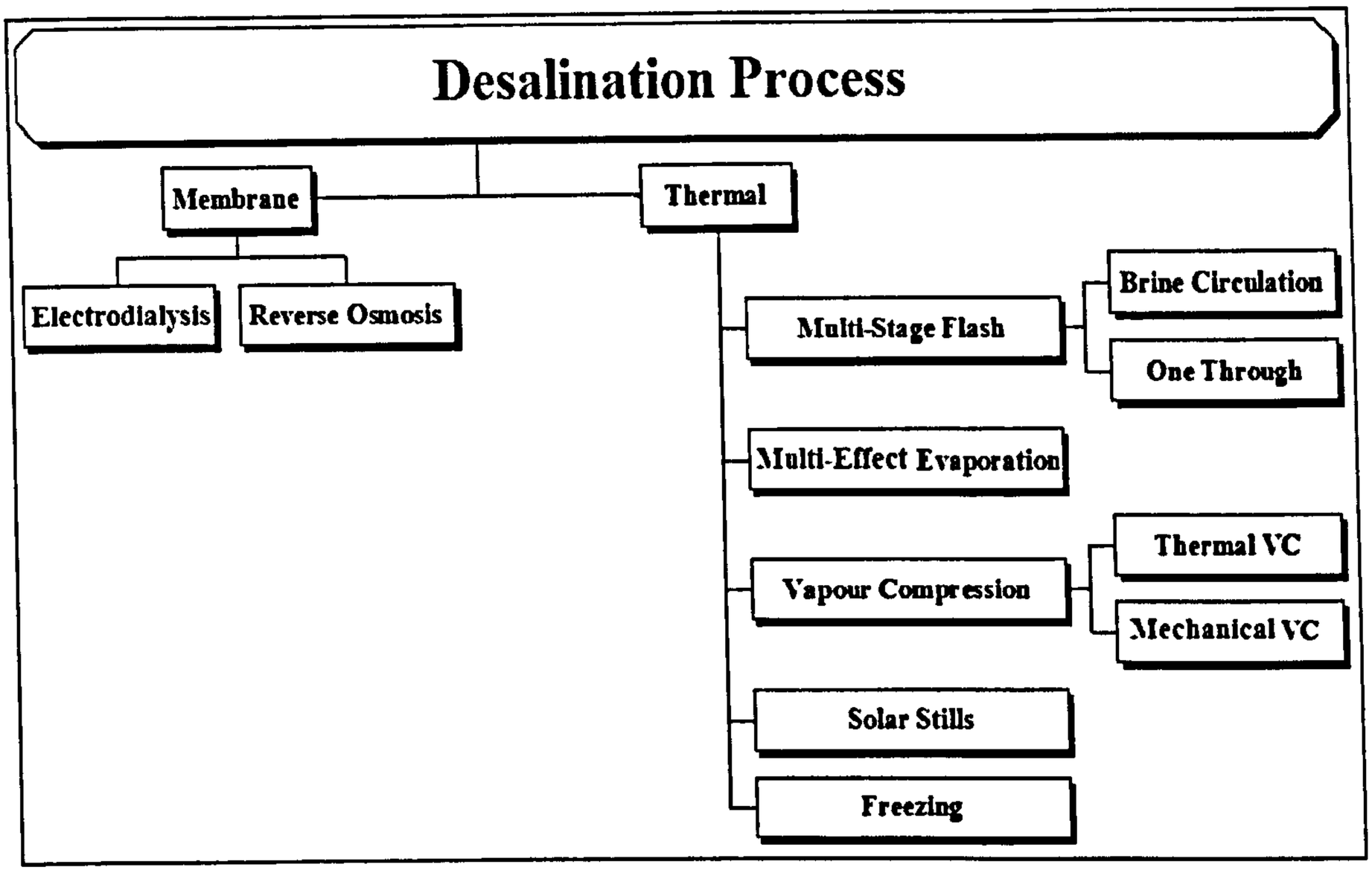

Figure 2-1 Desalination process categories

The main concept of desalination is to use a form of energy to separate the excess salt and other unwanted minerals from seawater or brackish water. One way of characterizing the desalination process is according to the form of energy used in the separation process, which can be thermal, mechanical or electrical energy. Thermal energy includes all the means of heating or cooling.

2.2.2 Thermal Desalination Process

Thermal desalination is also known as a phase-change separation process since it involves changes in the state of the water from a liquid state into either vapour (evaporation) or a solid state (freezing). In the following part of this chapter, only the most common process and techniques of the thermal desalination process will be mentioned.

- **Multi-stage flash**

Fifty years ago Weirs of Cathcart, a company in Scotland, gained the patent for inventing the multi-stage flash process (MSF), which had been outlined long before this by Waterhouse in 1900 [3]. The main concept of this process is using both pressure and temperature in order to

flash a portion of the seawater into steam in multiple stages. This process uses high-grade heat energy to boil the feed water, in addition to electric power for raising the pressure of feed water.

Figure 2-2 shows a single-stage of the multi-stage flash process. The process starts with the seawater being fed into a container called a "brine heater" to be heated under high pressure to a temperature between 90 and 120°C. Next, this high pressure stream of hot water is suddenly led to another container "stage", which has a pressure lower than that in the brine heater. This sudden change in pressure at a high temperature causes the water to boil rapidly and a portion of it to flash into steam; the remaining water will proceed to another stage at a pressure lower than the previous stage to repeat the same process of flashing. The generated steam condenses on tubes of heat exchanger carrying the feed seawater at an ambient temperature to the brine heater passing through each flashing stage. Simultaneously, this will heat-up the feed water which will reduce the thermal energy needed in the brine heater to increase its temperature [4, 5].

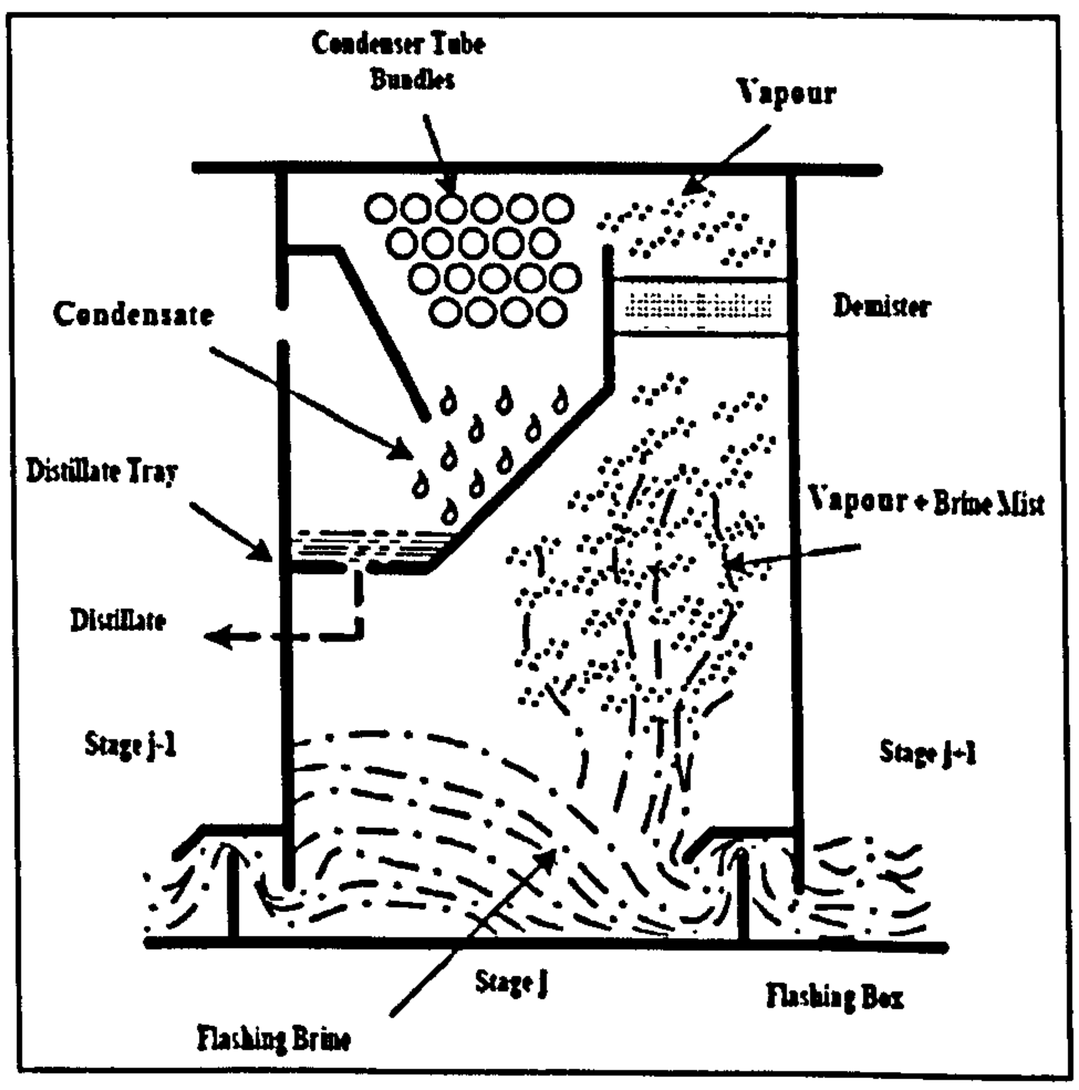

Figure 2-2 Multi-stage flash process (MSF) principle, reproduced from [3]

After the final stage the condensed steam is collected as potable water, which is then chemically treated to adjust its hardness before storage or usage. The distillate can be contaminated by brine mist coming from the sudden evaporation into water vapour, so a separator called a "demister" is used to separate it from the condensing vapour. The process described so far is called "once through MSF", which means that the remaining water from the last stage drains to the sea, while

all of the feed water is being pumped into the plant directly from the sea. In this method all of the feed water, which is roughly ten times the production quantity, must be treated chemically, considerably increasing the production unit cost. In order to minimize these extra costs a new design called "brine circulation" has been developed in which a heat-rejection section is added to the plant in order to circulate the remaining water from the last stage into the brine heater in addition to some make-up feed (MF) from the seawater through the last stage.

The multi-stage flash technology is one of the most mature technologies, distinguished by its simplicity in construction, operation and maintenance as it has no moving machine except for the normal pumps. As a result, a lifespan of up to 40 years is predicted for some large plants in the Middle East [4]. Such large plants may include up to 25 stages per unit with a maximum capacity of 100,000m^3/day and mostly operate with the dual purpose of producing both electricity and potable water. Statistically, the MSF process is the preferred one worldwide; 74% of the world's total desalted water in 2003 was produced using the MSF process, as can be seen in Figure 2-3.

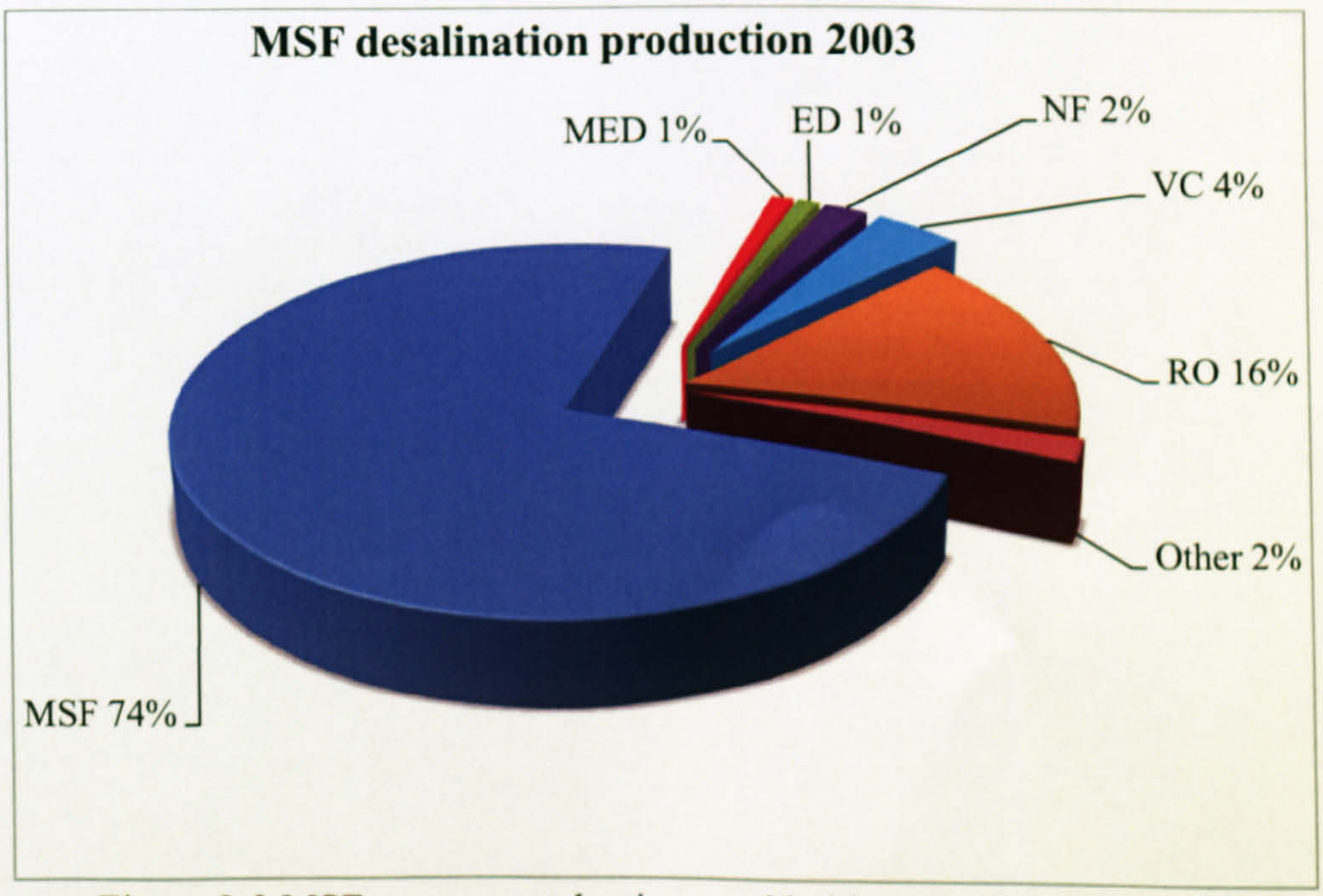

Figure 2-3 MSF process production worldwide, reproduced from [4]

However, the difficulties of this process are associated with its need to increase the top brine temperature (TBT) in order to improve its performance ratio (PR), which is limited to 120°C to avoid corrosion and control scale, even though anti-scale treatment is used [4, 6, 7]. The MSF desalination process typically consumes 4kWh of electric power in addition to 8m^3 of a steam at

a temperature between 90°C120°C and pressure lower than the atmospheric pressure to produce $1m^3$ of potable water [4]. Therefore, this process cannot be adopted in this study due to its high consumption of both electricity and high-grade heat energy.

- **Multi-effect distillation**

Multi-effect distillation (MED) principally uses distillation (evaporation and condensation) to produce potable water just like any other thermal desalination process. However, the MED desalination process uses boiling in order to evaporate seawater, which means that the distillate water will evaporate leaving salt on the heating surfaces, which diminishes their efficiency if the top boiling temperature was limited to 70°C. The MED process is similar to the MSF process; it takes place within a number of effects and uses the concept of reducing the pressure in each effect so that it is lower than the previous one to allow the seawater to boil and evaporate multiple times but without providing any extra thermal or electric energy after the first effect. Figure 2-4 illustrates the MED process where steam typically at a temperature of 70°C and with low pressure (0.2 to 0.4 bar) [4] is fed into a series of tubes where it release its heat and condenses, heating the surface of the tube.

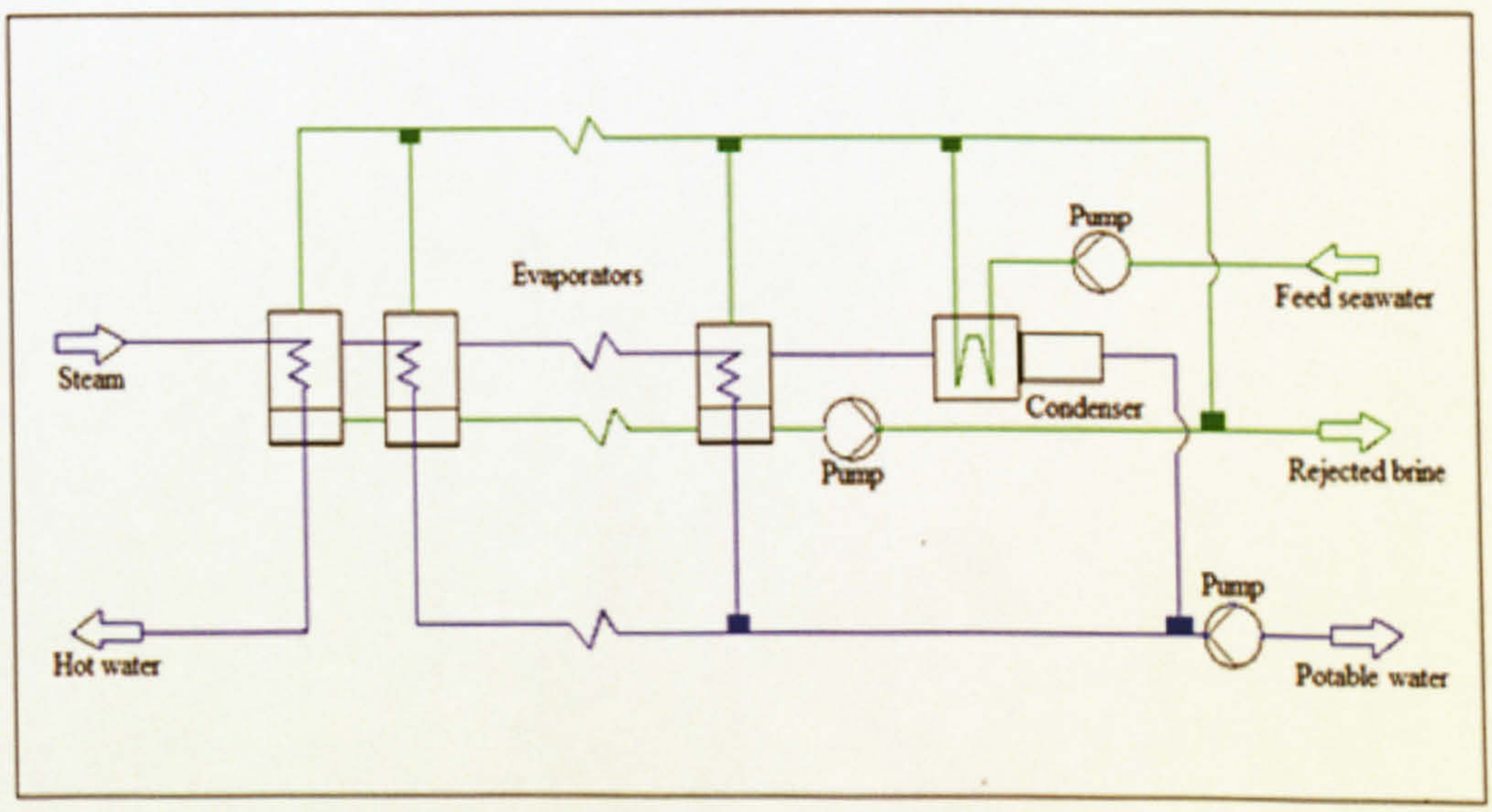

Figure 2-4 Multi-effect evaporation (MED)

The seawater is sprayed onto the evaporation tubes' surfaces to encourage fast boiling and evaporation. On the other side of the tubes the steam condenses and is recycled to be used in the boiler again, while the remaining seawater from the first effect is fed to the next effect, which

has a lower pressure than the previous one. After this the same process will be repeated in the subsequent effects. The steam generated from the final effect leads to a condenser to condense and preheat the feed seawater before entering the process [6, 7].

The first large land-based desalination plant was built in Tunisia in 1560 [3], which makes this process the oldest distillation process used for seawater desalination. The MED desalination process can be distinguished by its reliable design, high potable water quality, good operating history, relatively high unit capacity and high performance ratio. Additionally, unlike the MSF process, it is possible to improve the performance ratio by increasing the number of effects, which minimizes the cost of desalted water [4].

The MED process can be classified into two types according to the thermal energy source used: low temperature multi-effect distillation (LT-MED) and high temperature multi-effect distillation (HT-MED). In the first type the incoming steam temperature is 70°C while the last effect has a temperature of about 40°C, which eliminates scale formation and makes it possible to recover any type of waste heat efficiently, as well as allowing the use of cheaper material and enhancing the plant's availability. In the second type twice the capacity can be achieved and more effects can be built within the unit, but the scale formation must be controlled by a chemical pre-treatment [4, 5, 6].

The MED desalination process can be improved by installing a steam ejector that uses a high pressure steam (motive steam) that expands through the steam ejector's nozzle at high velocity. The high velocity steam entrains a low pressure suction steam extracted from the low pressure steam stream leaving the last effect in the MED plant. Both motive and suction steam are then forced into the mixing chamber and combined to power the MED brine heater. This reduces the steam needed to power the MED plant and this increases its thermal efficiency [6, 7]. Figure 2-5 shows an illustration of this process, which is known as thermal vapour compression multi-effect distillation (TVC-MED). The only difference between the MED desalination process and the TVC-MED desalination process is the steam ejector in the TVC-MED desalination process; other than that, the process is similar to the MED desalination process.

One issue that affects the performance of the MED desalination process is the flow of non-condensable gases inside its condenser and evaporators. These gases are mainly caused either by

a leakage of ambient air into the evaporators that are operating at vacuum pressure, or from the gases dissolved in feed seawater such as N_2, O_2 or CO_2 [8].

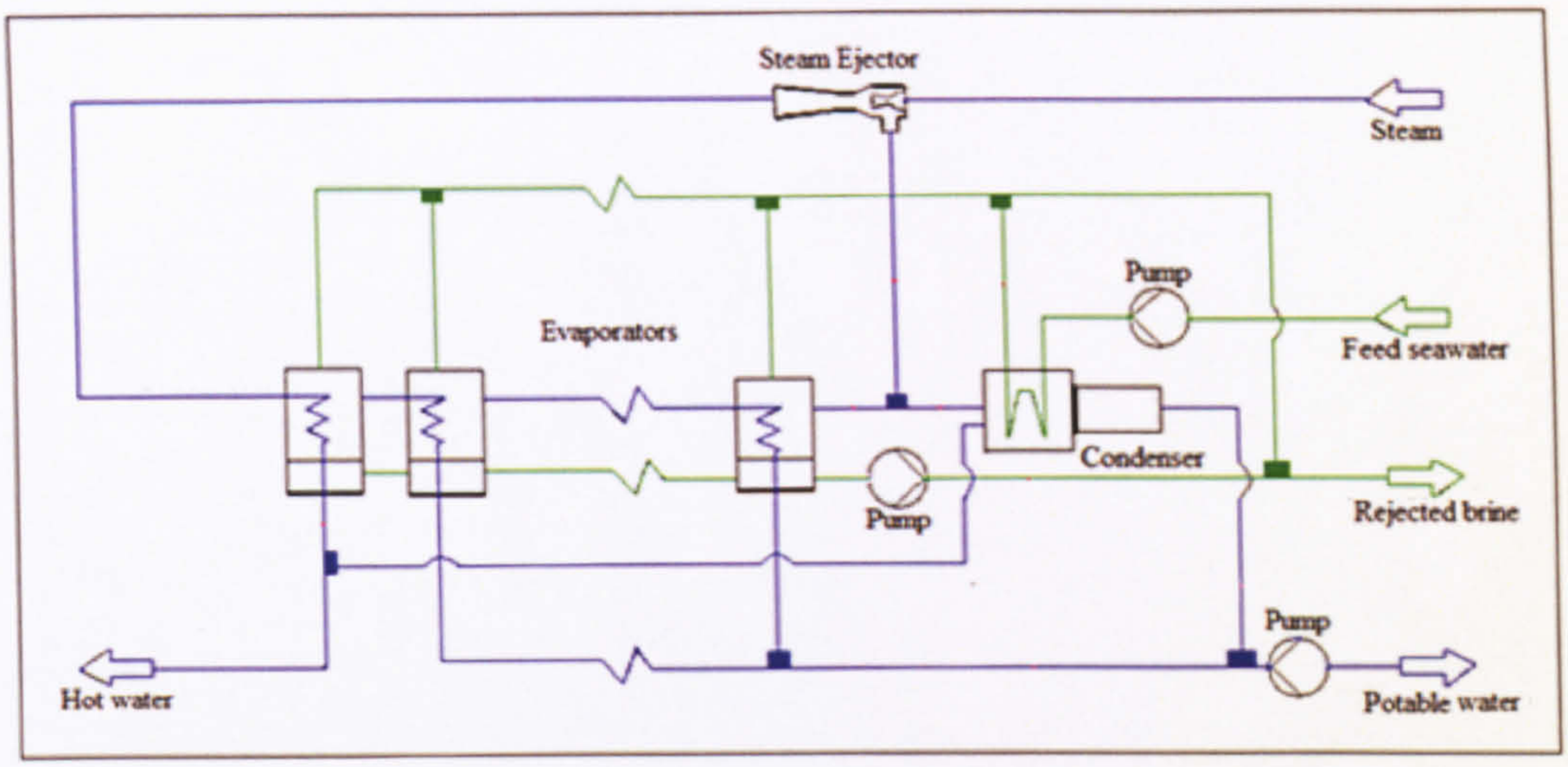

Figure 2-5 Thermal vapour compression multi-effect evaporation (TVC-MED)

According to Semiat and Galperin [9], these gases build a layer next to the heat transfer surfaces preventing the vapour reaching them, which reduces the heat transfer coefficient and then causes a reduction in the condensation rate. Furthermore, the presence of CO_2 in the condensate potable water lowers its acidity level (pH value), and the presence of O_2 in the feed seawater may cause a corrosion in the condenser tubes, while CO_2 released from the brine during the evaporation process encourages scale formation[8]. The non-condensable gases' affect on the desalination process can be eliminated by better designing, manufacturing and inspecting of outer surfaces to discover any leaks [8]. Chemical additives are also added to the feed seawater such as a scale inhibitor to reduce the corrosion caused by the dissolved gases in the feed seawater. However, a very low dosage is used in the MED desalination process in comparison with other desalination processes because it operates at a relatively low temperature [1, 10]. Corrosion may also take place on the evaporation tubes surfaces; however, in the MED process this is minimal due to the low evaporating temperature, which is in range of 40–70°C [7].

- **Vapour compression**

The vapour compression (VC) process is commonly used for small and medium-size seawater desalination units, with a maximum production capacity of about 5000m^3/day; it has been used in Europe since 1910 and in Japan since 1930. The main concept of this process is to compress

the water vapour, rather than the direct exchange of heat from steam coming from an external thermal energy source in order to evaporate the saline feed water, while the heat produced by the compression process is used to help evaporate the feed water, so the main energy required for this process is that used by compressors. Figure 2-6 shows a simple illustration of a single-effect vapour compression process, where the seawater enters the feed pre-heaters, which transfer the heat produced by the compression process either in the product water or in the rejected brine to the feed seawater [4, 5, 6].

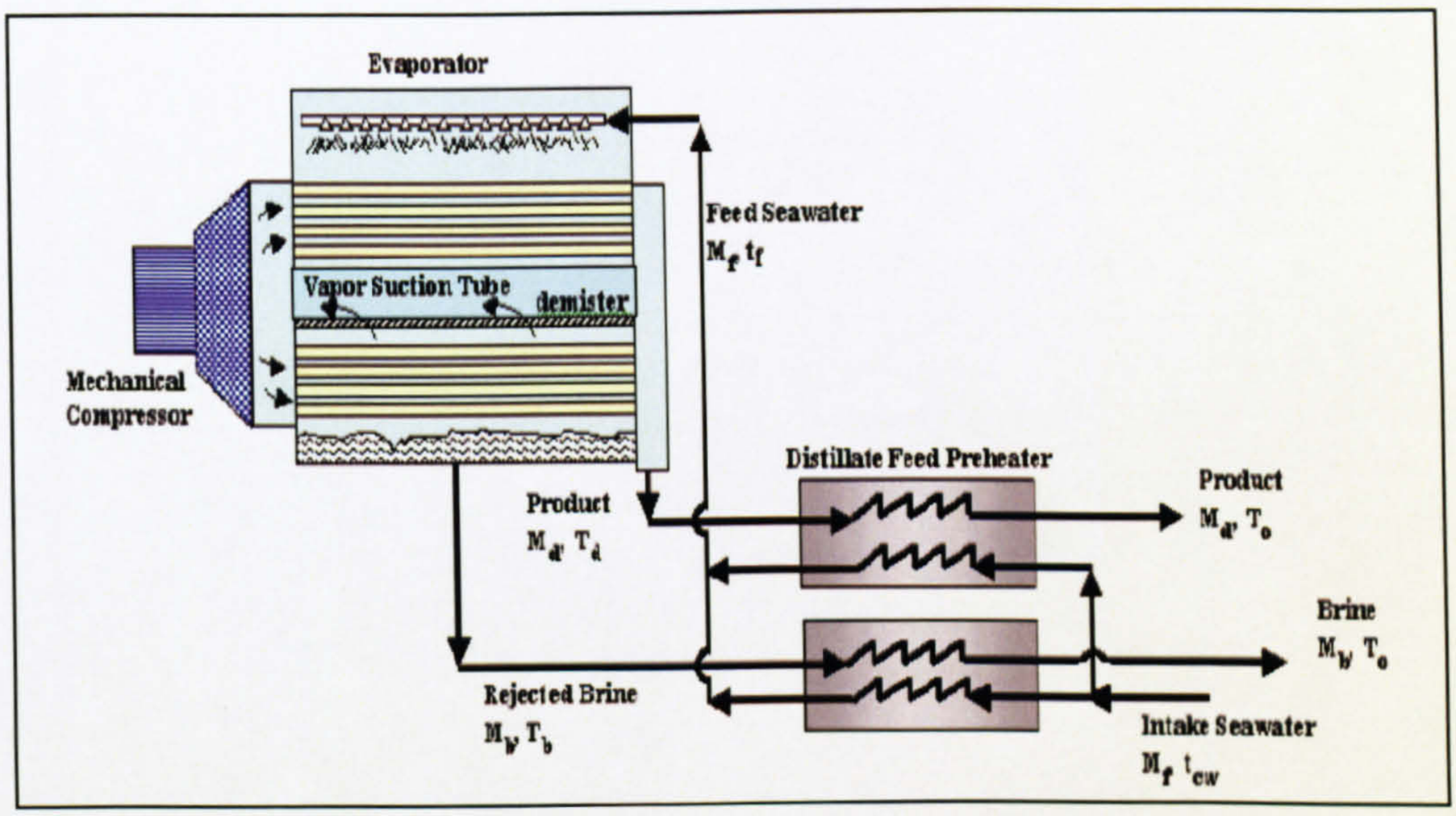

Figure 2-6 Vapour compression (VC) process, reproduced from [4]

The feed water is heated to its boiling point; the hot feed water with a portion of it evaporated already then enters the compression unit where it will be evaporated almost totally as a result of raising its pressure. The hot vapour condenses on the tubes and the potable water produced is drawn out of the unit through the feed pre-heater to benefit from its temperature in heating up the feed water and at the same time it is cooled for usage or storage [4, 5, 6]. The VC process can be classified according to the type of technique used in the compression process; the first is mechanical vapour compression (MVC) in which a mechanical compressor driven by an electric motor is used to compress the vapour. In this case, the only energy required is that consumed by the electric motor, and there is no need for any additional thermal heating source.

The second type is thermal vapour compression (TVC), in which the flow of an external stream at relatively higher pressure is used through a steam ejector to suck the vapour generated in the

evaporator through a suction pipe as it expands at high velocity and low pressure. The mixed stream then flows through a diffuser, which increases its pressure while reducing its velocity, and is then discharged through the evaporator bundle, where it condenses and forms the product distilled water. Generally, the VC process is considered one of the simplest technologies as it needs no cooling water, and this also allows it to be built in remote areas. Moreover, the low operation temperature allows the use of inexpensive materials and reduces the risk of corrosion and scale formation. However, the product quality and maintenance costs mean that the process's contribution to the worldwide water production is only 4% [4].

This process is not applicable in this study due to its dependency on electrical power (MVC) or high-pressure steam (TVC).

- **Solar**

Solar desalination is a process that simulates the natural water circuit (the hydrological cycle), where seawater is heated by sunlight to produce water vapour, which then condenses on cold surfaces as shown in Figure 2-7. The condensed water generated is then collected as a water product. It is believed that in the late 1500s Giovan Battista designed and described a solar still [3]. However, the first large-scale solar desalination plant was built in 1872 at Las Salinas, which is today known as northern Chile. It was designed by Charles Wilson, and produces about 23,000 litres a day [5].

Generally, the solar still is 50% efficient on summer days and 30% efficient during winter days, and usually $1m^2$ of surface area can produce about 4 litres of potable water a day, which makes it an expensive process compared to the other desalination methods, especially if an additional mechanism is used to improve the efficiency such as trackers that follow the sunlight all day. However, economically the solar desalination process appears to be one of the best ways to get potable water in some remote areas, due to the significant reductions in fuel consumption and low operational and maintenance costs [4, 5, 6]. A very good example of such a plant is the one in Abu Dhabi, which was built twenty years ago and consists of a solar collector field, a heat accumulator and a seawater evaporator with a total capacity of $100m^3$/day, and water costs estimated at $\$6.58/m^3$ [11].

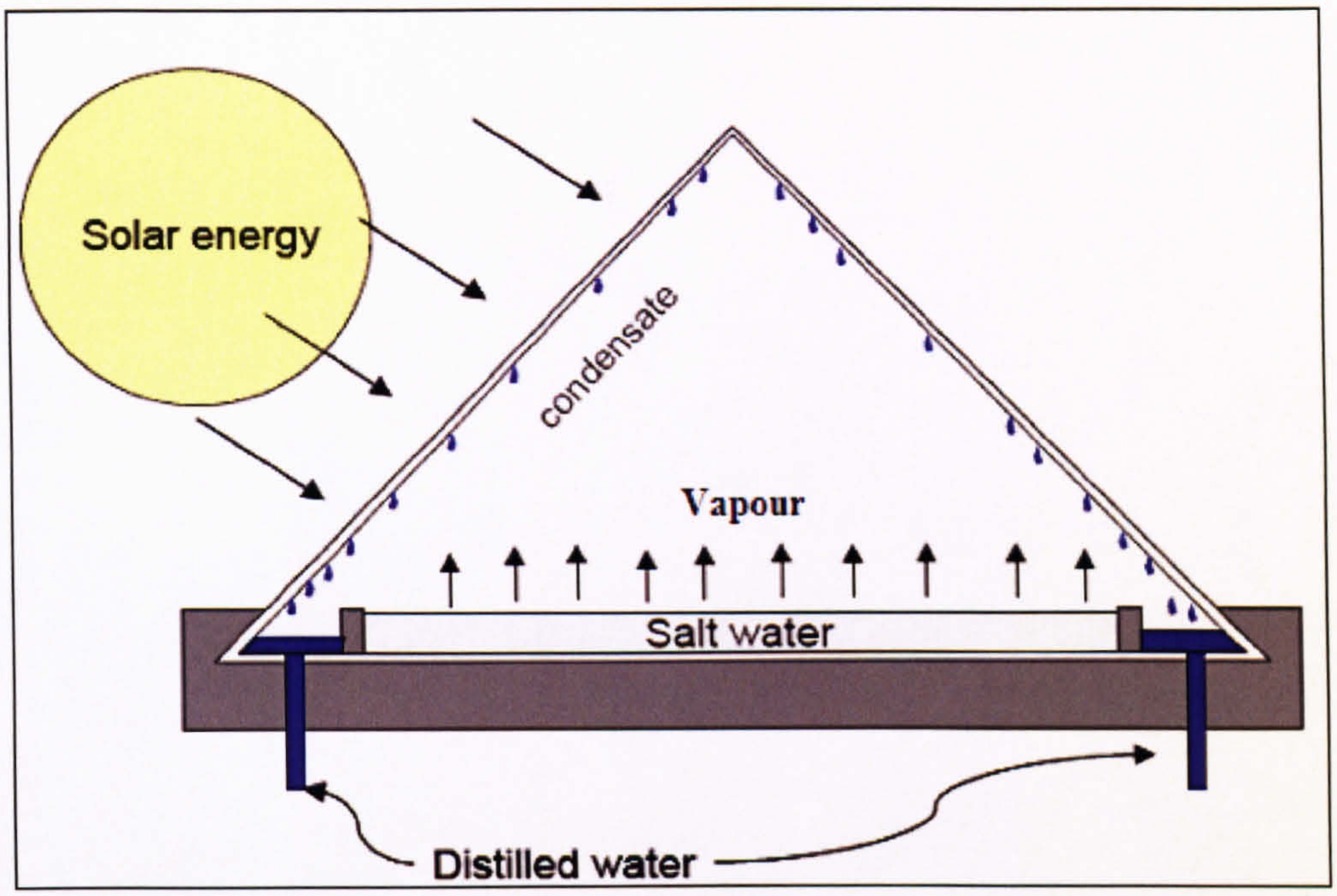

Figure 2-7 Solar desalination principle, reproduced from [5]

Solar energy, as one type of renewable energy, can be used directly to drive a solar desalination process. Alternatively, it can be used to produce electricity through photocells, which can then be used to drive the solar still. However, because solar energy depends on weather conditions this impedes it as a technology, which is motivating researchers to develop alternative ways to minimize this dependence and ensure full operational mode, for example using latent heat storage, or using more than one source of renewable energy to run the same desalination unit [4, 6, 7]

- **Freezing**

In the late 1700s Anton Maria published a paper in which he described an experiment that produced potable water by freezing seawater. However, most of the work that has been done to develop the freezing desalination process was carried out during the 1950s and 1960s. An illustration of the freezing desalination process is shown in Figure 2–8. This technique uses the difference between the freezing temperature point of potable water and that of the saline water; it is well known that the freezing point of saline water depends upon its salinity. For example, seawater has a salinity of about 35 parts per thousand and freezes at about -2°C, while potable water freezes at 0°C [6, 7, 12].

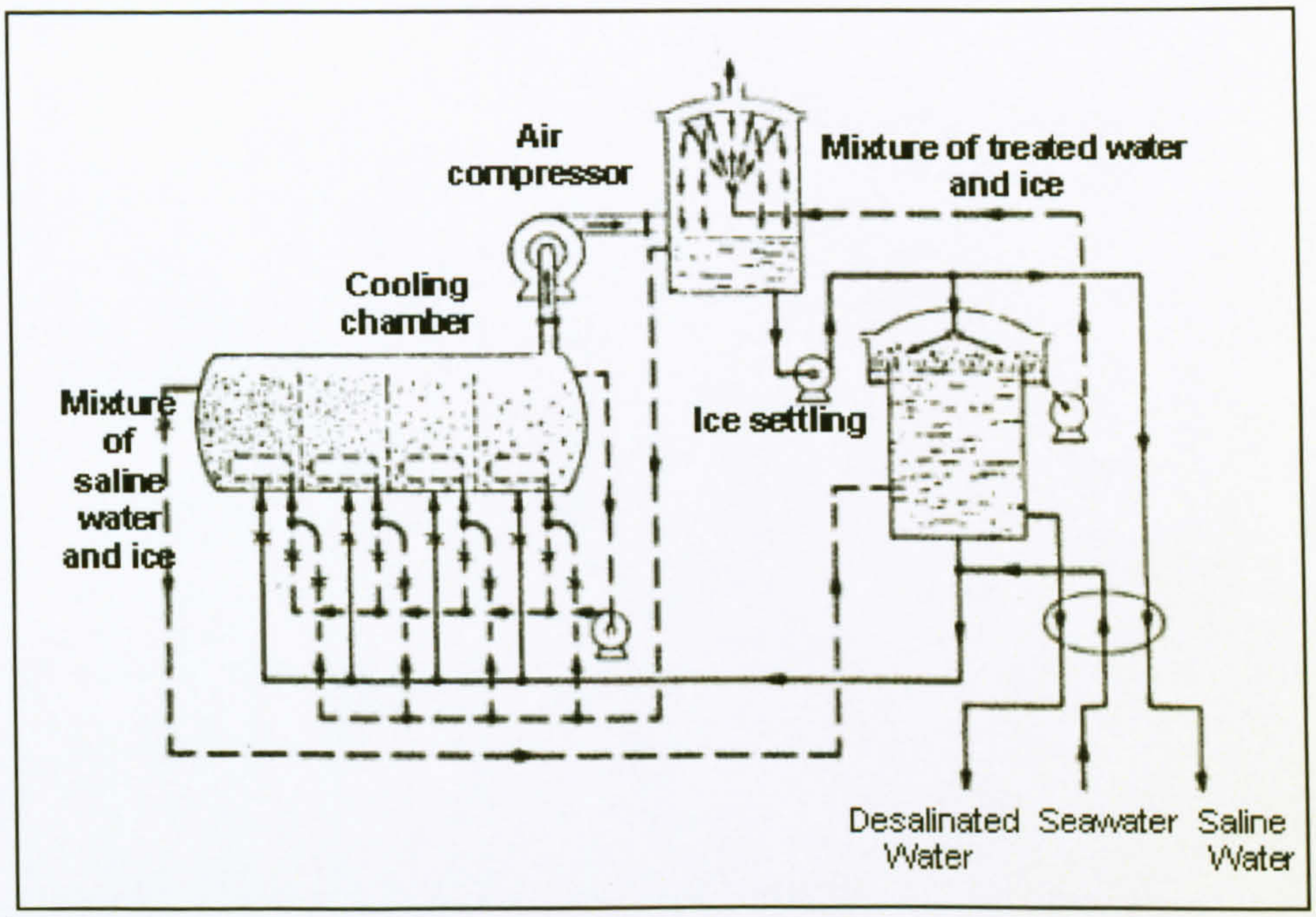

Figure 2-8 Freezing desalination process principle, reproduced from [12]

Therefore, lowering the seawater temperature below the freezing point of potable water, but above the freezing point of saline water, produces potable ice crystals surrounded by the salt water, which can then be washed away to leave pure fresh ice crystals to be finally melted into potable water. This technique has the advantage of a low operating temperature compared to other desalination methods and, therefore, avoids some corrosion and scaling problems. However, many drawbacks prevent this technique from competing commercially with the other methods of desalination. First, heating water is normally less costly than cooling it and, second, the handling, unit size and complexity problem all serve to limit the use of this method. An example was a plant built in Saudi Arabia in the 1980s, which was found to be inefficient and was, therefore, discarded [6, 7, 12].

2.2.3 Membrane Desalination Process

The word "membrane" can be defined as a semi-permeable barrier that allows water to pass through, but not salts. Regardless of the type or material of the membrane, this can be considered as the main concept of the membrane desalination process. A number of membrane techniques can be found, but this study will concentrate only on reverse osmosis (RO) and electro-dialysis (ED).

- **Reverse Osmosis**

The name clearly indicates the osmotic phenomenon that was observed in 1748 by the French cleric, Abbé Nollet. It is defined as that process where potable water flows through a membrane to dilute water with a higher salt concentration until both sides of the membrane reach an equilibrium condition, as shown in Figure 2–9.

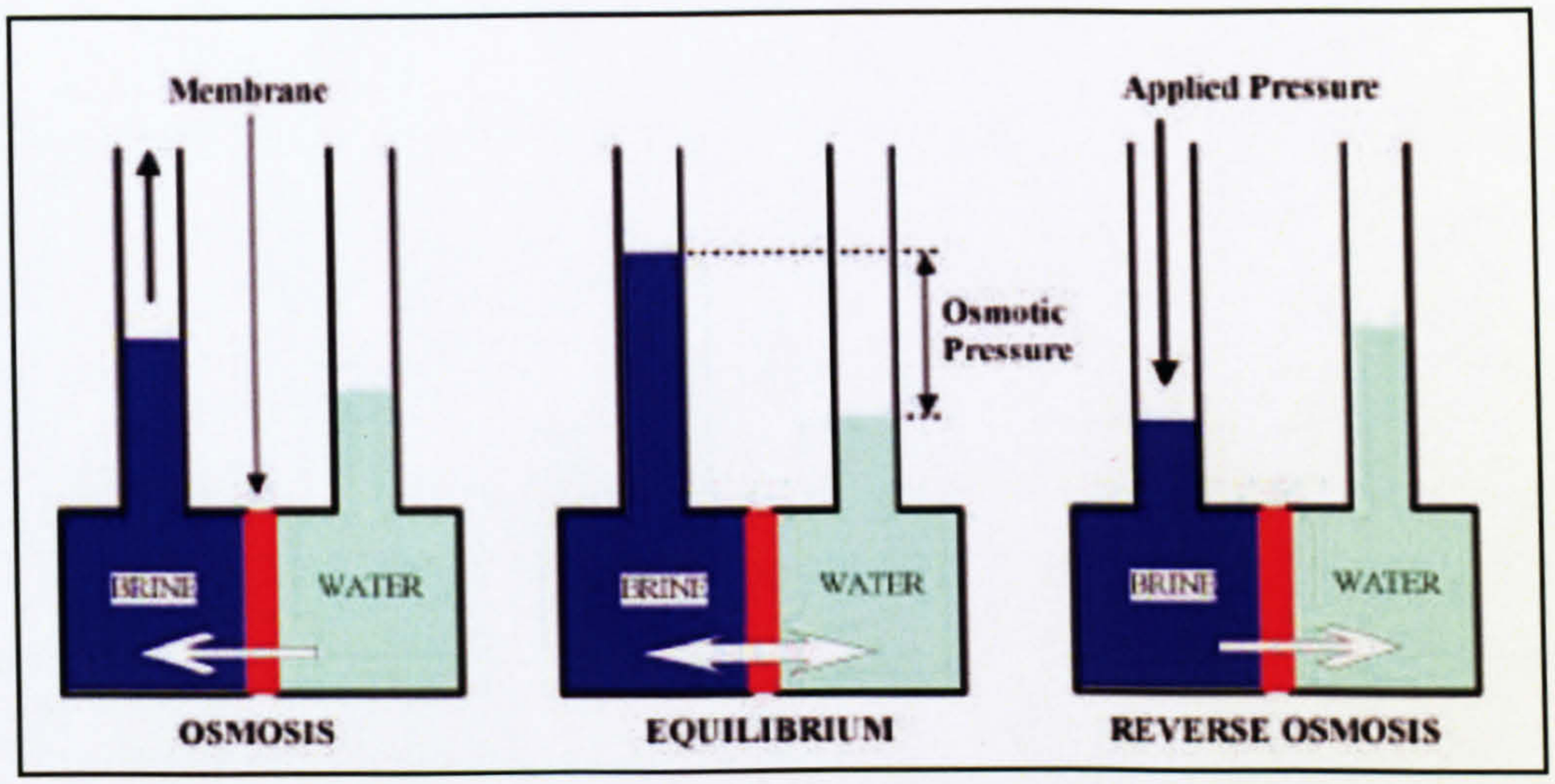

Figure 2-9 Reverse osmosis desalination principle, reproduced from [14]

Until 1867, the membranes were of animal or plant origin. The first synthetic membrane was made of copper ferro cyanide by Traub, as reported by Glater [13]. This process is a pressure-driven membrane process in which the natural flow of osmosis is reversed by applying pressure in excess of the osmotic pressure, as shown in Figure 2–9. In the operation the feed seawater passes through a pre-treatment unit to prevent salt precipitation or micro-organism growth, and then it proceeds to a pressure vessel in which it is pressurized, while at the same time its salt concentration is maintained, discharging a portion of it at this point before it passes through the membrane. The pressure at this point should be in the range of 17 to 27 bar, depending on a number of factors such as water temperature and salinity. After this, the potable water passes through the membrane assembly with a small amount of salt and then proceeds to the post-treatment unit where it is stabilized for storage or usage. Generally, the membrane used should have high salt rejection as well as high permeability with regards to the potable water; moreover, it should be stable in salty water and have good resistance against fouling and deformation [13, 14].

Two types of membrane are currently the most commonly used. The first is the hollow fibre made of a large number of fibres folded to form bundles, with a plastic tube inserted in the centre, and all the assemblies are wrapped and sealed inside a cylindrical shell. This allows the largest possible surface area per unit of volume, which leads to a compact overall design, and this makes it easier to maintain or change them. The second model is the spiral-wound model, which is made of a flat sheet membrane enclosed between layers of permeate carrier materials and cast onto a support fabric, forming a leaf. Usually, two or more leaves are rolled into a cylinder, and attached to a permeate tube. This model can be operated at high pressure, up to 80 bar, and has good resistance to fouling [5, 6, 7]. According to the United Nations report [4], published in 2001, 16% of the total potable water in the world was produced by the RO process in 2000.

- **Electro-dialysis**

Electro-dialysis (ED) is an electrical current-driven membrane process used to separate the salts and other minerals dissolved in the water in the shape of ions, either positive cations or negative anions, by which the ions move toward the electrodes with an opposite electrical charge while a suitable membrane is used to allow selective passage of either cations or anions, as shown in Figure 2–10.

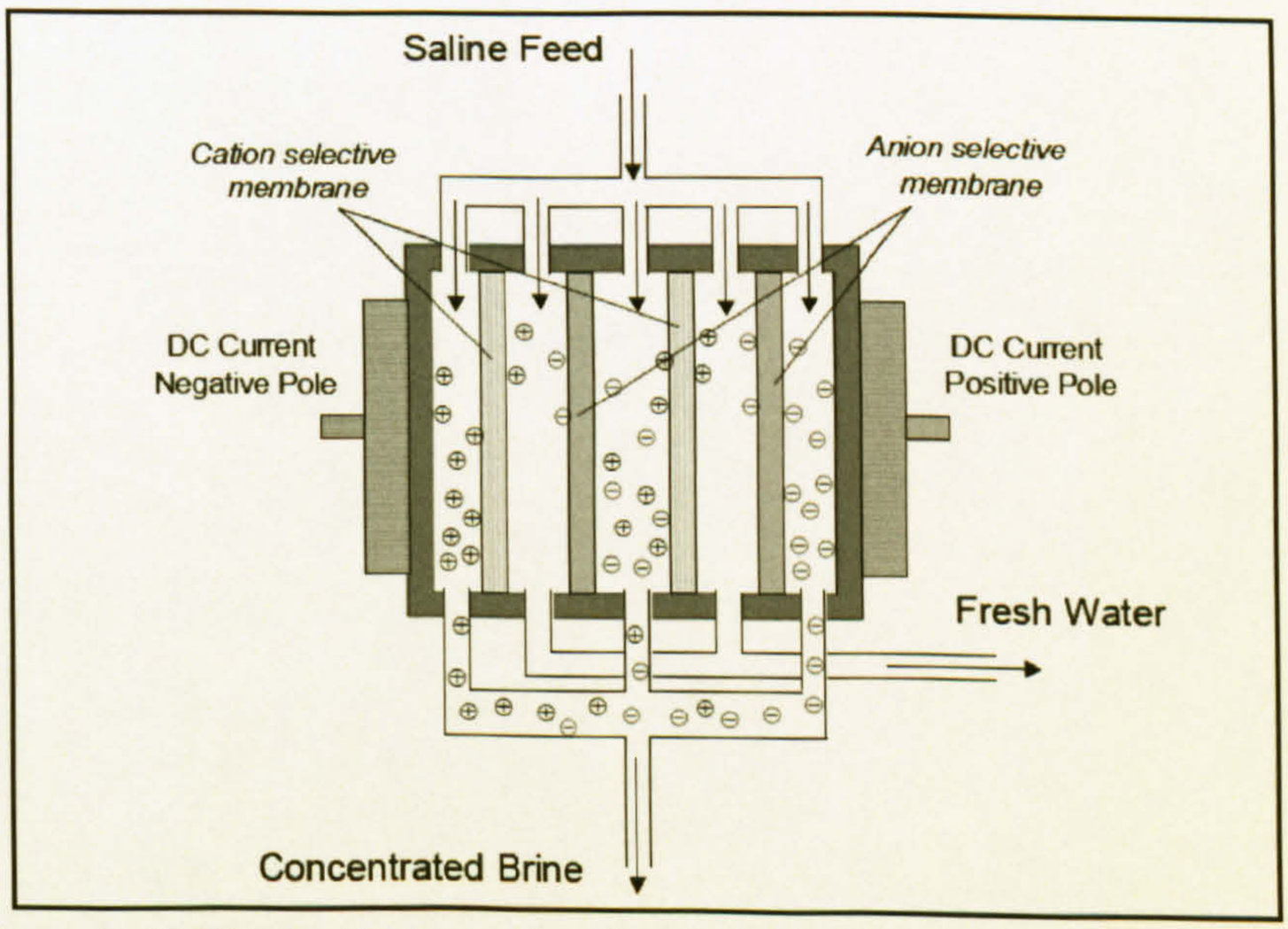

Figure 2-10 Electro-dialysis desalination principle, reproduced from [5]

Typically, the ED plant consists of a pre-treatment unit, a relatively low-pressure circulation pump system, a membrane stack and a post-treatment unit. The membrane stack consists of hundreds of cells, which combine two membranes and two spacers; the spacers distribute the flow of the feed water and brine solutions and direct them into parallel cells [5].

It is believed that the first ED plant was installed by the British company William and Boby Ltd in Tubruk city in Libya in 1959 and had a capacity of 55m^3/day [3]. Although this process was introduced ten years before the RO process, it is not as commonly used as the RO process, which can be explained by the difficulties and skills needed for the maintenance and operation of the ED process. Furthermore, this can be seen clearly in its contribution to the world's total distilled water production in the year 2000 — just 1% — as it is mostly used with brackish water rather than seawater, as mentioned in the United Nations report [13]. On the other hand, the ED process only consumes electric power and the product cost is comparable to that of the RO process; moreover, the ED unit can be built with a capacity of up to 104000m^3/day [4].

Another technique, called electro-dialysis reversal, has been derived from the ED process. It uses the same principle as ED except that both electrodes are similar, and their polarities are reversed three to four times per hour, while automatic valves are used to switch the flow streams at the same time. This helps in cleaning scale and other deposits in the cells, which minimizes the use of chemical additives and extends the life of the cell's electrodes as well as the membranes [6, 7].

In general, no membrane desalination processes are applicable in this study for its high electricity consumption rate.

2.2.4 Process Summary

A brief comparison of the most important properties of the processes mentioned is shown in Table 2–1. The product cost of the freezing desalination process was not defined due to the lack of data for this process as the most recent plant was built in 1985, as reported by Akili, et al. [7]. The data presented in Table 2–1 shows that the maximum capacity can be achieved using an MSF process. The MED process consumes the lowest amount of electricity. This makes it the ideal process for heat recovery utilization applications and it can be operated by low-grade heat energy. In addition, its corrosion resistance is better than other desalination processes, which also reduces its consumption of chemical additives and so reduces the product cost.

	Thermal Process					Membrane Process	
	MSF	MED	VC	Freezing	Solar	RO	ED
Maximum Capacity m^3/day	70,000	24,000	5,000	200	120	10,000	4,000
Steam Consumption m^3/m^3 of water	8	12	0	0	0	0	0
Electricity Consumption kWh/m^3 of water	4	1.8	9	17	0	8	6.6
Product Cost \$/m^3	0.5-1.5	0.5-1	0.5-1	no record	0.2-0.7	0.75-1	1

Table 2-1 Desalination process summary, collected from [15, 16]

2.3 Water Resources in Saudi Arabia

Saudi Arabia is an arid country with limited potable water resources. Therefore, it is becoming increasingly dependent on desalination; it was estimated that desalination will satisfy more than 70% of the domestic demand for water in Saudi Arabia by 2010 [17]. Saudi Arabia is the world's leading producer of desalted water, according to the United Nations report [4], published in 2001; it produced 21% of the world's desalinated water in the year 2000. Figure 2–11 shows the world's top desalinated water producing countries in 2000.

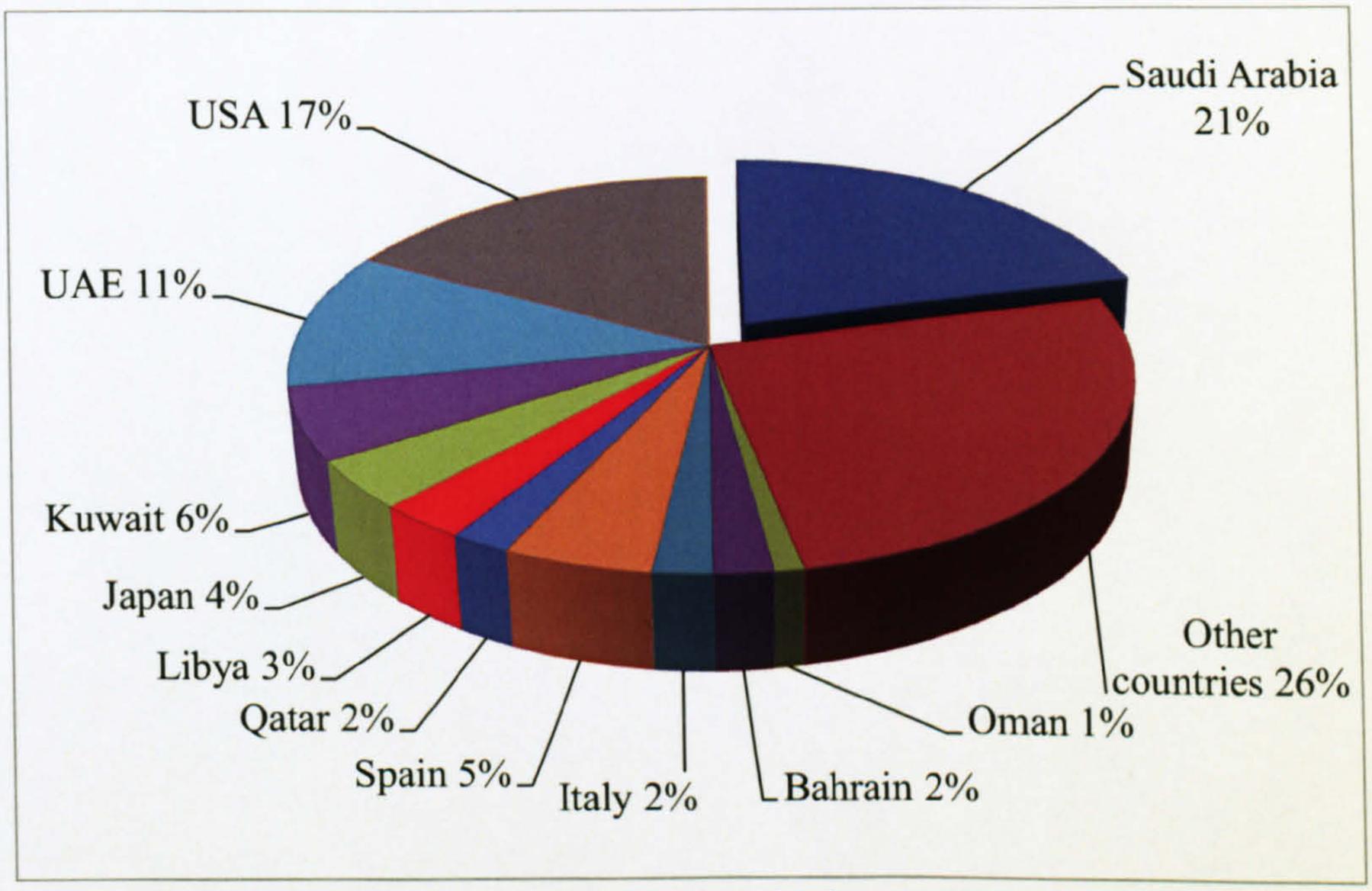

Figure 2-11 Desalted water — top-producing countries, in 2000 [4]

Saudi Arabia, the United States and United Arab Emirates account for about half of the total world production of water. Saudi Arabia has 30 plants on the eastern and western coasts using either the multi-stage flash (MSF) or the reverse osmosis (RO) process. Saudi Arabia also has the largest desalination plant in the world, located in Al-jubail on the western coast, with a total capacity of 1million m^3/day [18].

Although the first desalination plant in Saudi Arabia was installed in 1907, in the period of the Ottoman rule, the next installation took place 62 years later, when the new age of desalination had started in Saudi Arabia. Table 2–2 shows the history of all installations in Saudi Arabia since then according to the Saline Water Conversion Corporation in Saudi Arabia [19].

Year	Plant	Year	Plant
1969	Al-Wajh "Phase I". Duba.	1986	Al-Wajh "First Extension". Al-Khafji. Ummluj "Phase II".
1970	Jeddah "Phase I".		
1973	Al-Khobar "Phase I".	1987	Al-Aziziyah "Phase I".
1974	Al-Khafji "Phase I".	1989	Duba "Phase III". Al-Wajh "Second Extension" Jeddah RO "Phase I". Al-Shoaibah "Phase I". Al-Shuqaiq "Phase I".
1975	Ummluj "Phase I".		
1978	Jeddah "Phase II".		
1979	Al-Wajh and Duba "Phase II" Farasan "Phase I". Jeddah "Phase III". Haql "Phase I".	1990	Haql "Phase II". Farasan "First Extension".
1980	Yanbu "Phase I".	1994	Jeddah RO "Phase II".
1981	Al-Jubail "Phase I".	1999	Yanbu MSF. RO "Phase II".
1982	Rabigh "Phase I" Jeddah "Phase IV". Al-Birk "Phase I", Al-Jubail.	2001	Al-Khobar MSF "Phase III". Al-Jubail RO.
1983	Al-Khobar "Phase II".	2002	Al-Shoaibah "Phase II".

Table 2-2 History of all installations in Saudi Arabia [19]

Furthermore, the government, represented by the Saline Water Conversion Corporation (SWCC) has never stopped planning for and installing new desalination plants everywhere in the kingdom to meet the annual 3% increase in the potable water demand, as reported by A1-Sahlawi [15]. Moreover, the private sector has also contributed to the desalination industry in Saudi Arabia, with six desalination plants so far, having a total capacity of 3million m^3/day. On the other hand, there are 16 power plants along the eastern and western coasts, most of which are not dual-purpose plants according to the Saudi Electricity Company [20]. These power plants have the potential to produce potable water if integrated with a thermal desalination plant.

Although Saudi Arabia is the world's largest single producer of desalinised water, the domestic, industrial, and agricultural water demands are growing rapidly, which requires continuous upgrading of the current plants and building new plants using the latest technologies available.

2.4 Absorption Chillers

This topic explains the concept of the absorption chiller as an energy conversion system that utilizes a low-grade thermal energy source in order to generate a cooling effect used for air conditioning or refrigeration purposes, and discusses its ability to enhance gas turbine performance by maintaining the compressor air-intake temperature at or lower than the ISO level.

2.4.1 Historical Overview

According to Abrahamsson, et al. [21], in 1922 Baltzar von Platen and Carl Munters, from the Royal Institute of Technology in Stockholm in Sweden, submitted their degree project in which they invented the absorption refrigerator. One year later, they established two companies, AB Arctic and Platen-Munters Refrigeration System, and started the commercial production of the absorption refrigerator. By the 1960s, US manufacturers had 100% of the worldwide market for lithium bromide/water absorption chillers, and then the Japanese entered into the marketplace in the late 1960s, introducing direct-fired and multi-stage absorption chillers. However, at this time, oil prices were in the range of $3 per barrel, and so electricity was inexpensive, which has benefited electrical refrigerators [22].

The real development of the absorption system was mainly driven by the oil crisis in 1973, which directed researchers and manufacturers to look for a system that used energy in a more efficient way, and was capable of better utilization of waste heat energy. Since then, worldwide sales of the absorption refrigerator started growing, as can be seen in Figure 2–12, which is reproduced from an Oak Ridge National Laboratory publication [23].

The other factor that motivated the development and market growth of the absorption refrigerator was the categorization of chlorofluorocarbons (CFCs) in the early 1990s as one of the alkyl halides chemical group, which are believed to be responsible for some environmental issues such as ozone depletion, which triggered the search for alternatives. The Kyoto treaty [24], which calls for the reduction of greenhouse gas emissions, also encouraged the use of waste heat energy utilization systems such as absorption chillers.

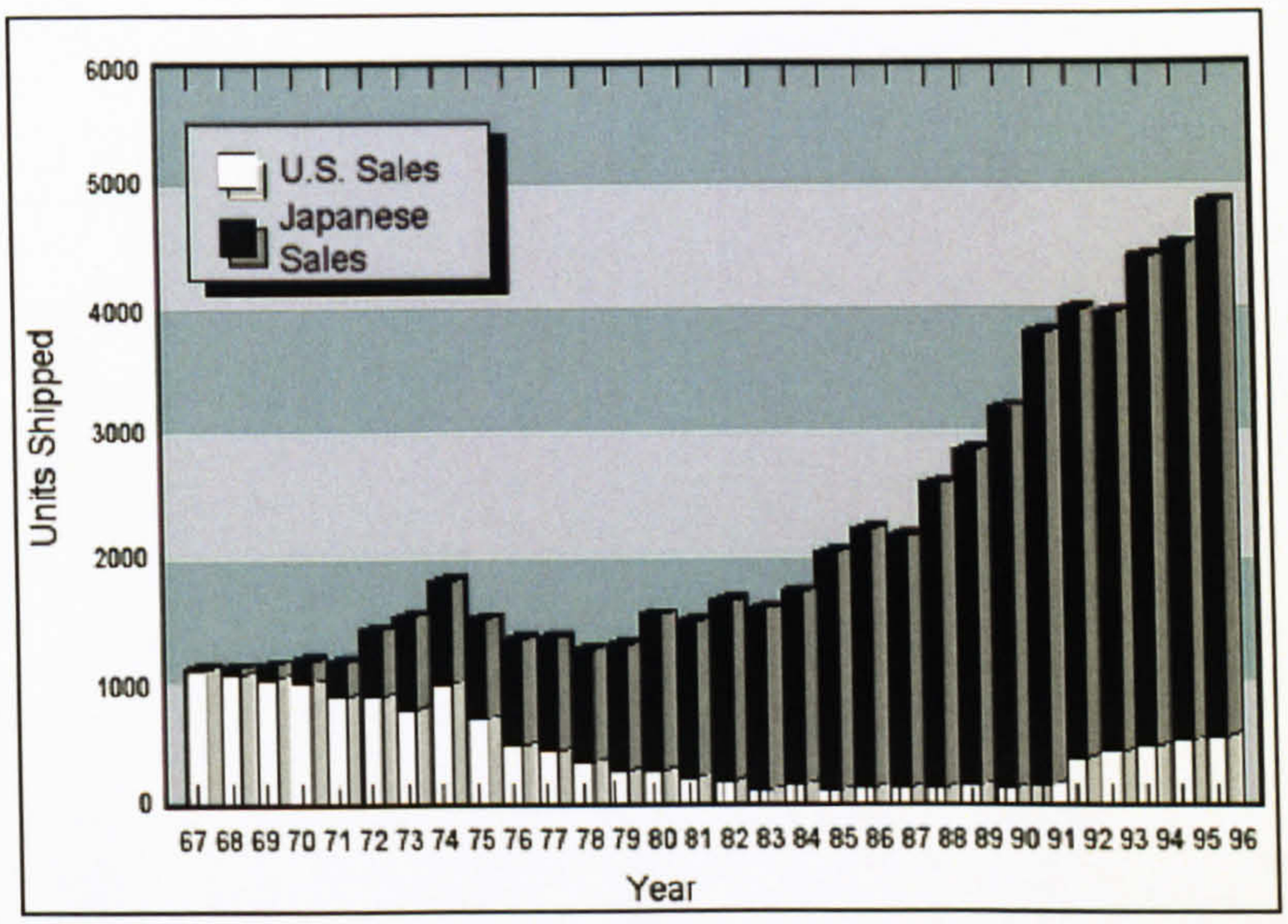

Figure 2-12 Worldwide sales of the absorption refrigerator [23]

2.4.2 System Fundamentals

The working principle of absorption chillers is similar to that of the normal refrigerator; both cycles evaporate the refrigerant at a relatively low pressure to create the cooling effect, and then condense it at high pressure to reject its heat. The main difference between the two cycles is the mechanism by which each cycle reaches the high-pressure level. While in the normal vapour compression refrigerator a compressor does this, in the absorption chiller cycle the compressor is replaced by an absorber, pump and generator, in addition to a secondary fluid that transports the refrigerant from the absorber to the generator [25].

Figure 2–13 shows an illustration of a single absorption chiller where the low-pressure mixture of vapour and liquid refrigerant (A) enters the evaporator, where it boils as a result of absorbing the heat from the warm water used to transfer the cooling effect to the cooling load. The low pressure vapour (B) is then drawn into the relatively lower pressure absorber, where it will be absorbed by the absorbent rejecting some heat to the coolant fluid. A small pump is then used to push the new mixture to the high-pressure side of the cycle, to the generator. A heat exchanger is used between the absorber and generator to transfer the heat between the mixture going to the generator and the absorbent going back to the absorber in order to reduce the heat energy required to boil the refrigerant in the generator, as well as pre-cooling the concentrated absorbent solution, which reduces the required flow rate of cooling fluid through the absorber. The external

heat energy is supplied to the generator in order to increase the mixture's temperature to the degree at which the refrigerant only evaporates and is separated from the absorbent, which needs a higher temperature to boil. The absorbent is then drawn back into the low-pressure side of the cycle, the absorber, to complete its cycle, while the high pressure vapour refrigerant (C) enters the condenser where it condenses while rejecting its heat to a coolant fluid. The high pressure liquid refrigerant (D) now passes through an expansion device that reduces its pressure to evaporate again using the heat of the relatively warm incoming chilled water.

The system has no moving parts except the pump, which is quieter and more economic than the compressor in the normal refrigerator. Moreover, the system can use low grade heat at a temperature in the range of 90˚C to 130˚C to separate the refrigerant from the absorbent [25, 26].

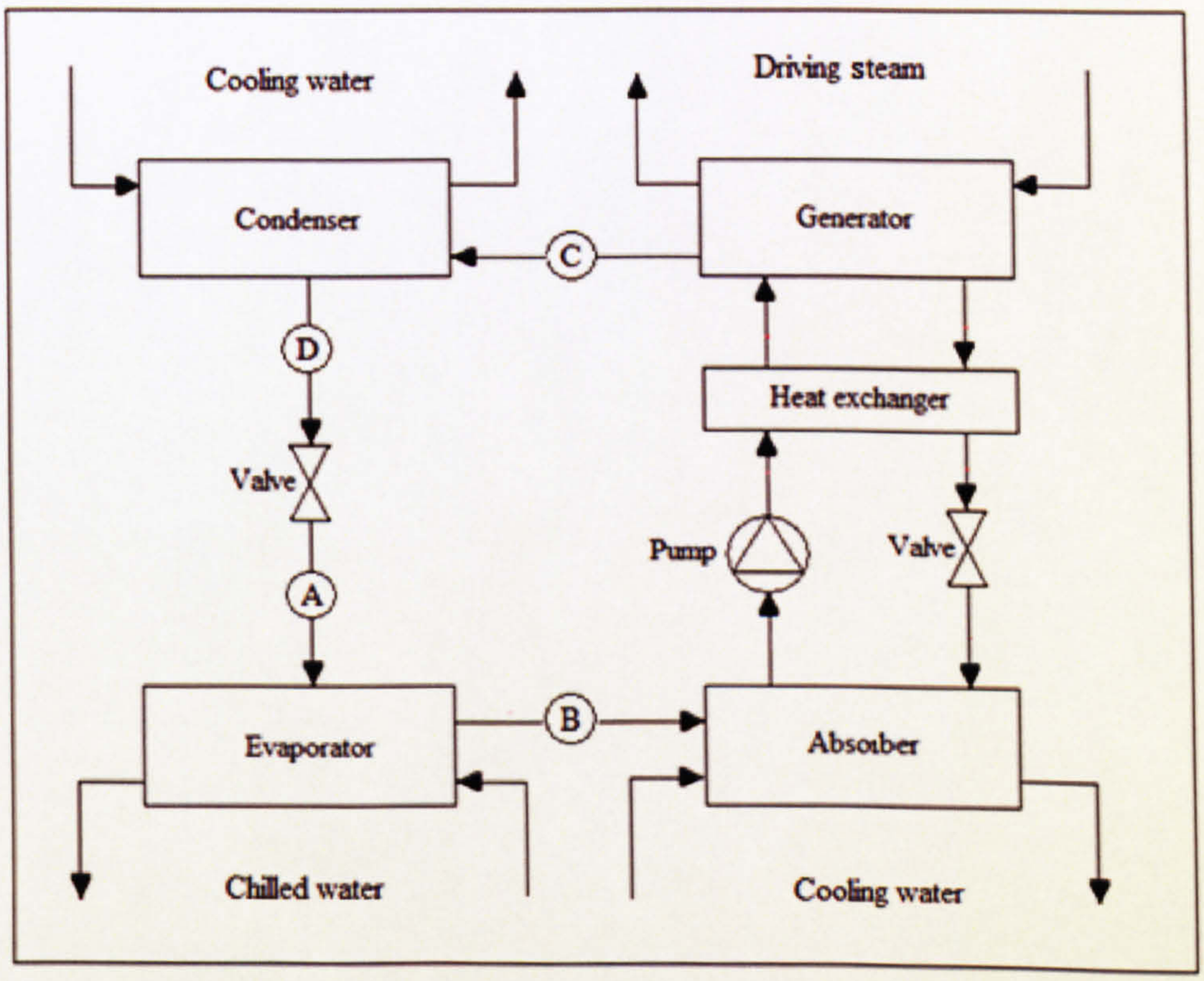

Figure 2-13 Single-effect absorption chiller principle.

A single absorption chiller can achieve a coefficient of performance (COP) in the range of 0.6 to 0.8, where the COP is defined as the ratio of evaporator cooling capacity to the heat energy required by the generator. Considering an average absorption chiller model, the absorption cycle refrigerant/absorbent mixture circuit can be analysed using the aqueous lithium bromide solution

equilibrium chart that is shown in Figure 2–14. At point (A), in Figure 2–15, the LiBr diluted solution leaves the absorber at 41°C at a pressure of 1.034 kPa and is preheated in the heat exchanger to 80°C at a fixed concentration (B) after it has been pumped into the generator at the high pressure side of the cycle at 10.34 kPa. In the generator, the water evaporates and the high pressure steam flows to the condenser. This increases the solution concentration in the generator from 59% to 64.5% at point (D), with an increase in the temperature to 102°C [25, 26].

The concentrated solution is now drawn back into the heat exchanger, where it is cooled to about 57°C (E). The cooled solution is then mixed with the diluted solution from the absorber to reduce its concentration to 62% and its temperature to about 48°C (F). The solution is pumped to a spray system in the absorber where its concentration decreases to 59% while rejecting some heat. The solution then completes its cycle at point (A) [25, 26].

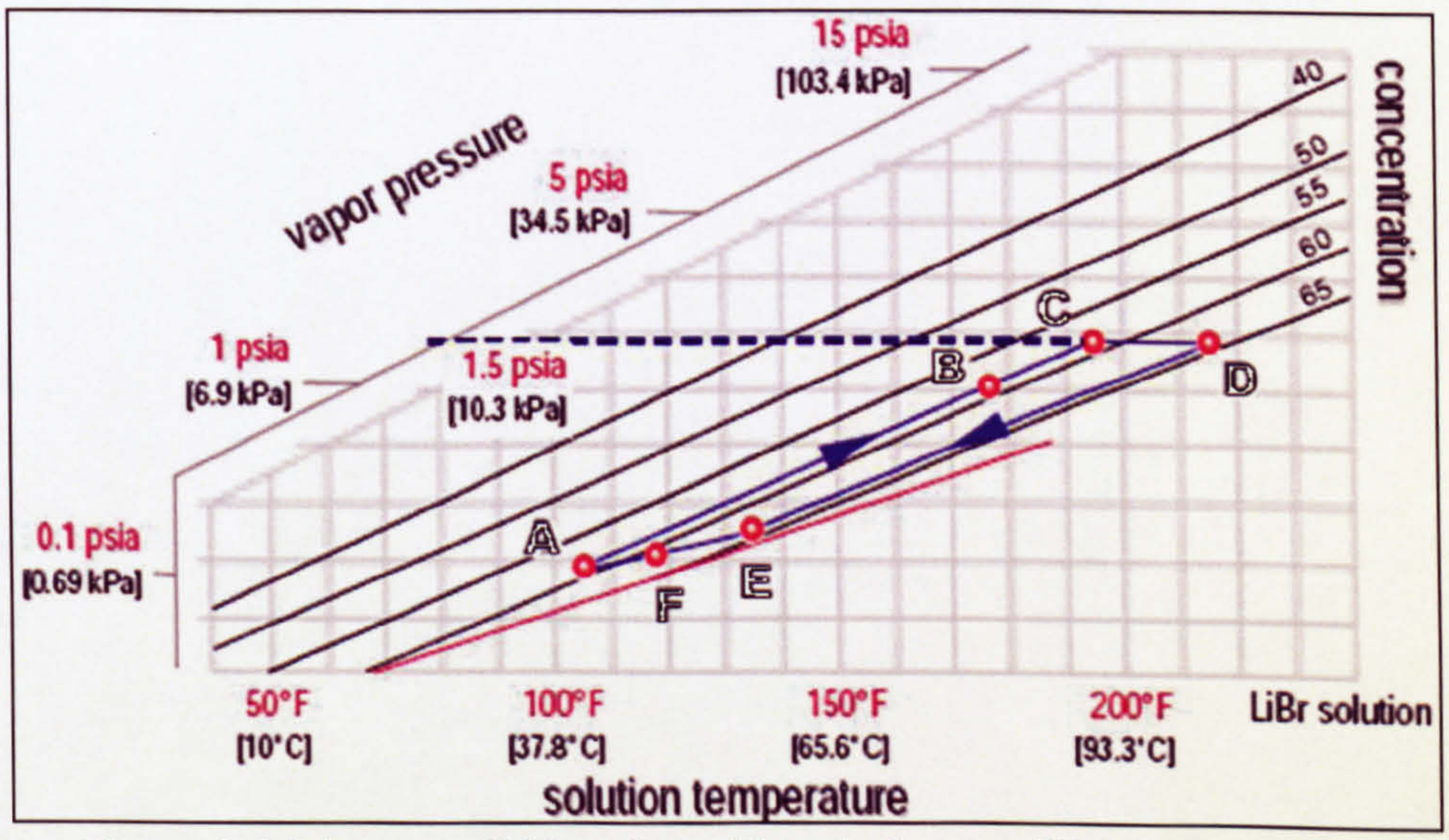

Figure 2-14 Aqueous lithium bromide solution equilibrium chart [25]

Moreover, one of the most dominant factors that limit the operation of the absorption chiller is the phenomenon of crystallization. Figure 2–15 shows the crystallization line of the LiBr solution with respect to temperature, pressure and concentration. It can be observed that if one or more of these variables changes, the salt leaves the solution in a solid crystalline form, making it inoperative. This could be due to electricity failure, a leak of air into the absorption chiller, cold cooling fluid or highly fluctuating temperatures in the case of the chiller being water-cooled. The result is a crystallized salt inside the heat exchanger interrupting the chiller's operation.

However, in the modern absorption chillers safety controls are used to monitor and control solution concentrations and temperatures to avoid crystallization.

The other issue that may affect the absorption chiller's efficiency is the accumulation of air inside the chiller. This may happen if the air leak into the chiller changes its operating pressure and temperature and is encouraged by the low pressure that the chiller is operated at. To resolve this, a purge system is necessary to detect any leaks, remove the air and maintain the chiller operating temperature and pressure [25, 26].

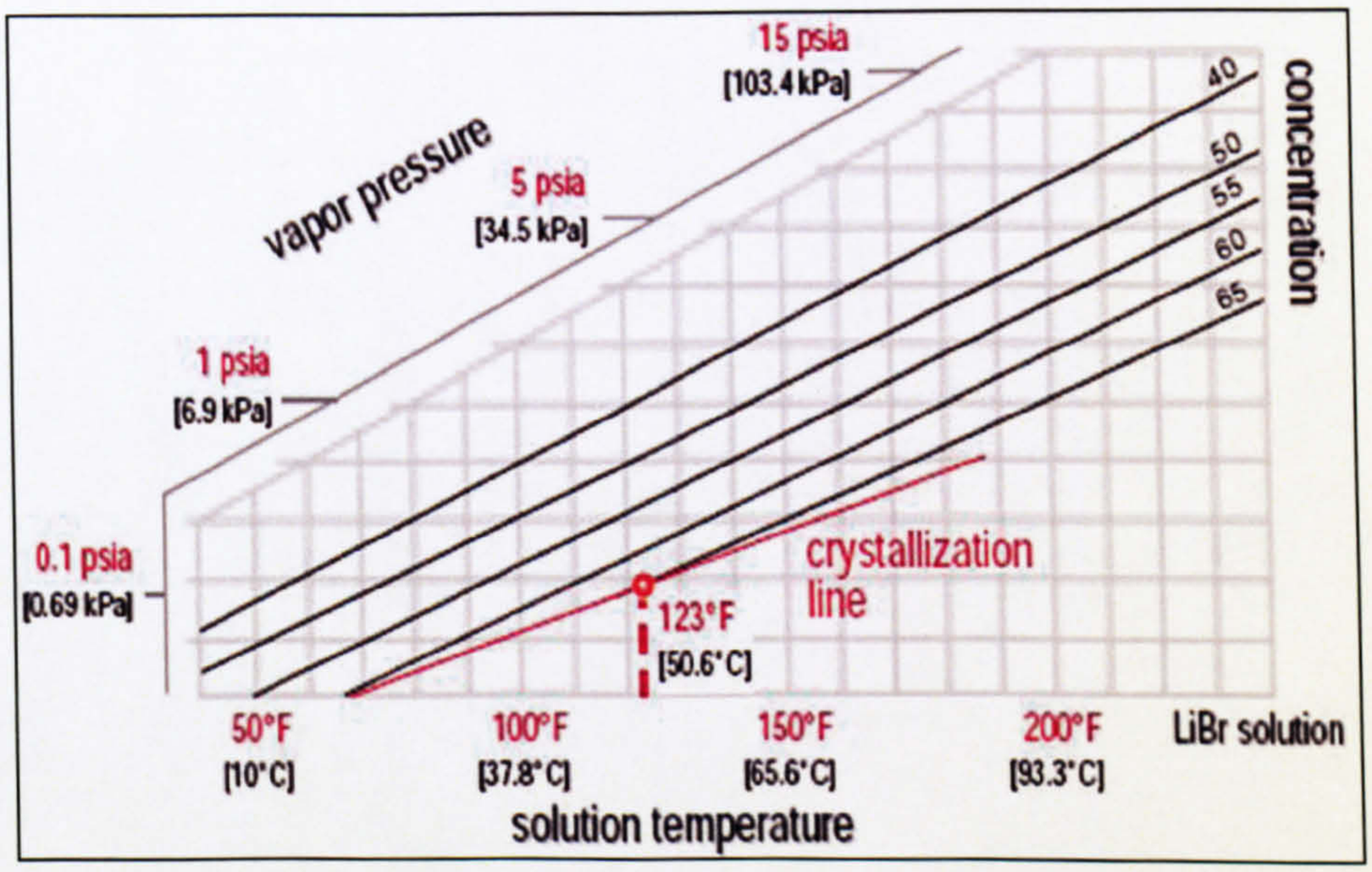

Figure 2-15 Crystallization line of the LiBr solution [25]

Furthermore, different designs of absorption chillers are commercially available and can be classified by the heat source, operating fluid type, effect number and coolant fluid. Table 2–3 lists the most common classification of absorption chillers with a brief comment on each type. The direct-fired chiller is not applicable for use with the waste heat recovery applications as it includes its powering mechanism.

The water-ammonia absorption chillers are similar to the LiBr-water chillers except that the operating fluid used is water-ammonia. Ammonia gas is classified as a toxic gas and it contributes to the ozone depletion issue as stated in the Montreal Protocol, which recommended ending the production of all chlorofluorocarbon compounds [27]. The air-cooled absorption chillers are similar to the water-cooled chillers that explained previously, except that the chillers

need cooling towers, which means extra economic costs. This chiller type is not an option if there is an open source for the cooling water, which is the case in this study.

Classification	Type	Comments
Heat Source	Direct-Fired	Includes a burner that operates on natural gas or fuel oil
	Indirect-Fired	Utilizes any eternal low-grade heat i.e. solar or waste
Fluid Type	Water-Ammonia	The water is used as an absorbent, while the ammonia is the refrigerant. Can achieve less than 0°C, but ammonia is a toxic gas
	LiBr-Water	The water is a refrigerant, while the LiBr is the absorbent
Effect Number	Single-Effect	Includes single generator, condenser, evaporator, absorber, heat exchanger and pump.
	Double-Effect	Includes additional generator, heat exchanger and pump.
Coolant Fluid	Water-Cooled	Both condenser and absorber are air-cooled; there is no need for a cooling tower
	Air-Cooled	Both condenser and absorber are water-cooled; there is a need for a cooling tower

Table 2-3 Absorption chiller classification [25, 26]

The double-effect absorption chiller uses the same principle as the single-effect chiller, except that it has two generators. The first generator is powered by an external heat source and the water vapour generated in this generator is used as a heating source for the second generator. This requires the temperature of the heat source needed to drive the first generator to be in the range of 155°C to 205°C, which is higher than that required for the single-effect absorption chiller [25]. Therefore, this type of chiller is not suitable for the waste heat utilization applications.

2.4.3 Gas Turbine Enhancement

One of the factors that affect gas turbine performance is the ambient conditions: temperature, pressure and humidity. Depending on the type and specifications of the gas turbine, its electric

power output and efficiency are sensitive to the changes in the ambient conditions [28]. Kehlhofer, et al. [29] stated that "*a gas turbine is a standardized machine, and can be used for widely different ambient conditions*", which means that the compressor of the gas turbine is designed for a constant volume of air [30].

Kehlhofer, et al. [29] also indicated that the increase in the ambient temperature causes a reduction in the air density. Due to this, the mass flow rate entering the compressor reduces and causes an increase in the compressor pressure ratio and specific work, and a reduction in the turbine pressure ratio but no change to its specific work. The reduction in the gas turbine pressure ratio is more than the increase in the compressor pressure ratio leading to a reduction in the gas turbine power output and efficiency. Bassily [31] confirmed that the increase in the ambient temperature leads to an increase in the compressor's specific work and expressed the compressor's specific work W_C as a function of the ambient temperature T_1 in the following equation:

$$W_C = T_1\, C_p \left(r_c^{\frac{\gamma_c - 1}{\gamma_c}} - 1 \right) \tag{2.1}$$

where C_p is the specific heat of air at a constant pressure, r_c is the compressor pressure ratio and γ_c is the specific heat across the compressor. The gas turbine cycle efficiency is a function of the compressor work, the turbine work (W_T), and the heat input (Q_{in}) as follows:

$$\eta_{cycle} = \frac{W_T - W_C}{Q_{in}} \tag{2.2}$$

Equation 2.2 confirms that the increase in the compressor's specific work causes a reduction in the gas turbine cycle efficiency. Hosseini, et al. [32] also indicated that the gas turbine compressor is designed for constant air volume flow, which makes the electric power output dependent on the ambient temperature through the specific mass flow rate. They added that the increase in the ambient temperature also decreases the compressor's output pressure, which reduces the gas turbine cycle efficiency, while the increase in the air density reduces the gas turbine's heat rate and increases its specific fuel consumption. They stated that, for each 1°C increase in the ambient air temperature, the electric power output of the gas turbine decreases by

0.5% to 0.9%, and by 0.27% for a combined cycle. Saravanamuttoo, et al. [33] also justified the reduction in power at higher ambient temperature by the reduction in the mass flow entering the gas turbine, and mentioned that the gas turbine cycle temperature ratio (T_3/T_1) also decreases with the increase in the ambient temperature causing a reduction in the turbine specific power.

Moreover, Kakaras, et al. [34] stated that "*the reduced air mass flow directly causes the gas turbine to produce less power output. On the other hand, the higher intake-air temperature results in an increase of the specific compressor work and, therefore, in a further reduction of the power output*". They also stated that for each 10°C increase in ambient temperature the electric power output of a gas turbine decreases by a percentage between 6% and 10%, and the specific heat consumption increases by a percentage between 1.5% and 4%, depending on the gas turbine type.

Kurz and Brun [35] confirmed the influence of ambient temperature on the gas turbine's power output, heat rate and optimum power turbine speed, and stated that "*Manufacturers typically provide performance maps that describe these relationships for International Organization for Standardization (ISO) conditions. These curves are the result of the interaction between the various rotating components and the control system*". In addition to the previously mentioned justifications, they added that at a higher ambient temperature on a two-shaft gas turbine the generator speed reduces to satisfy the equilibrium condition between the power requirement of the compressor and the generator. They then mentioned that the reduction in the generator speed causes a reduction in the gas turbine cycle efficiency, and suggested that the variable compressor guide vanes can keep the gas generator speed constant to avoid the drop in efficiency, which does not apply to the single-shaft gas turbine.

Ameri and Hejazi [36] observed that the variation in the ambient temperature causes a loss of 20% of the rated capacity of the 170 gas turbine units in Iran. They studied five gas turbines located in Chabahar city, where the difference between the ambient temperature and the ISO conditions is on average 11.8°C. They found that for each 1°C increase in ambient temperature, the power output was downgraded by 0.74%, and they suggested cooling the compressor's intake-air temperature to improve the gas turbine cycle efficiency. Hence, one of the most efficient applications of the absorption chillers is in cooling the inlet-air to a gas turbine

compressor to the ISO level (15°C), not just because this will improve the performance of the gas turbine itself, but also it utilizes the waste energy coming out of that gas turbine, which increases its energy utilization factor (EUF) and simultaneously lowers its CO2 emission rate. This is confirmed by a number of studies that have been published intensively since the early 1980s.

Boyce [37] pointed out the effect of ambient temperature on the power and heat rate produced by a gas turbine, and listed different cooling systems for cooling the compressor's inlet-air for improving the gas turbine's power output. He concluded that the power output can be increased in range from 3% to 21%, while the gas turbine cycle efficiency can be improved in range from 0.4% to 24%. These results are significantly high because he was using the compensation of two or three systems to cool the compressor inlet-air, but for an absorption chiller alone the increase in the power output and efficiency were by 11.5% and 2.5% respectively.

Adel, et al. [38] suggested using an absorption chiller powered from the waste heat of the exhaust gases to cool the compressor intake-air in Arabian Gulf areas where the average ambient temperature varies by more than 30°C from summer to winter. The study concluded that using gas turbine exhaust gas with a flow rate of 300kg/s at 450°C to cool the compressor intake-air temperature from 40°C to 30°C increased the power output by 10%. Although they achieved a 10% increase in the power output, it could have been even more than that if they had used a larger absorption chiller capacity in order to cool the inlet-air to the ISO conditions (15°C) or more as stated by Boyce [37] who confirmed that the absorption chiller can cool the inlet-air to 10°C.

Mohanty and Paloso [39] showed that using the LiBr/water absorption system to cool a gas turbine's intake-air to the ISO level increases the output power by up to 13%. They also stated that the investment, operation and maintenance costs are lower than for the normal air-cooling system. However, they used a double-effect absorption chiller that required steam with a temperature in the range of 150°C to 205°C, which forced them to use an auxiliary firing in the HRSG unit that powered the absorption chiller. This indicated that the plant's overall fuel consumption increased as a result of the auxiliary firing used in the HRSG unit, which could

have been avoided if they had used a single-effect absorption chiller that could have been powered by steam at a temperature in the range of 90°C to 130°C.

Moreover, Boonnasa, et al. [40] studied the performance improvement of an existing combined cycle power plant located in Bangkok that consisted of two gas turbines (110.76MW each), and one 115.14MW steam turbine in ISO conditions. The plant used an absorption chiller to cool one of the two gas turbine's intake-air to 15°C, in addition to having a thermal energy storage tank that stored the sensible heat of the chilled water to meet the varying daily cooling load. Low pressure steam from a heat recovery steam generator was used to drive the absorption chiller that was needed to meet a maximum load of 7049.58kW with the help of the thermal heat storage. As a result, the power output of the cooled gas turbine increased by 10%, improving the CC power plant's total power output by 6.24%. Economically, the study found that due to the low initial investment cost of retrofitting the absorption chiller the internal rate of return was 40%, and the payback period was just 3.81 years. However, the authors also reported a reduction by 2.85% in the steam turbine power output, which was due to powering the absorption chiller directly from the HRSG unit steam that was powering the steam turbine. This reduction in the steam turbine power output could have been avoided if they had used a boiler that utilized the waste heat energy from the stack after the HRSG unit.

Kakaras, et al. [34] pointed out that the variation in the ambient temperature could lead to a power loss of more than 20% and also an increase in the specific fuel consumption. They demonstrated this effect on a simple cycle gas turbine and on a combined cycle gas turbine using a computer simulation (IPSEpro) for the integration of an evaporative cooler and an absorption chiller to reduce the compressor intake-air temperature. They used an absorption chiller for cooling the combined cycle power plant, which was powered by steam extracted from the steam turbine. They also used an evaporator cooler to cool the compressor inlet-air in the gas turbine cycle, which was powered by a boiler that utilized waste heat energy from the gas turbine exhaust. The results indicated that for the gas turbine cycle both the power output and the efficiency improved by 6.8% and 0.44% respectively. For the combined cycle power plant, after retrofitting the absorption chiller, they reported an increase in the plant's total power output by 15% at an ambient temperature of 40°C, with a reduction in the plant's efficiency by 0.18% at the same ambient temperature. They justified this insignificant reduction in the plant's efficiency

by attributing it to the gas turbine's characteristics and efficiency curve, which as they showed was designed to reach its highest value at an ambient temperature of 20°C and to fall before and after this temperature. However, this can have also been justified by the fact that they powered the absorption chiller by a steam extracted from the steam turbine, which resulted in a reduction in the steam turbine power output and affected the plant's efficiency.

Ameri and Hejazi [36] confirmed an increase in both the plant's power output and its efficiency when they used an absorption chiller that was powered by a boiler which recovered waste heat energy from the gas turbine's exhaust system. They reported an increase in the power output of 11.3%, but did not mention by how much the plant efficiency was improved. Furthermore, Boonnasa and Namprakai [41] also studied the performance improvement of six different combined cycle power plants with a capacity from 100MW to 600MW using an absorption chiller to cool the compressors' inlet-air to 15°C. The study's results showed that for all the plants the gas turbine output power increased by 9.2%, while the steam turbine power output decreased by 3.4%. They justified this by powering the absorption chiller by steam extracted from the steam turbine.

On the other hand, Alhazmy and Najjar [42] studied the performance improvement of gas turbine power using two different air coolers to cool compressor intake-air. Firstly, they used a water spraying system, which improved the power output by 1.95% and the efficiency by 0.18% at an ambient temperature of 50°C. Secondly, they used a cooling coil cooler system, which improved the gas turbine power output by 18%. However, in their results the electric power consumed by the cooler system was not subtracted from the net output power; if the cooling coil electric power is considered the net electric power generated by the plant will reduce by 37.6%, and the plant efficiency drops by 30%. These results clearly showed that neither of the investigated cooling systems were as efficient as the absorption chiller.

The results of these studies and of many others [43–48] led to the same conclusion: using an absorption chiller to cool the intake-air of any gas turbine is economically viable, and this can both enhance the gas turbine's performance and reduce its impact on the environment. However, all the studies mentioned previously only used the first law analysis to evaluate the performance improvement of the power plant after retrofitting the cooling system. In addition, none of them

reported the environmental benefit of such integration. Therefore, this study is set to use both the first and second law analysis (exergy analysis) in the assessment of the power plant after the improvement and to investigate the environmental benefit of it.

2.5 Waste Energy Recovery

Over the last two decades, this topic has been one of the main concerns not only for engineers but also for most economists and environmentalists. Waste energy, and in particular waste heat energy, is the main focus of this study. The following part of this chapter is a brief review of this type of energy and its applications.

2.5.1 Introduction

A number of energy sources are available, but most of them need to be converted into more usable forms, such as electrical energy, mechanical energy or thermal energy. Due to the limitation of the second law of thermodynamics, almost any energy conversion process is inefficient, that is it involves loss of the energy being converted. Therefore, developing new technologies that benefit from that waste energy is essential, not just economically, but also environmentally.

A number of theories have explained the increase in the global average temperature and the rise in the sea levels as a natural cycle or phenomenon, such as the Milankovitch theory, which considers the climate changes to be an expected result of the changes in the Earth's orbit around the Sun [49]. However, the majority prefer the man-made global warming theory, which is based on an old theory introduced by Svante Arrenius in 1896, and states that the continual emission of carbon dioxide caused by combustion of coal would intensify the greenhouse effect, which will cause global warming [50]. Hence, it is believed that the industrial revolution, which started around 1800, has caused the most dramatic increase in the carbon dioxide level [49, 50]. Furthermore, as stated by the Kyoto Protocol, by September 2006 a total of 169 countries had signed the agreement calling for a reduction in the emissions of certain greenhouse gases such as carbon dioxide (CO_2), methane (CH_4), nitrous oxide (N_2O), sulphur hexafluoride (SF_6), perfluorocarbons (PFCs) and hydrofluorocarbons (HFCs) [24]. Chae, et al. [53] suggested that

utilizing industrial waste heat energy would contribute to the reduction in the emission of greenhouse gases.

2.5.2 Waste Heat Energy Utilization in Desalination Plants

Waste energy can be recovered in any thermal system. However, one of the most important and efficient uses of all is in desalination plants, as the demand for potable water is continuously increasing, while the available sources of potable water are decreasing. In addition, the waste heat energy could significantly reduce desalination plant operational costs, which will ensure a low-cost product and enhance desalination plant reliability and availability. In this section, there will be review of a number of studies that have been published concerning the utilization of waste heat energy of different industry applications to operate different types of desalination processes, using different coupling techniques.

One of the oldest papers about utilizing waste thermal energy in desalination plants was written by Chaffiotte in 1967 [54], where he suggested using exhaust gases from a gas turbine to power a desalination plant as a low temperature energy source. Currently, there are more than 350 desalination plants worldwide operated by waste heat energy [1]. Ophir and Lokiec [1] presented a number of examples of some commercial LT-MED desalination plants, such as the one installed in the US Virgin Islands in the 1980s. It is powered by steam in the range of 1.5 bar to 2.5 bar extracted from a cogeneration power plant to power a 15-effect MED desalination plant. The other example was also an MED desalination plant installed in India at the Reliance Refinery, consisting of four MED sub-plants, which has been in operation since 1998 and produces 10% above its capacity, which is about 48,000m^3/day. This proves the reliability and flexibility of MED desalination process. Another example was the Kompania di Awa e Electrisidad (KAE) of Curacao, which was installed in 1988, and uses a combination of extraction steam with an auxiliary turbine to produce 10000m^3/day with electric power consumption below 5kWh/m^3.

Rautenbach, et al. [55] indicated the viability of utilizing waste heat from electric-arc furnaces in the steel industry to drive two MSF desalination plants of 1000m^3/day. The MSF desalination plant was designed with a specific heat consumption of 312kJ/kg, to utilize the water that cools the furnace and the gases of the dust collection processes. Moreover, it is believed that the first

paper describing the usage of such a source in RO desalination plants was published in 1981 by Tidball and Kadaj [56]. They suggested using a turbine to supply electrical energy to the high pressure RO's pumps. The turbine was designed to utilize the energy from the high pressure discharged waste brine from the RO plant itself to provide 30% of the electricity required by the plant's pumps. They succeeded in designing a plant that produces 750m^3/d of potable water consuming approximately 2.5kWh/m^3. Lastly, they concluded that the economic feasibility of such a system is dependent on the temperature and availability of the waste heat source and the seawater salinity.

Kronenberg [57] stated that using diesel engine waste heat to power a MED desalination plant could increase the thermal efficiency of the diesel engine power plant from 40% to 80%. He also mentioned that using such a low temperature energy source diminishes the risk of scale formation and corrosion, which extends the operation period of the plant without the need for chemical cleaning for up to five years. Consequently, this improves its reliability and availability. In addition, he presented a number of designs for LT-MED plants that became commercially available through IDE Technologies Ltd. The first design was a steam turbine-cogeneration and it included three different coupling techniques: firstly, extraction steam coupling where the MED desalination plant is powered by steam at a pressure of 1.5 bar extracted from a steam turbine; secondly, back pressure coupling, which uses the back pressure generated by a combined cycle power plant; and thirdly, a combination of extraction steam with an auxiliary turbine where the extraction steam is used to start the turbine (which produces electricity) and discharges steam at a pressure of 0.3 bar to power an MED plant.

Tay, et al. [58] investigated the use of the low pressure, low temperature waste thermal energy of a steam turbine to power a vacuum desalination system through a superheated vapour heater. They examined the effect of the temperature of the waste heat source on the system's production rate and found that increasing waste heat temperature above 70°C did not enhance the productivity of the system, while raising it from 62°C to 68°C enhanced the production rate by 70%.

All types of waste heat source can be used to power a desalination plant, even municipal solid waste (MSW) as reported by Dajnak and Lockwood [59]. They recommended the use of MSW

waste heat energy to operate an RO desalination plant with electrical consumption from 3 to 9kWh, and estimated that 188m^3 of potable water can be produced by burning one ton of waste. They also introduced the MSW incinerator in London as an example, which was designed to burn over 400,000 tons of refuse each year and generate 32MW of electricity. They concluded that such a plant would be able to produce 75Mm^3/day of potable water, if it was coupled to an RO desalination plant. Likewise, a chemical complex forms a great source of the waste heat energy that can be utilized in desalination plants, as reported by Lovato, et al. [60], where they discussed the idea of recovering low temperature waste heat, at approximately 50–60°C, from the absorption and drying tower coolers of a sulphuric acid plant, which will not require any major modification to the main plant to operate an MED desalination plant that is able to produce 4300m^3/day of potable water with an availability factor of 96%. The study concluded that investment in recovering waste heat from a sulphuric acid plant is economically viable and environmentally efficient.

A recently published paper by Maidment, et al. [61] proposed the use of a new barometric flash-type desalination driven by waste heat from a power plant. They performed a mathematical model and used it to investigate the thermodynamic performance and economic viability of the proposed system using water- and electricity-supply data for the island of Cyprus. They claimed that the proposed simple-to-manufacture system could provide an efficient and useful use of the power plant's waste heat, and stated that the total heat rejection rate from all electricity power plants in Cyprus is able to produce 11.25 million m^3/year of potable water.

Cohen, et al. [62] assessed the possibility of cooling the flue gases of a typical coal-fired power plant prior to entry to the flue gas desulphurization scrubber and utilized the rejected heat in an MED desalination plant. A heat exchanger was assumed to be installed after the flue gas desulphurization scrubber to recover heat from the flue gases and transfer it to water in a closed loop. They introduced two different integration schemes. In the first one the cooling effect was achieved by heating water in the closed loop. The pressurized water entered a closed low pressure flushing chamber with a pressure at 0.35 bar and saturation temperature of 72°C. The saturated steam produced flows to the MED desalination plant as motive steam. In the second scheme, the heated water flowed through the heat exchanger to enter an evaporator steam converter. The heated water flowed inside the evaporator tubes while producing saturated steam

from the sprayed water on the outside of the evaporator. The low pressure steam at 0.75 bar and a saturation temperature of 88°C was expanded down to 0.35 bar in a single-stage back-pressure turbine, where it was used as motive steam for the MED desalination plant. The results indicated that the energy utilization was more efficient in the second design, but the production rate was less in this design.

Furthermore, as a solution for the shortage of potable water in Cyprus, Aypar [63] published a paper in which he suggested building an MED desalination plant to recover the 300 tons of saturated and pressurized waste water coming out of a boiler that utilized the waste heat of two 60MW gas turbine power plants. He concluded that the temperature difference in the MED desalination plant affects its production rate. At a temperature difference of 10°C the MED desalination plant will be capable of producing about $80m^3/h$.

The MSF, MED, TVC-MED and RO have all been employed in the previous reported studies, but a few studies have performed a comparison between two or more processes in order to address the ideal desalination process for such a source of energy. One of those studies is a very important study that was published recently by Henry and Teresa [64], in which they investigated the best desalination process for the utilization of waste heat energy of a 1000t/day sulphuric acid plant. Based on the first law analysis they compared the MSF, MED and TVC desalination processes. They concluded that economically the MED process was the best with a unit product cost of $0.9\$/m^3$, followed by the TVC-MED with $1.74\$/m^3$. The TVC-MED produced $5680m^3$/day, while the MED produced $3400m^3$/day and the MSF $1150m^3$/day. Likewise, Shih [65] published a study that included a comparison between the MSF and MED desalination processes. A sulphuric acid plant located in Morocco was employed as a waste heat source. The sulphuric acid plant's heat exchanger was used to recover the heat from circulating acid and preheat the feed seawater of the desalination process. The purpose of integrating the desalination process was to satisfy the sulphuric acid plant's demand for cooling water. The study concluded that the MED process was able to produce $54720m^3$/day of potable water, which was more than the sulphuric acid requirements, and also found that the process was very sensitive to the operating mode of the sulphuric acid plant as the primary service was to cool the acid stream. On the other hand, it was found that it was impossible to operate the MSF process by such a source if the amount of seawater was limited for the benefit of the waste heat source

plant. Even if this was not the case for such a source the MSF process only produced 18,288m^3/day at a very low thermal efficiency of 1.78 in comparison with 4.48 for the MED. Shih defined the performance ratio as the amount of produced water divided by 2326kJ.

Methnani [66] also performed a comparison between the RO and MED processes operated by two different power plants: a 600MW combined cycle power plant and a 660MW gas-cooled reactor. The MED process in the gas-cooled reactor plant was coupled at the pre-cooler and the inter-cooler, while in the CC power plant the HRSG unit powered it. The RO processes in both plants were powered directly by the power plant. He concluded that the MED processes in both power plants performed similarly, producing 100,000m^3/day at the GOR value of 8 and specific heat consumption of 80.67kWh/m^3, but in the CC power plant the thermal energy utilization was better by 12.7%. The RO processes also performed the same in both plants producing 100,000m^3/day and consuming 285MWh of the power plant's electricity. Economically, he indicated that the potable water cost was lower in the RO than in the MED process. However, this economic result is contrary to the result of a similar study published by Nisan and Benzarti [67], who compared the RO and MED processes and concluded that the MED process was the most profitable.

Kamali and Mohebinia [68] developed a computer simulation tool to investigate the difference between the MED and TVC-MED processes. They concluded that the GOR in TVC-MED improved to 8.8 in comparison with to 8 in the MED process; similarly, the potable water production rate increased to 18000m^3/day from 1536 in the MED process. They also reported that the performance of the TVC-MED process was dependant on the condenser parameters. Hence, the GOR can be improved by increasing the condenser's heat transfer area.

All the studies mentioned so far and many others [69-75] confirmed the economic and thermodynamic benefits of using waste heat energy to operate a desalination process, but none reported the environmental benefits of such an integration. Therefore, it is one of this study's aims to investigate the impact of such an application environmentally before and after improvements, not just by evaluating the thermal utilization of the fuel, but also by calculating the amount of carbon dioxide that the plant emits in kgCO_2/kW. Moreover, all the reported studies and many others [69-75] only used the energy analysis to evaluate the plant performance

thermodynamically and none employed the exergy analysis, which provides more accurate and precise results. Hence, this study aims to fill this gap and evaluate plant performance before and after improvement by using both the energy and exergy analyses.

In conclusion, a considerable number of studies have been published investigating the performance and economic feasibility of utilizing waste heat from different types of sources, including gas and steam turbine power plants, combined cycle power plants, chemical complexes, refineries, municipal solid waste, the steel industry, sulphuric acid plants, etc. However, according to Nordell [76], most of the increase in the carbon dioxide emissions is caused by the burning of fossil fuels, which are used to generate 90% of the world's electrical energy [77, 78]. This makes power plants an ideal source of waste heat, if the aim is to reduce the CO_2 emission rate in order to control global warming. Likewise, a number of desalination processes have been integrated for such an application including MSF, RO, MED, TVC-MED, etc, and a few studies have performed comparisons between two or more of them. The desalination processes that were reported to be the most efficient and economical in the literature were the TVC-MED process followed by the MED process. Therefore, these two desalination processes have been selected for this study to determine the best process based on its impact on the environment and on both the energy and exergy analyses.

The TVC-MED process is considered as an improvement on the traditional MED process; the MED process is chosen, based on number of factors that were discussed throughout the previously mentioned studies and summarized by Kronenberg and Lokiec [75] as follows:

- A long plant life that exceeds 25 years due to low corrosion rates and the use of a mild anti-scalant. This is mainly because of the low operating temperature 70°C.
- High thermal efficiency due to the use of a large heat transfer area.
- High-purity production that satisfies the potable water standard.
- A low product cost as a result of consuming low-grade heat energy and less operating and maintenance costs.
- High reliability and availability (typically 95%) and minimal maintenance, due to the low level of corrosion and scaling rates.

- Flexibility and short start-up time and heating-up time.

Lastly, different coupling techniques were reported in this section including steam extraction, back pressure, through the HRSG unit, etc. The most common technique was steam extraction. However, most of these techniques somehow affect the base plant or vice versa. Hence, the steam extraction coupling technique is adopted in this study in addition to a new proposed coupling technique that aims to provide more flexibility for both plants.

2.6 Exergy Analysis

This study involves exergy analysis for evaluating the performance of all the plants employed in this study before and after the integration. Therefore, this topic is set to define exergy, introduce its fundamentals and review a number of studies that use the exergy analysis to investigate the performance of similar plants to that employed in this study.

2.6.1 Introduction

While the first law of thermodynamics states that energy cannot be destroyed, the second law states that the entropy of an isolated system that is not in equilibrium will tend to increase over time. The increase in entropy causes a portion of the energy to be degraded. Hence, exergy defined as the maximum theoretical useful work obtainable as the system interacts to equilibrium. The use of exergetic analysis can clarify precisely the inefficiencies among the plant's components and defines the true magnitude, cause and location of any degradation of energy. Neglecting the nuclear, electrical, surface tension, and magnetic effects, the total exergy of a system consists of four components: kinetic exergy E^{KN}, potential exergy E^{PT}, chemical exergy E^{CH} and physical exergy E^{PH} [79,80].

$$E = E^{KN} + E^{PT} + E^{CH} + E^{PH} \tag{2.3}$$

If equation (2.3) is expressed on the basis of mass it will denote the total specific exergy (e) and can be written as follows:

$$e = e^{KN} + e^{PT} + e^{CH} + e^{PH} \tag{2.4}$$

Defining the kinetic exergy as the exergy of a system due to its motion and the potential exergy as the stored exergy within the system as a result of its position they can be written as follows:

$$e^{KN} = \frac{1}{2}V^2 \tag{2.5}$$

$$e^{PT} = gz \tag{2.6}$$

In this study both the kinetic and potential exergies are neglected as there is no variation in the system speed or elevation [79-81]. The chemical exergy (E^{CH}) is the maximum theoretical work obtainable as it passes to a chemical equilibrium with the reference environment at a constant

temperature and pressure [82]. Modelling the fuel stream as an ideal gas its chemical exergy is calculated as follows [83]:

$$E_{Fuel} = \Theta \times \eta_{COM} \times \dot{m}_{Fuel} \times LHV \tag{2.7}$$

where (Θ) denote the molar Gibbs function of formation. For all the other streams the chemical specific exergy can be calculated as follows:

$$e^{CH} = \bar{R}T_o ln x_i^e \tag{2.8}$$

where $\bar{R}$ and x_i^e denote the universal gas constant and the mole fraction of gas (i) in the environmental gas phase, and T_o represent the environmental temperature [79]. The chemical exergy value of most streams tends to be small and they cancel each other out during the analysis as they do not change across most of the system components. Thus it can be ignored, causing a negligible error in subsequent calculations [79-81] except that for the fuel chemical exergy calculated as shown in equation 2.7.

The physical exergy (E^{PH}) is the maximum theoretical work achievable when the system passes from its initial state at pressure P and temperature T to the reference condition at pressure P_o and temperature T_o. Treating the working fluid as an ideal gas the physical exergy of a closed system can be expressed as follows [84]:

$$e^{PH} = (h - h_o) - T_O \times (s - s_o) \tag{2.9}$$

where h and s denote the enthalpy and entropy respectively and the subscript (o) denotes the reference condition. Assuming that all components are operating in a steady state then the exergy balance can be expressed as follows [85, 86]:

$$\sum \dot{m}e_{in} = \sum \dot{m}e_{out} + \sum_j \left(1 - \frac{T_o}{T_j}\right) \dot{Q} + \dot{W}_{net} + \dot{E}_D \tag{2.10}$$

where $\dot{E}_D$ is the exergy destruction rate, which is dependant of the boundary selection. In the case of T_o being equal to the temperature of surface conditions (T_j) the exergy destruction will be only due to the friction and the irreversibility of the heat transfer within the component. The second term on the right-hand side of the exergy balance represent the exergy loss associated with heat transfer between the surface of the boundary chosen and the reference conditions. Moreover, based on the system boundary selection this term vanishes if $T_o = T_j$. Assuming that

the system is well insulated, this term will be ignored in this study as the boundary chosen satisfies $T_o = T_j$ [77, 81, 83].

The exergetic efficiency (η_{II}) is used as a performance parameter to evaluate the thermodynamic performance of each sub-plant as well as the entire plant, and is defined as the ratio between the exergy of the product and the exergy of the input fuel [79]:

$$\eta_{II} = \frac{E_p}{E_{Fuel}} \tag{2.11}$$

In addition, two exergy destruction ratios of a component (i) are used to compare the component (i) exergy destruction to the plant total exergy destruction rate (Ψ_D), and to the rate of fuel supplied to the system (Ψ_{Fuel}) and can be expressed as follows [79]:

$$\Psi_D = \frac{E_{D,i}}{E_{D,tot}} \quad and \quad \Psi_{Fuel} = \frac{E_{D,i}}{E_{Fuel}} \tag{2.12}$$

Using the exergy balance equation (2.10) the exergy destruction for each component can be calculated and then used to calculate other exergy parameters. After defining exergy and introducing its fundamentals, a number of exergy analysis studies will now be introduced in the next section.

2.6.2 Power Plant

A number of studies have been published recently using exergy analysis to evaluate the performance of power plants. For example, a study by Kanoglu, et al. [87] used exergy analysis to evaluate the performance of a 10MW steam power plant. They indicated that exergy analysis is mainly used to evaluate the plant components separately and to define their exergy destruction, which can be used to improve the performance of the plant by reducing the exergy destruction. The results showed that the exergetic efficiency (77%) is much higher than the energy efficiency (34%), which is justified by the exergetic efficiency definition as the ratio of the work output to the fuel exergy (potential to do work), while in the energy efficiency it is the ratio to the total heat input of the fuel. The total exergy destruction of the investigated power plant was found to be 75% of the input exergy, being mainly caused by the steam turbine's condenser, which accounts for 47% of the plant's total exergy destruction. Unfortunately, they did not provide any

explanation for the high exergy destruction rate in the condenser, which was not the main source of the exergy destruction in a different study for a similar plant published by Aljundi [88], who indicated that the main source of the plant's irreversibility was the boiler not the condenser. Aljundi studied a 56MW steam turbine and found that the boiler accounted for 76.7% of the plant's total exergy destruction followed by the turbine, which caused 12.9% of the plant's exergy destruction. He also suggested that the boiler's exergy destruction could have been reduced by reheating the combustion air and reducing the air-fuel ratio.

Ameri, et al. [89] performed an exergy analysis for a 420MW combined cycle power plant; the plant had two gas turbines, two compressors, two HRSG units, two deaerators, one steam turbine and one condenser. In the gas turbines, the main source of the exergy destruction was caused by the combustion chamber due to the chemical reaction and the large temperature difference between the burner and the working fluid as they indicated. The results also showed that the gas turbine's cycle had the highest exergetic efficiency in comparison with the other components of the plant. The second source of the exergy destruction in the plant was found to be the HRSG units. The exergetic efficiency of the plant was 44% and 45.5% if the HRSG units were unfired. They concluded from the results that the HRSG units needed to be optimized in order to improve the plant's overall exergetic efficiency.

Shi and Che [83] confirmed most of the previous study's results in their study, which investigated a 320MW combined cycle power plant consisting of a gas turbine, two-pressure-level HRSG units, a steam turbine, an deaerator and a condenser. They also found that the combustion chamber was the main cause of the plant's exergy destruction, followed by the gas turbine and then the HRSG unit. The plant's overall exergetic efficiency was 52%.

2.6.3 Desalination Plant

A few studies have used exergy analysis to investigate the performance of desalination plants in comparison with the studies published on energy analysis. For example, a study by Choi, et al. [90] employed exergy analysis to evaluate the performance of a TVC-MED desalination plant. They tested four TVC-MED plants with different numbers of effects (four, five, eight and nine) and production capacity (from 4500m^3/day to 20000m^3/day). They indicated that the exergy destruction in the desalination plant was due to the heat transfer process in the steam ejector,

evaporators and condenser or due to a pressure drop in the condenser, pumps, valves and evaporator during the flashing process or because of the evaporator's demister. The results showed that the main causes of the plant exergy destruction were the steam ejector and the evaporator, which accounted for more than 70% of the plant's total exergy destruction. The highest exergy destruction was found in the plant with five effects, which they did not provide a justification for, but it could have been due to the fact that for each plant there are an optimum number of effects defined by motive steam and seawater properties. Unfortunately, they did not report a value for the plant's exergetic efficacy. However, their results were not in agreement with the results of a similar study published by Hamed, et al. [91], where they found that the steam ejector was not the main cause of the plant's exergy destruction. They reported the first effect of the evaporators as the main cause of the plant's exergy destruction. They compared the TVC-MED with the mechanical vapour compression (MVC) and the MED process and concluded that the most effective process was the TVC-MED with total exergy destruction rate of 135kW in comparison with 142kW and 117kW for the MVC and MED respectively.

Sayyaadi and Saffari [85] performed an exergy analysis to investigate the performance of a seven-effect TVC-MED desalination plant. They reported an exergetic efficiency of 10.7%, with a total exergy destruction rate of 1.87MW, which was mainly caused by the steam ejector, while the evaporator only caused 524kW exergy destruction. Mabrouk, et al. [92], confirmed this result; they compared the TVC-MED and the MVC-MED processes in addition to the RO and MSF processes. Both MED plants had two effects and a capacity of 5000 m^3/day. The results showed that the steam ejector in the TVC-MED plant was the main cause of the plant's exergy destruction of 1.03MW followed by the condenser and then the evaporators. They indicated that the TVC-MED process had the lowest specific power consumption and exergy destruction.

2.6.4 Absorption Chiller

A few exergy analysis studies have been published for the absorption chiller in comparison with energy analysis studies. For example, Kaushik and Arora [93] developed a computer programme to study the performance of a 2357kW single-effect water-cooled water/LiBr absorption chiller with a COP value of 0.76. They found that the absorber was causing the highest exergy destruction in the cycle (191.72kW), followed by the condenser (109.76kW) and then the

evaporator (86.28kW) and the generator (55.5kW). They reported an exergetic efficiency of 11.75%. However, these results are not in agreement with Misra, et al.'s [94] results, which indicated that the evaporator was the main cause of the plant's exergy destruction, followed by the generator. They also studied a single-effect water/LiBr absorption chiller with a COP value of 0.71. Moreover, they reported two water streams with negative exergies — those entering and exiting the evaporator towards the absorber — which they justified by the fact that these two streams' pressure and temperatures were below reference conditions. The results also showed that the overall exergy destruction was 21.125kW, which led to an exergetic efficiency of 11.13%. Different results were reported by Sencan, et al. [95]; they also investigated a single-effect water/LiBr absorption chiller with a COP value of 0.78. They indicated that the generator was the main cause of the cycle exergy destruction, followed by the heat exchanger and then the condenser and the evaporator. Moreover, Talbi and Agnew [96] developed a computer programme to investigate a similar absorption chiller. They found the generator to be the main cause of the cycle exergy destruction, followed by the absorber and then the evaporator and the heat exchanger. They stated that exergy destruction in the plant was due to the heat transfer process, and also reported an exergetic efficiency of 26.23%.

In conclusion, the exergy analysis results greatly vary from one study to another even for similar plants; this is due to the fact that the reference condition, system boundary, exergy destruction and efficiency equation definitions are all defined by the researcher. Therefore, the exergy analysis is mainly a tool to investigate system components in order to improve system performance [79].

2.7 Closing Remarks

This chapter introduced the different topics covered in this study including desalination plants, absorption chillers and waste energy recovery. A brief review of the water resources in Saudi Arabia was also introduced. Finally, the exergy analysis fundamentals were presented with a number of studies that used it in power plants, desalination plants and absorption chillers.

In conclusion, a number of guidelines have been drawn from this chapter to be used in this study for a number of reasons mentioned in detail earlier, and these can be summarized as follows.

- A combined cycle power plant will be used as a waste heat energy source.
- A single-effect water/LiBr absorption chiller will be adopted as a cooling system.
- TVC-MED and MED processes will be compared to choose the better one
- The steam extraction coupling technique will be used in this study.
- Exergy analysis will be performed.
- The system's impact on the environment will be evaluated in detail.

Chapter 3

Methodology

3.1 Introduction

This chapter introduces the tools used in modelling, simulating and examining the proposed thermal model. This includes the simulation software and with all its modules and library models employed in this study. The chapter then continues with a description of the first law analysis including first law efficiency, effectiveness-NTU methods, pinch analysis and other first law performance parameters that were used to evaluate the system performance. The chapter then presents a second law analysis or exergy analysis including the methods of calculating the entropy and enthalpy of some streams. The weather data for Yanbu city, the location intended for this study, are also presented in this chapter as well as the real data collected for the modelling of each sub-plant employed in this study.

3.2 Modelling and Simulation Tools

Computational modelling and simulation has become a keystone in all studies, training and certification applications. It saves time and money, offers flexibility and enables repeatability and control. Thus, for industrial scale studies, this is an ideal method for testing models and examining their performance in different conditions [35]. The software used in this study was IPSEpro; it is a set of software modules that create, analyse and utilize models of a new or existing process plant.

The core of IPSEpro is an extremely flexible modelling system for calculating heat balances and simulating processes. It has the ability to represent any problem as a network of collected and connected components; this is the first level in which the model is represented mathematically and graphically using the model development kit (MDK). The second level performs the calculations and generates results in the process simulation environment (PSE). IPSEpro goes far beyond calculating heat balances, as it can be made to predict design and off-design performance, verify and validate measurements during acceptance tests and plan modifications and re-powering of existing plants.

The IPSEpro design suite consists of a number of modules; however, only four of them were used in this study. Although, this software has gained credit within the industrial and research companies such as Rolls-Royce and NaREC, it was subjected to validation throughout this study

where it was proven to be accurate. The real data collected for this study was modelled accurately using this software and provided the same output as the real plant. Moreover, the entropy and enthalpy of certain streams were validated with manually calculated ones. In the following pages each of the used modules and the component libraries will be briefly introduced [97].

3.2.1 Model Development Kit (MDK)

MDK is IPSEpro's Model Development Kit, designed to translate components into a form that can be used by the Process Simulation Environment module (PSE). It consists of two functional units. The first is MDK's model editor, which defines the component graphically by designing an icon that represents the model, and mathematically by describing the component behaviour using the model description language (MDL). The second functional unit is MDK's model compiler, which translates the model descriptions into a binary format that is solved in the PSE [98]. MDK was used in this work to combine three existing libraries: desalination, refrigeration and advance power plant libraries. This newly created library will then simplify the modelling and simulation of the proposed plants that consist of components from all three libraries.

3.2.2 Process Simulation Environment (PSE)

PSE is the core of IPSEpro. It allows the creation of a process model based on components from a model library. This is then simulated via optimized mathematical methods that assure fast and accurate calculations. Any process that consists of one or more objects or process models can be easily modelled in an easy-to-use flow sheet editor by selecting the components as icons from a model library shown as a sidebar in the PSE screenshot (Figure 3–1), then connecting them and entering all the data related to the process model directly in the flow sheet. Mathematically, PSE first analyses the system and then works out the numerical solution. In the analysis stage, PSE determines the optimum solution method for the equation system. PSE combines and solves several equations simultaneously. During the analysis phase, PSE also chooses the optimum numerical method. In the numerical solution stage PSE solves the equations in the order pre-established by the analysis, and uses the numerical methods that have also been chosen in the analysis stage [97].

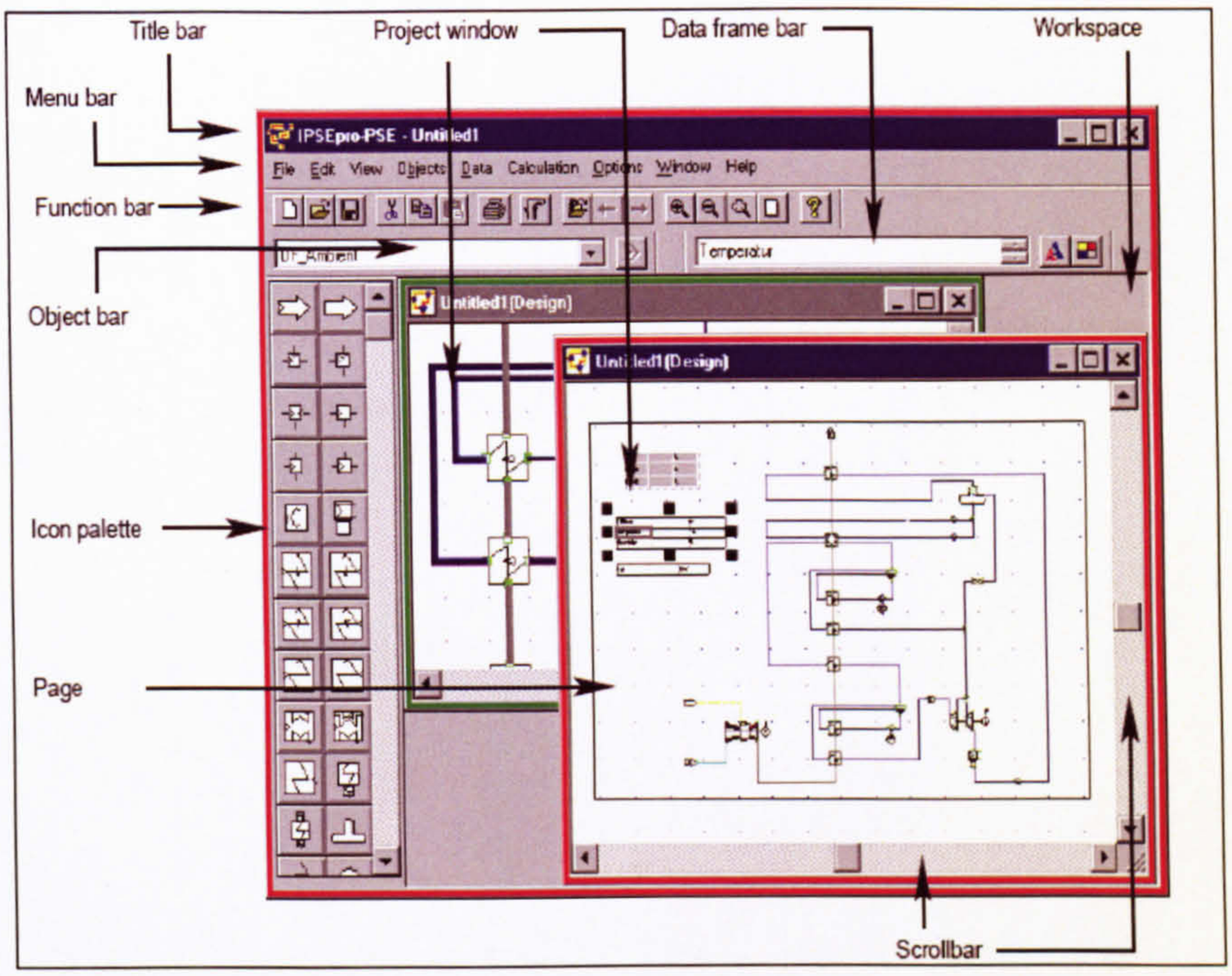

Figure 3-1 IPSEpro screenshot, from [97]

3.2.3 Process Simulation MS Excel (PSExcel)

PSE-MS Excel Integration is a module that allows data exchange between PSE and MS Excel. It provides a special MS Excel template (PSExcel.xlt) and an MS Excel add-in (PSExcel.xla), which supports this data exchange. It incorporates data from PSE projects into an Excel worksheet, which can illustrate a report about the project. PSE-MS Excel can also be used to generate a series of different calculations in a PSE project, by varying the values of some items of the component models. These item variations are then input from an Excel worksheet.

This module can easily invoke a variation of a PSE-project and allow displaying the variation results in the form of diagrams or curves in MS Excel. The term "variation" of a PSE project stands for the fact that the process calculation can be performed (n) times, adopting different input data each time. Depending on the number of variation parameters the variation can be two- or three-dimensional. Once a variation has been created, it can be updated whenever necessary. Furthermore, the PSE-MS Excel integration module can be used to create a diagram to show the values of a certain item belonging to different library models of a process. This can generate a lot of information about the library models used in a project, and especially about their relationship within a process [99].

3.2.4 Libraries

In addition to the ability to create a new library through MDK, SimTech provides a number of libraries that cover a wide range of process plants. Three of them have been employed in this study.

- **Advanced power plant library**

The library contains 49 units that represent any power plant component, for example turbine, boiler, condenser, heat exchanger, valve, motor, mixer, etc. Nonetheless, a new unit can be built and added to the library using the MDK. Specialized off-design models are available for each unit of the advanced power plant library. The library also includes a database of physical properties for water and a wide range of chemical components that might be used in the combustion system [100].

- **Desalination process library**

This library contains all the necessary component models for designing all the following desalination processes:

- MSF, multi-stage flash
- MED, multi-effect distillation
- MVC, mechanical vapour compression
- TVC, thermal vapour compression
- RO, reverse osmosis.

The library includes equipment, such as heat exchangers, pumps, valves, etc, as well as some core components of standard desalination processes, for example individual stages of multi-stage processes (MSF), single-effect of multi-effect distillation cell (MED) and reverse osmosis membrane module (RO). The library can also be edited or upgraded using MDK. Moreover, the library includes mathematical functions that describe the physical properties of pure water and aqueous salt solutions, in addition to a database of physical properties for water and a wide range of gaseous chemical components.

The library defines seawater as an aqueous salt solution of various constituents, with sodium chloride, magnesium chloride and sulphate, calcium sulphate and potassium sulphate. As a generally accepted simplification these constituents are represented by one key parameter, which is the salinity or salt content [101].

- **Refrigeration process library**

The refrigeration process library allows modelling of a number of advanced thermal processes using more than 50 refrigerants. It was modelled in agreement with data that were obtained from the US National Institute of Standard and Technology for the development of a reference data programme. It contains all the necessary component models for designing and analysing both absorption refrigeration systems and the vapour compression systems. Some of these component models (for example, generator, absorber, evaporator and reflux cooler) were designed for both design and off-design analyses. Most of the common components are repeated for the NH_3/H_2O mixtures, $LiBr/H_2O$ solutions and for other refrigerants. In addition to the physical property database that contains the properties of water/steam and a series of gases, the library also provides a physical property database that includes a wide range of refrigerants and refrigerant mixtures for both compression and absorption processes [102].

3.3 Energy Analysis

This analysis includes a number of performance parameters that used throughout this study to evaluate the performance of the base and proposed plants. For the power plant, a generic model was used to simulate the gas turbine that includes its compressor and combustion chambers. Based on the first law of thermodynamics the net amount of energy received through heat interaction is equal to the net energy transferred out in work interaction [79].

$$\sum \dot{Q}_{cycle} = \sum \dot{W}_{cycle} \tag{3.1}$$

From this the thermal efficiency of the gas turbine cycle defined as the ratio of work generated to the total energy input into the cycle [79] as follows:

$$\eta_{GT} = \frac{\dot{W}_{net}}{\dot{Q}_{in}} = \frac{\dot{W}_{GT} - \sum \dot{W}_{pump}}{\dot{m}_{Fuel} \times LHV} \tag{3.2}$$

The combined cycle power plant's efficiency was then defined as the ratio of the net total electric power to the energy input through the fuel [79]:

$$\eta_{cc} = \frac{\dot{W}_{net\ ,output}}{\dot{Q}_{in}} = \frac{\dot{W}_{GT} + \dot{W}_{ST} - \sum \dot{W}_{pump}}{\dot{m}_{Fuel} \times LHV} \tag{3.3}$$

The energy utilization factor (EUF) was also used in this study to evaluate the performance of the cogeneration plant and was defined as the ratio of the total output work plus the useful heat energy to the fuel energy supplied [103]:

$$EUF = \frac{\dot{W}_{net\ ,output} + \dot{Q}_{net\ ,output}}{\dot{Q}_{in}} = \frac{\dot{W}_{output} - \sum \dot{W}_{Pump} + \dot{Q}_{output} - \dot{Q}_{cw}}{\dot{m}_{Fuel} \times LHV} \tag{3.4}$$

Anther performance parameter used in this study was the carbon dioxide (CO_2) emission rate and was defined as the amount of carbon dioxide emitted for the production of each kWh of electric power and useful heat energy.

$$CO_2\ Emission\ Rate = \frac{\dot{m}_{Fuel} \times \alpha}{\sum \dot{W}_{useful\ ,net} + \sum \dot{Q}_{useful\ ,net}} \tag{3.5}$$

where α is the amount (kg) of CO_2 produced for each ton of the consumed fuel. The natural gas used in this study produces 3142 kg of CO_2 per ton [104]. For the heat recovery, steam generator (HRSG) the pinch analysis was used to ensure the best heat recovery and an acceptable pinch

point as well as approach point Δt. The amount of heat transfer in the economizer, evaporator and super heater were calculated as follows [83]:

$$\dot{Q}_{\text{Economizer}} = \dot{m}_{\text{h,w}} \times \left(h_{hw,out,Ecn} - h_{hw,in,Ecn}\right) = \dot{m}_{gas} \times \left(h_{gas,in,Ecn} - h_{gas,out,Ecn}\right) \quad (3.6)$$

$$\dot{Q}_{\text{Evaporator}} = \dot{m}_{\text{s}} \times \left(h_{sat-s,out,Eva} - h_{sat-s,in,Eva}\right) = \dot{m}_{gas} \times \left(h_{gas,in,Eva} - h_{gas,out,Eva}\right) \quad (3.1)$$

$$\dot{Q}_{Super\ Heater} = \dot{m}_{s} \times \left(h_{s,out,SH} - h_{sat-s,in,SH}\right) = \dot{m}_{gas} \times \left(h_{gas,in,SH} - h_{gas,out,SH}\right) \quad (3.2)$$

The gas-steam temperature profile of the HRSG then plotted to pinpoint the pinch point and approach point Δt [118, 119].

$$\Delta T_{pp} = T_{gas,out,Eva} - T_{sat-s,out,Eva} \quad (3.3)$$

$$\Delta T_{app} = T_{sat-s,in,Eva} - T_{hw,out,Ecn} \quad (3.4)$$

The effectiveness-NTU method was also used in this study to ensure realistic and commercially available heat exchangers. Assuming steady state and steady flow, no heat generation in the heat exchanger, negligible kinetic and potential energy difference, adiabatic processes and constant specific heat the heat exchanger effectiveness. The effectiveness was defined as the ratio of the actual heat transfer to the maximum possible heat transfer [118, 119].

$$\varepsilon = \frac{\Delta T_{\text{actual}}}{T_{h,in} - T_{c,in}} \quad (3.5)$$

where ΔT_{actual} is for the fluid experiencing the larger temperature difference in the heat exchanger. The NTU for a single-phase heat exchanger was calculated by dividing the overall thermal conductance of the heat exchanger (UA) by the minimum heat capacity rate (C_{min}) [119].

$$NTU = \frac{UA}{C_{min}} \quad (3.6)$$

The UA was read directly from the simulation software while the C_{min} was determined after calculating the heat capacity rate for both hot and cold streams in the heat exchanger as follows:

$$C = \dot{m} \times C_p \quad (3.7)$$

In the case of an evaporator or condenser where there was phase change in one of the heat exchanger streams, this phase change stream had the C_{max}.

For evaluating the performance of the desalination plant, the gain output ratio (GOR) parameter was used and defined as the ratio of the potable water mass flow rate (kg/s) to the driving steam mass flow rate [4].

$$GOR = \frac{\dot{m}_{potable\ water}}{\dot{m}_{driving\ steam}} \tag{3.8}$$

The amount of heat energy required to produce one kg of potable water is known as the specific heat consumption and was calculated as the amount of heat transferred in the first effect divided by the mass flow rate of the produced potable water [65, 68]:

$$ShC = \frac{\dot{Q}_{1^{st}\,effect}}{\dot{m}_{Potable\ \ water}} \tag{3.9}$$

To measure the rejected brine salinity in regard to intake seawater salinity the concentration factor parameter was used and defined as follows [65,68]:

$$CF = \frac{w_{Relected\ \ brine}}{w_{In\,take\ \ seawater}} \tag{3.10}$$

where (w) denotes the mass fraction of salt in the seawater.

For the absorption chiller the coefficient of performance (COP) was used to express its efficiency excluding the pump's electrical energy, and was defined as the ratio of the cooling capacity produced from the evaporator to the heat energy provided to the generator [25]:

$$COP = \frac{\dot{Q}_{Evaporator}}{\dot{Q}_{Generator}} \tag{3.11}$$

3.4 Exergy Analysis

In addition to the introduction to exergy analysis that was presented in the previous chapter, the exergy destruction equation for each component in each plant will be introduced in the following chapter. In this chapter, the method used to calculate the enthalpy and entropy for each stream, in addition to some assumptions, is introduced. Firstly, the nuclear, electrical, surface tension, and magnetic effects were ignored [79, 80]. Moreover, both the kinetic and potential exergy were neglected as there is no variation in the system speed or elevation [79–81]. The chemical exergy (E^{CH}) was calculated for the fuel stream as an ideal gas as follows [83]:

$$E_{Fuel} = \Theta \times \eta_{COM} \times \dot{m}_{Fuel} \times LHV \tag{3.12}$$

where (Θ) denotes the molar Gibbs function of formation and for natural gas is equal to 1.04 according to Shi and Che [83]. For all other streams, the chemical exergies tended to be small and canceled each other during the analysis, as they do not change across most of the system components. Thus it was neglected causing negligible error in subsequent calculations [79–81]. The physical exergy (E^{PH}) was calculated as follows [84]:

$$E^{PH} = (h - h_o) - T_o \times (s - s_o) \tag{3.13}$$

where h and s denote the enthalpy and entropy respectively and the subscript (o) denotes the reference condition. The reference condition for all streams was taken to be at a temperature of 15°C and at a pressure of 1.013 bar. The enthalpy and entropy of air, water, fuel composition and exhaust gas composition streams were read directly from the simulation software IPSEpro after being validated with those values available in tables. The entropy of LiBr-H_2O mixture streams and both the entropy and enthalpy for seawater streams were calculated manually as the software does not provide a reading for them. For the LiBr-H_2O mixture stream entropy the Kaita's method [105] was adopted.

For the seawater streams the entropy and enthalpy were calculated manually [106–109]. The seawater is a mixture of pure water and salt; the enthalpy and entropy of pure water is taken from the simulation software IPSEpro, while those of salt were calculated from the following equations:

$$h_{salt} = h_{salt,o} + C_{p.salt}(T - T_o) \tag{3.14}$$

$$s_{salt} = s_{salt,o} + C_{p,salt} \ln\left(\frac{T}{T_o}\right) \tag{3.15}$$

where C_p is the salt specific heat that is equal to 0.8368 kJ/kg.K. h_o and s_o are respectively the enthalpy and entropy of salt at the reference condition. Typically, seawater with a concentration less than 5% can be considered as a dilute solution that behaves closely to an ideal solution with negligible error [106–109]. Thus, its enthalpy is the sum of the enthalpy of its individual components (salt and pure water), and was calculated as follows:

$$h_{seawater} = w_{salt} \times h_{salt} + w_{water} \times h_{water} \tag{3.16}$$

where w_{salt} and w_{water} are the mass fractions of salt and water respectively. This does not apply to the calculations of the seawater solution entropy, as the entropy of each individual component in the solution tends to be greater than its entropy when it exists alone at the mixture temperature and pressure. Therefore, the entropies of both salt and water were calculated separately at the solution temperature and pressure as follows [106–109]:

$$s = s_{i,pure}(T_{sol}, P_{sol}) - \overline{R} \ln x_i \tag{3-17}$$

where $\bar{R}$ is the universal gas constant in kJ/kmol.K and $s_{i,pure}$ is the entropy of the (i) component at the solution temperature and pressure and they were calculated by equation 3.30 using the reference conditions mentioned previously. The mole fraction (x_i) of the (i) component in the solution was calculated as follows [106–109]:

$$x_w = w_w \frac{M_{sol}}{M_w} \text{ and } x_{salt} = 1 - x_w \tag{3.18}$$

where M_{sol} is the molar mass of the solution, which was calculated as follows [106–109]:

$$M_{sol} = \frac{1}{\frac{w_w}{M_w} + \frac{w_{salt}}{M_{salt}}} \tag{3.19}$$

M_{salt}, and M_w are the molar masses of salt and water respectively and they were taken as 58.5kg/kmol for salt, and 18 kg/kmol for water [106–109]. The entropy of the seawater solution was then calculated as follows:

$$s = w_{salt} \times s_{salt,pure}(T_{sol}, P_{sol}) + w_w \times s_{w,pure}(T_{sol}, P_{sol}) - \overline{R} \times (x_{salt} \ln s_{salt} + x_w \ln s_w) \tag{3.20}$$

Knowing the entropy and enthalpy for each stream in the plant the exergy and specific exergy were calculated for each stream. Furthermore, by applying the general exergy balance over each component of the plant the exergy destruction and efficiency were calculated. Assuming that all components are operating at a steady state, the exergy balance was written as in equation 2.10 [85, 86].

3.5 **Weather Data**

This study is applicable in any area worldwide; however, there will be some challenges in the warmer areas due to the effect of ambient conditions on the performance of the power plant as discussed in the Literature Review. Therefore, a hot city in Saudi Arabia has been chosen as a location for this study. This city is an industrial city called Yanbu and is located in Saudi Arabia at 24°05′N, 38°00′E. It is a major Red Sea port in the Medina region of western Saudi Arabia, as shown in Figure 3–2.

Figure 3-2 Location of Yanbu city

Yanbu is an important petroleum-shipping terminal, and is home to 34 basic and secondary industries and 224 light industries, including three oil refineries, a plastics facility and several other petrochemical plants. It is the country's second biggest port after Jeddah. Yanbu is the location for a cogeneration power plant and MSF desalination plant built in 1981 and updated in 1999. In total they generate 285MW of electric power and 215,000m^3/day of potable water. The 107,000m^3/day RO desalination plant was built in 1999 and is the largest RO plant in the world [110]. These plants supply Medina, Yanbu and other adjacent cities. The weather data was obtained from the Presidency of Meteorology and Environment, Saudi Arabia [111], which is a branch of the Ministry of Defence and Aviation.

The temperature data obtained is in the form of mean and extreme readings for each month over a 23-year period from 1985 to 2008. The mean values include maximum, minimum and mean readings. The extreme readings include the maximum and the minimum recorded values during this period of time and are provided with the data about when the readings were recorded. All the temperature values are on a monthly basis as shown in Appendix A as obtained. Figure 3–3 simplifies the data in a chart form.

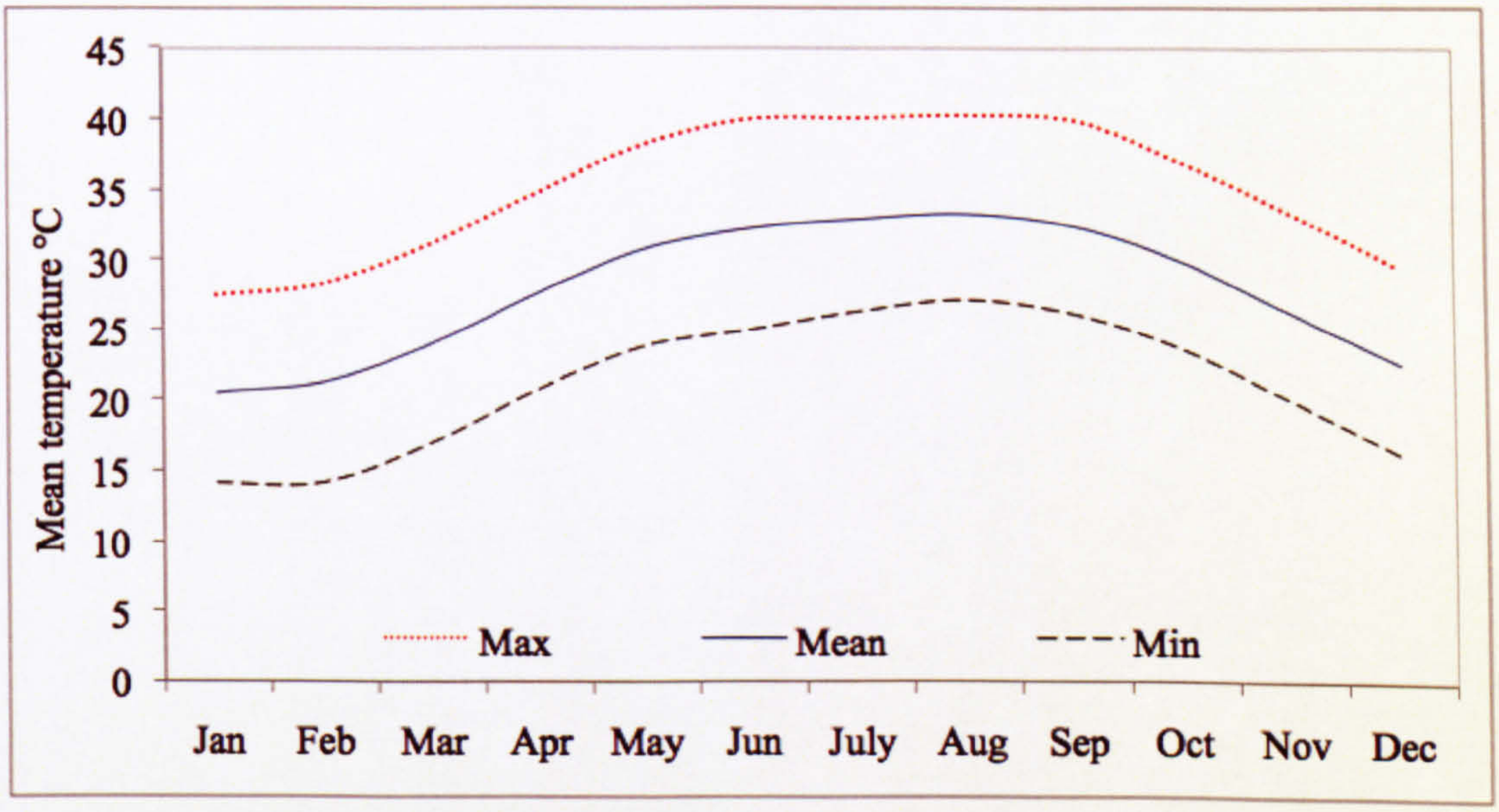

Figure 3-3 Mean, maximum, minimum and temperature of Yanbu city [111]

As shown in Figure 3–3, the mean temperature in Yanbu city during the year varies from a minimum value of 14.1°C to a maximum value of 40.3°C. However, the maximum-recorded temperature over the period from 1985 to 2008 was 49.5°C, while the minimum during the same period was 4.7°C, recorded just once on 3 January 2000.

Relative humidity data was also obtained from the same source over the same period of time. The relative humidity values were provided in the form of maximum, minimum and mean readings. The data as obtained is presented in Appendix A in tabulated form, while Figure 3–4 represents it in a chart form. As can be seen in Figure 3–4, the relative humidity varies from a minimum value of 4.7% to a maximum value of 100% over the period of time from 1985 to 2008. The mean humidity value is in the range of 50% to 60%.

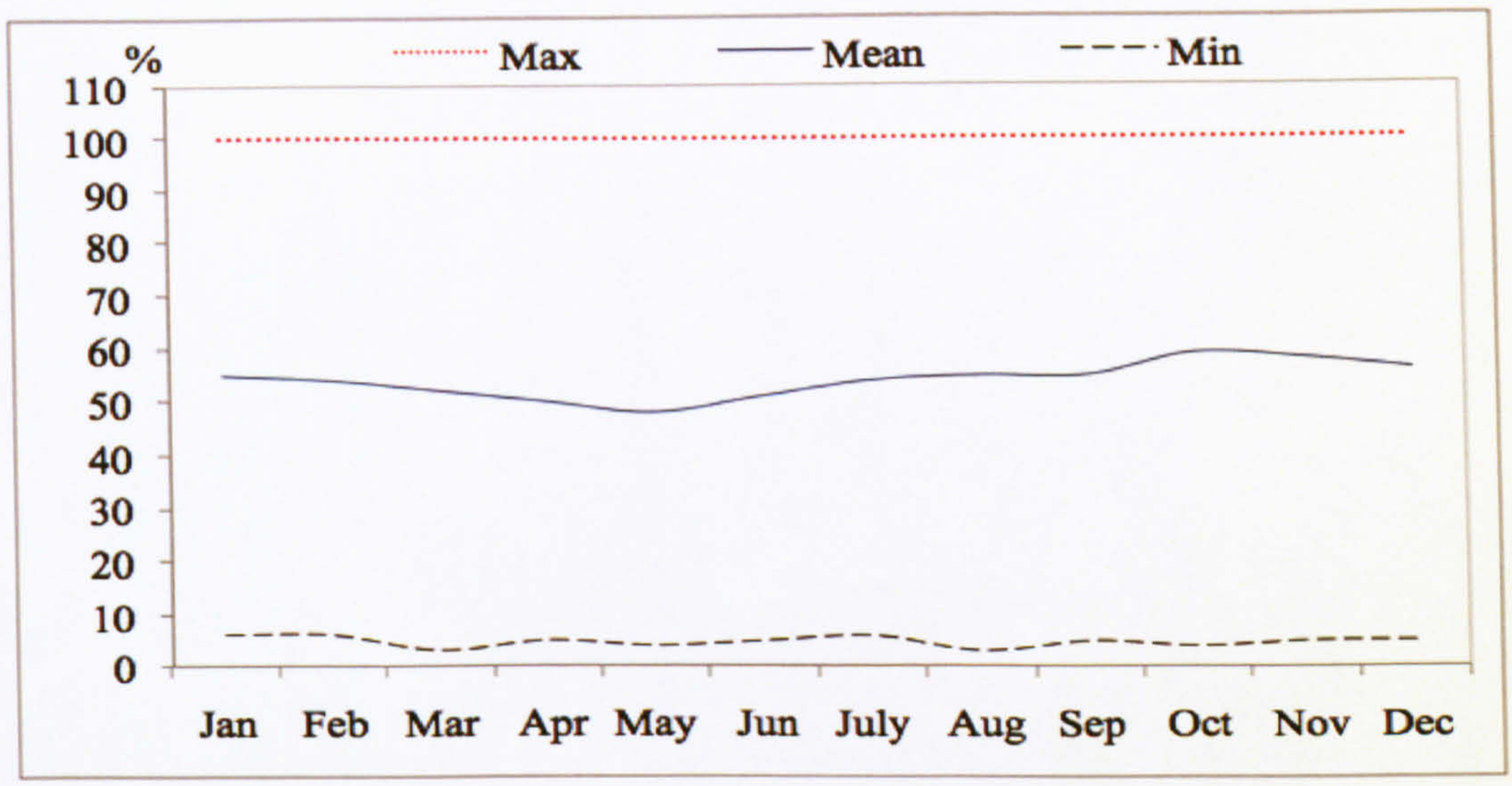

Figure 3-4 Yanbu's maximum, minimum and mean relative humidity [111]

The Red Sea oceanography is critical data for this study as the seawater is the main input for the MED desalination plant and for the absorption chiller and steam turbine condenser as cooling water. The Red Sea high surface temperatures coupled with high salinities make it one of the hottest and saltiest bodies of seawater in the world. The average surface water temperature of the Red Sea during the summer is 26°C and 20°C during the winter months. As a result of the scarcity of rainfall, the absence of potable water sources and the excess evaporation that reaches 205cm per year, the Red Sea salinity varies from 0.036kg/kg to 0.04kg/kg [111]; these values were carefully considered in the parametric studies.

3.6 Plants Modelling Data

This section presents the real data collected for the modelling of each plant employed in this study. The real modelling data supports this study in two different ways: firstly, it validates the main tool used in this study — the simulation software IPSEpro; secondly, it adds to the credibility and applicability of the study. The data was collected from different sources as follow.

3.6.1 Gas Turbine

The gas turbine used in this study was modelled as an AAB gas turbine model that was installed in 1995 in a combined cycle power plant located in Benghazi city in Libya. The technical

specification and performance curve data was obtained from an operation engineer working in the same plant. Table 3–1 lists all the gas turbine's technical specifications.

Specifications	Description/code
Manufacturer	ABB
Model	GT 13LE1
Fuel	NG and LFO
Frequency	50 Hz
Year	1995
Compressor	Axial
Generator	WY217-092LLT
Number of compressors	One, axial
No. of shaft	One single spool
No. of compressor stages	21
No. of turbine stages	5
Shaft rotor type	Hollow concentric
Shaft diameter	40 cm
Shaft speed (rpm)	3000 rpm
No. of combustors	One
No. of burners per combustor	One
Compression ratio	13.8-14
Design power	141.44 MW
Design thermal efficiency	0.3837
Design exhaust temperature	524.4 °C
Design exhaust mass flow	496.4 kg/s
Lower heat value (LHV)	42070
Design inlet pressure loss	0.0114
Design exhaust pressure loss	0.0127
Design operation altitude	0 m
Relative power drop due to inlet pressure	-1.25 bar^{-1}
Power drop due to outlet pressure drop	-0.475 bar^{-1}
Power change due to barometric pressure	0.98 bar^{-1}
Efficiency drop due to inlet pressure drop	-0.65 bar^{-1}
Efficiency drop due to outlet pressure drop	-0.56 bar^{-1}
Design ambient barometric pressure	1.0133 bar

Table 3-1 ABB gas turbine's specifications, from Benghazi power plant

The performance characteristic curves were provided in tabulated form at loads 0.25, 0.5, 0.75 and full load at varius ambient temperatures from 5°C to 50°C. These curves indicate the behaviour of the output power, efficiency, exhaust mass flow rate in kg/s and exhaust gas temperature in °C. The data as obtained is presented in Appendix B and figures 3–5 to 3–8.

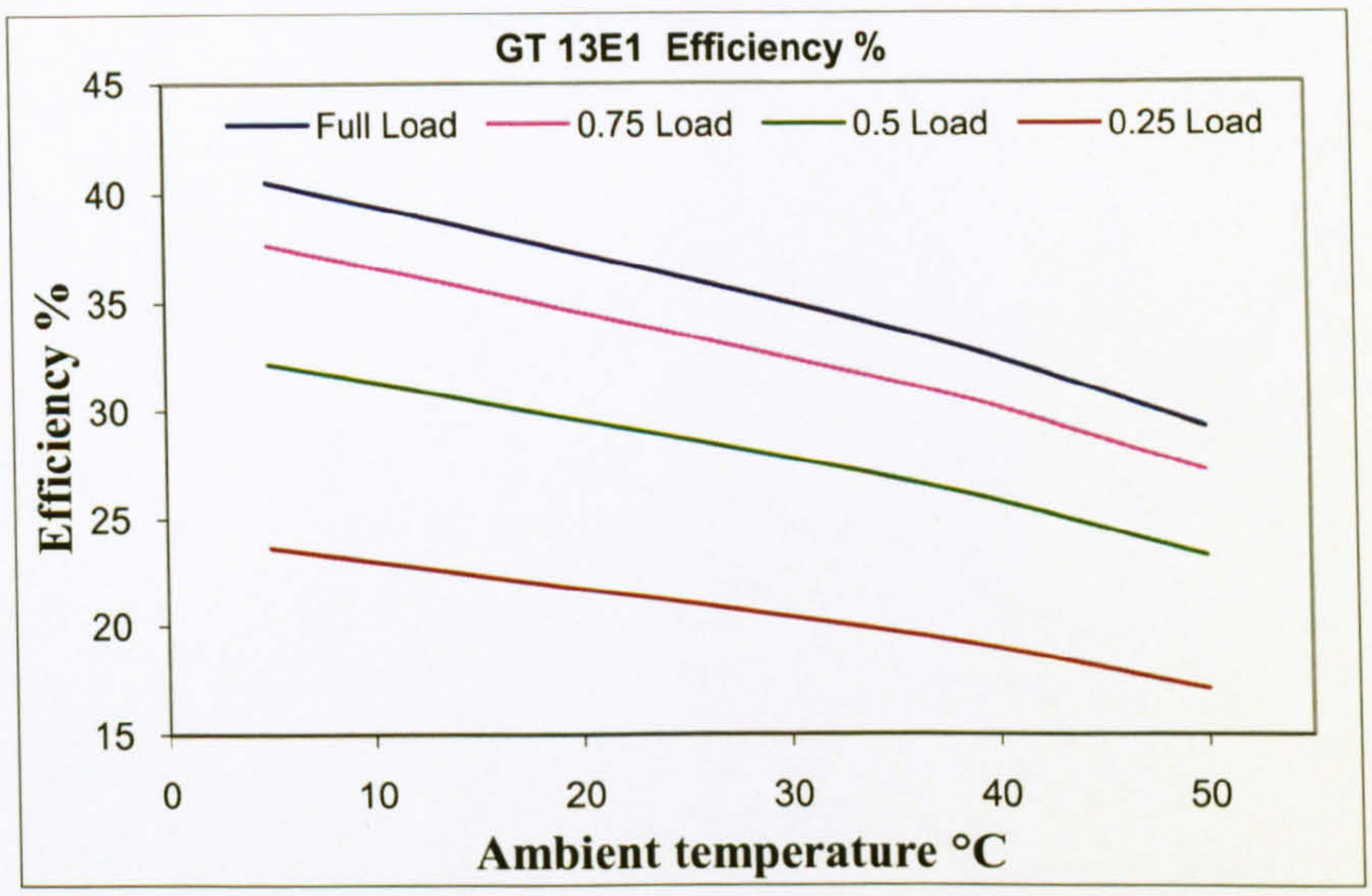

Figure 3-5 ABB gas turbine's efficiency performance curve

Both the gas turbine's efficiency and output power decline as the ambient temperature increases according to these two figures. The ambient temperature affect on the gas turbine power output is lower at partial load.

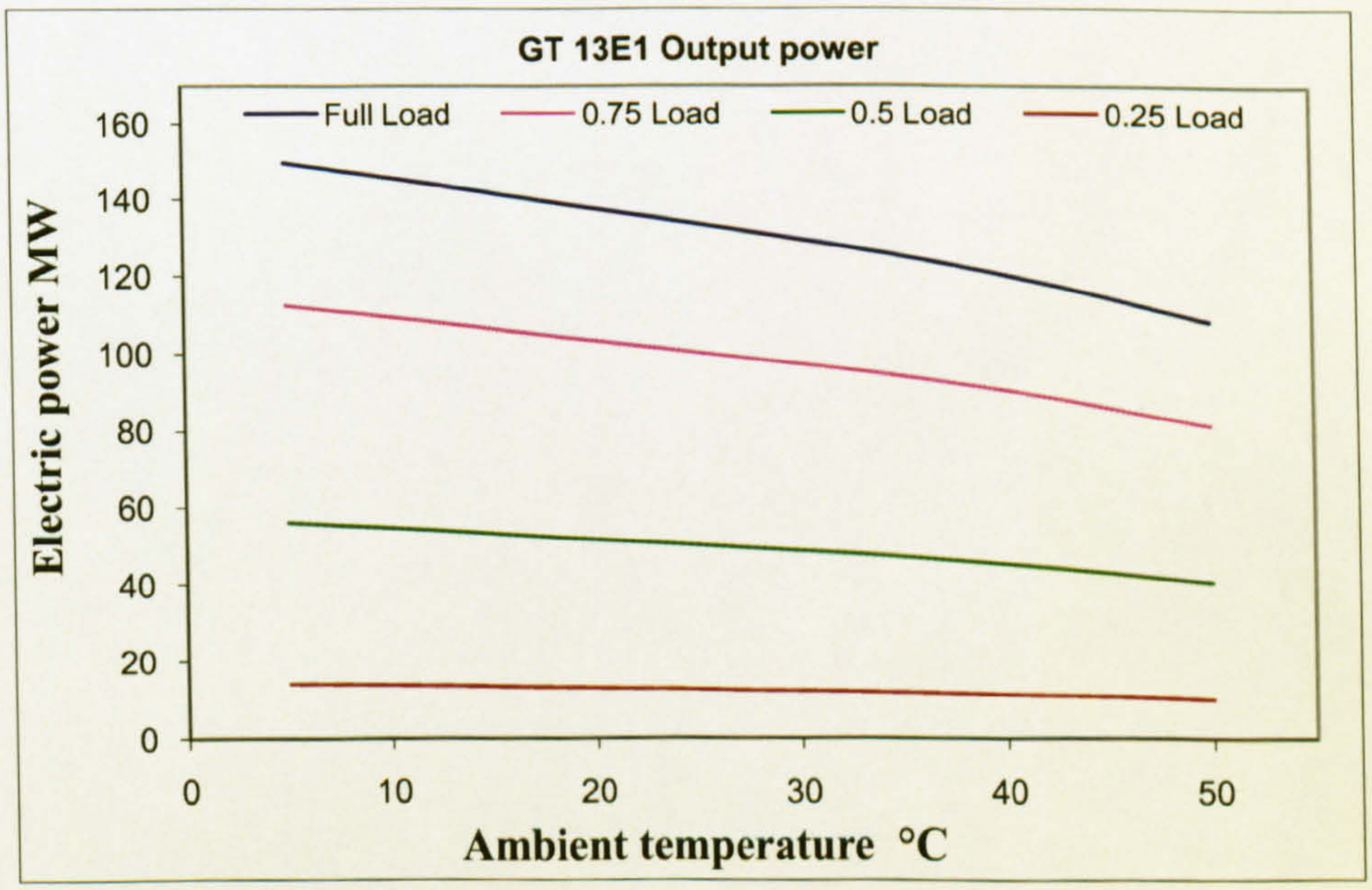

Figure 3-6 ABB gas turbine's output power performance curve

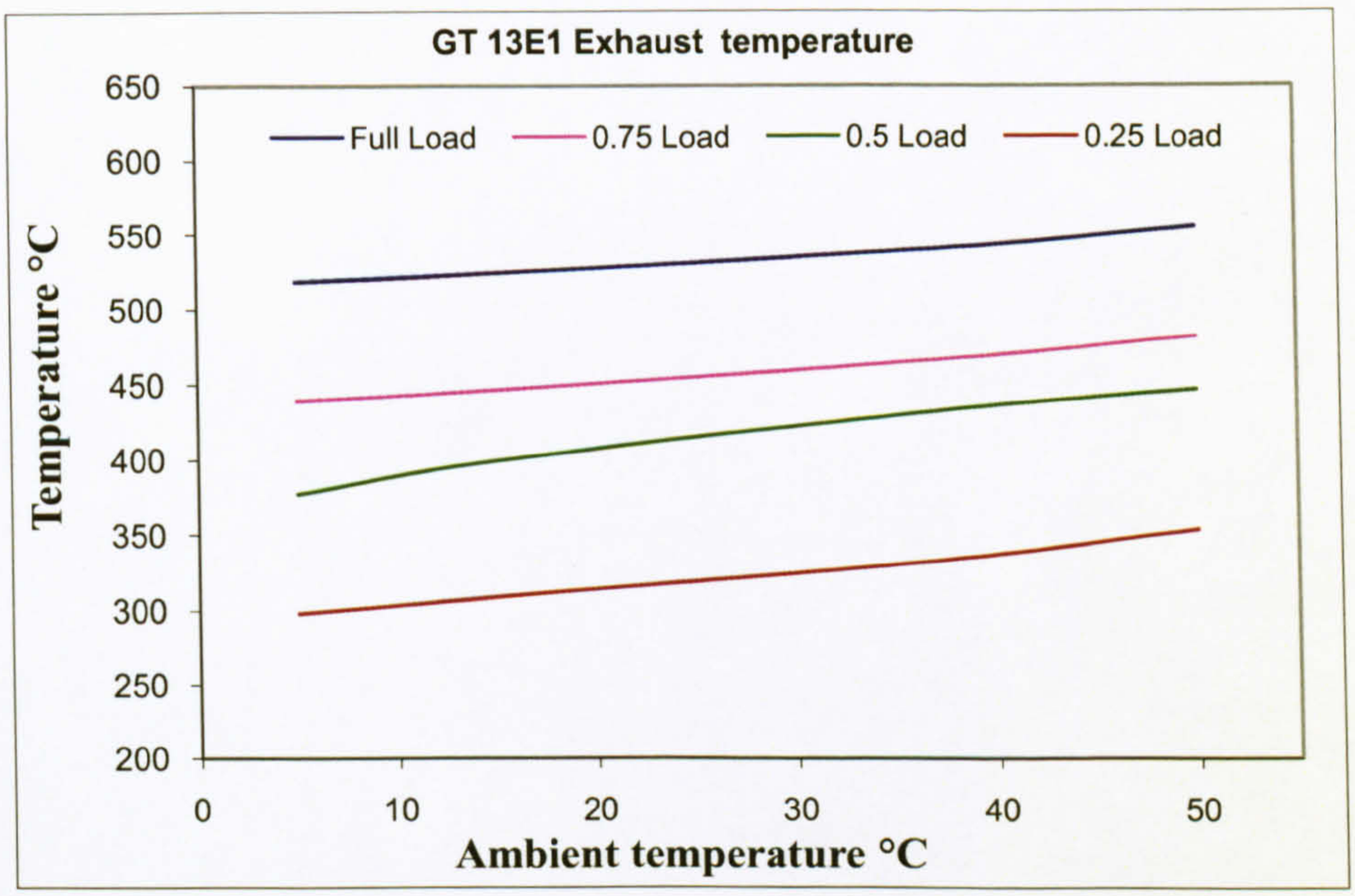

Figure 3-7 Temperature performance curve of the ABB gas turbine's exhaust

These curves are not the designed curves; the gas turbine was installed in 1995 and these curves were obtained after a performance test performed on 10 August 2004. Hence, the gas turbine is not expected to perform as it was designed.

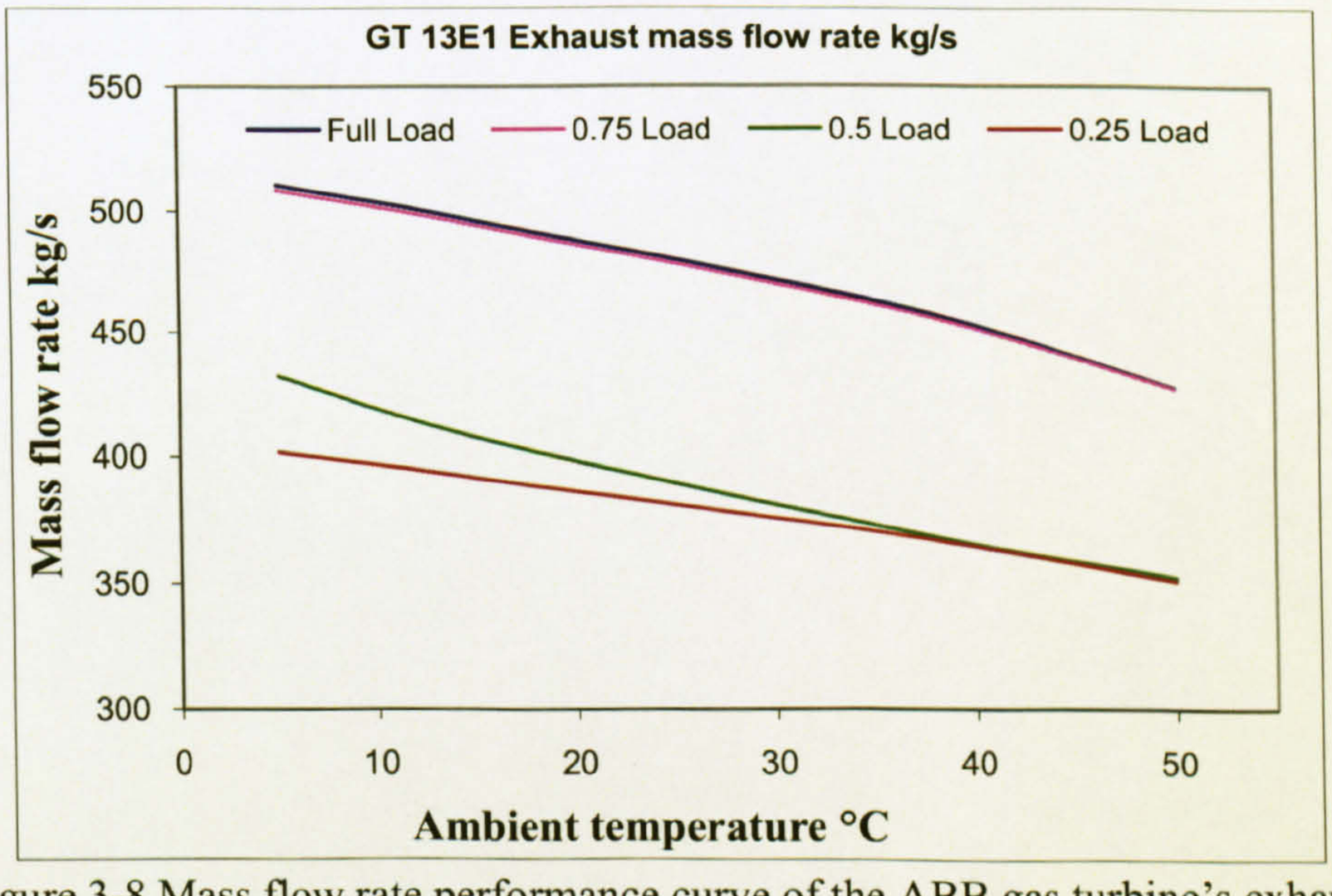

Figure 3-8 Mass flow rate performance curve of the ABB gas turbine's exhaust

These curves are used as input data in the generic gas turbine model used in this study in tabulated form. The tables show the variation in the output power, efficiency, exhaust mass flow and temperature as the operating load and ambient temperature vary. The following equation was

used to obtain the required value at the specified load and ambient temperature from the given data:

$$V(T,L)=\frac{V_{design}}{V_{curve}(T,L)} \tag{3.21}$$

where V_{design} is the parameter designed value, and V_{curve} is the value read from the curves at the specified temperature and load.

3.6.2 Steam Turbine

The steam turbine used in this study was modelled according to the 60MW steam turbine built by the China National Electric Wire and Cable Import and Export Corporation. The technical specification was obtained from the company catalogue [112]. Table 3–2 below lists the technical specifications of the steam turbine.

Specifications	Unit	Designation/code
Code		G38#
Model		C60. 8.83/1.27
Type		Impulse-tandem
Rated output	MW	60
Isentropic efficiency	%	87
Mechanical efficiency	%	95
Max. output	MW	63
Speed	RPM	3000
Steam pressure	M Pa	8.83
Steam temperature	°C	535
Rated steam flow	t/h	372
Max steam flow	t/h	410
Cooling water temperature	°C	20
Heat rate (extract/condense)	kJ/kWh	5870/9860
Steam rate (extract/condense)	Kg/kWh	7.084/3.770
Height of last vane	mm	540
Overall size (L x W x H)	m	8.0x5.0x3.5
Turbine weight	t	192
Cooling surface of condenser	m^2	3500

Table 3-2 Steam turbine's specifications [112]

The heat recovery steam generator (HRSG) unit used to power the steam turbine is a typical single pressure, vertical flow and forced circulation with a deaerator heater. It was modelled to provide the steam turbine requirements, with both the pinch point ΔT and approach point ΔT set to 33°C and 11°C respectively. These settings were made as a result of a pinch point analysis and pinch point parametric study that investigated the optimum pinch point ΔT value on the basis of the first and second law efficiencies and heat transfer area [83, 113, 114].

3.6.3 Absorption Chiller

The absorption chiller used in this study was modelled according to a 9304 kW absorption chiller built by BROAD Air Conditioning Co., Ltd. The technical specifications were obtained from the company's manual [115]. Table 3–3 lists the technical specifications of the selected model. This model was also validated against the Dühring P-T chart and will be presented in the next chapter.

Specifications	Unit	Value
Code	-	BHE-800
Power source temperature	°C	97.7
Rated chilled W inlet temperature	°C	6.6
Rated chilled W outlet temperature	°C	13.7
Lowest permitted outlet temperature for chilled	°C	5
Lowest permitted inlet temperature for cooling	°C	10
Adjustable chilled water flow rate	%	50~120
Pressure limit for chilled W, cooling W	bar	7.99
Adjustable load	%	5~115
LiBr solution concentration	%	52
Chilled water flow rate	kg/s	316.8
Capacity	kW	9304
COP	-	0.79

Table 3-3 BHE-800 absorption chiller's specifications [115]

3.6.4 Med Desalination Plant

The desalination plant used in this study was modelled according to a 40000m^3/day multi-effect distillation desalination plant built by IDE Technologies Ltd [116]. The data was obtained from the company's global marketing vice president. Table 3–4 below lists the specifications of the modelled plant.

Specifications	Unit	Value
Potable water production rate	m^3/day	40000
Number of effects	-	10
Number of units	-	2
Driving steam pressure	Bar	0.32
Specific heat consumption	kJ/kg	318
Concentration factor	-	1.6
Electricity consumption	kW	290
Top brine temperature	°C	70.5
Gain output ratio	-	7-8
Reliability	%	99
Availability	%	98 yearly

Table 3-4 MED desalination plant's specification [116]

3.7 Closing Remark

In this chapter, the tools used in the study were introduced including the simulation and modelling software IPSEpro with all of its modules and libraries. Then the first and the second low performance parameters used were presented. Following this, the weather data for Yanbu city was introduced followed by the real modelling data for each plant employed in this study.

Chapter 4

Base Plants Modelling and Results

4.1 Introduction

This chapter presents the modelling, simulation, performance assessment and off-design studies for all the base plants. These are the CC power plant, multi-effect distillation desalination plant, thermal vapour compression multi-effect distillation plant and the absorption chiller. The performance assessment and analysis are on the basis of both the first and second laws of thermodynamics. The modelling real data collected and presented in the previous chapter are used in this chapter to simulate and assess the sub-plants employed in this study.

4.2 Combined Cycle Power Plant

This study can be applied to any power plant arrangement to utilize its waste energy efficiently and to improve its performance and reduce its environmental impact. However, a combined cycle power plant was simulated for this study based on real gas turbine and steam turbine models. As shown in Figure 4–1 the power plant model combines a gas turbine and a steam turbine and each of them drives a generator. A single pressure level, vertical flow and forced circulation heat recovery steam generation unit (HRSG) is employed to utilize a portion of the gas turbine's exhaust heat energy in the steam turbine. The HRSG unit consists of an evaporator, super heater and economizer. The HRSG also includes a deaerator to control the dissolved oxygen level in the makeup water. The deaerator is supported with a heater to improve HRSG efficiency [117]. Figure 4–1 also shows the exhaust chimney, gas turbine air-intake, fuel stream source, steam turbine condenser and condenser cooling water streams.

The gas turbine in ISO conditions (International Standards Organization) consumes 8.763kg/s of natural gas fuel (lower heating value of 42070kJ/kg) according to the data presented in the previous chapter. It produces 135.74MW of electric power and emits 485.7kg/s of exhaust gases at a temperature of 537.16°C. The HRSG unit utilizes 60.42% of the heat energy out of the gas turbine exhaust stream and powers the steam turbine, which generates 60MW of electricity. The plant emits 144.4MW of waste heat energy as exhaust gases from the stack at a temperature of 219.74°C, and consumes 837.1kW of electricity to drive the HRSG pumps. The overall electrical efficiency of the plant in ISO conditions is 52.94%, and its CO_2 emission rate is 506.62kg of CO_2/kW, according to equation 3.5 and assuming that each ton of the fuel consumed produces 3142kg of CO_2 [104]. The HRSG unit was evaluated using the pinch analysis, effectiveness and

NUT method. Also, a parametric study was performed to investigate the optimum pinch point value.

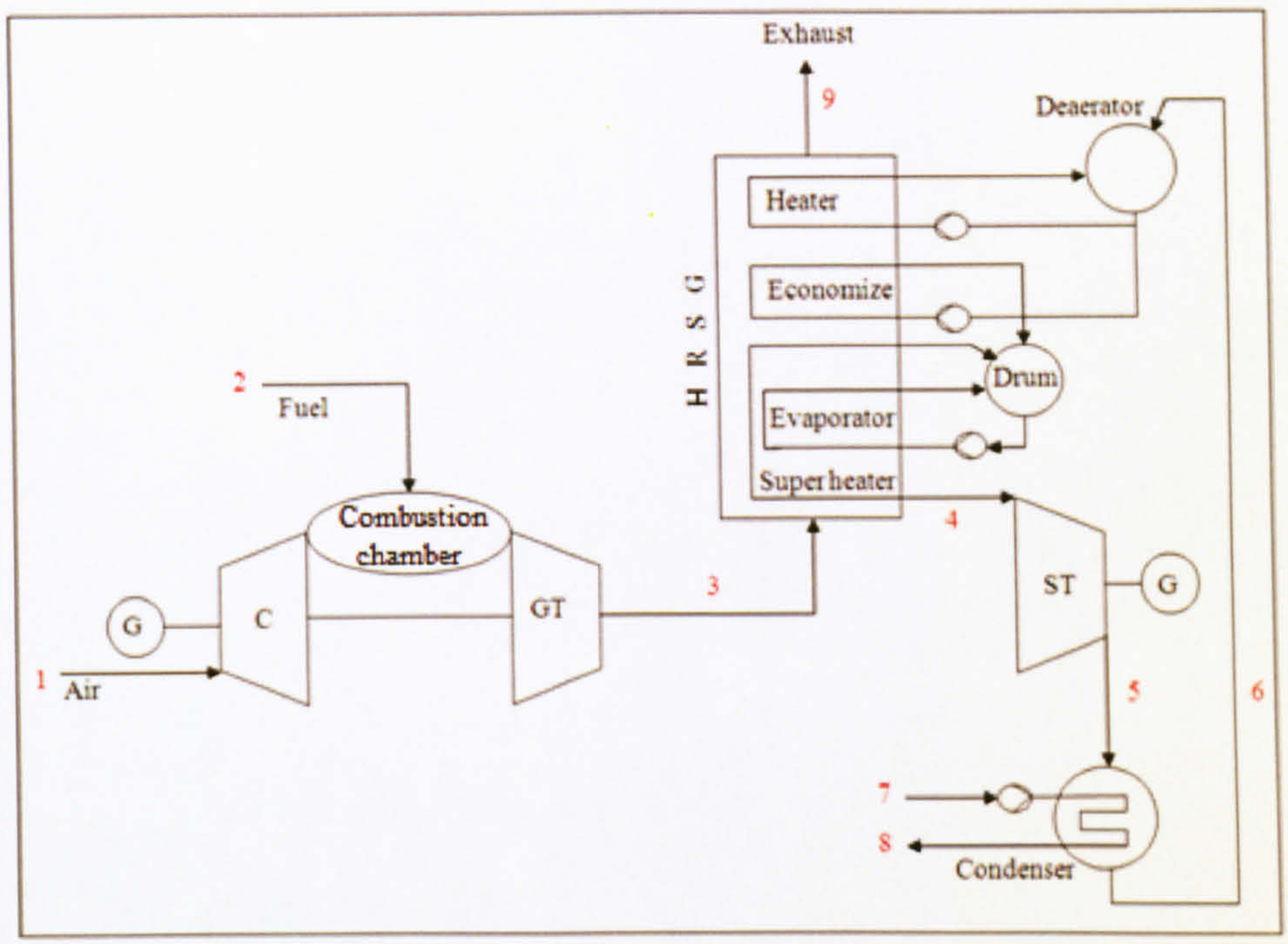

Figure 4-1 Modelled combined cycle power plant

The lower pinch point temperature increases the HRSG efficiency as it utilizes more heat energy from the gas turbine exhaust gas, but requires a larger heat transfer area, which may affect the plant's economic visibility. Boyce [37] in his book *Gas Turbine Engineering Handbook* suggested a value between 22°C and 33°C. However, the effectiveness-NTU method analysis confirmed that the lower acceptable value for the modelled plant was 33°C, as any value less than that would have increased the effectiveness and NTU of the HRSG heat exchangers indicating the larger heat transfer area. Table 4-1 lists the effectiveness-NTU analysis results for each heat exchanger used in the HRSG as well as the steam turbine condenser at a pinch point value of 33 °C. All the effectiveness and NTU values fell in the typical range reported in the literature [118, 119].

	Effectiveness	**NTU**
Deaerator	0.80	1.87
Economizer	0.80	2.16
Evaporator	0.81	1.67
Super heater	0.80	1.93
ST condenser	0.80	1.60

Table 4-1 Effectiveness and NTU values

The pinch analysis confirmed the same value for the pinch point, while an approach temperature of 11°C and a circulation ratio of 3 were set according to the typical values of the forced circulation HRSG that are reported in the literature [37, 117,120, 121]. Figure 4–2 shows both the pinch and the approach temperature located on the HRSG temperature profile.

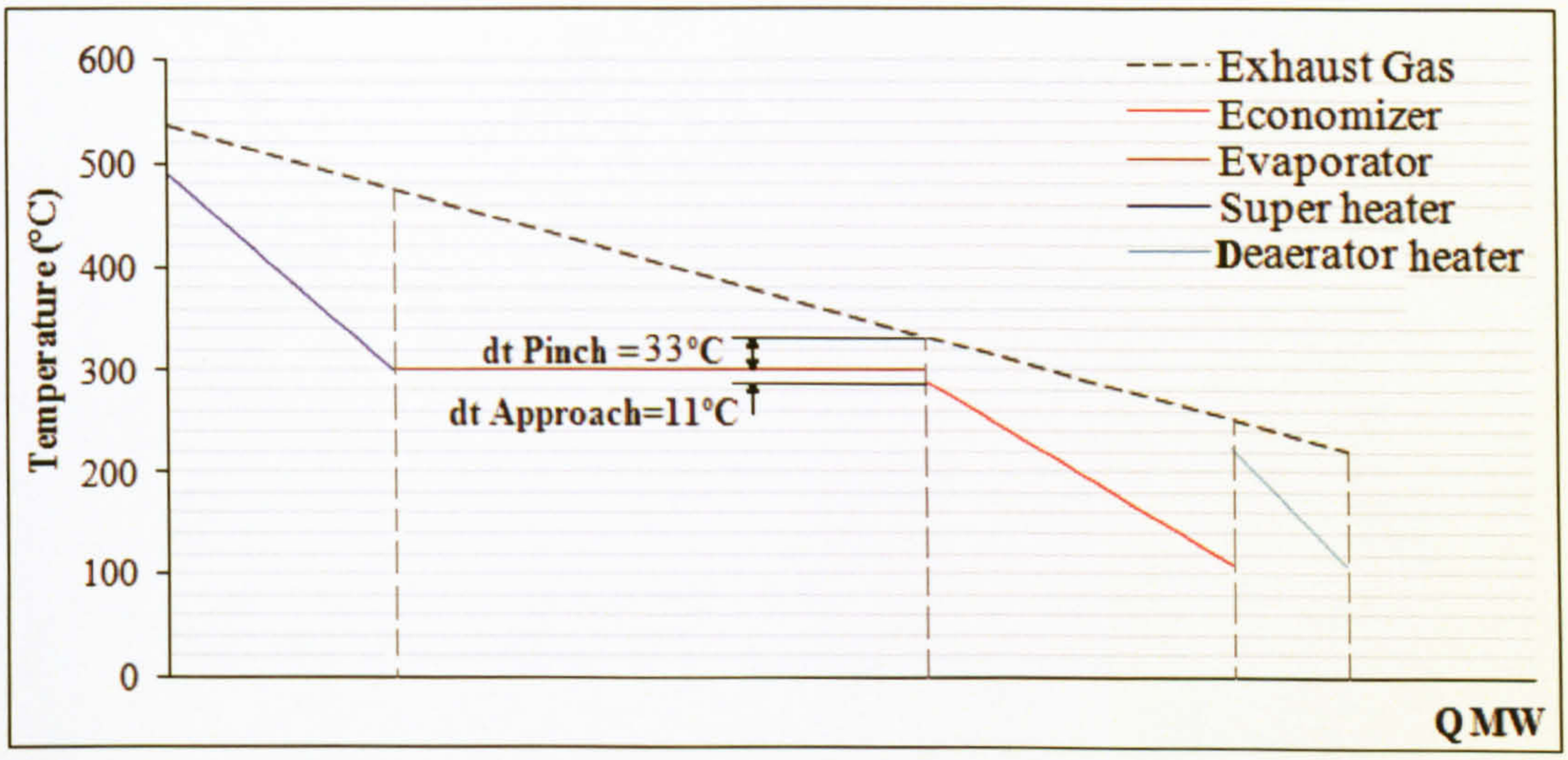

Figure 4-2 HRSG temperature profile

A parametric study was also carried out to support these values where the overall plant performance was examined against a variation in the pinch point from 15°C to 40°C at ISO conditions and the gas turbine was at full load. The results show an increase in the UA value by 10% on average for each 5°C reduced in the pinch point value accompanied by just a 2.3% increase in the HRSG thermal efficiency as shown in Figure 4–3.

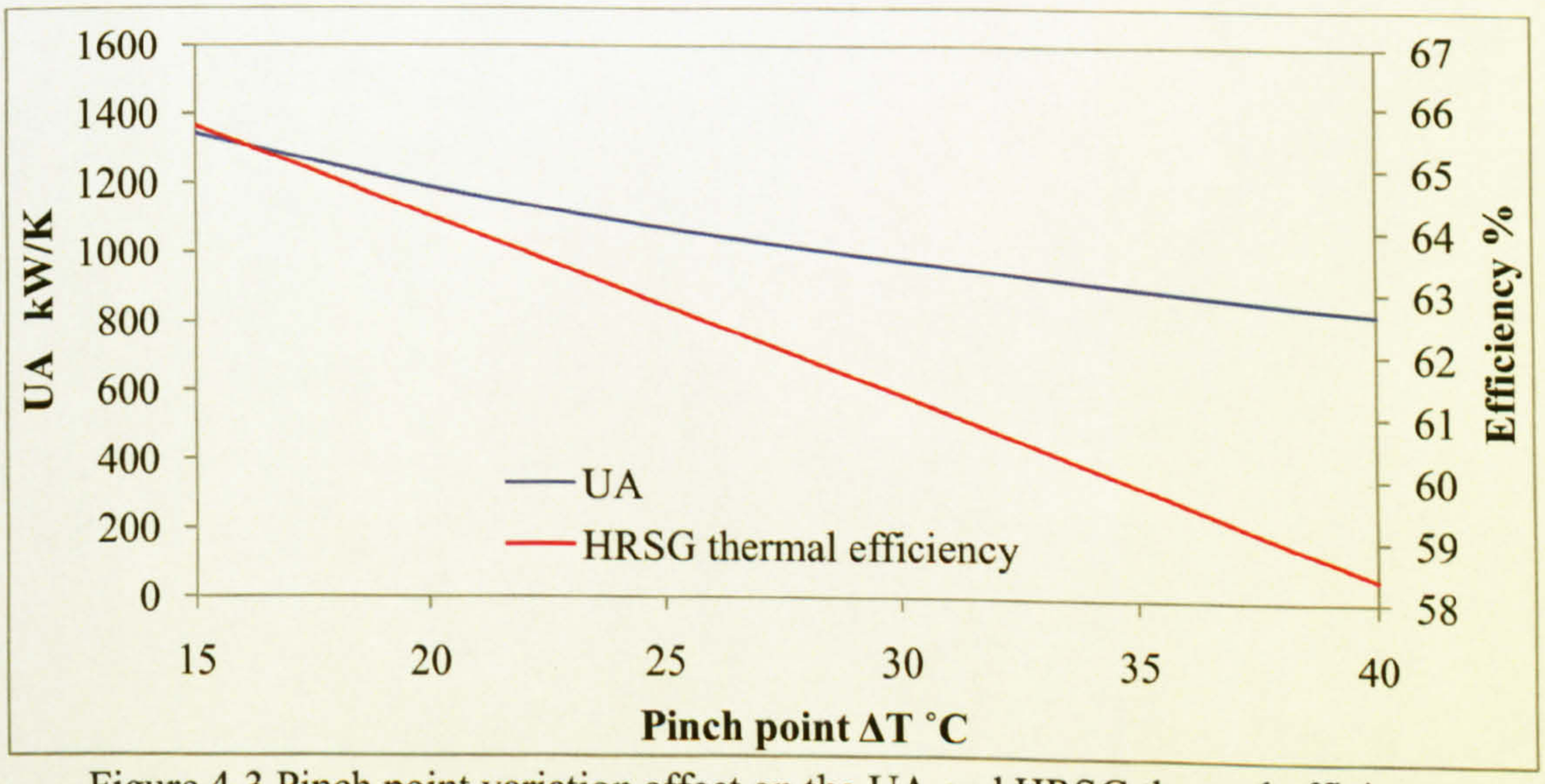

Figure 4-3 Pinch point variation affect on the UA and HRSG thermal efficiency

The steam turbine output power was also affected by the value of the pinch point in a way that its power was enhanced by 2.38% for each 5°C decrease in the pinch point value as seen in Figure 4–4. Likewise, the stack exergy destruction and the CO_2 emission rate were reduced on average by 1.7MW and 3.67 kg CO_2 /kW respectively for each 5°C decrease in the pinch point value as shown in Figure 4–4. All the other results of this parametric study are listed in Table 1 in Appendix C. All the results clearly enforce the minimum possible pinch point value except the HRSG heat transfer area. However, in order to achieve reasonable effectiveness and NUT values that ensure acceptable and economical heat exchangers sizes, the pinch point should not be lower than 33˚C.

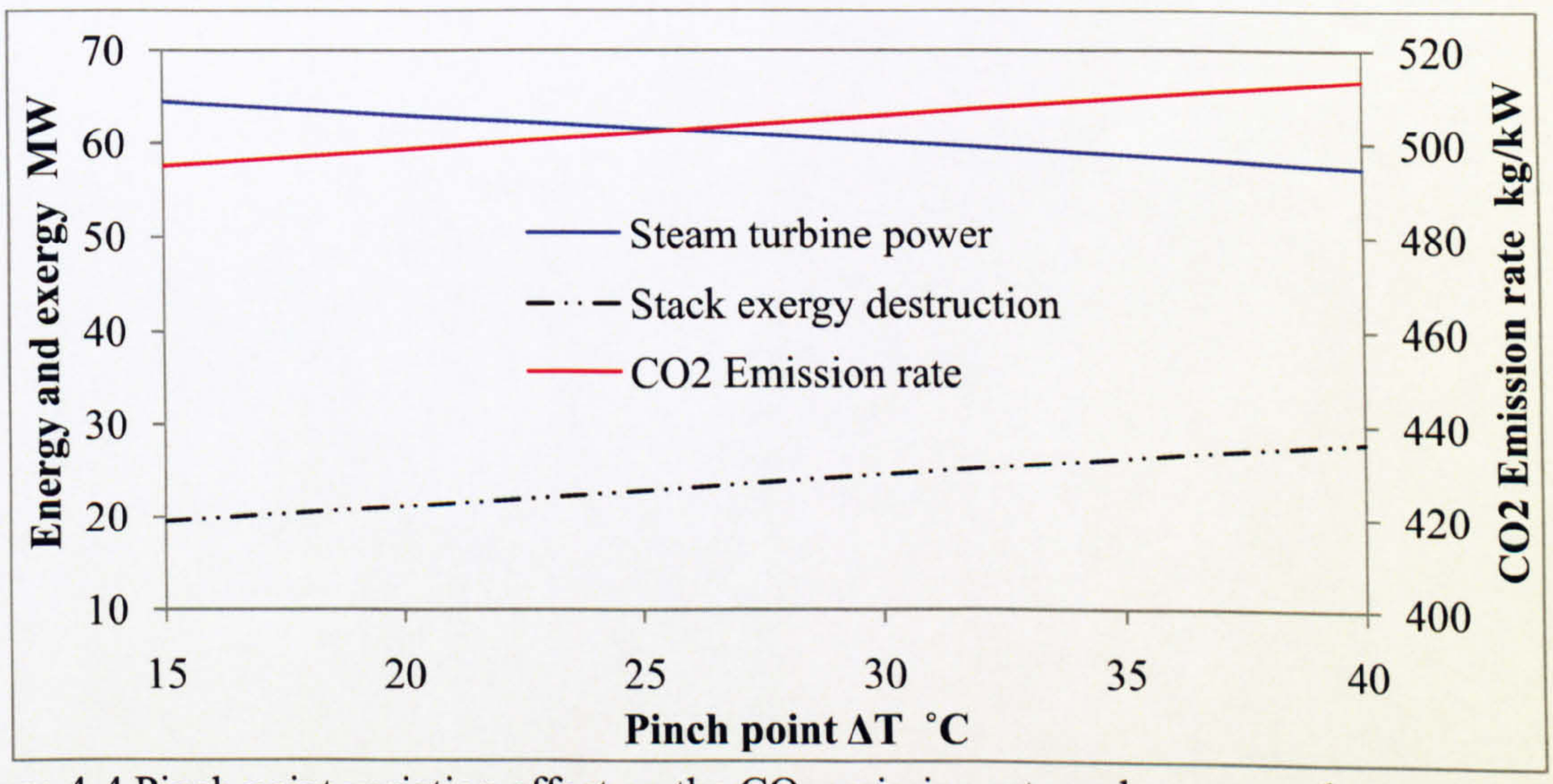

Figure 4-4 Pinch point variation affect on the CO_2 emission rate and exergy and energy analysis results

On the basis of the second law analysis, the exergy was calculated for each stream in the plant. Then the exergy destruction for each component in the plant was calculated according to the equations shown in Table 4–2, which are based on the exergy balance equation presented in the previous chapter.

Component	Exergy Destruction
Gas turbine	$e_1 \times \dot{m}_{Air} + e_2 \times \dot{m}_{Fuel} - e_3 \times \dot{m}_{Exhaust} - \dot{W}_{GT}$
HRSG	$\dot{m}_{Exhaust} \times (e_3 - e_9) + e_6 \times \dot{m}_w - e_4 \times \dot{m}_{Steam} + \sum \dot{W}_{pump}$
Steam turbine	$\dot{m}_{Steam} \times (e_4 - e_5) - \dot{W}_{ST}$
ST condenser	$e_5 \times \dot{m}_{Steam} - e_6 \times \dot{m}_w + \dot{m}_{C,w} \times (e_7 - e_8) + \sum \dot{W}_{pump}$
Stack	$e_9 \times \dot{m}_{Exhaust}$

Table 4-2 Exergy destruction equation for the power plant components

With reference to Figure 4–1, the exergy and specific exergy of each stream in the plant are listed in Table 2 in Appendix C, while the exergy destruction of each component in the power plant is shown in Figure 4–5.

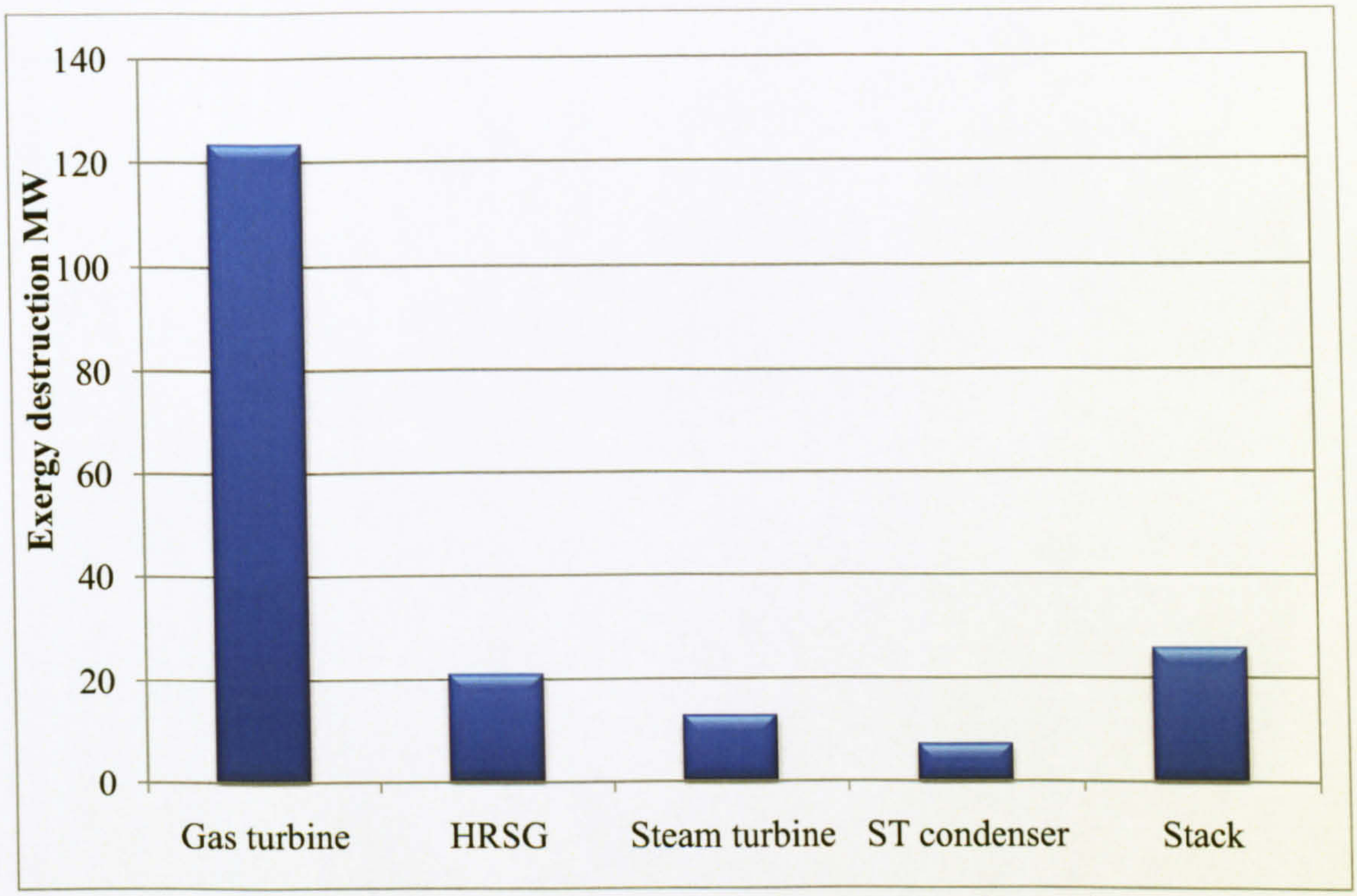

Figure 4-5 Base power plant components' exergy destruction

The modelled power plant's exergy analysis indicated that the gas turbine including its compressor, generator and combustion chamber was the main source of the plant irreversibility; consuming 32% of the fuel exergy it represented 64.9% of the total exergy destroyed in the plant. This can be justified by the exergy degraded during the compression, combustion and expansion processes taking place in the gas turbine components. The exegetic efficiency of the gas turbine was 52.26%, which was comparable to the typical values reported in the literature [89, 122, 123]. The gas turbine emitted 125.26 MW of exergy in the exhaust gases stream, which was utilized in the HRSG at an exergetic efficiency of 79.17%.

The HRSG unit consumed 5.47% of the fuel exergy and formed 11% of the total exergy destroyed in the plant to provide the steam turbine with a stream of saturated steam that had an exergy of 79.6MW causing an exergy destruction of 21.06MW, and emitting 25.6MW of its input exergy out of the stack. The stack formed 13.47% of the plant's total exergy destruction

and came second after the gas turbine as a source of the plant's irreversibility. This amount of exergy destroyed through the stack indicated the applicability of improving the plant's performance through more utilization. Furthermore, with an exergetic efficiency of 83.2% the steam turbine consumed 3.32% of the fuel exergy and represented 6.73% of the plant's total exergy destruction. The condenser only caused 3.82% of the plant's total exergy destruction and it only consumed 1.89% of the fuel exergy. The plant's overall exergetic efficiency was 54.47%, which is comparable to the typical values (50–60%) reported in the literature [83, 89, 122–125].

The plant's partial load performance was investigated by varying the gas turbine load from half load to full load while monitoring all the energy and exergy performance parameters. The study was performed in ISO conditions and a cooling water temperature of 22°C. All the results are listed in Table 3 in Appendix C, while the most significant results are plotted in graphs and discussed. Figure 4–6 shows the gas turbine load against the steam turbine and net plant electric output power. Operating the gas turbine at half load reduced the steam turbine output power by 69%. This is typical according to the gas turbine performance curves that were presented in the previous chapter.

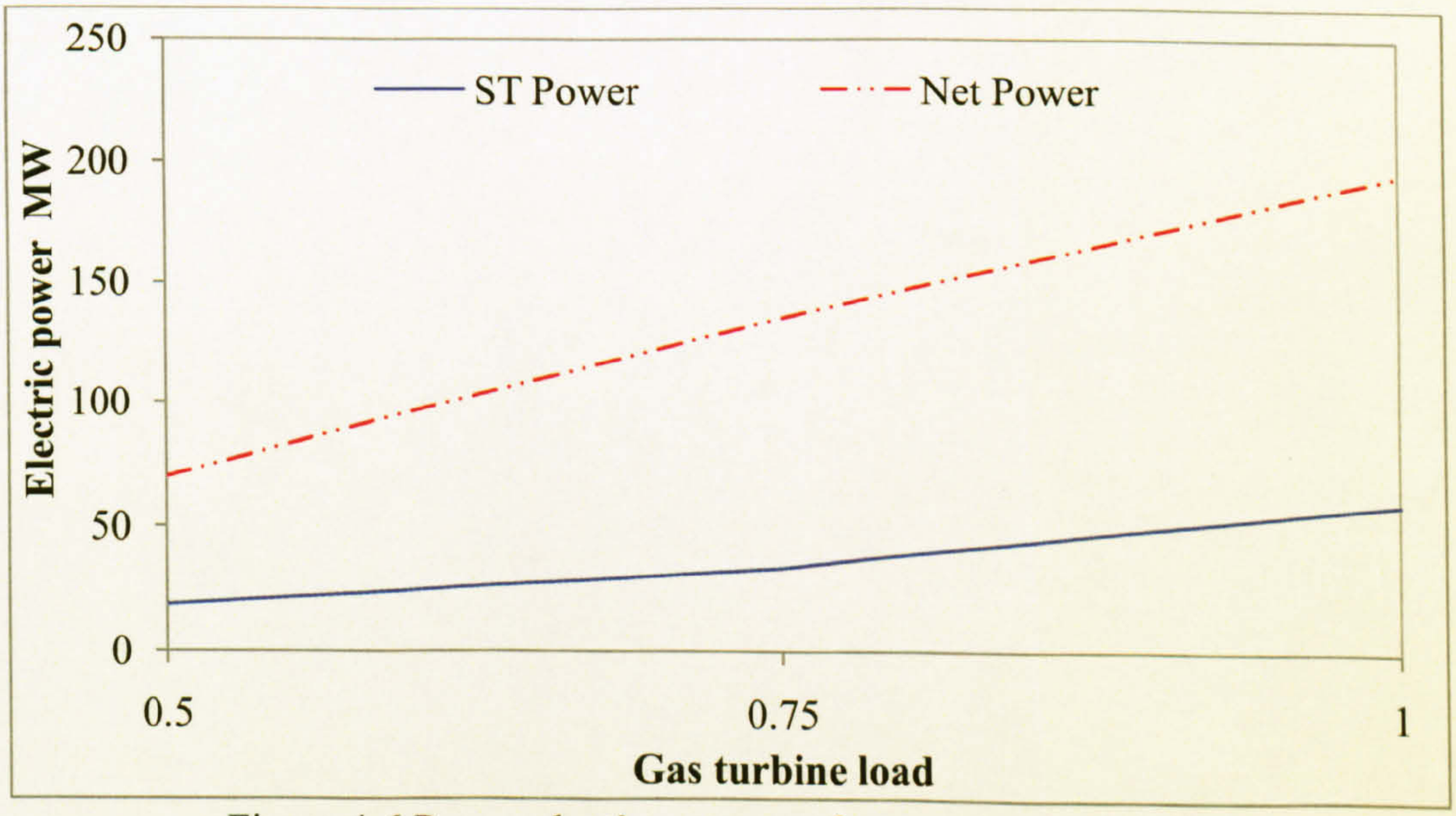

Figure 4-6 Power plant's power performance at partial load

The plant's CO_2 emission rate increased as the gas turbine load decreased to half by 34.1% due to the higher reduction in the plant's output electric power by 64.1% in comparison with the reduction in the gas turbine's fuel consumption by 51% as shown in Figure 4–7.

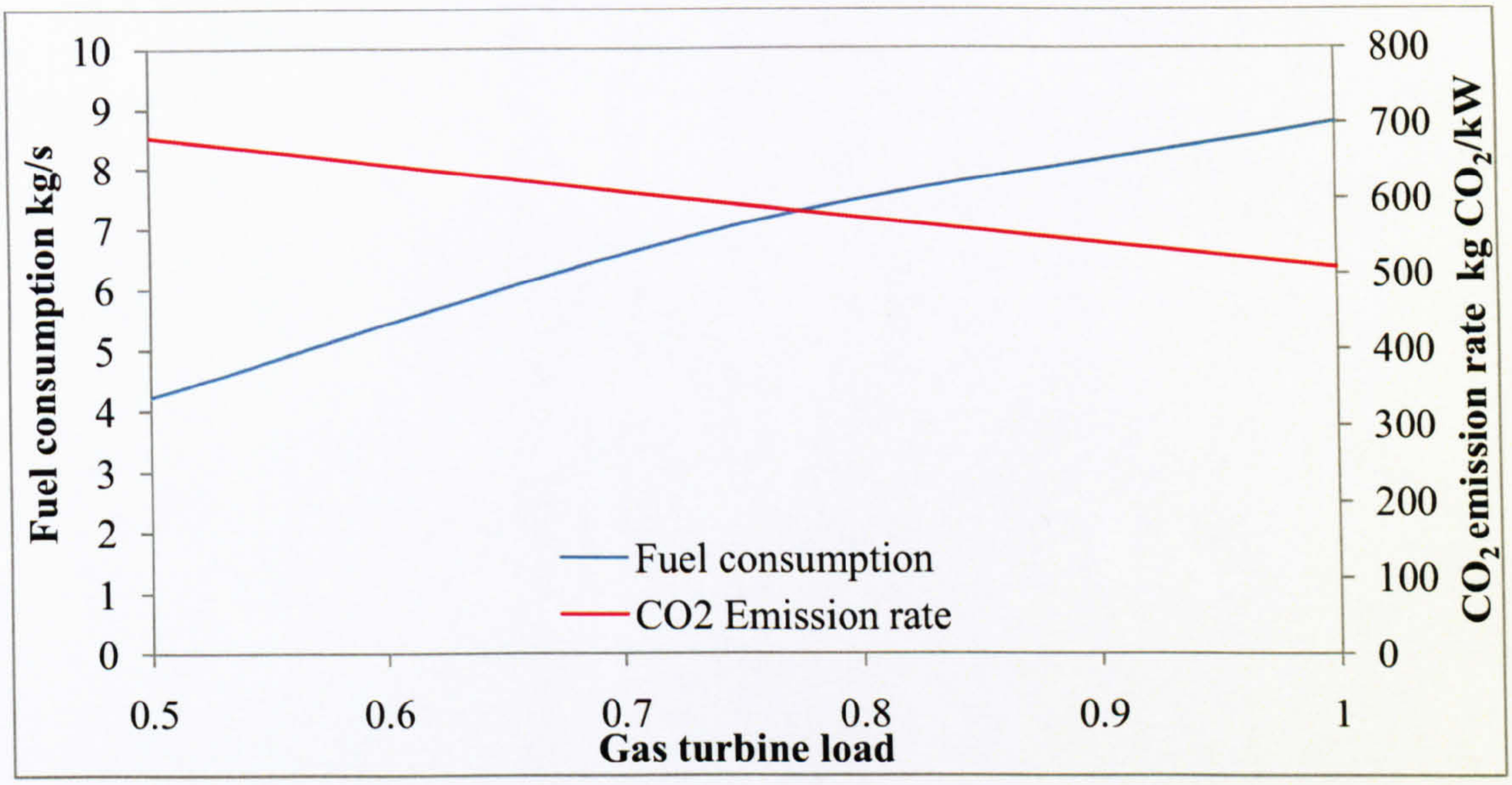

Figure 4-7 Fuel consumption and CO_2 emission rate performance at partial load

Figure 4-8 shows the gas turbine's and the plant's overall energy and exergetic efficiency at partial load. Both energy and exergetic efficiency were reduced as the gas turbine load decreased. This behaviour of the plant under partial load was imposed by the gas turbine's characteristic curves, which indicate the amount of fuel required for any operating load mode. In comparison with other combined cycle power plants the plant's performance under partial load was found to be typical and in agreement with what has been reported in the literature [29].

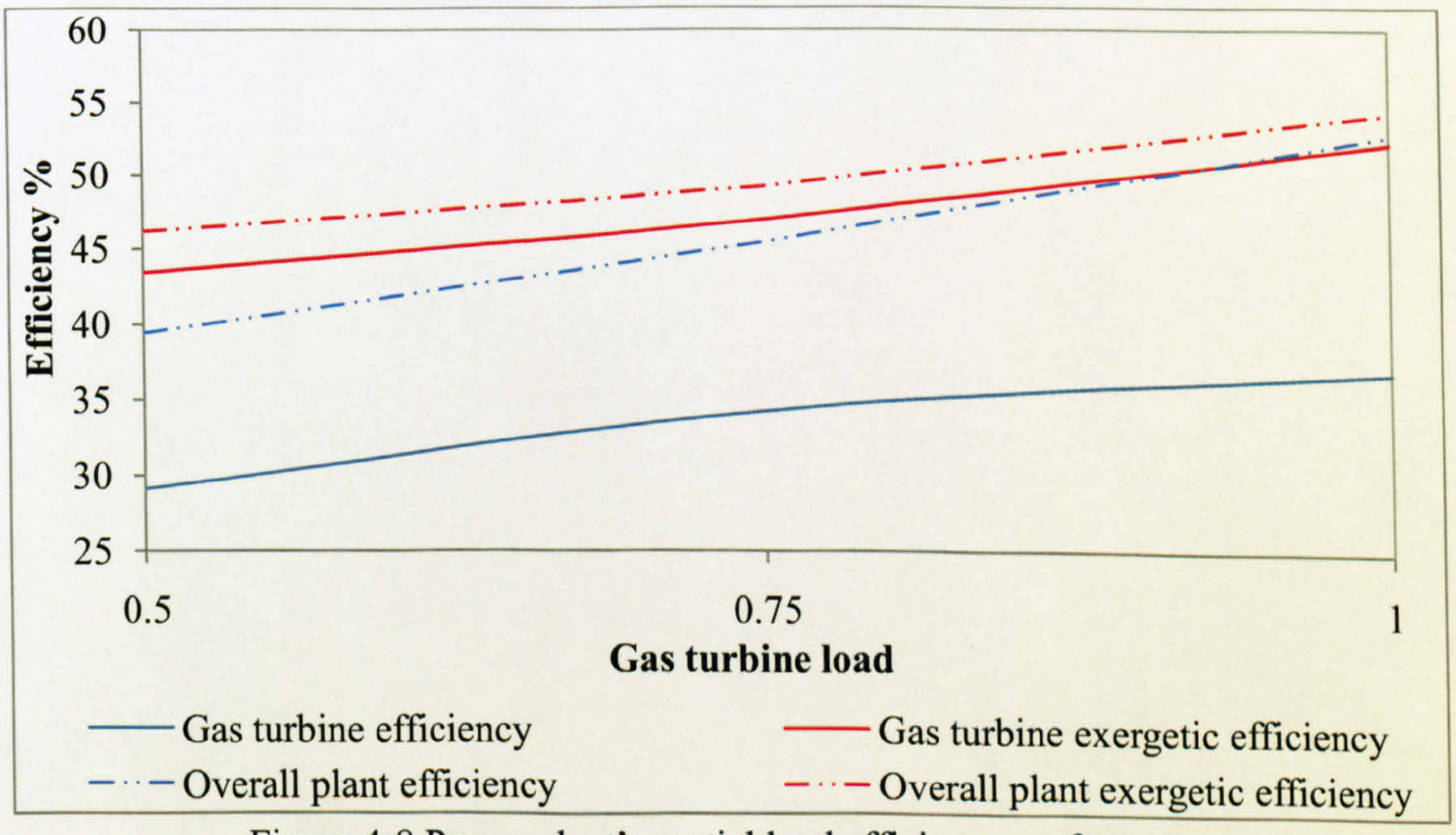

Figure 4-8 Power plant's partial load efficiency performance

The plant's off-design performance was evaluated by a number of parametric studies that investigated the effect of the variation of environmental parameters on the plant's overall performance. Firstly, the ambient temperature variation was investigated at full gas turbine load, with an ambient pressure of 1.013 bar and a cooling water temperature of 22°C. According to the weather data presented in the previous chapter the mean temperature of Yanbu city is 27.5°C, while the maximum and minimum recorded temperatures are 59.5°C and 4.7°C respectably. Thus the modelled plant performance was investigated under a variation in the ambient temperature from 5°C to 50°C.

Appendix C includes all the study's results in Table 4, while the most significant results are presented and discussed in this chapter. As the ambient air temperature increased its density decreased and the air intake mass flow rate to the compressor was then reduced. The compressor then generated less pressure for the same work. This decreased the gas turbine cycle temperature ratio (T_3/T_1) only if the fuelling was constant and this resulted in a reduction in the output power, as explained in more detailed in Chapter 2. Figure 4–9, shows that the air intake mass flow rate decreased on average by 2.1% while the gas turbine temperature ratio decreased on average by 4.1% for each 5°C increase in the ambient air temperature. These results are governed by the turbine's characteristic curves, which control the performance of the gas turbine.

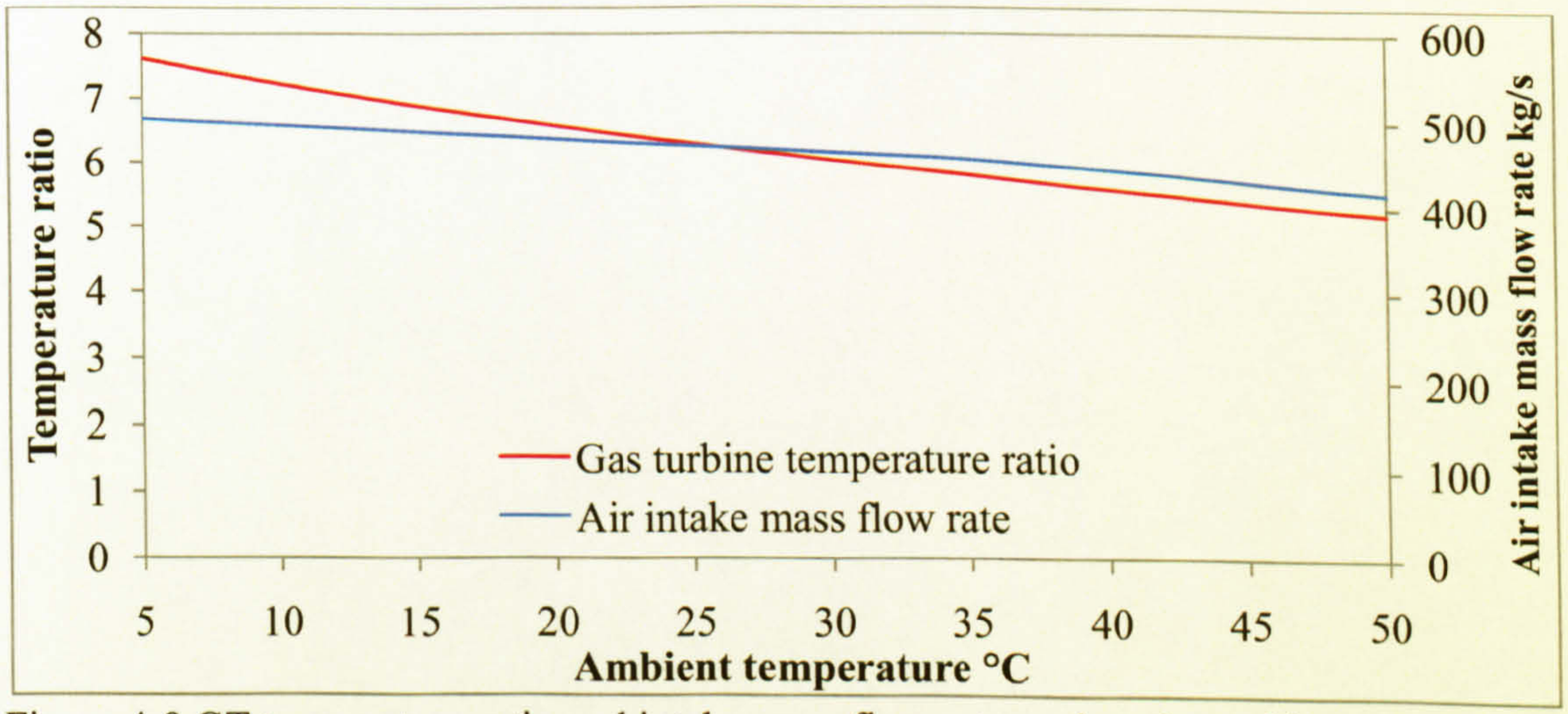

Figure 4-9 GT temperature ratio and intake mass flow rate against the ambient temperature

The reduction in the plant output is shown in Figure 4–10. This reduction was mainly caused by the reduction in the gas turbine's output electric power on average by 3.8% for each 5°C increase in the ambient air temperature.

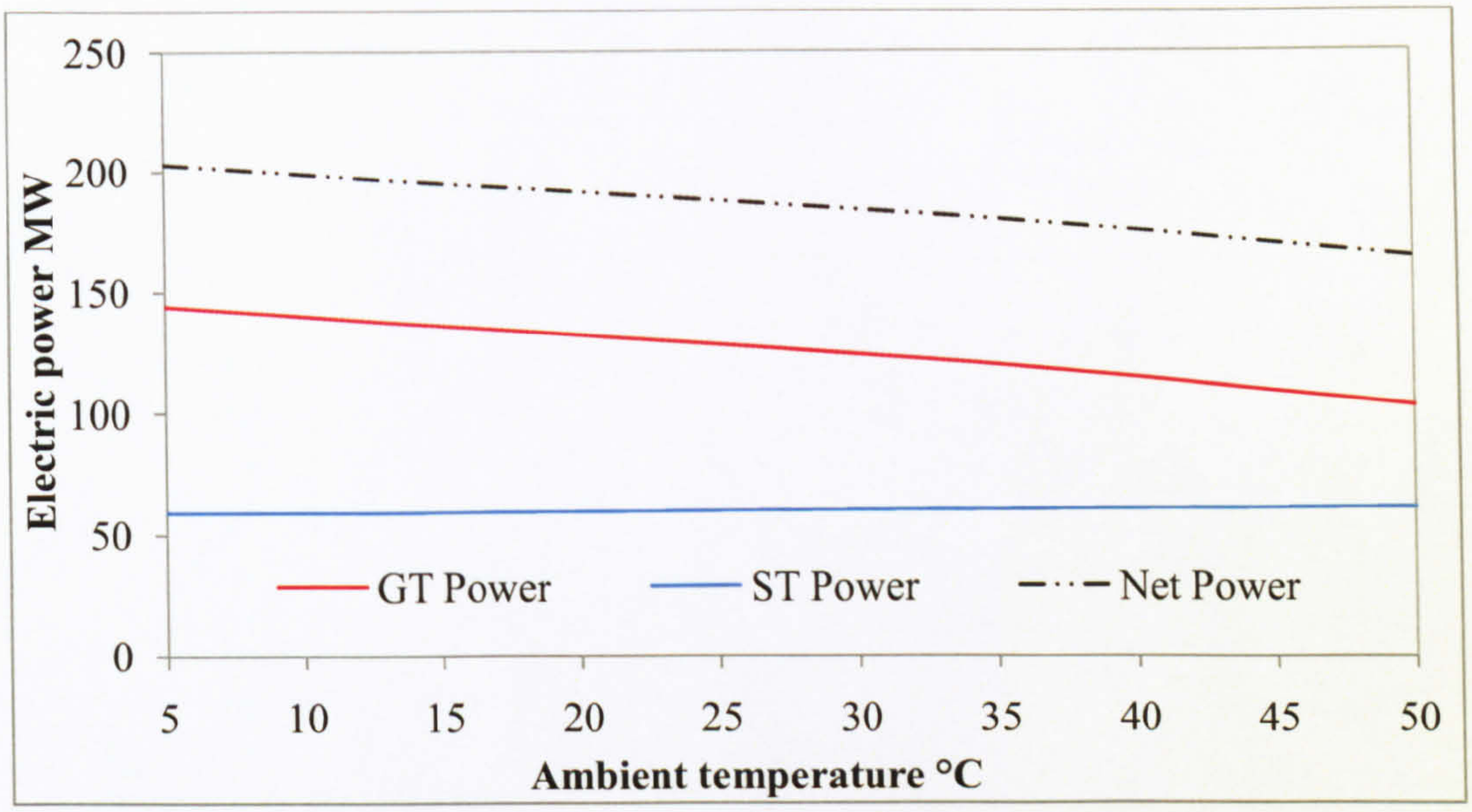

Figure 4-10 Power plant's electric power versus ambient temperature

The steam turbine benefited from the increase in the exhaust gases temperature (Figure 4–11), where its output power increased slightly by 0.31% for each 5°C increase in the ambient air temperature. Figure 4-11 shows an increase in the CO_2 emission rate by 2.37% for each 5°C increase in the ambient air temperature as a result of the reduction in the plant's total output power by 2.4%.

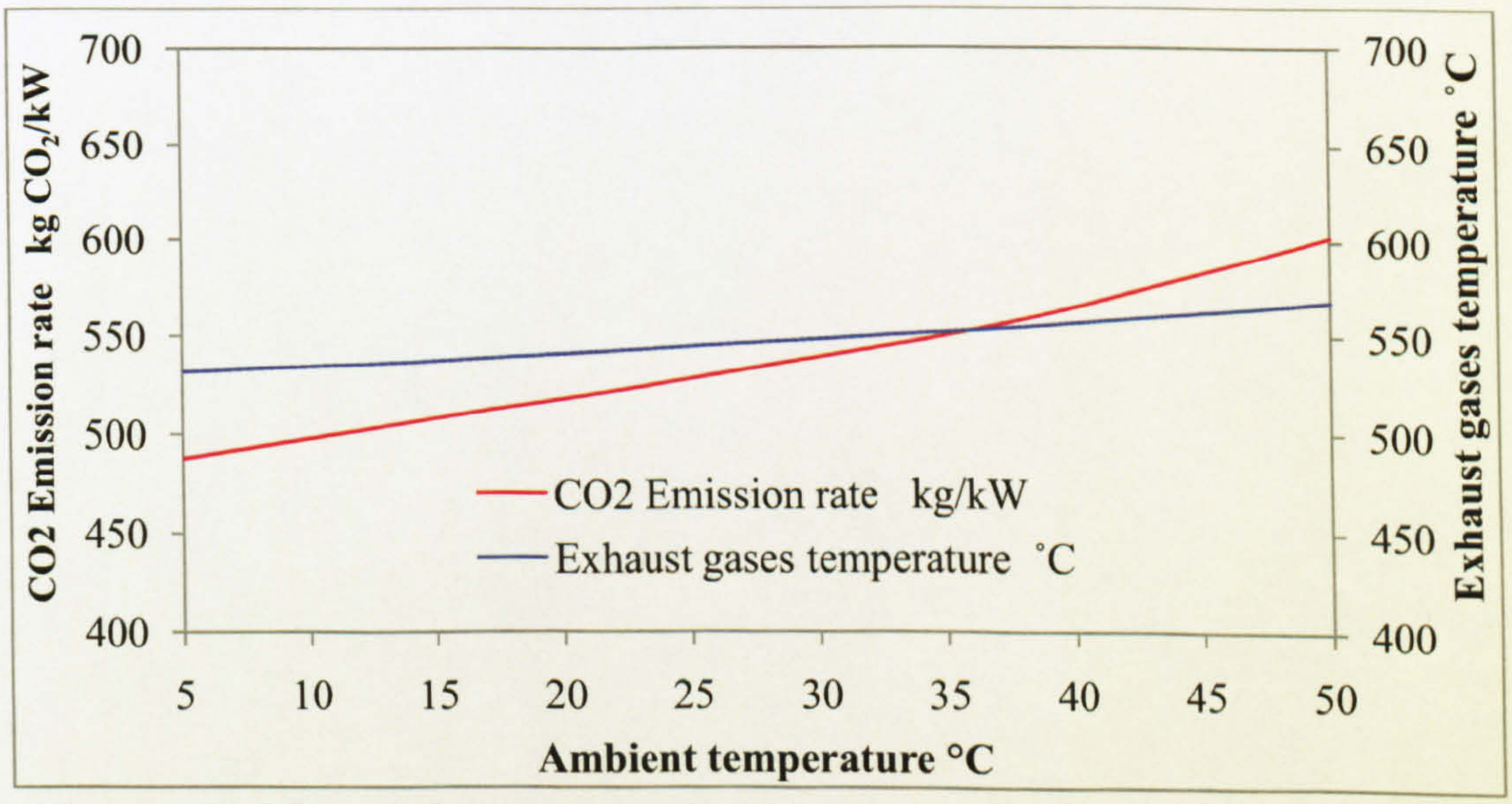

Figure 4-11 CO_2 emission rate and exhaust temperature versus ambient temperature

The effect of the ambient air temperature variation on the plant's total exergy destruction was found to be mainly caused by the gas turbine. Figure 4–12 shows the most significant results of

the plant's component exergy destruction. The gas turbine exergy destruction increase was mainly produced by the reduction in its output power.

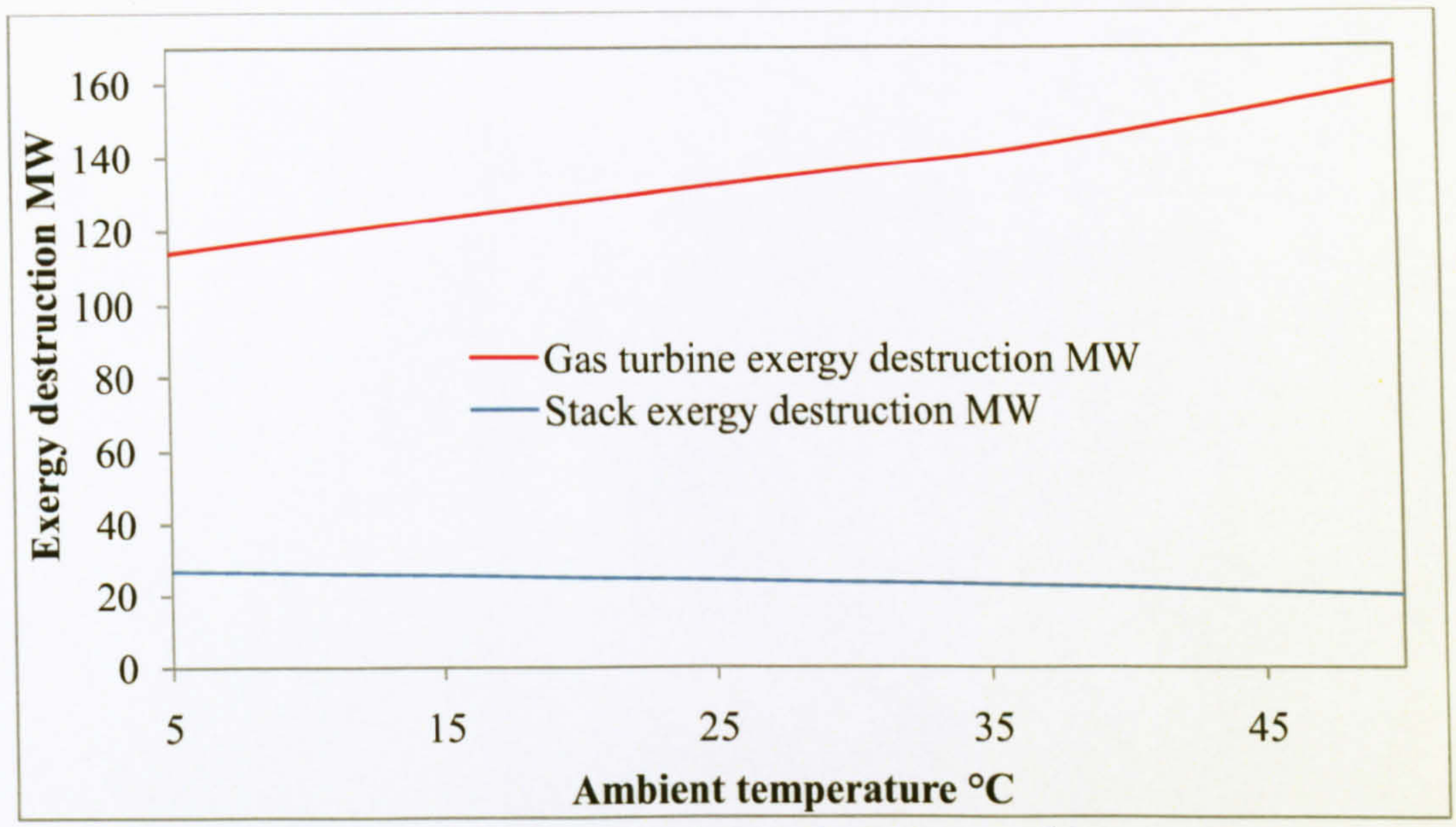

Figure 4-12 GT and stack exergy destruction versus ambient temperature

The stack exergy destruction (Figure 4–12) was reduced due to the reduction in the mass flow rate of the compressor air intake, which is shown in Figure 4–9. The plant's overall energy and exergetic efficiency followed the gas turbine's efficiency as it was the largest energy and exergy consumer and producer component in the plant. Figure 4–13 indicates the inversely proportional relationship between the ambient air temperature and the plant and its components energy and exergy relative efficiency. The HRSG and steam turbine performed steadily under the variation in the ambient temperature, whilst the gas turbine relative exergetic efficiency was inversely propositional to the increase in the ambient temperature. These results were in agreement with what have been reported in the literature [28–48].

The relative humidity was the other parameter that was investigated, even though most of what has been reported in the literature indicates that the humidity affect on the plant is insignificant and ignorable [29, 34]. As presented in the previous chapter Yanbu city's mean relative humidity varied from a minimum value of 4.7% to a maximum value of 100% over the period of time from 1985 to 2008. The mean humidity value was in the range of 50% to 60%. Thus a variation in the relative humidity value from 4% to 100% was introduced to the modelled plant while monitoring its performance.

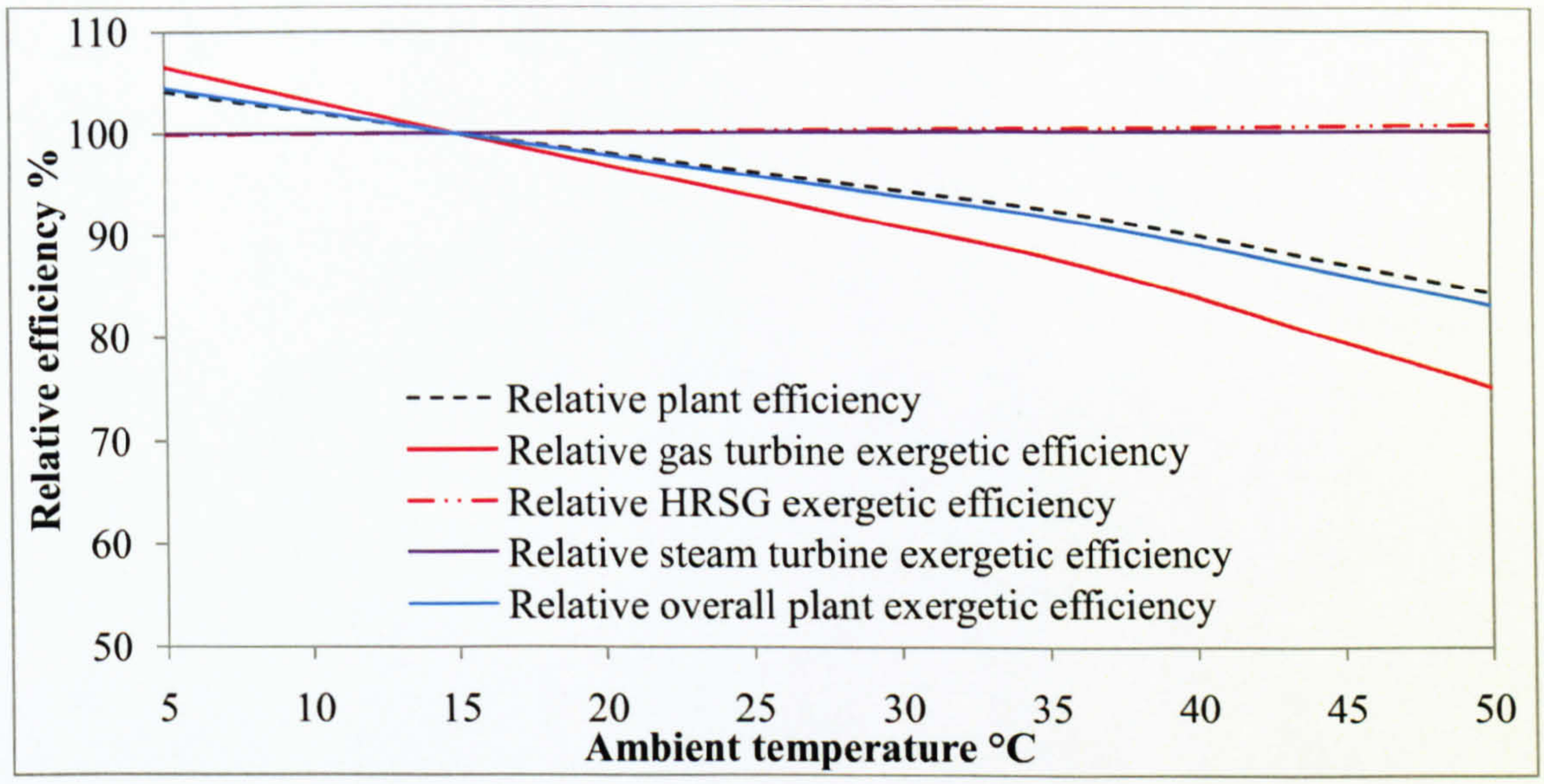

Figure 4-13 Power plant's efficiency versus ambient temperature

The study was performed in ISO conditions with the gas turbine operated at full load and the steam condenser cooling water at a temperature of 22°C. The increase in the air relative humidity increased the water content in the working medium of the plant, which reduced the enthalpy drop through the gas turbine, leaving more exhaust energy for utilization in the HRSG [29]. This is shown in Figure 4–14, which shows the relative exhaust gas enthalpy and entropy versus the relative humidity.

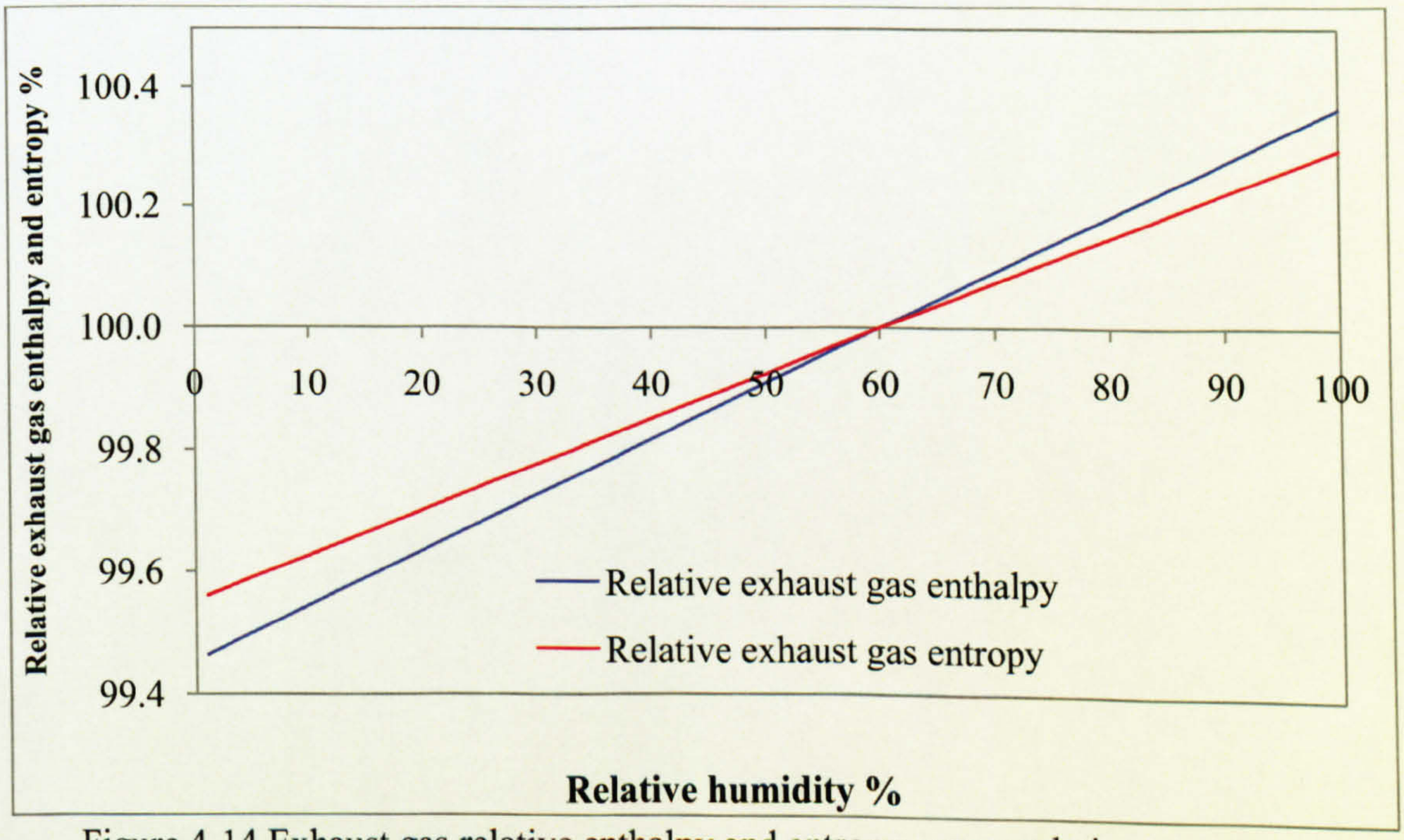

Figure 4-14 Exhaust gas relative enthalpy and entropy versus relative temperature

The relationship between the relative humidity and the exhaust gas stream enthalpy and entropy was almost linear on a normal scale graph. However, the scale was reduced to clarify this effect, which only took place with 1%. Increasing the relative humidity from 1% to 100% would have increased the enthalpy and entropy of the exhaust gas stream by 5.28kJ/kg, and 0.06kJ/kg K respectively. These finding justified the effect of the relative humidity variation on other performance parameters, which was also insignificant. All the results are presented in Table 5 in Appendix C. The increase in the exhaust gas stream energy insignificantly increased the plant's total output power by 558kW when the relative humidity increased from 1% to 100% as shown in Figure 4–15. Figure 4–15 also shows the plant's overall energy and exergetic efficiency versus the relative humidity. The increase in both of them was less than 0.2% over the whole range of relative humidity change. Moreover, it was mainly driven by the increase in the output power of the steam turbine.

As mentioned earlier the effect of the relative humidity on the power plant was insignificant and can be ignored as reported in the literature [29].

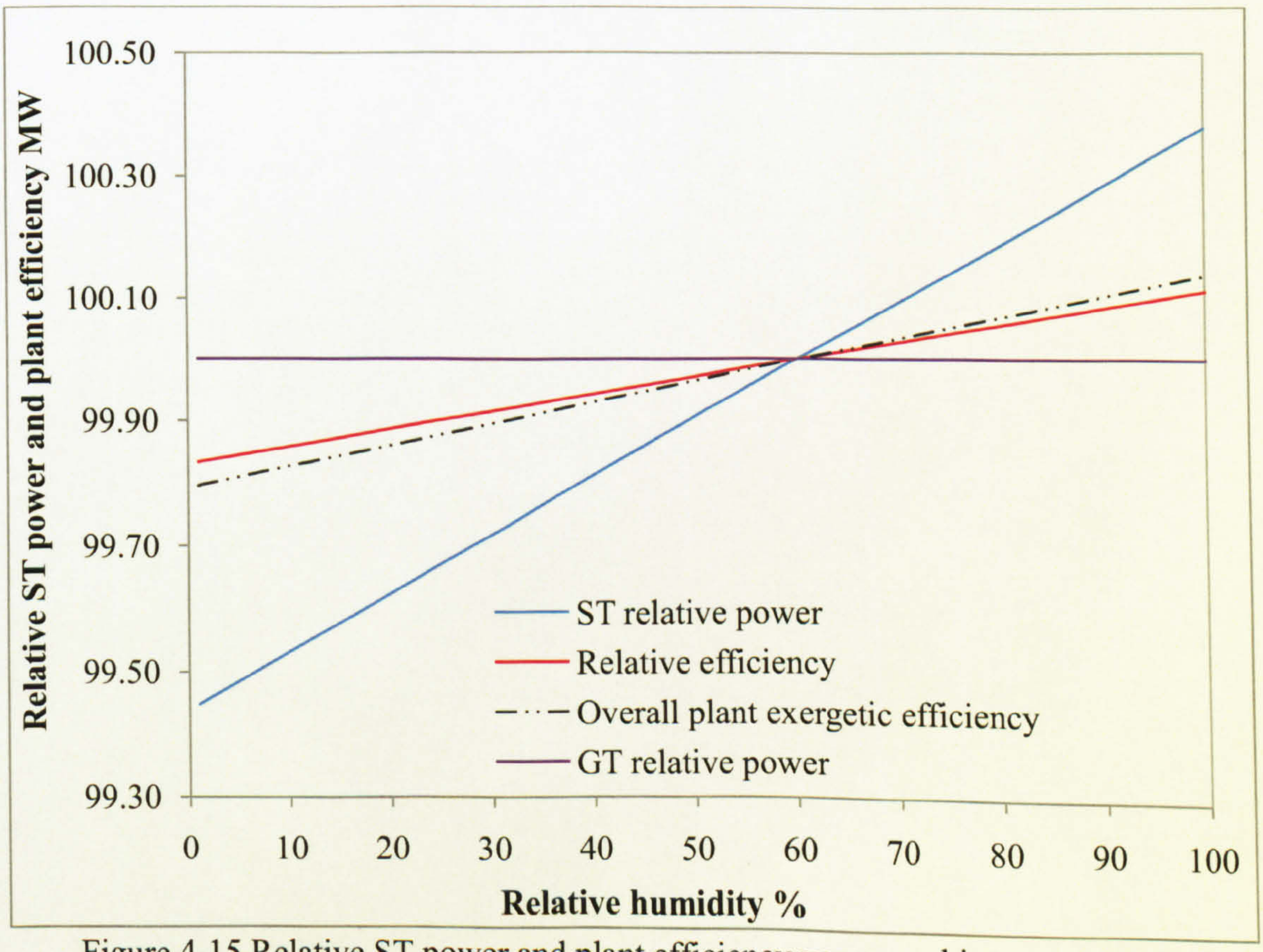

Figure 4-15 Relative ST power and plant efficiency versus ambient temperature

4.3 MED Desalination Plant

Any thermal desalination plant is applicable to this study; however, the multi-effect distillation (MED) desalination technology was chosen as it can be operated totally with low-grade waste heat energy. Based on a maximum typical heat consumption value of 390kJ/kg for the MED desalination plant and a boiler typical effectiveness value of 0.8 [118, 119], the modelled gas turbine was able to produce 43,000 m^3 of potable water per day. Therefore, a 40,000m^3/day MED desalination plant model was designed based on data obtained from IDE Technologies Ltd. The main components of the MED desalination plant, as shown in Figure 4–16, were single-effect distillation cells (evaporators), a condenser and pumps.

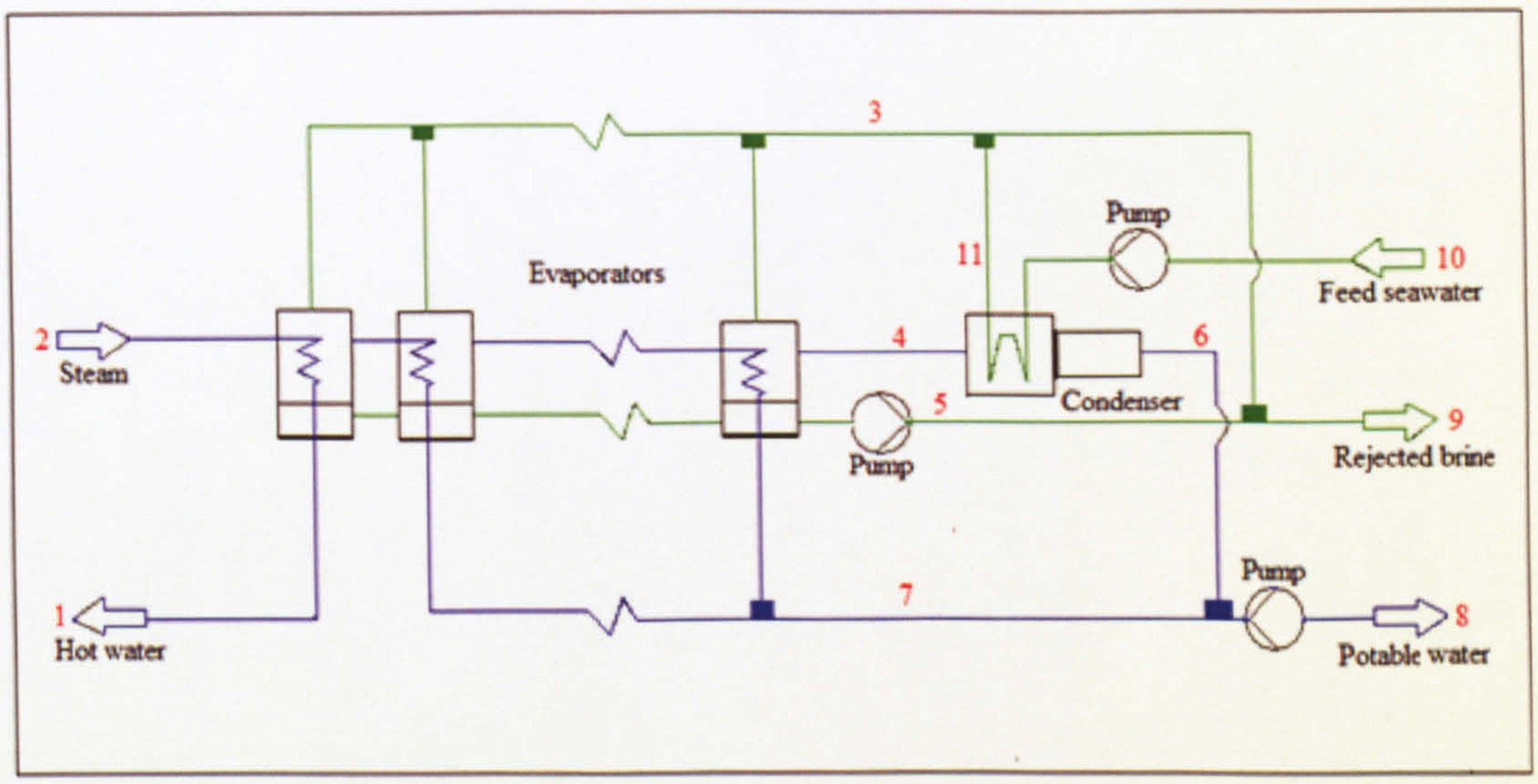

Figure 4-16 Multi-effect desalination plant model

The number of effects was defined mainly by the real MED model data and validated by a parametric study that investigated the performance of the model against varying the number of effects from two to ten The study was performed for a seawater temperature of 22C° and salinity of 0.04kg/kg according to the Red Sea oceanography data that was presented in the previous chapter, and for a constant potable water production rate of 40,000m^3/day. The results are listed in Table 6 in Appendix C, while the most significant results are plotted and discussed here. One of the MED desalination's advantages over other technology is that its thermal performance can be improved by adding more effects, which will improve the gain output ratio (GOR) and reduce the specific heat consumption [64, 68]. Figure 4–17 shows the desalination plant's GOR versus

the number of effects. For each extra effect, the GOR would have improved on average by 20.8% as a result of the reduction in the input heat energy required to produce the 40,000m^3/day on average by 16.4% for each an additional effect as seen in Figure 4–17. The reduction in the input heat energy was due to the increase in the total heat transfer area, as each effect had the ability to evaporate a portion of the feed seawater. Adding an extra effect that had a lower pressure made it possible for the rejected brine to be evaporated once more using the heat energy in the steam produced from the previous effect.

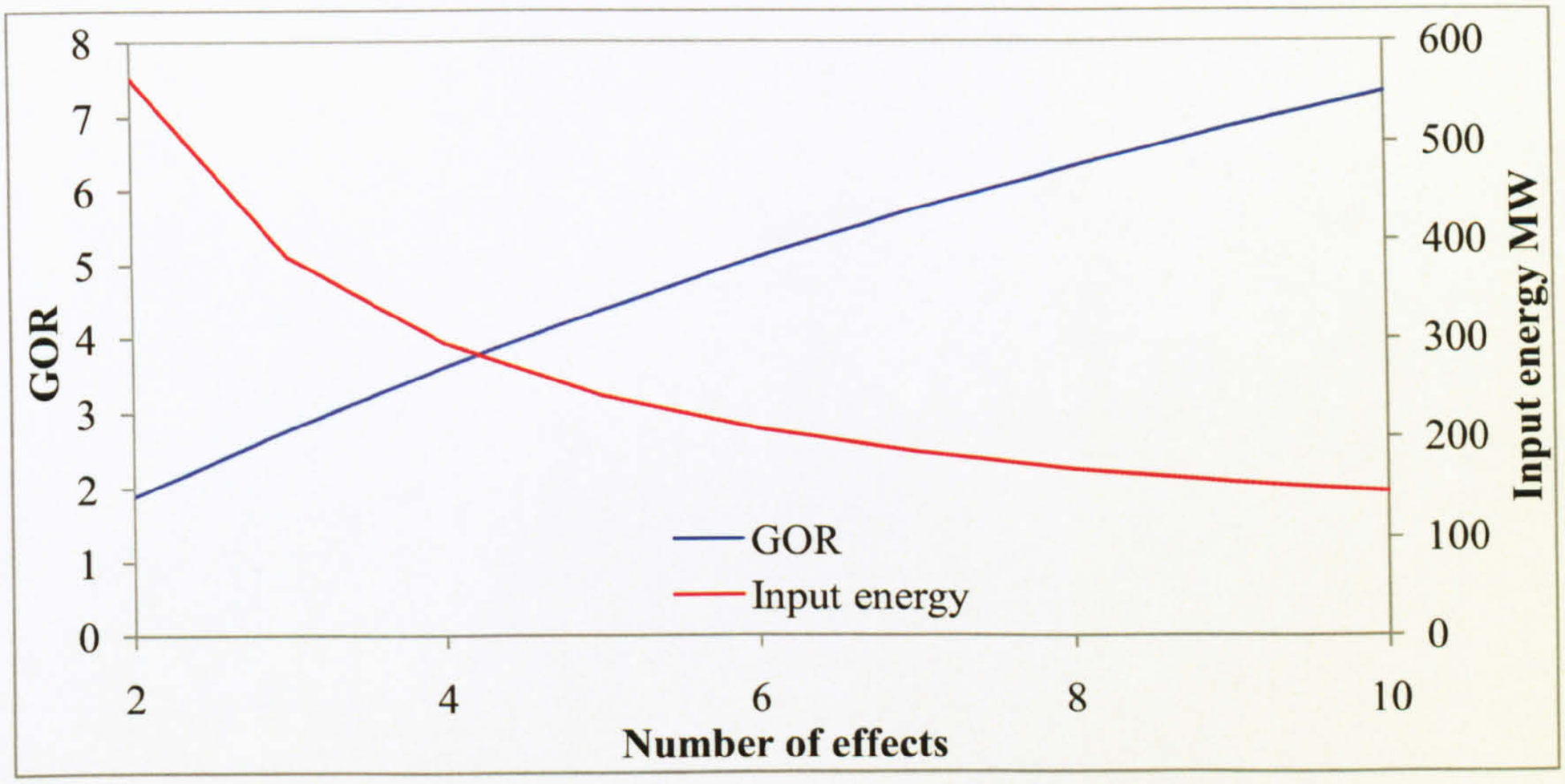

Figure 4-17 GOR and input energy versus number of effects

Figure 4–18 shows a reduction in the MED model's specific heat consumption with the increase in the number of effects. The plant's concentration factor increased slightly by 0.2% for each extra effect as a result of the increase in the rejected brine water concentration due to the further evaporation that took place in the additional effect. All these results were in agreement with those reported in the literature [126, 127]. In conclusion, the number of effects defined by the real model as ten effects was found to be the optimum number of effects for this plant.

Assuming that the seawater salinity was 0.04kg/kg and it had a temperature of 22°C the MED desalination modelled plant consumed 318.5kJ/kg of heat energy to produce 40,000m^3/day of potable water at a concentration factor of 1.6, and a gain output ratio (GOR) of 7.32. The modelled plant consumed 291kW of electricity to drive three pumps at the seawater feed and drain, as well as at the potable water sink. The effectiveness-NTU was used to ensure an

economical size of the condenser; it was designed with an effectiveness value of 0.8 and 1.83 NTU, which is in agreement with the literature [118, 119]

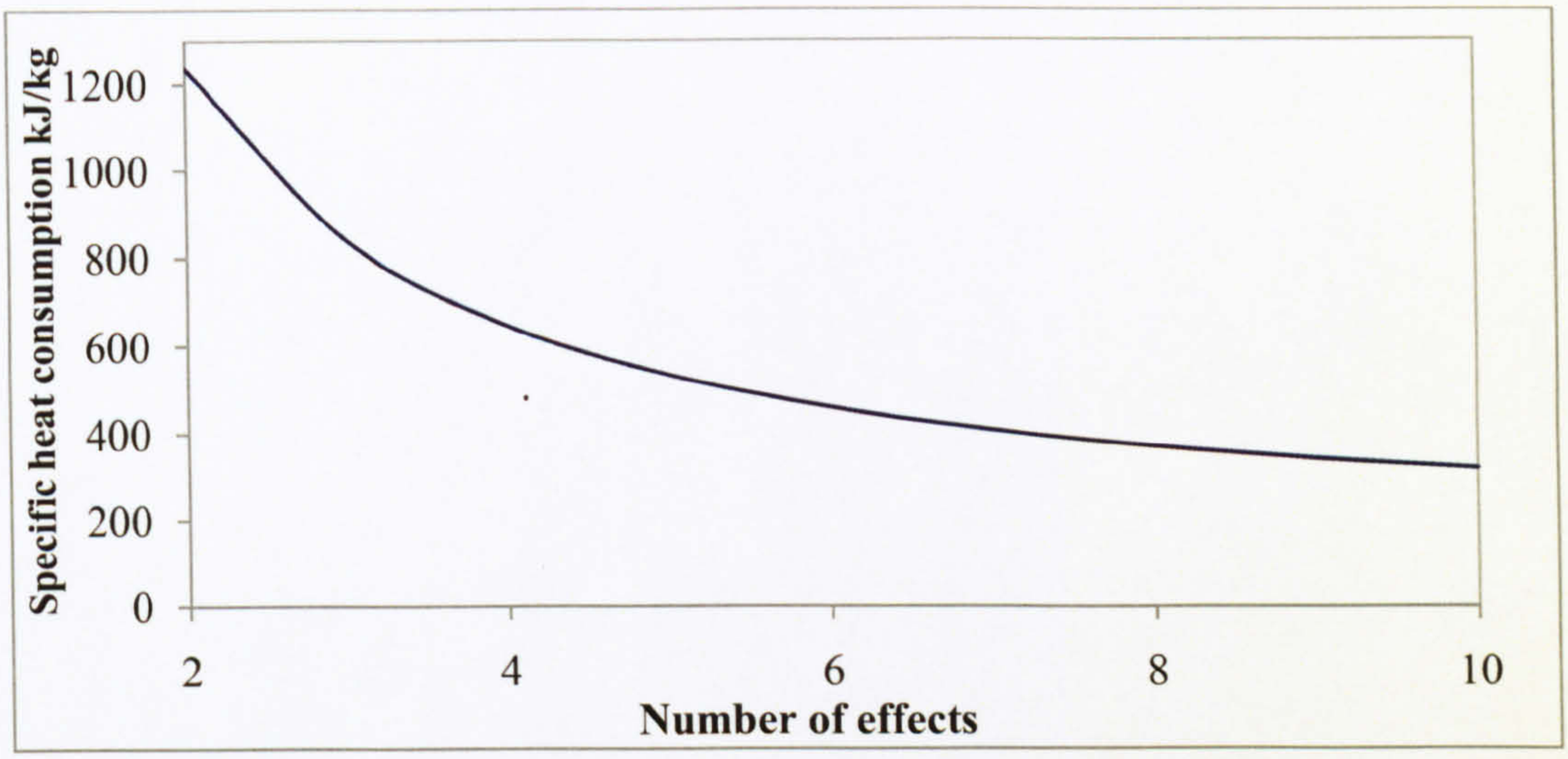

Figure 4-18 Specific heat consumption versus number of effects

Based on second law analysis the specific exergy and exergy was calculated for each stream in the model to calculate the exergy destruction in the evaporators as one unit and in the condenser. Firstly, the enthalpy and entropy of each seawater and brine water stream were calculated according to the methodology presented in the previous chapter. The salt reference conditions were taken to be at a temperature 15°C and a pressure of 1.013 bar, where the enthalpy and entropy of salt in these conditions were h = 12.552kJ/kg, and s = 0.04473kJ/kgK respectively.

Table 4–3 lists all the exergy and specific exergy results for each stream as numbered in Figure 4–16. Both rejected brine streams, 5 and 9, had positive exergy unlike in the results of some similar studies [106–109] in which the brine water had a negative exergy. It was justified by the fact that the salt concentration was higher than that of the reference conditions, which meant that this brine stream required energy in order to dilute its concentration to bring it to the reference condition concentration. However, the change in the brine water stream's exergy was a function of both its salinity and temperature; while the increase in its salinity reduced its exergy the increase in its temperature increased it. In this study the exergies of both brine streams were positive due to the fact that the chosen reference condition was 15°C which is low in comparison with similar studies. For example, Kahrman, et al. [107] used a reference condition of 35°C. This made the change in exergy due to the temperature increase higher than that due to the increase of

salinity, and the sum of both generated positive exergy. Table 7 in Appendix C lists all the seawater and brine water entropy and enthalpy calculation results. The ten evaporators' exergy destruction values were calculated as follows based on the exergy balance presented in the previous chapter:

$$E_{D,Eva} = \dot{m}_2 \times (e_2 - e_1) + e_3 \times \dot{m}_3 - e_7 \times \dot{m}_7 - e_4 \times \dot{m}_4 - e_5 \times \dot{m}_5 + \dot{W}_{pump,5}$$

while the condenser exergy destruction was calculated as follows:

$$E_{D,Cond} = \dot{m}_{10} \times (e_{10} - e_{11}) + \dot{m}_4 \times (e_4 - e_6) + \dot{W}_{pump,10}$$

Point	Stream	e (kJ/kg)	E (MW)
1	Water	19.80	1.23
2	Steam	396.45	24.66
3	Seawater	5.88	5.76
4	Water	262.47	11.29
5	Brine	4.34	2.27
6	Water	7.16	0.31
7	Water	14.49	5.97
8	Water	13.87	6.31
9	Brine	4.65	3.19
10	Seawater	0.33	0.38
11	Seawater	5.88	6.71

Table 4-3 MED model's exergy and specific exergy results

The results show that the evaporators consumed 33% of the total exergy input to the plant and this represented 76.51% of the plant's total exergy destruction with an exergy destruction of 9.65MW. This significant amount of exergy destroyed in the evaporators was mainly due to the heat transfer process, especially in the first effect, which dealt with the maximum heat energy input. The pressure drop from one effect to the other was also a source of the evaporators' irreversibility, as well as the destruction caused by the pump [90]. The condenser consumed 15.65% of the total exergy input into the plant and formed 32.73% of the plant's total exergy destruction with an exergy destruction of 4.57MW. This exergy destruction in the condenser was mainly due to the heat transfer process. The plant operated at an overall exegetic efficiency of 39.42% and caused a total exergy destruction of 14.22MW. This performance was acceptable and in agreement with that published in the literature [85, 90, 92].

The off-design performance of the plant was investigated based on the first and second laws of thermodynamics. Firstly, the effect of the seawater temperature variation on the plant's performance was examined by a parametric study that varied the seawater temperature from 20°C to 28°C with a seawater salinity of 0.04kg/kg. All the results are presented in Table 8 in Appendix C, while the most significant results are plotted and discussed here. Figure 4–19 shows an increase in the GOR of the modelled MED plant with the increase in the seawater temperature as a result of the reduction in the input heat energy source mass flow rate.

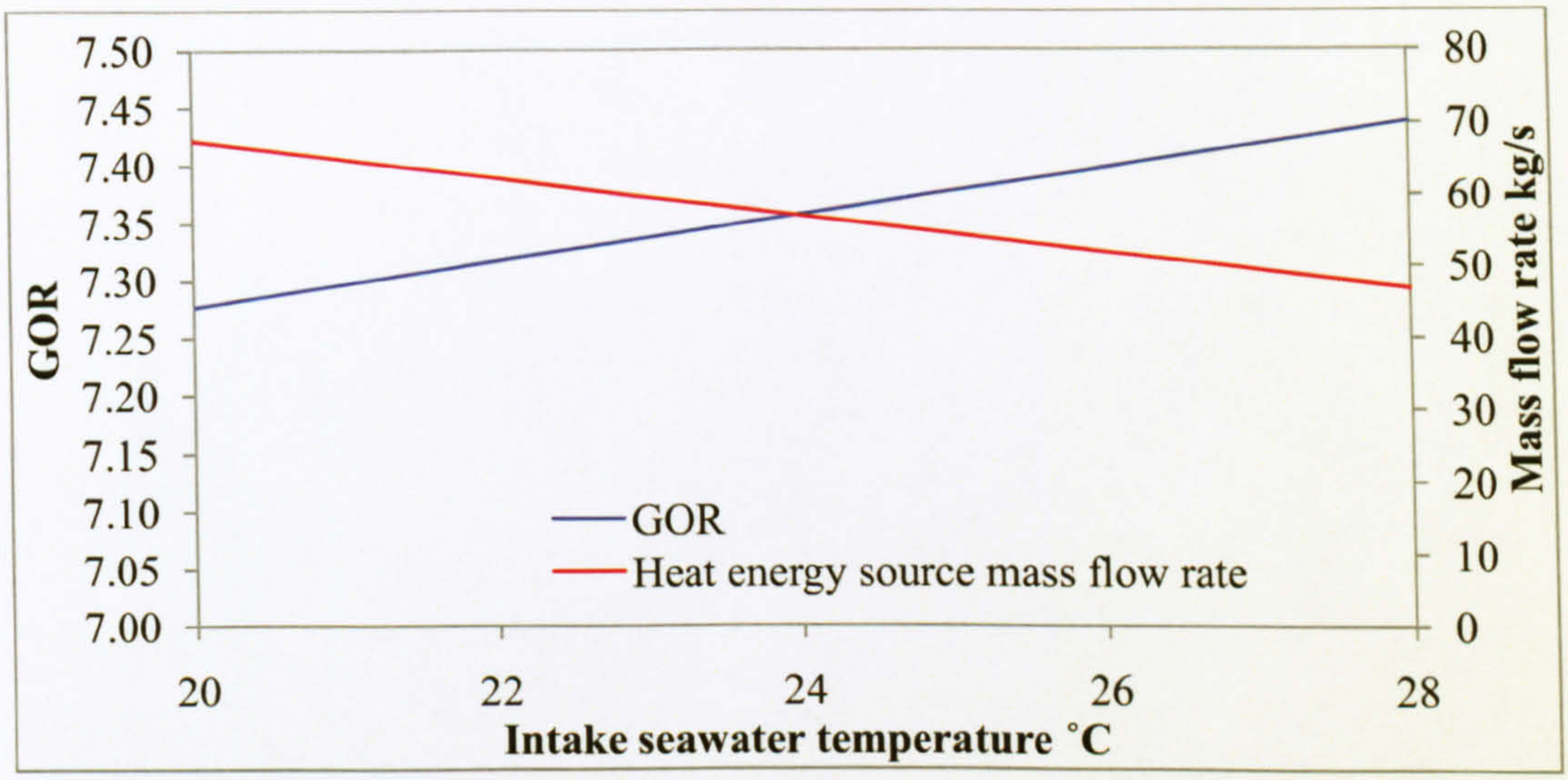

Figure 4-19 GOR and heat energy mass flow rate versus seawater temperature

This was due to the fact that less heat energy was required in the first effect in order to increase the seawater temperature to boiling point, at which it evaporates; the heat transfer in the first effect was reduced on average by 8.6% for each 2°C increase in the intake seawater temperature. This response to the intake seawater temperature variation is in agreement with what has been published by Alasfour, et al. [126] and many others. The plant's specific heat consumption decreased on average by 1.76kJ/kg for each 2°C increase in the intake seawater temperature driven by the reduction in the heat transfer in the first effect. The heat transfer in the first effect declined by 8.6% as a result of the increase in the intake seawater temperature, which required less input heat to evaporate it. Figure 4–20 shows the effect of the seawater temperature variation on both the specific heat consumption and the heat transfer in the first effect. The exergy destroyed in the condenser tended to decline on average by 6.5% for each 2°C increase in the intake seawater temperature. This was because of the increase in the condenser input exergy while its output exergy did not change.

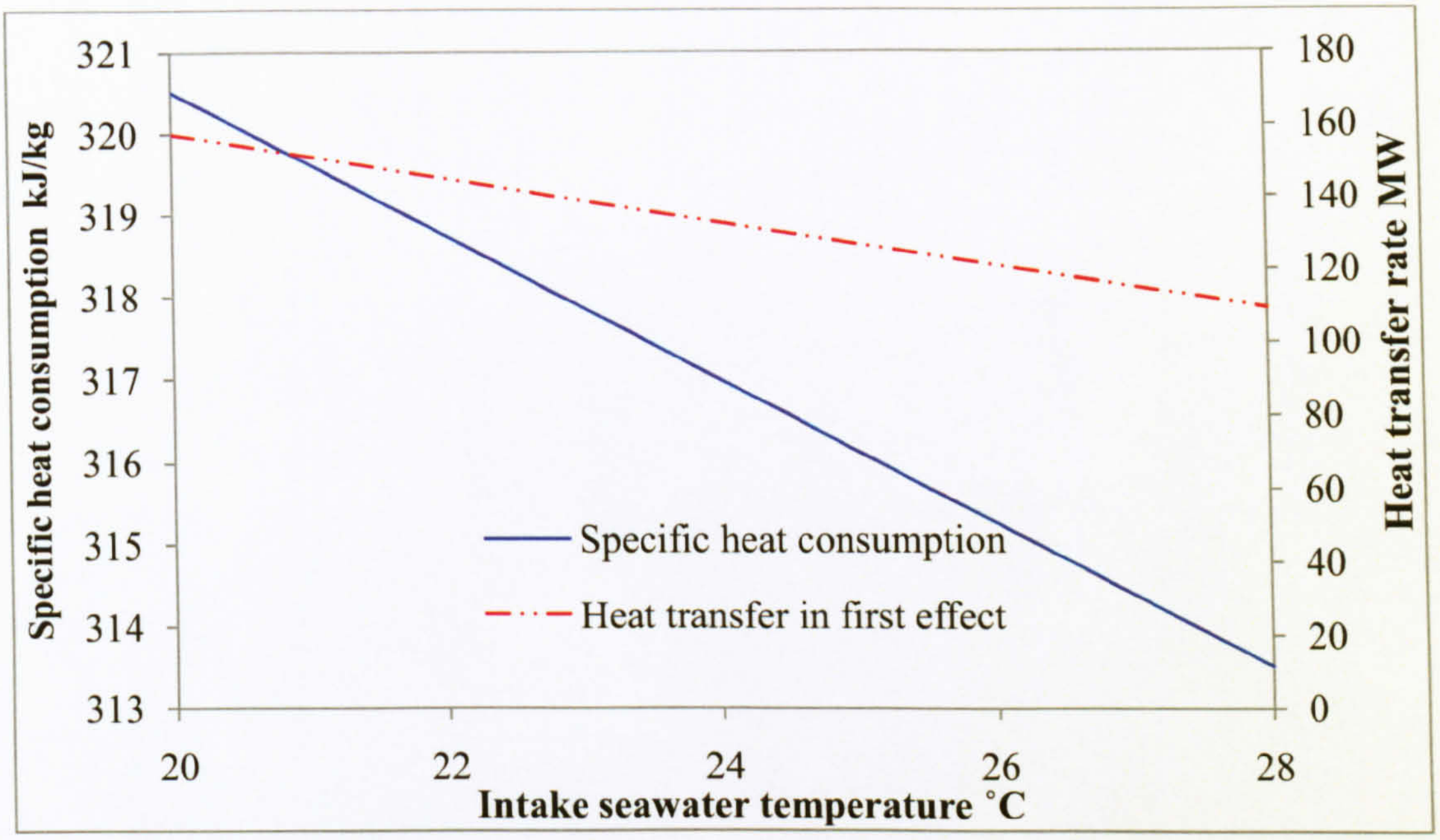

Figure 4-20 Specific heat consumption and heat transfer rate versus intake seawater temperature

The evaporators' exergy destruction increased insignificantly on average by 1.1% for each 2ºC increase in the intake seawater temperature, due to the reduction in input heat energy as shown in Figure 4–21. The plant's exergetic efficiency responded to the condenser's exergy destruction reduction with an increase on average by 15% for each 2ºC increase in the intake seawater temperature as seen in Figure 4–21.

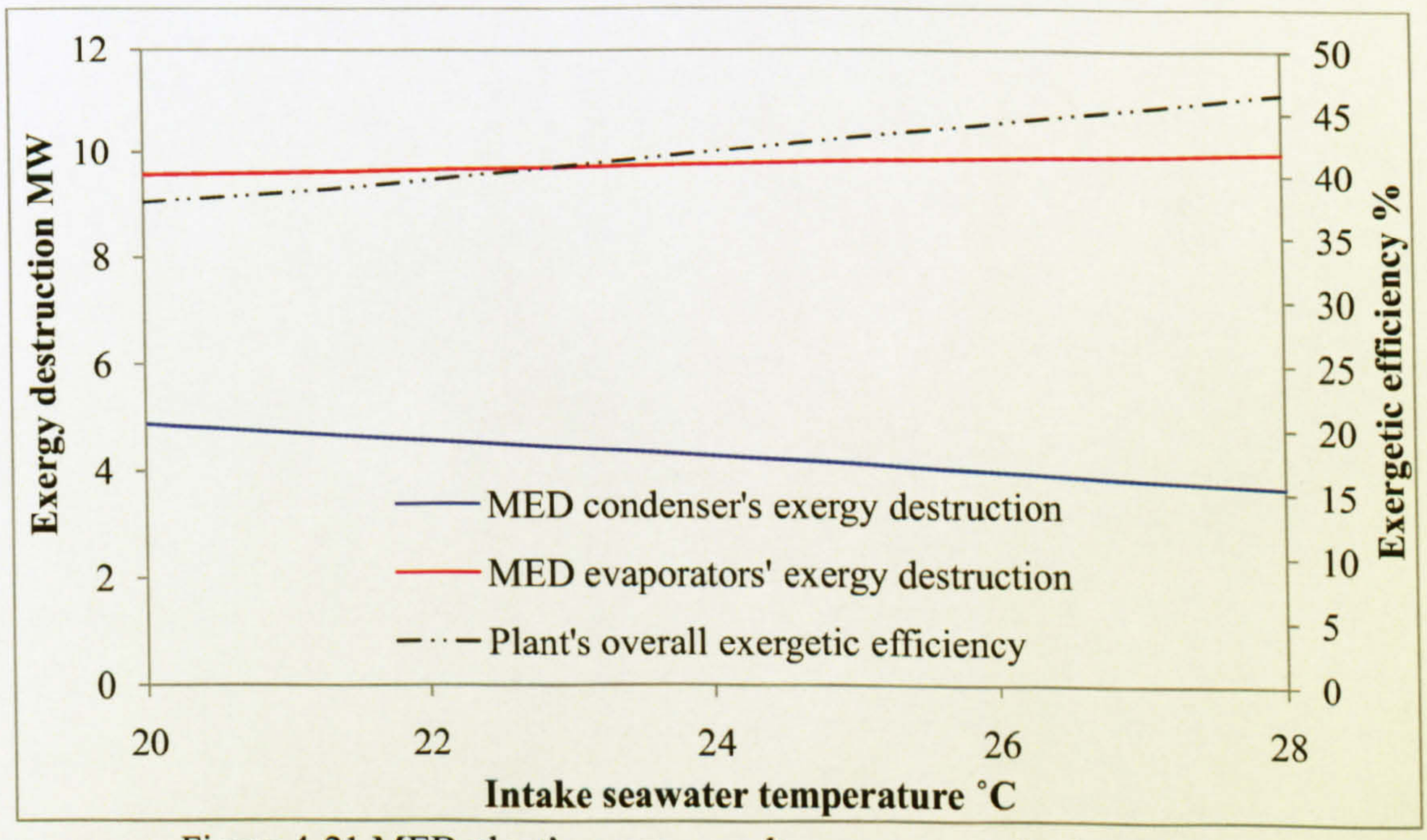

Figure 4-21 MED plant's exergy results versus seawater temperature

The second parametric study investigated the MED plant's model performance under varying input heat energy temperatures ranging from 50°C to 150°C. All the results of this study are listed in Table 9 in Appendix C. One of the advantages of the MED desalination plant over the other thermal desalination technologies is the fact that it can be operated with low-grade heat energy. This helps minimizes the potential for fouling of the pipes corrosion; however, it requires a bigger heat transfer area [7]. Figure 4–22 indicates that the GOR of the modelled plant declined as the input heat energy temperature increased as a result of the increase in the input heat energy mass flow rate on average by 1.2% for each 10°C increase in the input energy temperature due to the reduction in the first-effect heat transfer area.

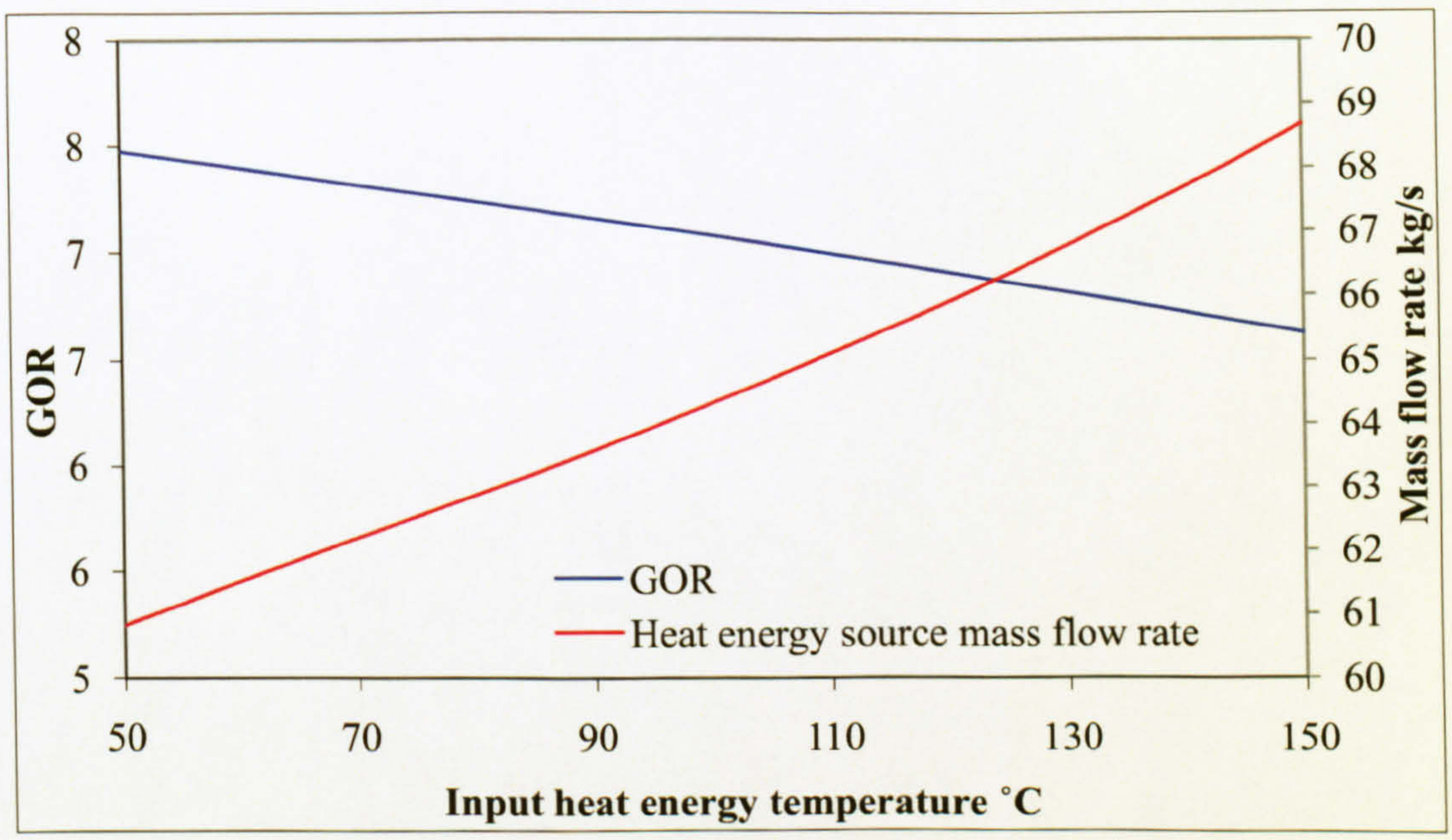

Figure 4-22 GOR and heat energy mass flow rate versus input heat temperature

On the basis of the second law analysis, Figure 4–23 shows the exergy destruction in the evaporators and the MED plant's exergetic efficiency against the increase in the input heat energy temperature. The condenser's exergy destruction was not affected by the increase in the input heat energy temperature; therefore, the drop in the plant's exergetic efficiency on average by 8.5% for each 10 °C increase in the input energy temperature was mainly caused by the increase in the evaporators' exergy destruction. The increase in the evaporators' exergy destruction was on average 31.3% for each 10°C increase in the input energy temperature. This significant increase in the evaporator's' exergy destruction was mostly generated from the first effect which received the extra heat energy.

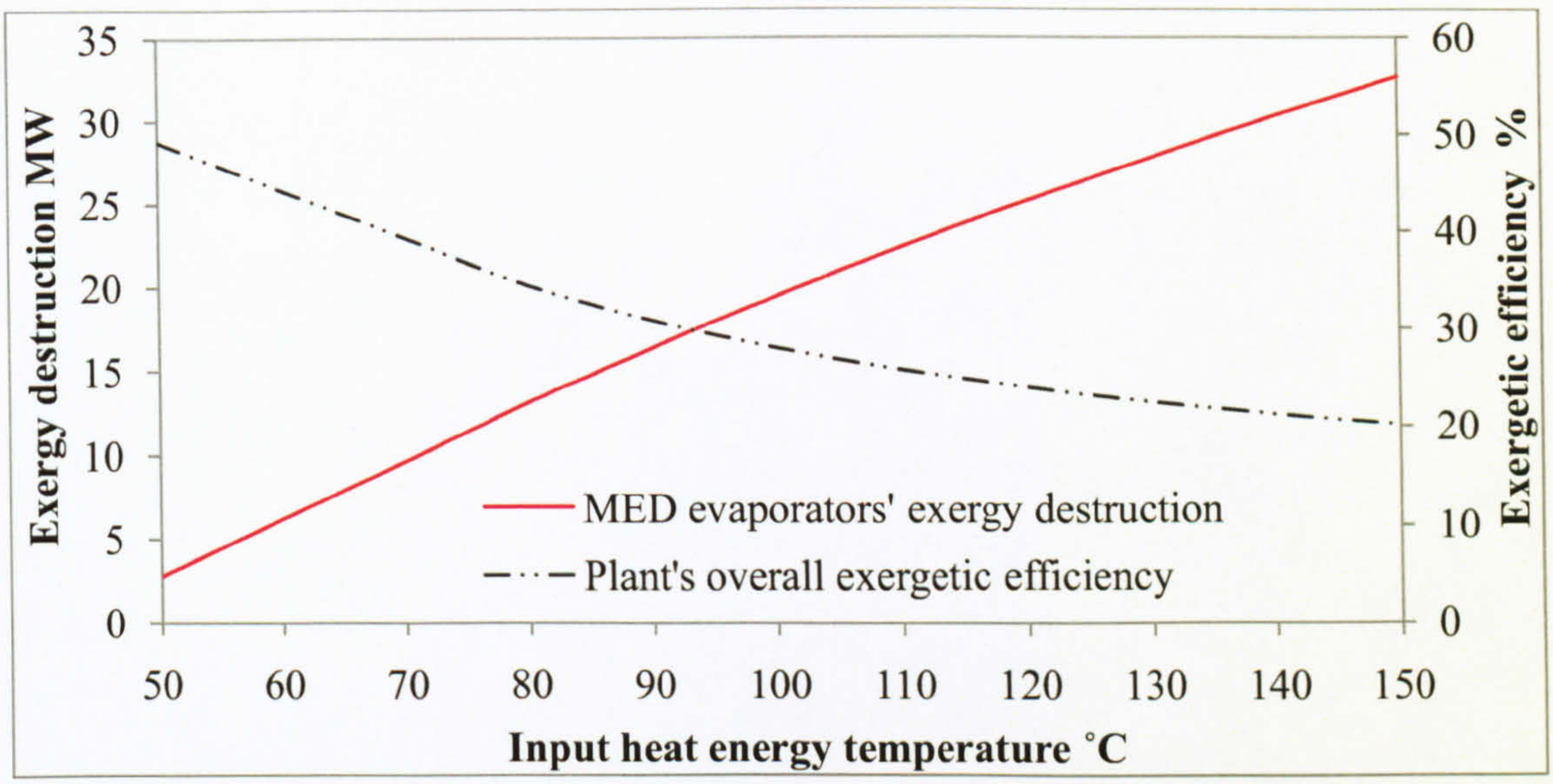

Figure 4-23 MED exergy analysis results versus input heat temperature

The third parametric study investigated the MED desalination plant's model performance under varying seawater salinity ranging from 0.036kg/kg to 0.045kg/kg at a seawater temperature of 22°C. All the results are listed in Table 10 in Appendix C. Figure 4–24 shows an insignificant reduction in the model GOR as a result of increasing the plant's specific heat consumption. The increase in seawater salinity reduced its enthalpy and entropy. Thus, it required additional heat energy in order to evaporate at the specified pressure in each effect. Therefore, this would have led to an increase in the input heat energy, which reduced the GOR and increased the model's specific heat consumption.

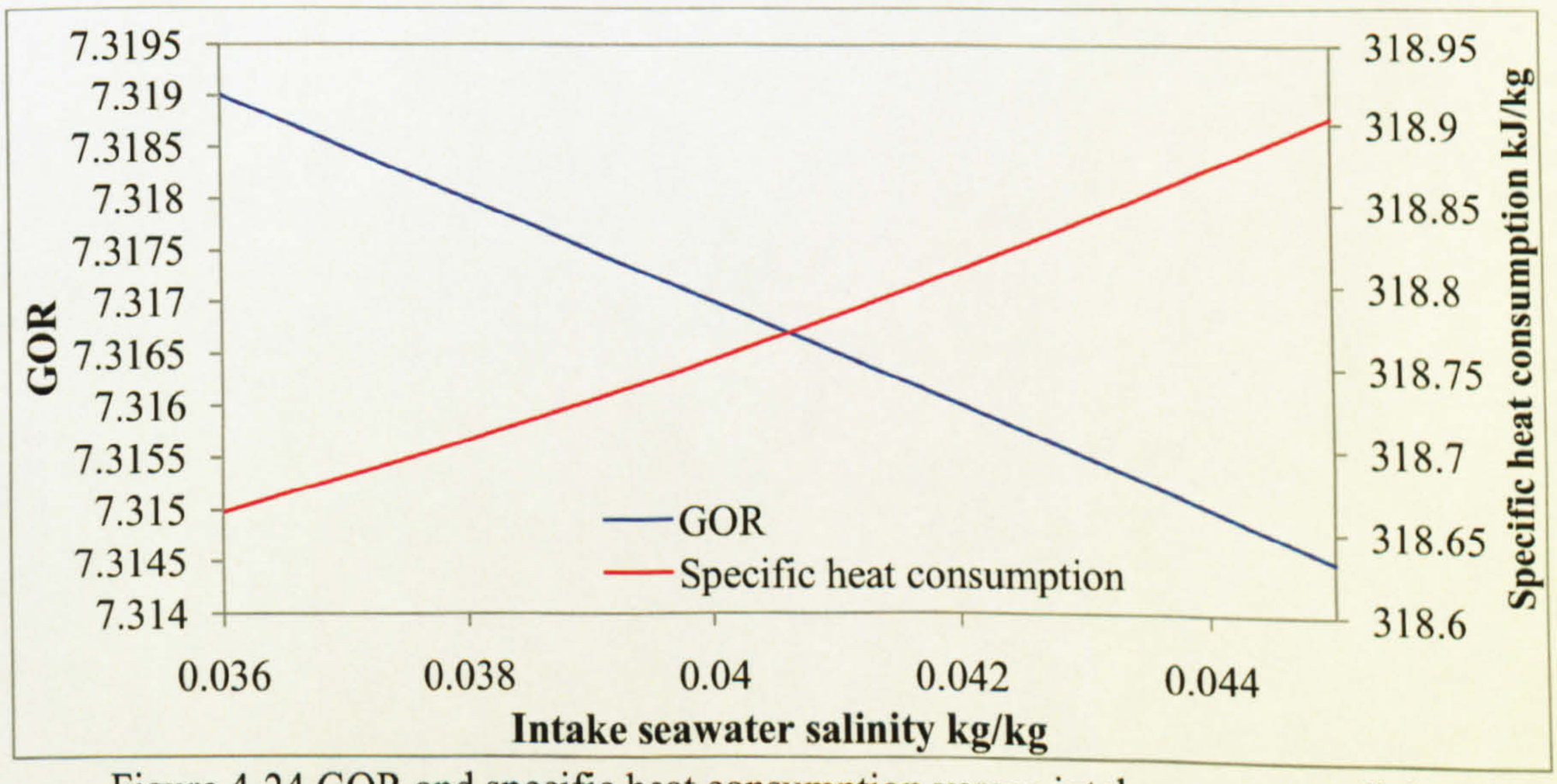

Figure 4-24 GOR and specific heat consumption versus intake seawater salinity

It was noticed that the exergy destruction in the evaporators increased with the increase in the seawater salinity, while the condenser's exergy destruction was almost constant. The increase in the input heat energy caused an increase in the evaporators' exergy destruction, which affected the overall exergetic efficiency of the model. The model exergetic response to the seawater salinity was very small and insignificant as can be seen in Figure 4-25.

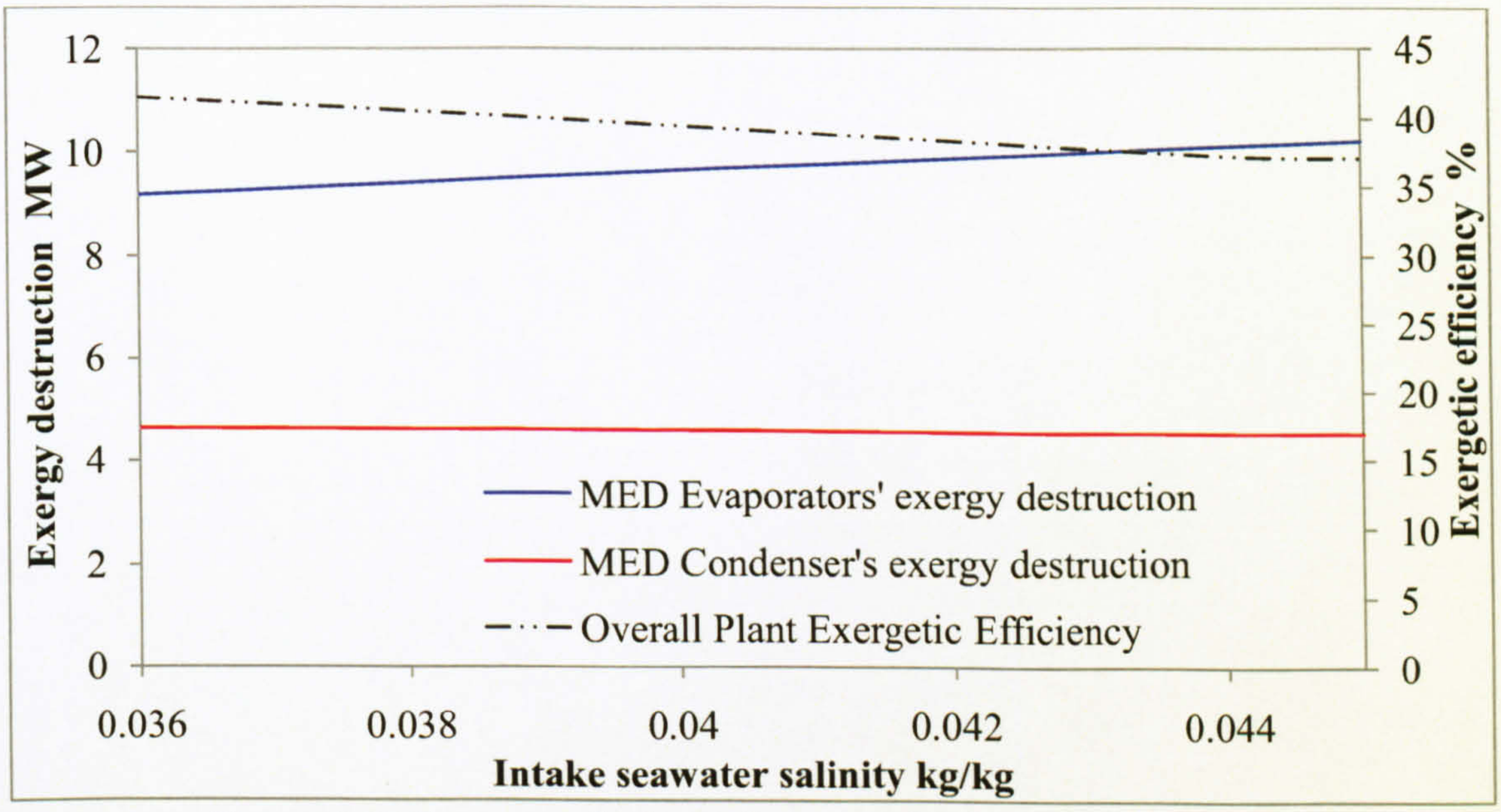

Figure 4-25 Exergy analysis results versus intake seawater salinity

4.4 TVC-MED Desalination

The thermal vapour compression multi-effect distillation desalination plant (TVC-MED) is basically a MED desalination plant that is improved by a steam ejector. The steam ejector uses a high pressure steam (motive steam) that expands through the steam ejector's nozzle at high velocity. The high velocity steam entrains a suction low-pressure steam extracted from the low-pressure steam stream leaving the last effect in the MED plant. Both motive and suction steam are then forced into a mixing chamber at the end of the steam ejector and combined to power the MED brine heater. This process reduces the steam needed to power the MED plant and that increases its efficiency. The steam ejector was modelled according to the available suction steam pressure, and the required steam properties, namely pressure, mass flow and temperature. The steam pressure after the last effect in the MED plant was 0.12 bar, while the steam needed to drive the MED brine heater had to be 0.32 bar; the steam ejector's compression ratio C_R was then 2.66, based on the following definition:

$$C_R = \frac{P_{drain}}{P_{Suction}}$$

The suction steam pressure also defines the steam ejector's number of stages. According to Figure 4–26 such suction pressure can be utilized by a single-stage steam ejector, where 0.12 bar is equal to 90mmHg. The ratio of suction mass to motive mass is called the "entrainment ratio" and was set to the minimum possible value in order to achieve the best GOR. An entrainment ratio value of 0.11 was chosen and confirmed to be within the production range of Schutte and Koerting's steam ejector manufacturing company, as reported by El-Dessouky, et al. [128]. The isentropic compression and expansion efficiency was set to 80% and 85% respectively in accordance with Hegazy [129]. The evaporators and condenser were modelled exactly as the basic MED plant according to the real modelling data mentioned in the previous chapter. A parametric study that investigated the optimum number of effects confirmed a similar result to that performed for the MED plant. Ten effects were found to be the optimum number that ensured the highest GOR value and the lowest specific heat consumption value. All the results of this study are listed in Table 11 in Appendix C. Figure 4–27 shows the GOR and motive steam mass flow rate versus the number of effects. The highest value of the GOR was obtained at ten

effects, where it started to decline after this due to the increase in the motive steam mass flow rate by 2kg/s on average for each extra effect.

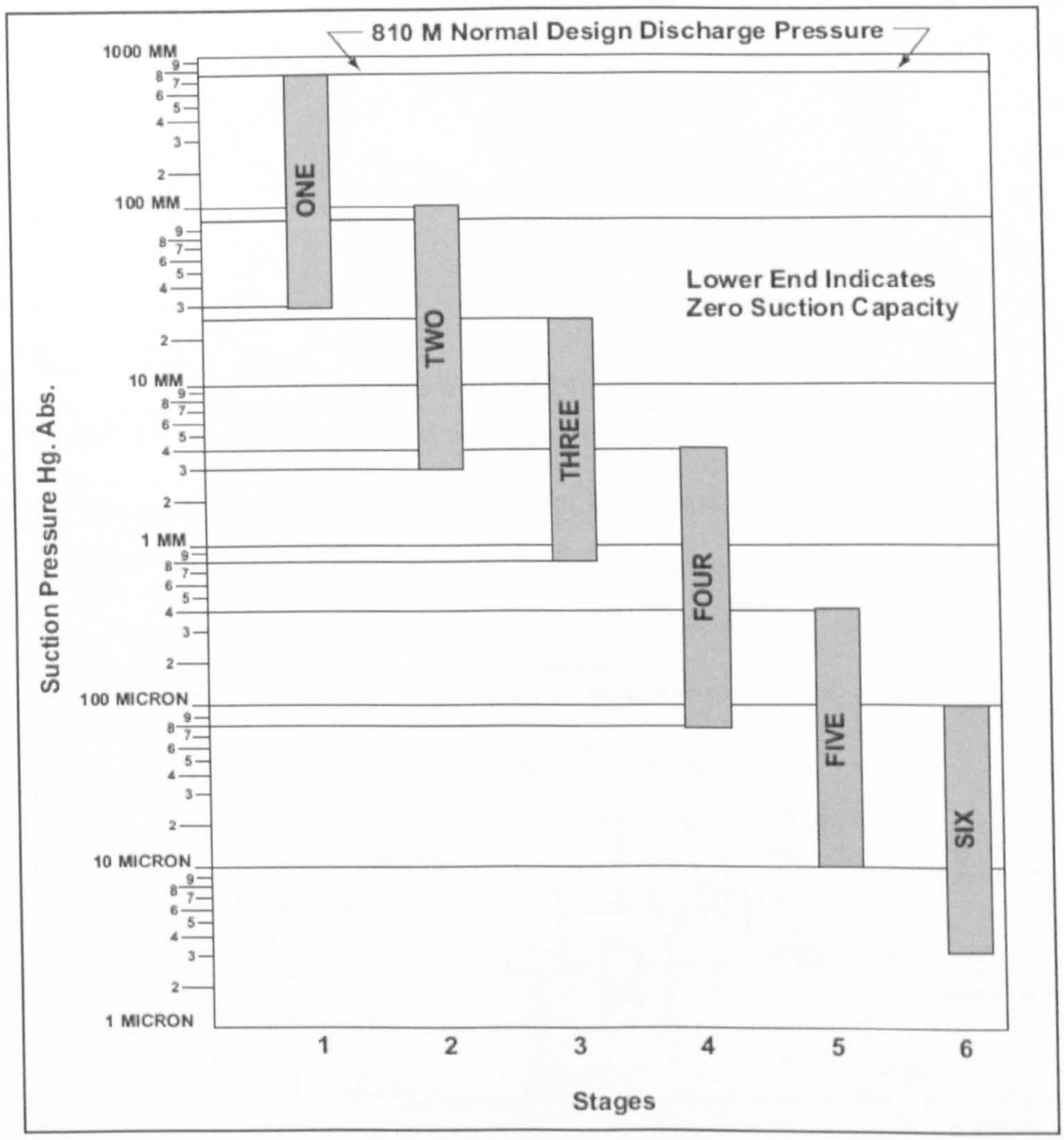

Figure 4-26 Suction pressure versus number of stages for steam ejector [130]

In comparison with the MED plant model, the GOR of the TVC-MED improved from 7.31 to 8.14 as a direct result of the reduction in the input steam's mass flow rate from 62.19kg/s to 55.89kg/s at a similar potable water production rate of 40000m^3/day. The specific heat consumption was not changed as it was a function of the first-effect heat transfer and the potable water production rate, and both were the same in both models.

The concentration factor increased from 1.66 in the MED plant model to 1.8 in the TVC-MED plant model as a result of the extraction from the steam entering the condenser which in return reduced the amount of seawater rejected after the condenser and before entering the brine heater.

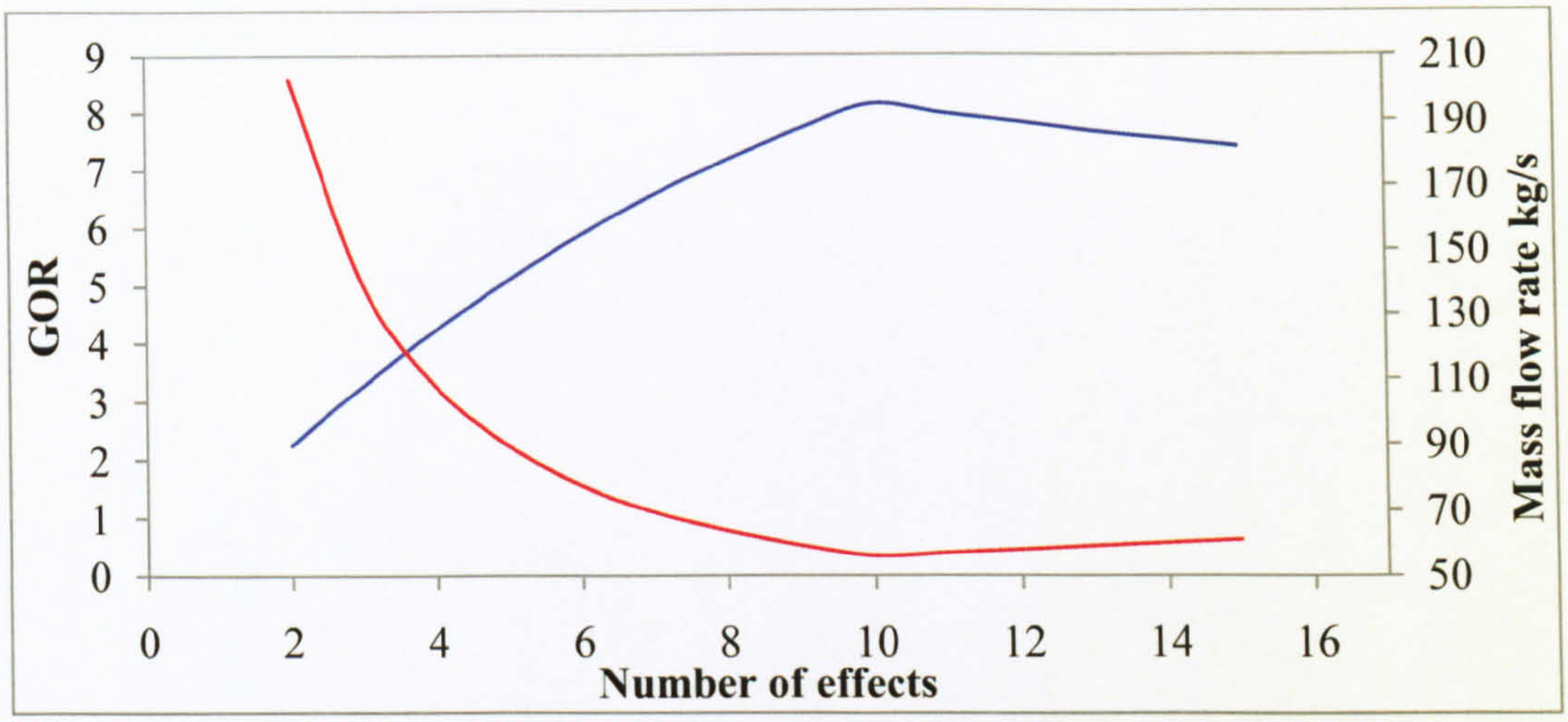

Figure 4-27 GOR and motive steam mass flow rate versus number of effects

On the basis of exergy analysis, the ten evaporators' exergy destruction values were calculated in accordance with TVC-MED plant model's illustration in Figure 4–28:

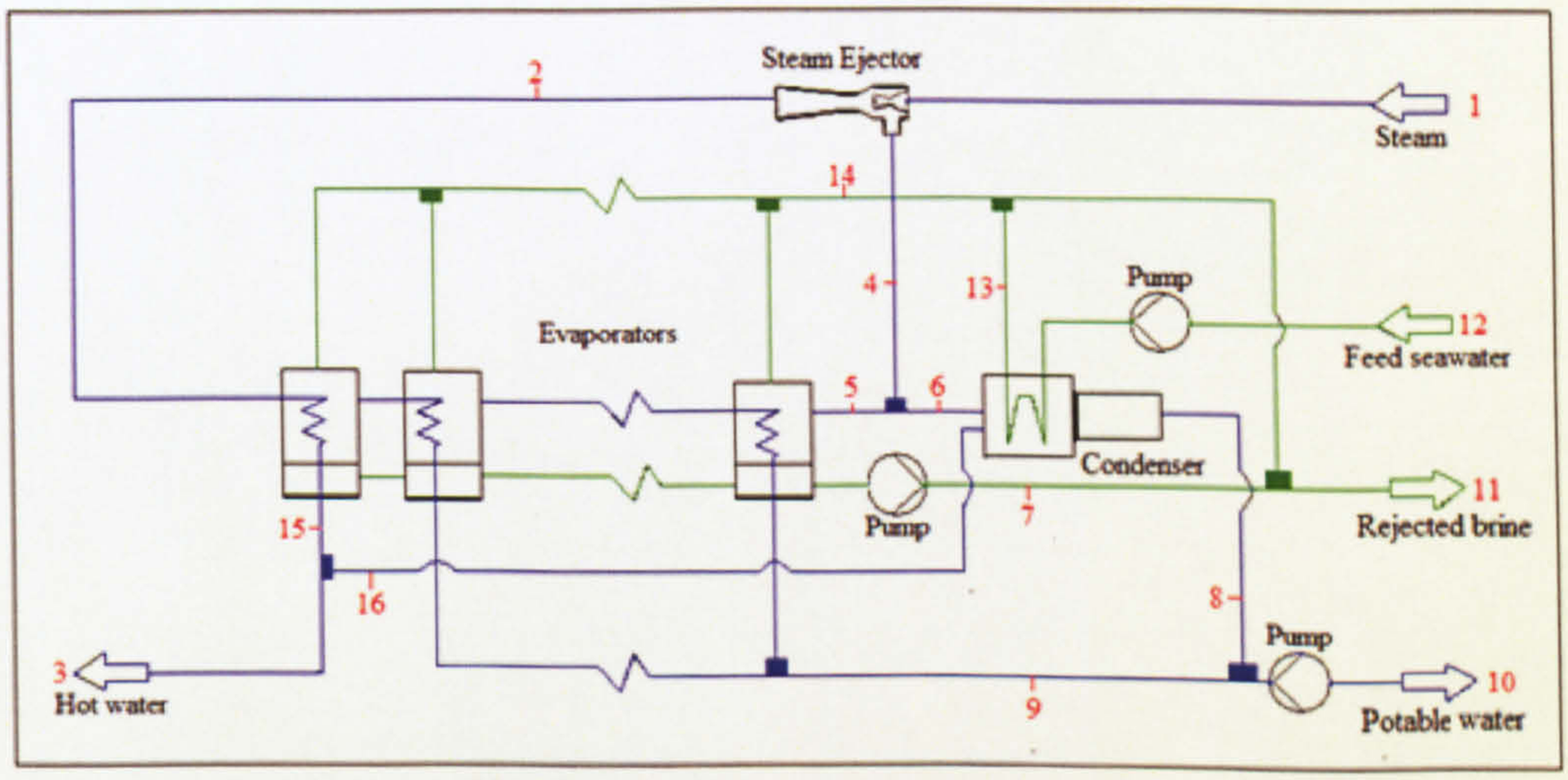

Figure 4-28 TVC-MED plant model

$$E_{D,Eva} = \dot{m}_2 \times (e_2 - e_{15}) + e_{14} \times \dot{m}_{14} - e_5 \times \dot{m}_5 - e_7 \times \dot{m}_7 - e_9 \times \dot{m}_9 + \dot{W}_{pump\,,7}$$

while the condenser's exergy destruction value was calculated as follows:

$$E_{D,Cond} = \dot{m}_{12} \times (e_{12} - e_{13}) + \dot{m}_6 \times (e_6 - e_8) - \dot{m}_{16} \times h_{16} + \dot{W}_{pump\,,12}$$

The steam ejector's exergy destruction value was calculated as following:

$$E_{d,Ej} = \dot{m}_1 \times e_1 + \dot{m}_4 \times e_4 - \dot{m}_2 \times e_2$$

The entropy and enthalpy of each seawater and brine water stream were calculated exactly as in the MED plant model. All entropy and enthalpy values are listed in Table 12 in Appendix C. Then the specific exergy and exergy were calculated for each stream in the plant as shown in Table 4–4. The reference conditions were taken to be at 15°C and a pressure of 1.013 bar.

Point	Stream	e (kJ/kg)	E (MW)
1	Steam	503.19	28.12
2	Steam	396.96	24.68
3	Water	19.86	1.11
4	Steam	262.47	1.65
5	Steam	262.47	11.29
6	Steam	262.47	9.65
7	Brine	4.34	2.27
8	Water	7.16	0.31
9	Water	14.49	5.97
10	Water	13.87	6.31
11	Brine	4.36	2.29
12	Seawater	0.33	0.33
13	Seawater	5.89	5.77
14	Seawater	5.89	5.764
15	Water	19.86	1.23
16	Water	19.86	0.12

Table 4-4 TVC-MED plant's exergy and specific exergy results

Using the exergy destruction equations the performance of the steam ejector, condenser and the evaporators was calculated. The steam ejector consumed 19% of the total exergy input into the plant and accounted for 27% of the plant's total exergy destruction as shown in Figure 4-29. The ten evaporators consumed 36% of the total exergy input and formed 52% of the plant's total exergy destruction. The condenser caused 4.02MW of exergy destruction, which was 21% of the plant's total exergy destruction, and consumed 15% of the plant's input exergy. The plant's total destruction was 18.94MW, and its exergetic efficiency was 31%. In comparison with the MED plant the evaporators and condenser performed similarly. The main difference was caused by the addition of the steam ejector, which caused an extra 5.09MW of exergy destruction. Although the motive steam mass flow rate was reduced by 9.8% in the TVC-MED plant, its entropy increased from 7.37 in the MED plant to 7.74 in the TVC-MED plant. This increased the input steam exergy to 28.12MW in the TVC-MED plant from 24.66MW in the MED plant.

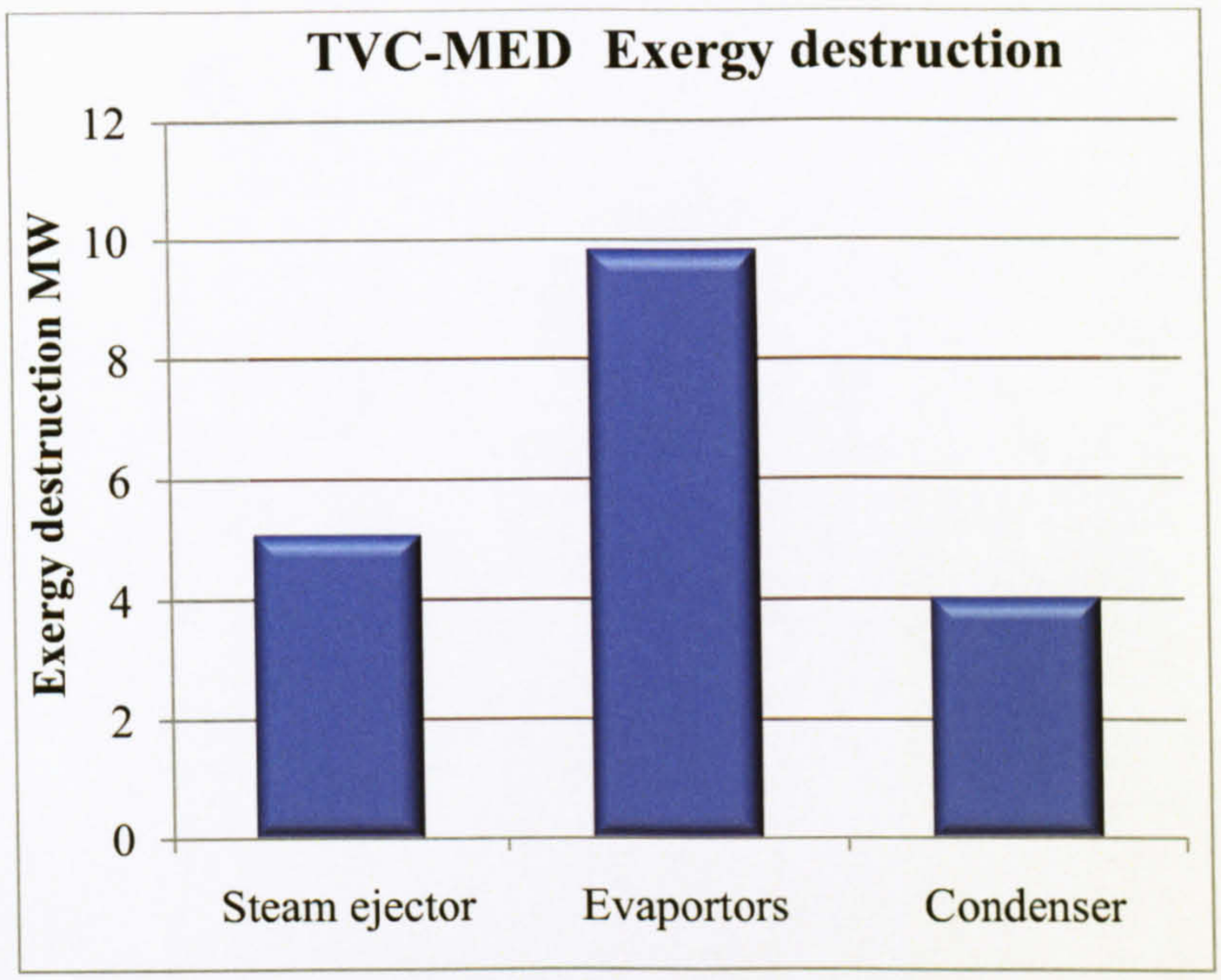

Figure 4-29 TVC-MED plant exergy destruction percentage

The increase in the total exergy destruction of the TVC-MED plant caused its exergetic efficiency to drop from 39.42% in the MED plant to 31.77 %. Table 4-5 shows a full comparison between both plant models on the basis of first and second laws. The second-law analysis indicated that the MED was more efficient than the TVC-MED as it generated less irreversibility.

Parameter	Unit	MED	TVC-MED
Steam ejector's exergy destruction	MW	-	5.09
Evaporators' exergy destruction	MW	9.63	9.82
Condenser's exergy destruction	MW	4.58	4.02
Total exergy destruction	MW	14.21	18.93
Plant's overall exergetic efficiency	%	39.42	31.77
Capacity	m^3/day	40000	40000
GOR	-	7.32	8.14
Specific heat consumption	kJ/kg	318.59	318.59
Concentration factor	-	1.66	1.87
Heat transfer in first effect	MW	144.97	144.97
Heat energy source mass flow rate	kg/s	62.16	55.89
Condenser effectiveness	-	0.80	0.80
Condenser NTU	-	1.84	1.84

Table 4-5 Comparison between TVC-MED and MED desalination plants

The effect of the variation in intake seawater temperature on the TVC-MED plant's model performance was investigated in a parametric study that varied the seawater temperature from 20°C to 28°C. All the results of this study are listed in Table 13 in Appendix C. Figure 4–30 shows that the TVC-MED plant model's performance under varying seawater temperatures, which was similar to the performance of the MED plant model. The GOR increased with the increase in the seawater temperature as a result of the reduction in the required motive steam mass flow rate for evaporating the higher temperature intake seawater. This type of performance is in agreement with what have been published in the literature by Alasfour, et al. [126], Kamali, et al. [127] and Ameri, et al. [131].

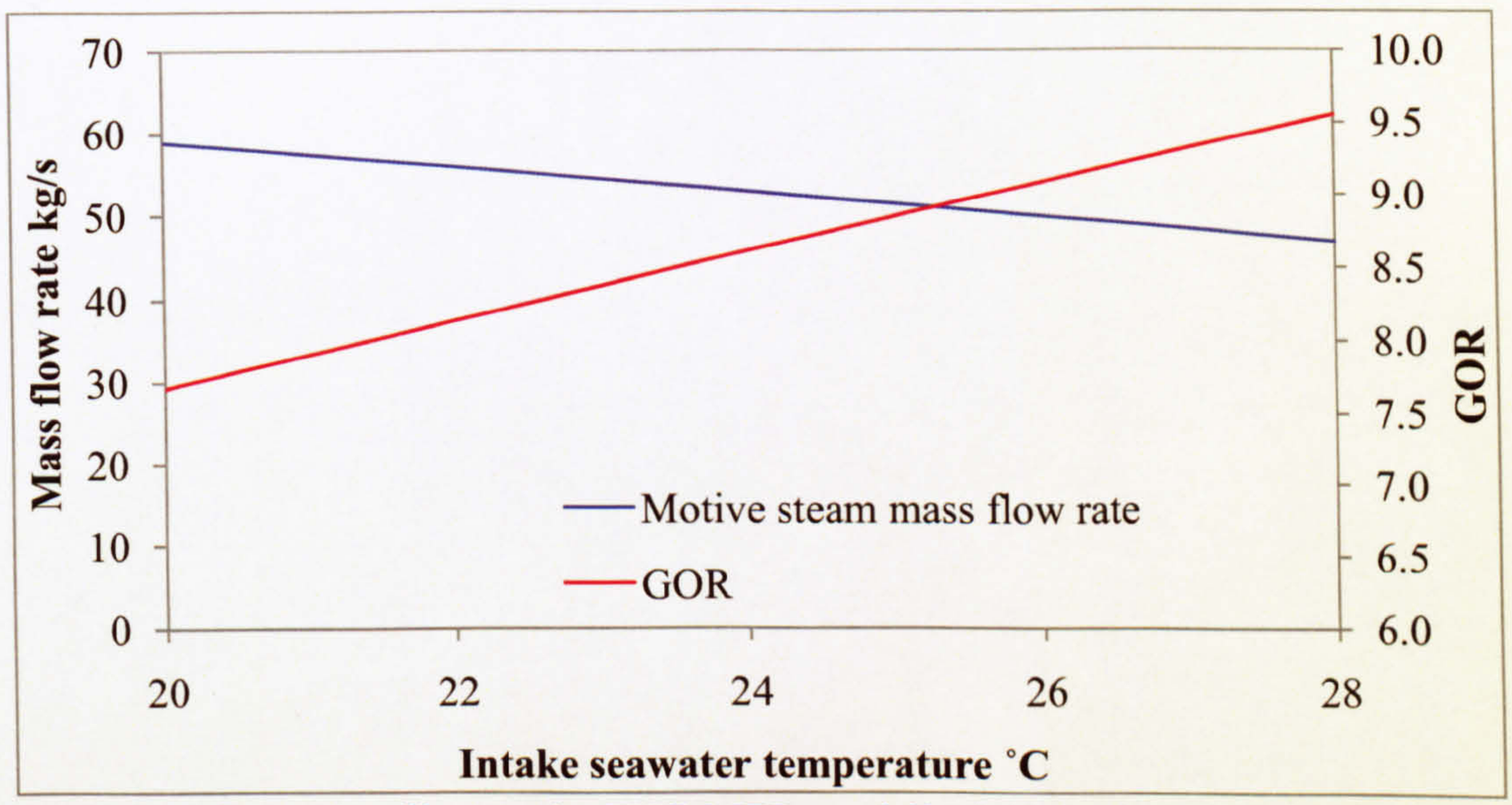

Figure 4-30 Seawater effect on the TVC-MED model's GOR and motive mass flow rate

The plant specific heat consumption (kJ/kg) was a function of the heat transfer in the first effect: heat extracted from the input steam. The input steam decreased as the seawater temperature increased causing the heat transfer in the first effect to decrease by 4.4% for each 2°C increase in the intake seawater temperature. The drop in the first-effect heat transfer led to the reduction in the specific heat consumption by the same percentage of 4.4% for each 2°C increase in the intake seawater temperature as shown in Figure 4-31. Based on exergy analysis, the exergy destroyed in the condenser tended to decline on average by 6.59% for each 2°C increase in the intake seawater temperature. As the intake seawater increased the condenser input exergy increased while its output did not change. The evaporators' exergy destruction increased insignificantly on average by 0.9% for each 2°C increase in the intake seawater temperature. The increase in the

evaporators' exergy destruction was due to the reduction in the specific heat consumption as shown in Figure 4–31.

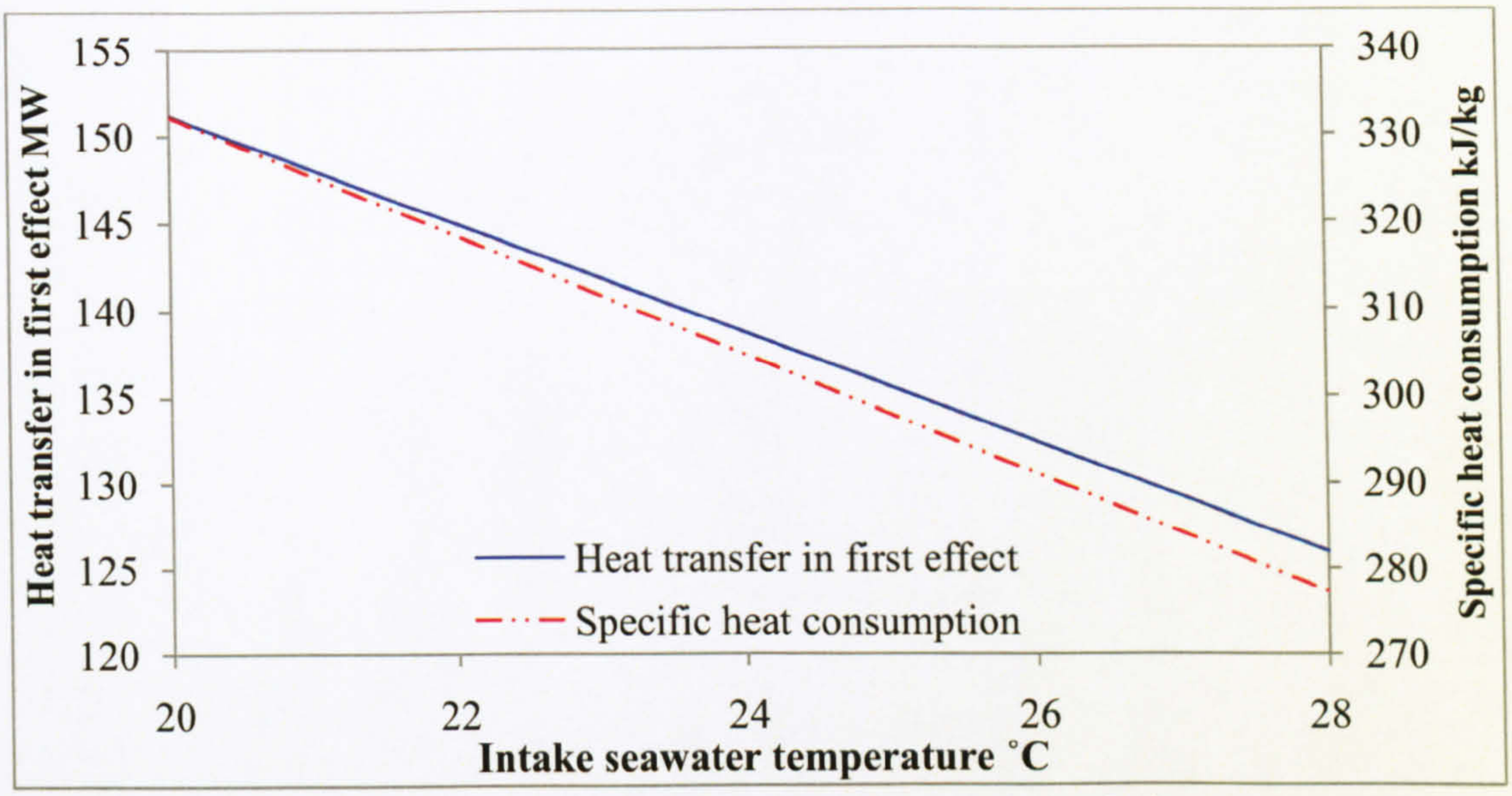

Figure 4-31 Seawater effect on the TVC-MED model's specific heat consumption

The steam ejector's exergy destruction increased insignificantly by 0.88% for each 2ºC increase in the intake seawater temperature. This increase was encouraged by the reduction in its output exergy. The plant's exergetic efficiency increased on average by 5.6% for each 2ºC increase in the intake seawater temperature as seen in Figure 4-32 as a result of the reduction in the motive steam mass flow rate.

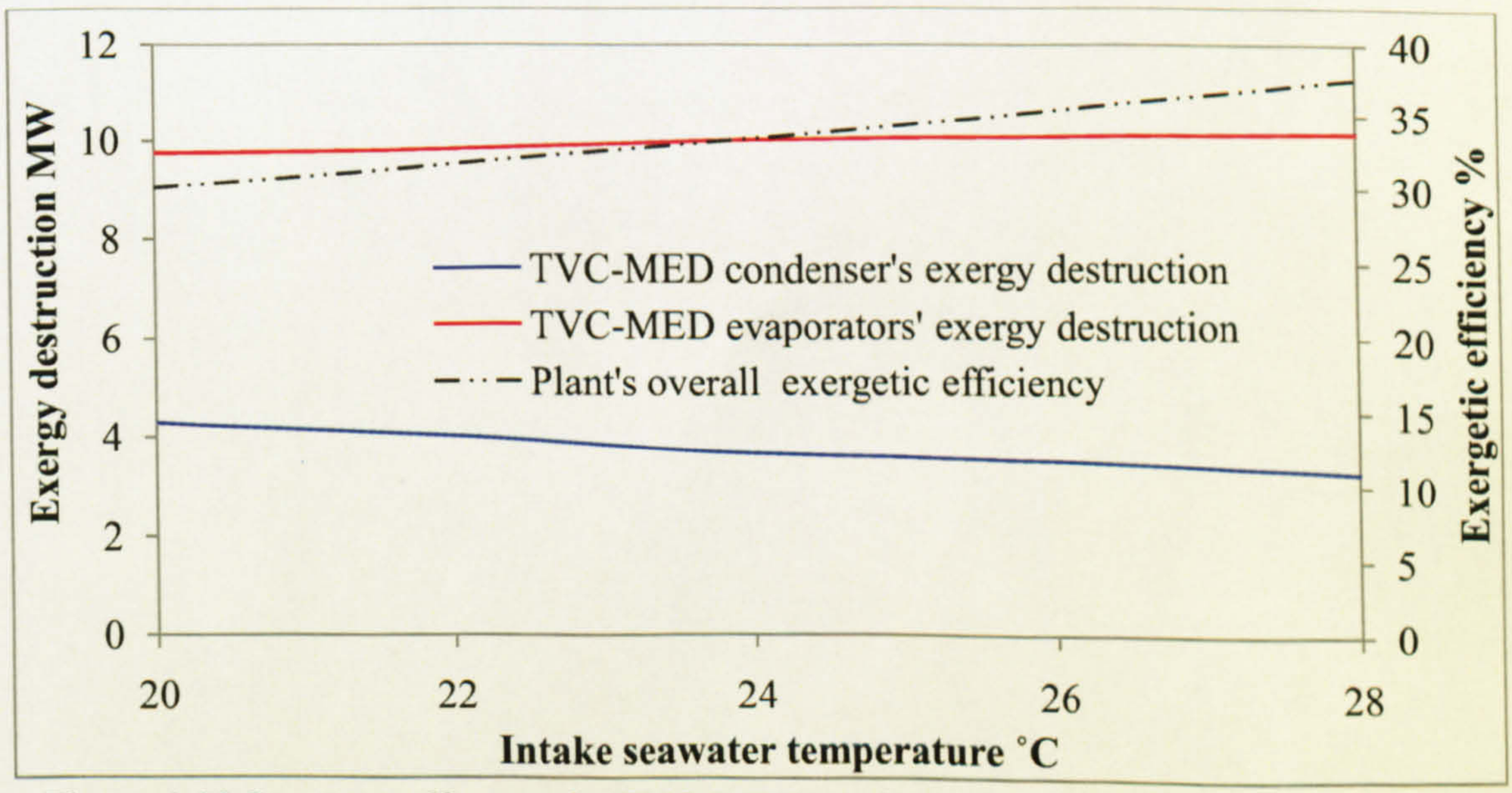

Figure 4-32 Seawater effect on the TVC-MED model exergy destruction and efficiency

From the results of this parametric study, it can be concluded that the TVC-MED desalination plant will perform in a similar manner to the MED plant if the other variables are the same.

4.5 **Absorption Chiller**

The third module used in this study was a water-cooled single-effect lithium-bromide/water absorption chiller with a capacity of 9304kW. It was modelled to resemble the BHE-800 absorption chiller built by BROAD Air Conditioning Co., Ltd [115] as mentioned in the previous chapter. The model consisted of a generator, absorber, evaporator and condenser, in addition to two expansion valves, a small pump and a heat exchanger between the generator and the absorber as shown in Figure 4-33.

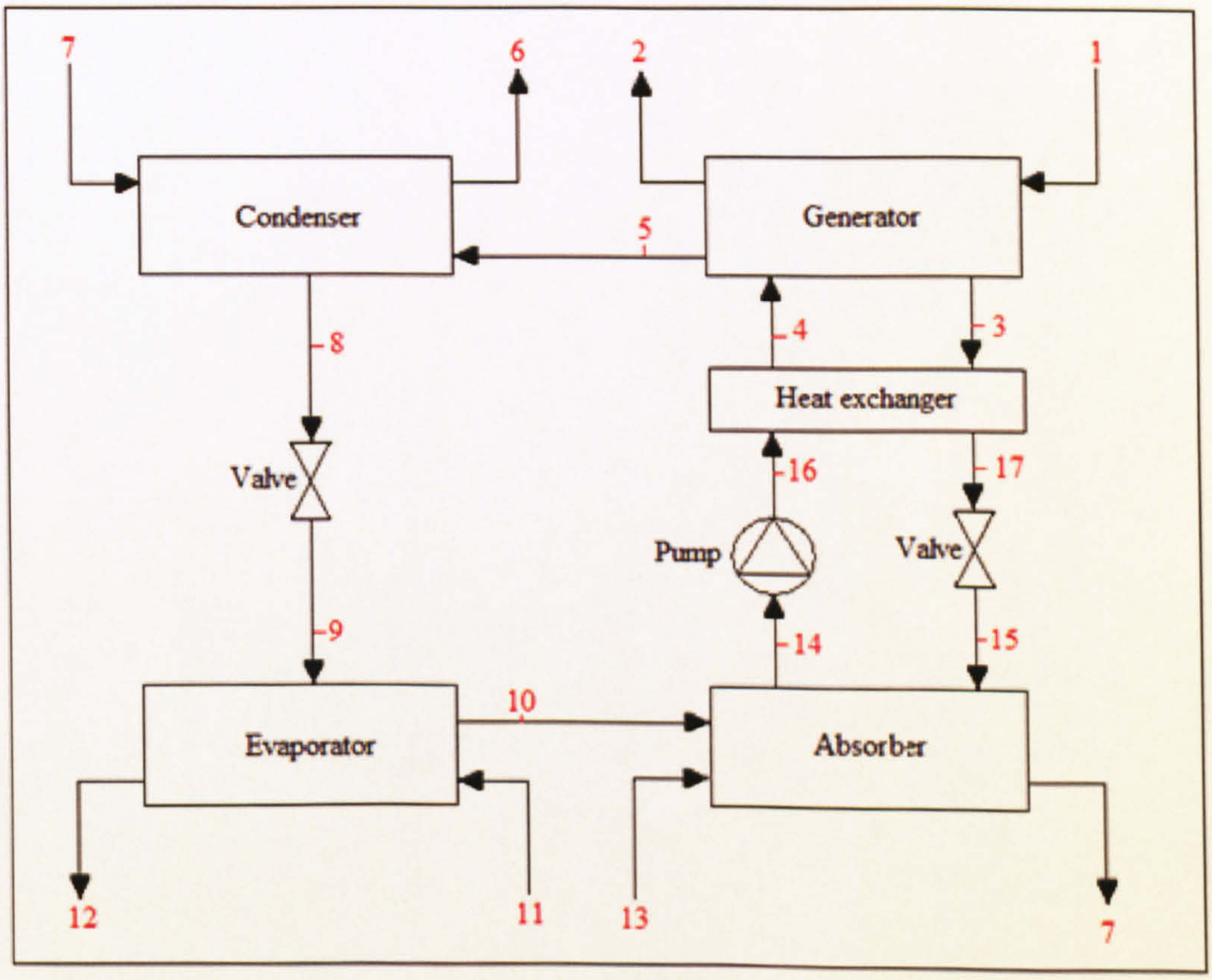

Figure 4-33 Absorption chiller plant model

Table 4-6 lists all the operating conditions for the cycle. The absorption chiller's performance was defined by the coefficient of performance (COP), which is the ratio of the evaporator's heat transfer to that of the generator. In addition, an exergy analysis was also performed. The absorption chiller model's cycle was plotted against the Dühring P-T chart and it was found that

it did not to touch the crystallization curve as seen in Figure 4-34. The model consumed 11.7 MW as heat energy in the generator to produce the 9.3MW cooling effect from the evaporator. The model used a stream of seawater at a temperature of 22°C to cool the absorber; then it proceeded to cool the condenser.

No	Stream	Enthalpy kJ/kg	Entropy kJ/kg K	Mass flow rate	Temperature °C	Pressure Bar	Mass fraction
1	Water	409.71	1.28	156.77	97.7	1.013	1
2	Water	334.46	1.07	156.77	79.8	0.913	1
3	LiBr/Water	177.85	0.48	41.76	78	0.08	0.57
4	LiBr/Water	145.09	0.45	45.86	67.8	0.08	0.52
5	Steam	2639.02	8.42	4.1	74.4	0.08	1
6	Seawater	166.315	0.58	239.85	41.09	1.113	0.04
7	Seawater	125.85	0.45	239.85	31	1.013	0.04
8	Water	173.85	0.59	4.1	41.51	0.08	1
9	Water	173.85	0.63	4.1	3.76	0.008	1
10	Steam	2445.5	8.83	4.1	3.76	0.008	1
11	Water	57.63	0.21	316.7	13.7	1.013	1
12	Water	28.25	0.1	316.7	6.7	0.913	1
13	Seawater	89.42	0.32	239.85	22	1.013	0.04
14	LiBr/Water	55.42	0.18	45.86	26	0.008	0.52
15	LiBr/Water	90.41	0.2	41.76	34.6	0.008	0.57
16	LiBr/Water	55.42	0.18	45.86	26	0.08	0.52
17	LiBr/Water	90.41	0.2	41.76	34.6	0.08	0.57
Heat transfer in the generator						11.7	MW
Heat transfer in the absorber						9.02	MW
Heat transfer in the evaporator						9.3	MW
Heat transfer in the condenser						10	MW
COP						0.79	

Table 4-6 Absorption chiller's operating conditions

The model achieved a COP of 0.79, confirming the real model specification. On the basis of the second law analysis, the entropy of each LiBr/H_2O stream was read from the entropy curve that was reported by Kaita [105]. The cooling seawater enthalpy and entropy were calculated as mentioned in the previous chapter [106-109]. All the results for the entropy and enthalpy calculations are listed in Table 4-6. Then the exergy and specific exergy were calculated for each stream as shown in Table 4-7. The negative exergies of streams 9 and 10 were justified by the stream thermodynamic conditions that fell below the reference thermodynamic conditions and this was an indication of a stored exergy in these two streams [94, 132].

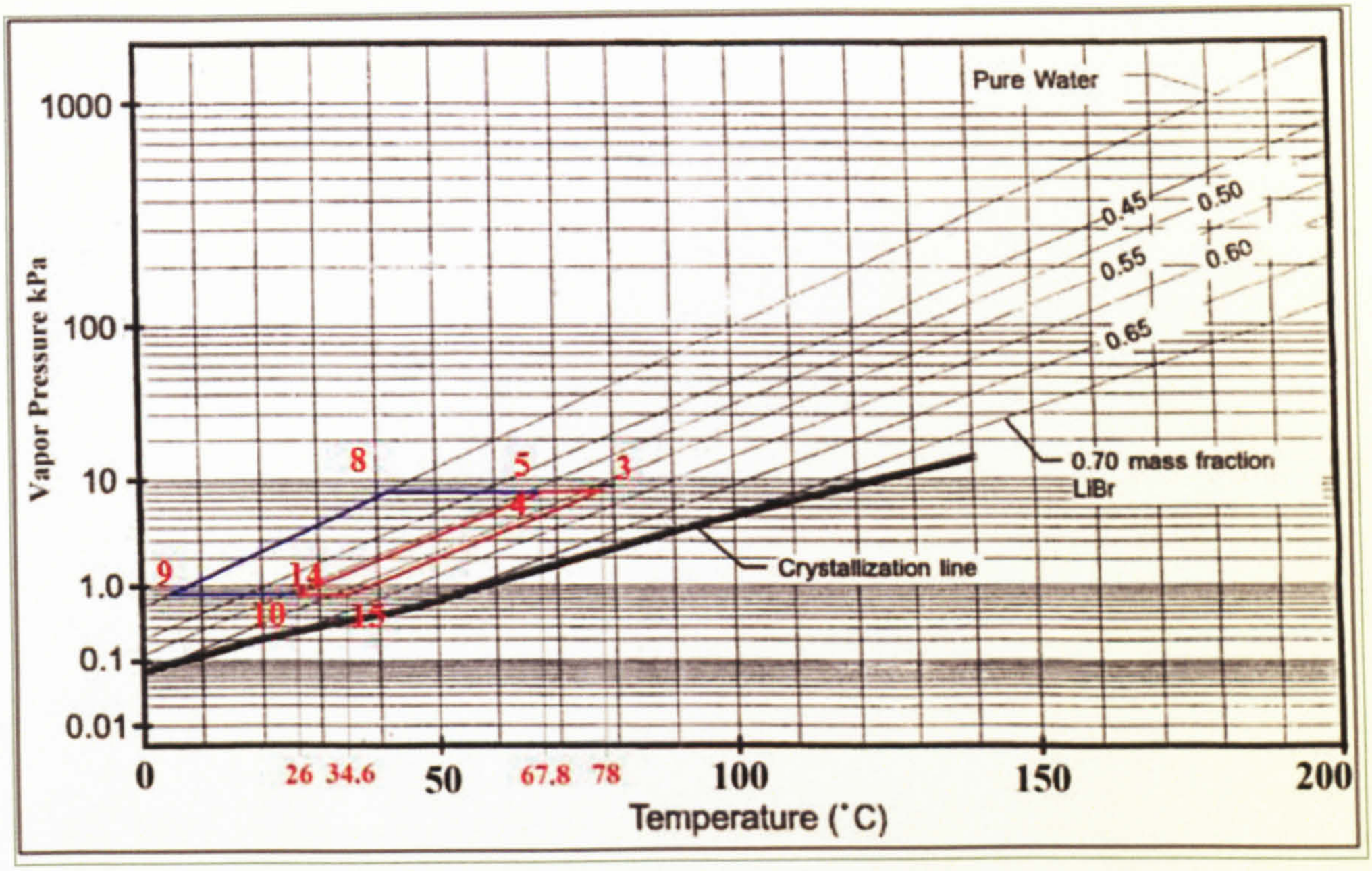

Figure 4-34 Water/LiBr Dühring P-T diagram

point	Stream	e kJ/kg	E MW
1	Water	42.33	8.04
2	Water	29.28	5.56
3	LiBr/Water	38.98	1.66
4	LiBr/Water	9.22	0.43
5	Steam	216.49	0.89
6	Seawater	4.52	1.08
7	Seawater	1.75	0.42
8	Water	4.74	0.02
9	Water	-5.42	-0.02
10	Steam	-97.68	-0.4
11	Water	0.02	0.01
12	Water	0.56	0.18
13	Seawater	0.33	0.08
14	LiBr/Water	2.09	0.1
15	LiBr/Water	26.58	1.13
16	LiBr/Water	2.09	0.1
17	LiBr/Water	26.58	1.13

Table 4-7 Absorption chiller's exergy and specific exergy results

The exergy destruction in each component was calculated as listed in Table 4-8 based on the exergy balance presented in the previous chapter:

Component	Exergy destruction equation	Value kW
Generator	$\dot{m}_1 \times (e_1 - e_2) + \dot{m}_4 \times e_4 - \dot{m}_5 \times e_5 - \dot{m}_3 \times e_3$	361.69
Absorber	$\dot{m}_{13} \times (e_{13} - e_7) + \dot{m}_{10} \times e_{10} + \dot{m}_{15} \times e_{15} - \dot{m}_{14} \times e_{14}$	296.43
Condenser	$\dot{m}_7 \times (e_7 - e_6) + \dot{m}_5 \times e_5 - \dot{m}_8 \times e_8$	206.64
Evaporator	$\dot{m}_{11} \times (e_{11} - e_{12}) + \dot{m}_9 \times e_9 - \dot{m}_{10} \times e_{10}$	204.1
Heat exchanger	$\dot{m}_{16} \times (e_{16} - e_4) + \dot{m}_3 \times (e_3 - e_{17})$	195.81
Expansion valve	$\dot{m}_8 \times (e_8 - e_9)$	41.63

Table 4-8 Absorption chiller components' exergy destruction equation and values

The solution expansion valve, between the heat exchanger and the absorber, and the pump's exergy destruction were neglected due to their insignificant contributions (less than 1%) to the absorption chiller model's total exergy destruction. Figure 4-35 shows the proportion of each component's exergy destruction. The generator consumed 14.59% of the total input exergy into the model and represented 27.69% of the plant's total exergy destruction, 361.69 kW. This was produced by the irreversibility caused by the heat transfer between the heat energy source and the absorption chiller fluids, and because of the $LiBr/H_2O$ separation process that took place in the generator. This result was in agreement with those of a number of studies, such as Abdul-Khaliq [124].

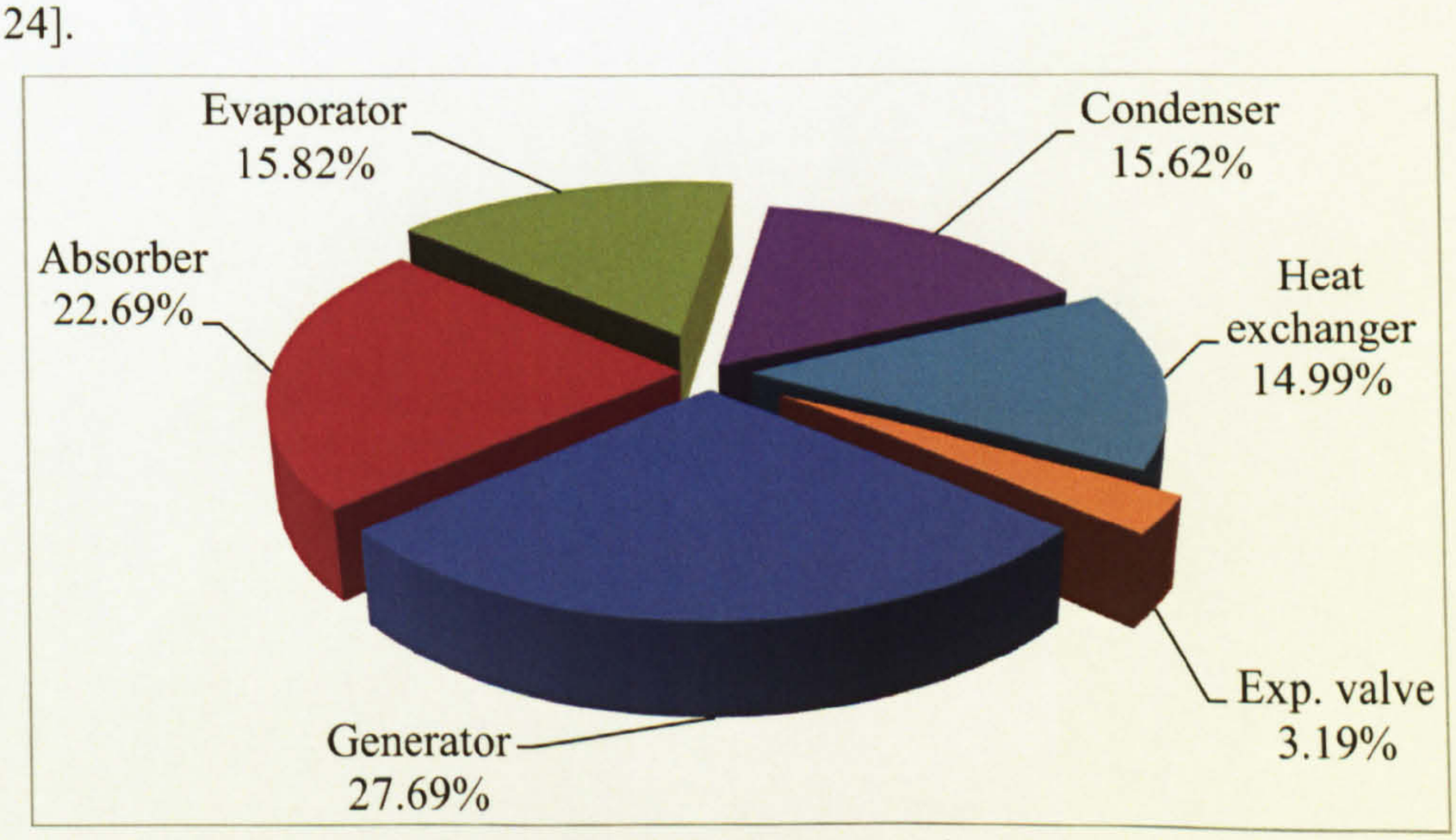

Figure 4-35 Absorption chiller's exergy destruction ratio ψ_D

The absorber came second with an exergy destruction value of 296.43 kW, consuming 11.96% of the total input exergy and forming 22.69% of the total exergy destruction. The evaporator consumed 8.34% of the total input exergy and accounted for 15.82% of the total exergy

destruction, while the condenser caused 15.62% of the model's total exergy destruction, consuming 8.23% of the input exergy. The heat exchanger accounted for 14.99% of the model's total exergy destruction, consuming 7.9% of the input exergy. The refrigerant expansion valve between the condenser and the evaporator produced 3.19% of the model's total exergy destruction with only 41.63kW. The overall absorption chiller model's exergetic efficiency was 6.91%. This value of exergetic efficiency fell within the typical range reported in the literature [93, 94, 95].

The affect of the evaporator's inlet water temperature on the model's behaviour was investigated, assuming that the inlet cooling water temperature was 22°C, the solution mass fraction at the generator outlet was 0.52% and at the absorber outlet was 0.57%, the generator inlet mass flow rate and temperature were 190kg/s and 97.9°C respectively, the evaporator mass flow rate was 316.7kg/s and the outlet chilled water temperature was 6.7°C according to the real model's data. The evaporator's inlet water temperature varied from 10°C to 22°C while monitoring all the used parameters of the first and second laws. All the results of this study are listed in Table 14 in Appendix C. Figure 4-36 shows the heat transfer in the generator, absorber, evaporator, condenser and heat exchanger versus the increase in the evaporator inlet water temperature.

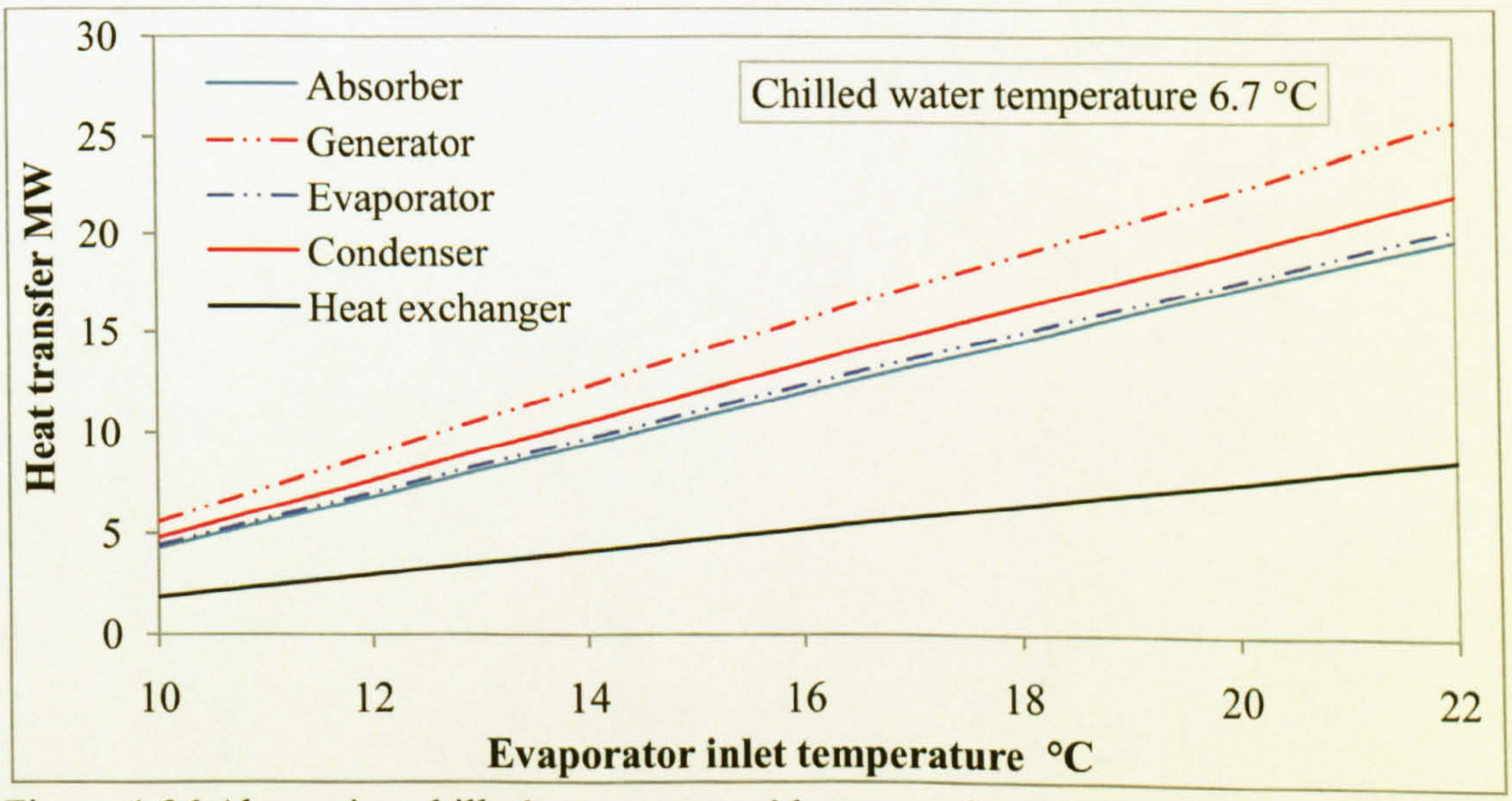

Figure 4-36 Absorption chiller's components' heat transfer versus evaporator inlet water temperature at a fixed chilled water temperature

For each 2°C increase in the evaporator inlet water temperature the heat transfer in all the absorption chiller's heat exchangers increased on average by 22% to overcome the increase in

the evaporator inlet water temperature and meet the required chilled water temperature of 6.7°C. This increase was mainly driven by the increase in the mass flow rate of all the cycle fluids in order to have the capacity for cooling the evaporator inlet water to the predefined temperature as shown in Figure 4-37. If the chilled water temperature was not set, the only changes would have been in the evaporator's exergy destruction and the chilled water temperature as shown in Figure 4-38. The evaporator's exergy destruction would have increased on average by 41.2% as a result of increasing its input exergy through increasing its inlet water temperature.

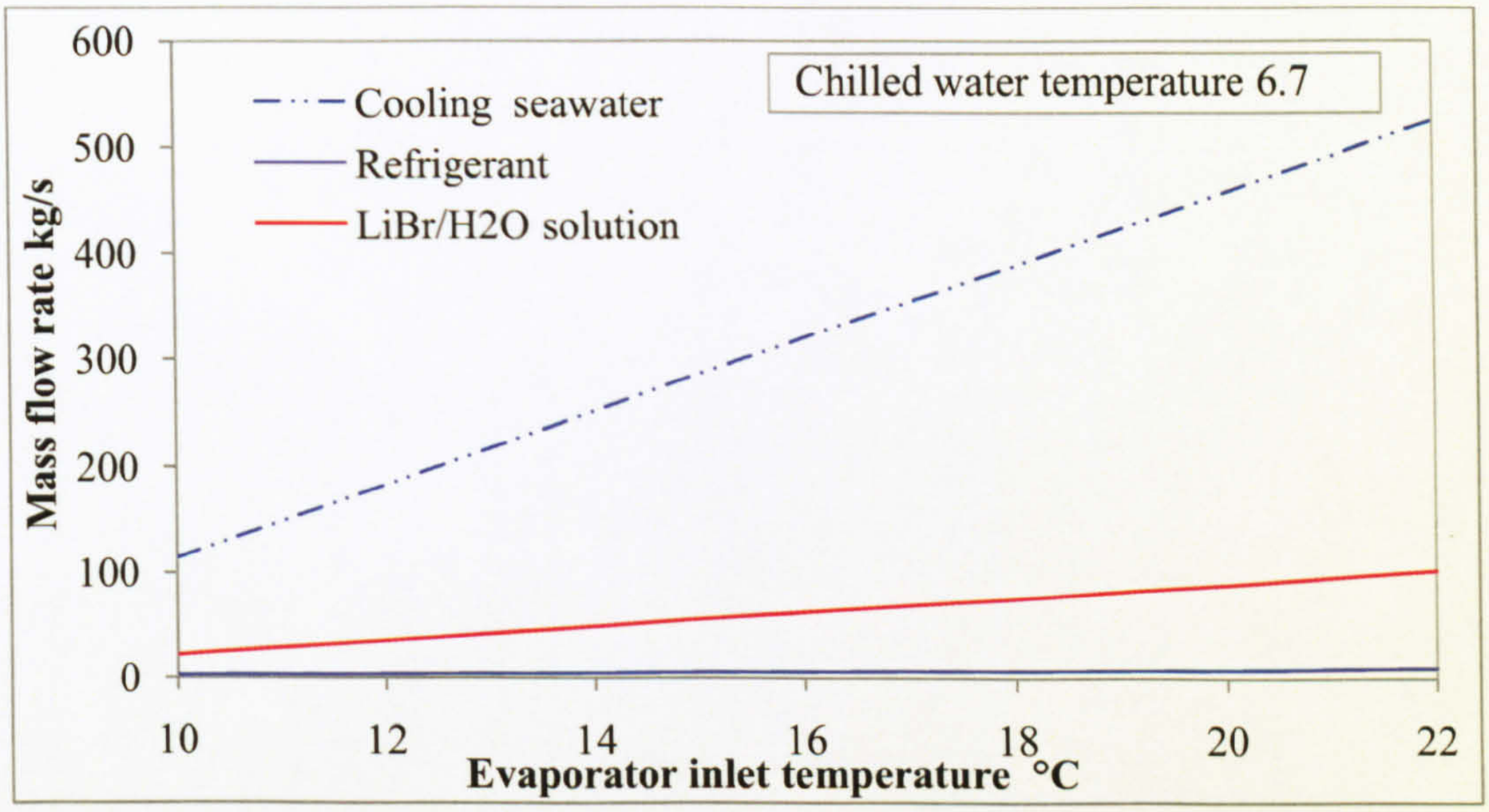

Figure 4-37 Absorption chiller's fluid mass flow rate versus evaporator inlet water temperature at a fixed chilled water temperature

The increase in the evaporator's exergy destruction would have led to a drop in the model's overall exergetic efficiency. This indicated the need for the circulation of the chilled water between the cooling load and the evaporator in order to limit this effect and utilize the chilled water after the cooling load. This parametric study also confirmed the accuracy and reliability of the second-law analysis over the first law. The first law's COP parameter was only a function of the energy flow in both the evaporator and the generator; therefore, the COP showed no changes, while the exergy analysis reflected all the model's factual responses to any changes in its design variables. In the case of the chilled water temperature being set to 6.7°C, the exergy destruction caused by the absorber, condenser, heat exchanger and refrigerant expansion valve responded to an increase in the evaporator inlet water temperature in a similar way to that of the heat transfer as shown in Figure 4-39.

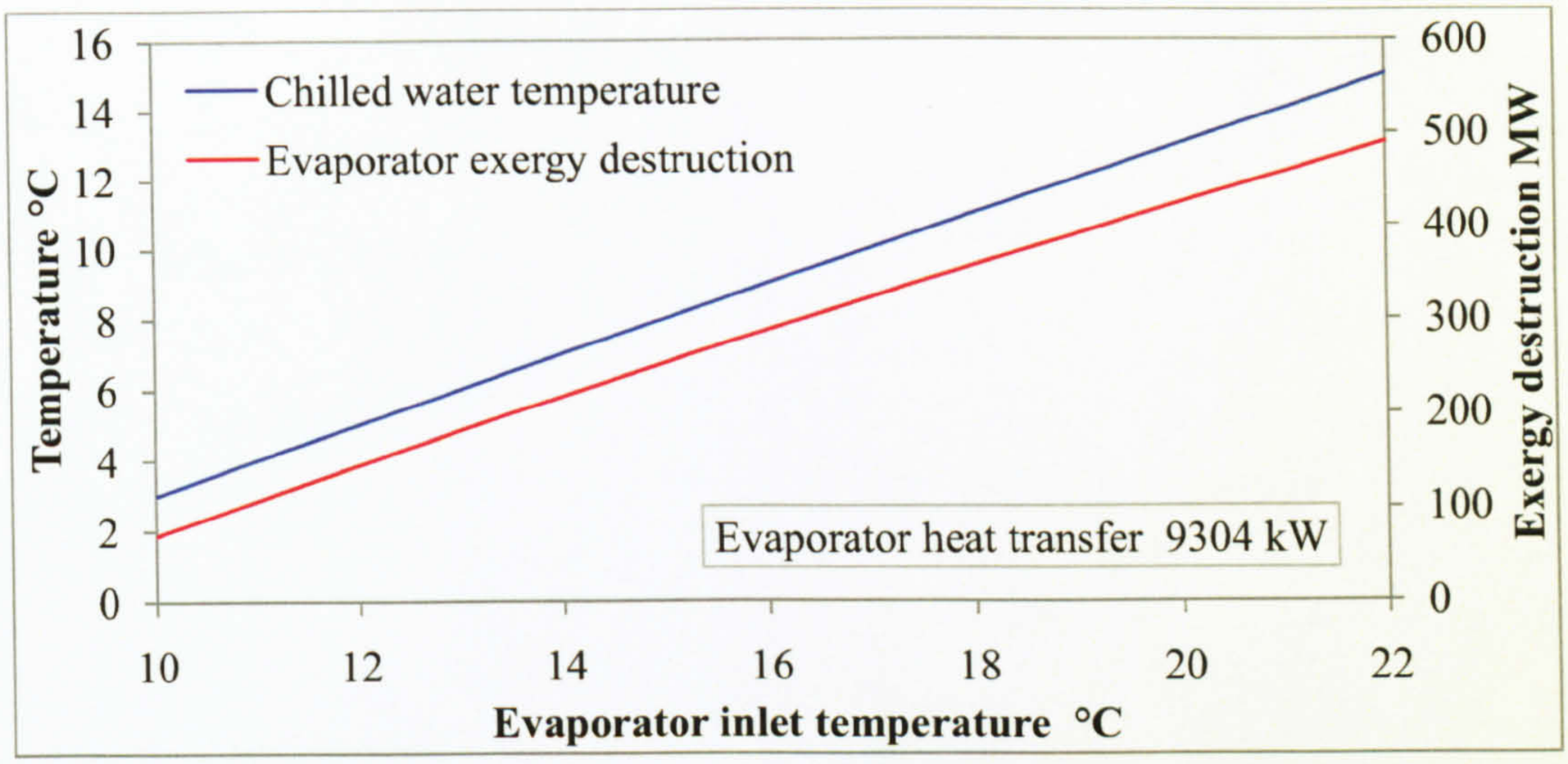

Figure 4-38 Evaporator's exergy destruction and chilled water temperature versus evaporator's inlet water temperature at a fixed evaporator heat transfer

This increase in the exergy destruction of these components can be also justified by the increase in the cycle fluids mass flow rate that is shown in Figure 4-37. The generator and evaporator responses were different as shown in Figure 4-40. The evaporator's exergy destruction increased nonlinearly in a way that was affected by the nonlinear curve of its input exergy that driven by the increase in the evaporator inlet water temperature. The generator's exergy destruction increased until it reached its maximum value at an inlet water temperature of 15.6°C and then started to decline back to the value of a lower evaporator inlet water temperature.

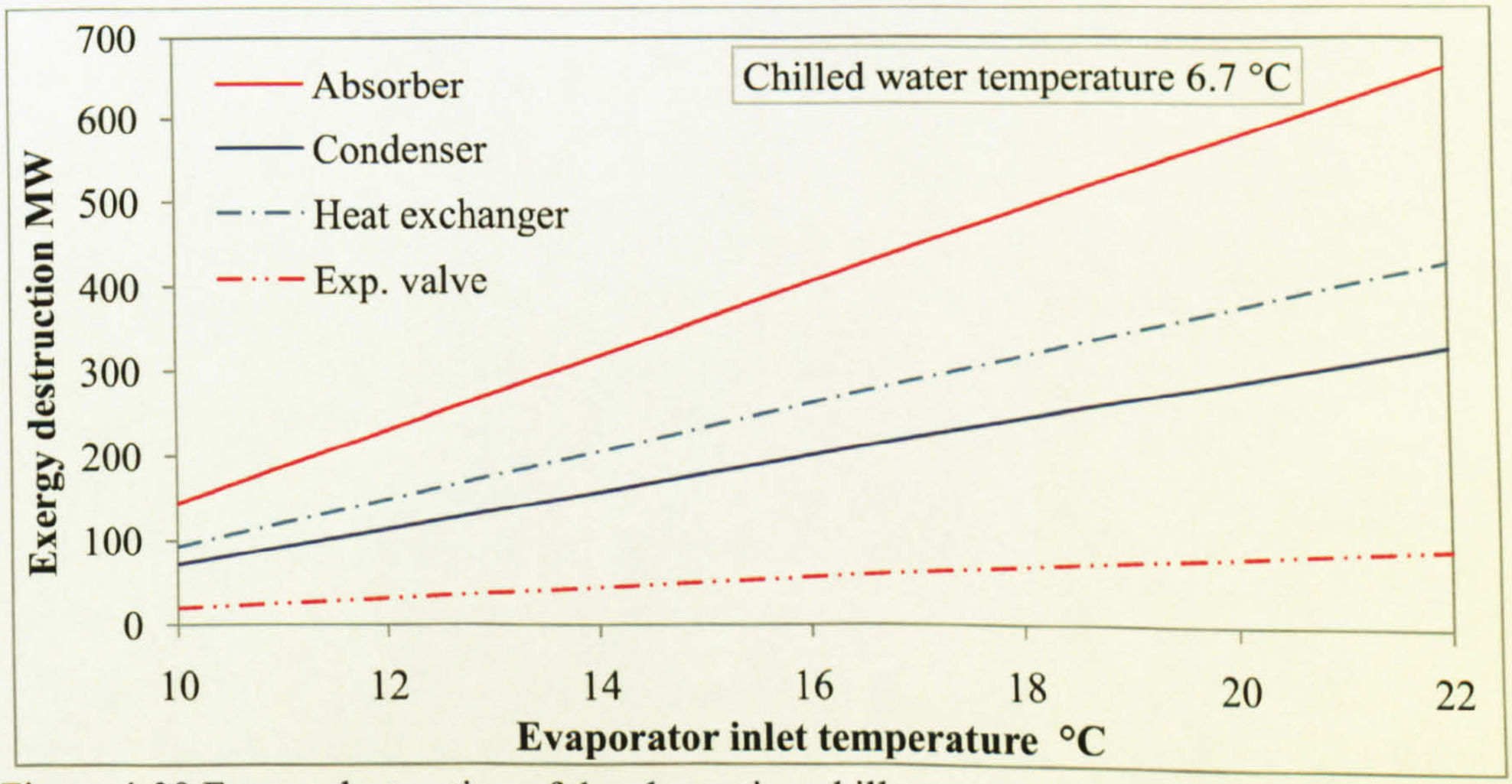

Figure 4-39 Exergy destruction of the absorption chiller components versus evaporator inlet water temperature at a fixed evaporator heat transfer

This form of response could have been explained by the relative temperature of the hot water stream rejected out of the absorption chiller from the generator (T_2), to that of the LiBr/H_2O solution leaving the generator and going to the heat exchanger (T_3). Figure 4-41 shows this parameter's (that is, T_2/T_3) performance under varying evaporator inlet water temperatures; this temperature ratio (T_2/T_3) dropped as the evaporator inlet water temperature increased as a result of the increase in the cycle fluids mass flow rate. This then required extra heat to separate the refrigerant from the LiBr/H_2O solution.

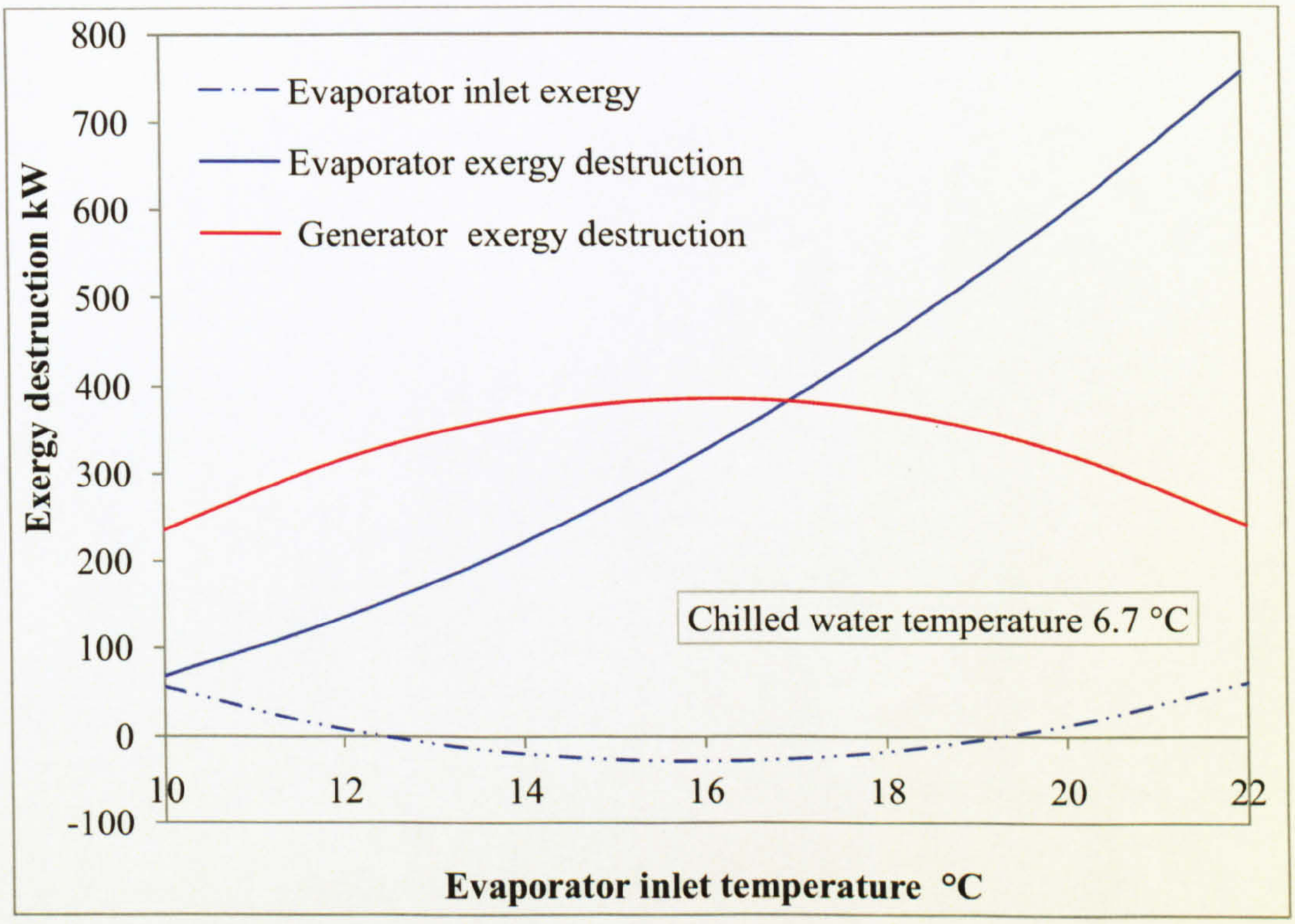

Figure 4-40 Evaporator's and generator's exergy destruction values versus evaporator's inlet water temperature at a fixed evaporator heat transfer

The drop in the T_2/T_3 parameter would have caused an increase in the generator's exergy destruction until it reached 100% at a temperature of 15.6°C where the generator reached its maximum value of exergy destruction. Then it forced the generator's exergy destruction to decrease as it dropped below 100% where the hot water stream temperature (T_2) became less than that of the LiBr/H_2O solution stream (T_3). The extra heat was extracted from the heat source stream and this meant further utilization of its energy and the rejection of less heat (that is, a lower temperature at T_2), while T_3 was predefined by the LiBr/H_2O solution concentration at the generator outlet toward the heat exchanger.

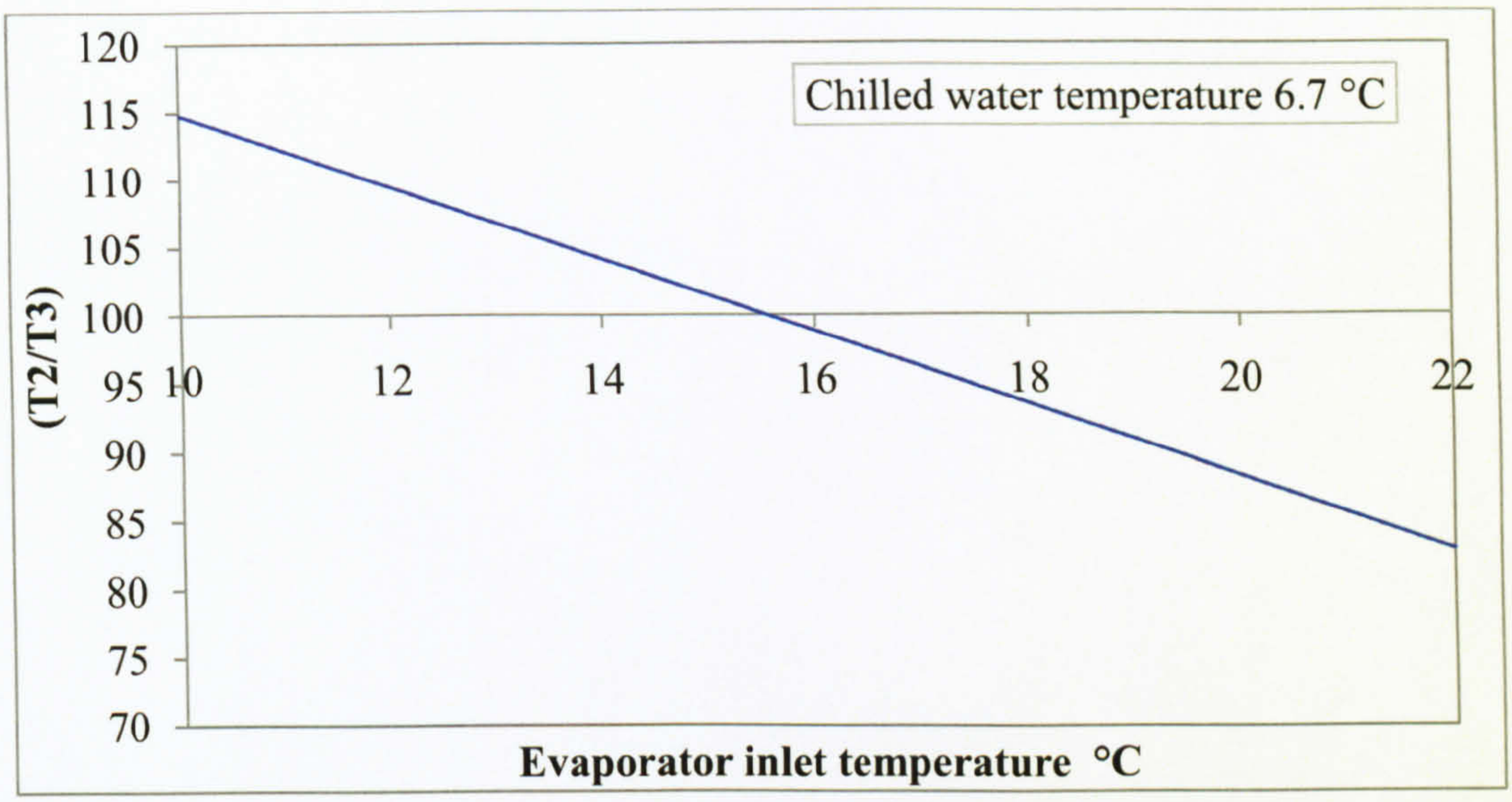

Figure 4-41 T_2/T_3 versus evaporator inlet water temperature

The model's exergetic efficiency declined with the increase in the evaporator inlet water temperature as a result of the increases in all the cycle components' exergy destruction values. Figure 4-42 shows the inversely proportional relationship between the evaporator's inlet water temperature and the model's exergetic efficiency.

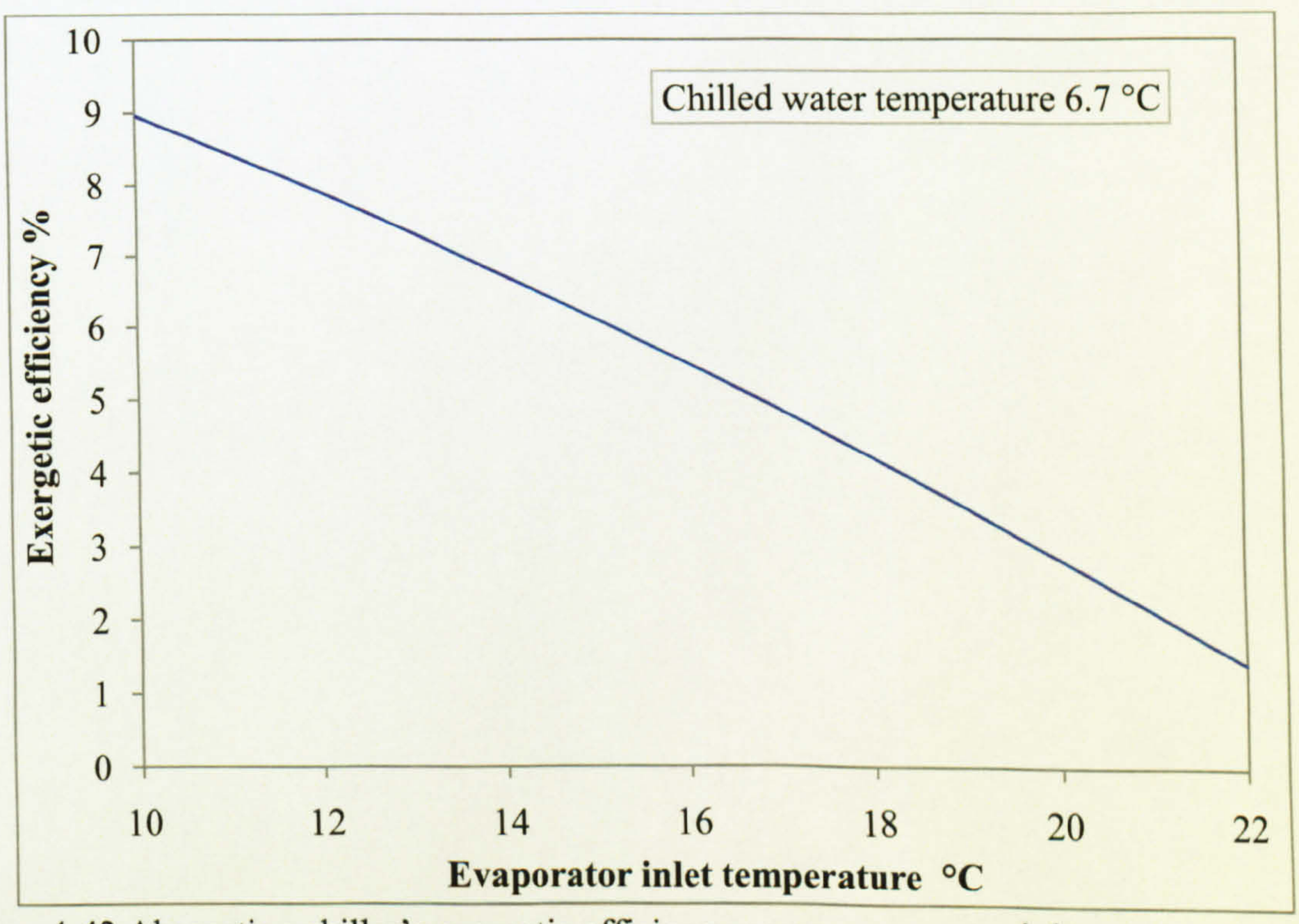

Figure 4-42 Absorption chiller's exergetic efficiency versus evaporator inlet water temperature

The performance of the absorption chiller model under varying cooling water temperatures was investigated from 20°C to 28°C to mach the variation in the temperature of the Red Sea, which was presented in the previous chapter. The LiBr/H_2O solution concentration was set at the absorber and generator outlet in addition to the inlet mass flow rate of the energy source. All the results are listed in Table 15 in Appendix C, while the most significant results will be discussed in this section. Figure 4-43 shows the increase in the cooling water mass flow rate with the increase in its temperature in order to cool the absorber and the condenser to a certain degree that is defined by the evaporator capacity for the condenser and by the LiBr/H_2O solution concentration for the absorber.

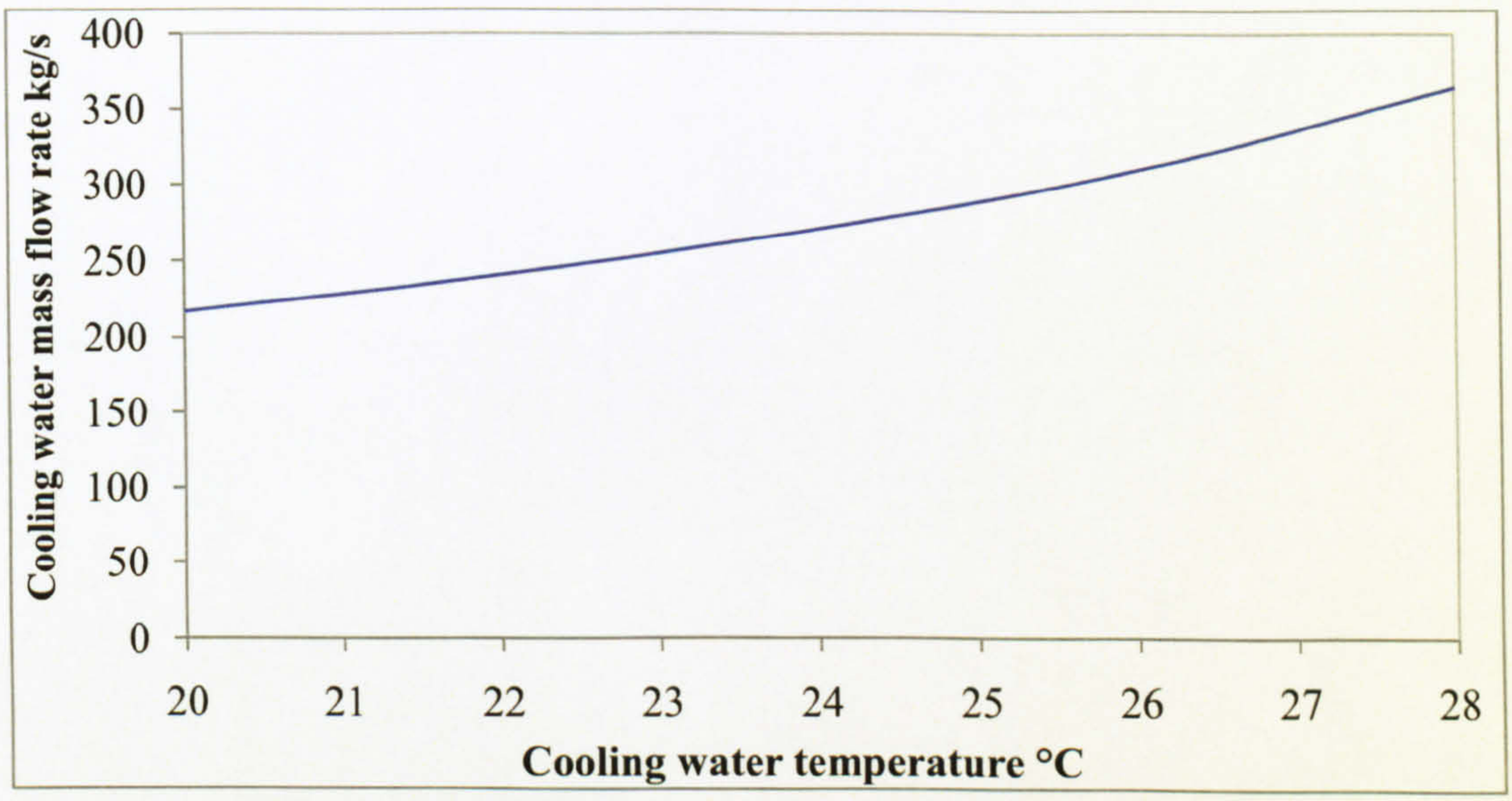

Figure 4-43 Cooling water mass flow rate versus its temperature

Figure 4-44 shows the exergy destruction of both the absorber and condenser with the increase in the cooling water temperature. The absorber's exergy destruction decreased by 14.7% and the condenser by 6.6% for each 2°C increase in the cooling water temperature. This was due to the change in the input and output exergy rates. In the case of a set cooling water mass flow rate, the exergy destruction of both the absorber and condenser would have been increasing not decreasing. This told us that the extra mass flow rate of the cooling water was what made the change in the exiting exergy of both components more than that of the entering exergy, which resulted in reduced exergy destruction. The absorption chiller's exergetic efficiency was not affected by this change in the absorber's and condenser's exergy destruction values because it was only a function of the evaporator and generator parameters.

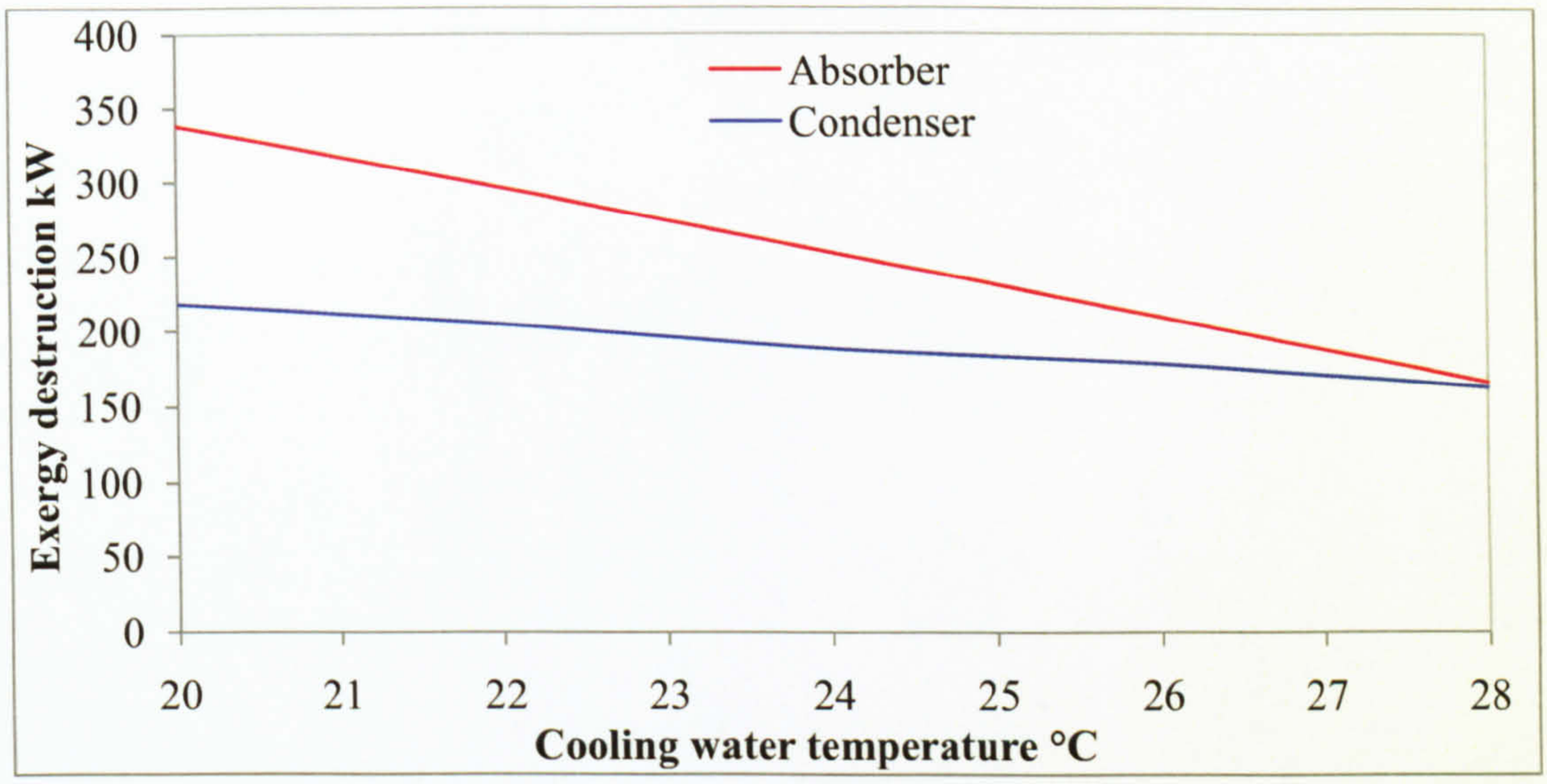

Figure 4-44 Absorber's and condenser's exergy destruction versus cooling water temperature

The performance of the model was also examined under varying inlet hot water temperatures. The same assumptions made for the previous study were also considered here. The variation in the heat energy source temperature was limited to 99°C to avoid boiling point of the hot water to comply with the real model's data. All the results of this study are listed in Table 16 in Appendix C, while Figure 4-45 shows the affect of the generator's inlet hot water temperature on both its mass flow rate and its exergy destruction.

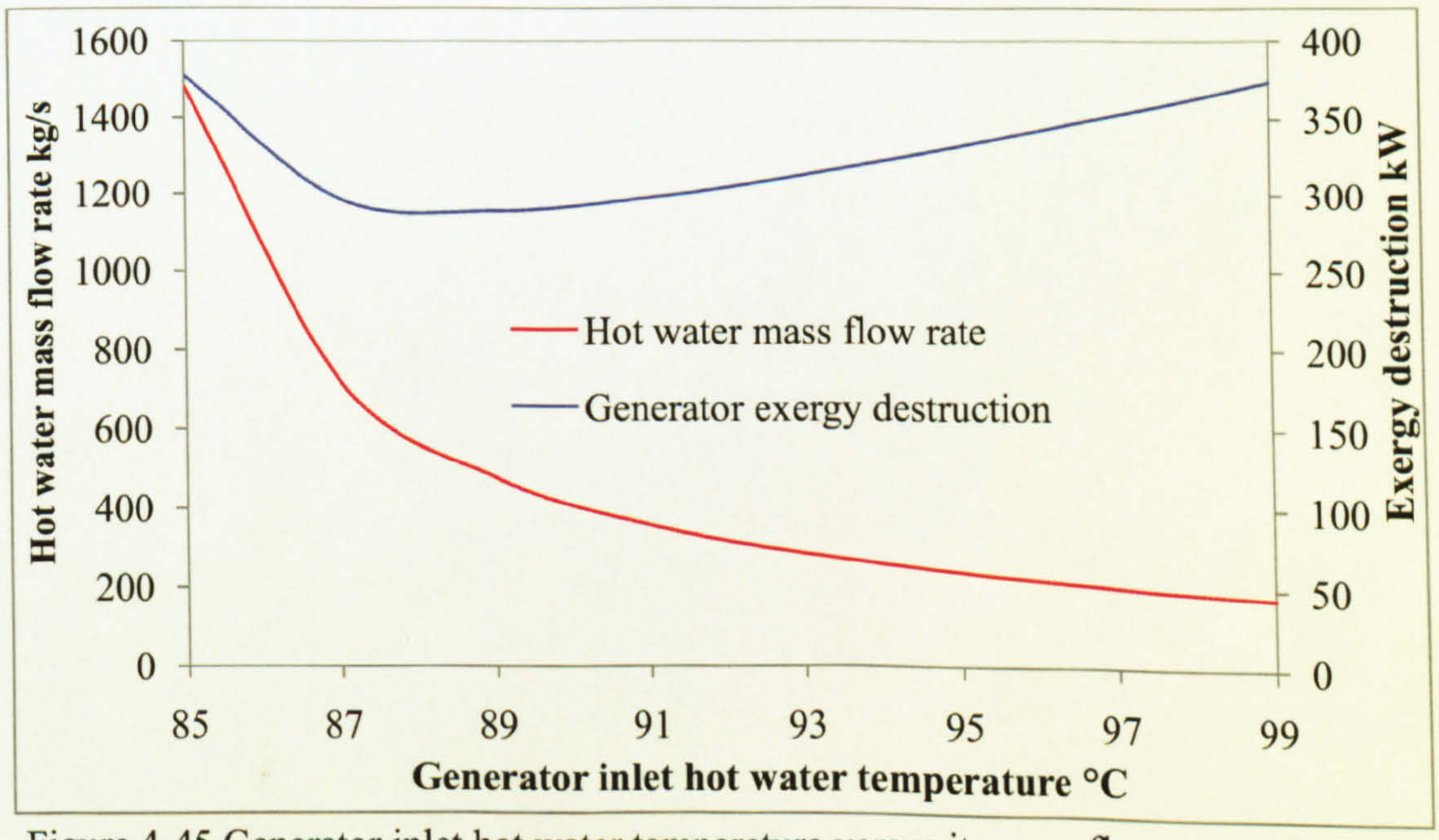

Figure 4-45 Generator inlet hot water temperature versus its mass flow rate and exergy destruction

The generator's exergy destruction rate increased, with its minimum value being at a temperature of 88˚C; below this temperature value both the exergy destruction and the hot water mass flow rates increased rapidly. Above 88˚C, the generator's exergy destruction rate increased on average by 5.3% for each 2˚C increase in its input hot water temperature. The input hot water's mass flow rate typically decreased on average by 17% above this temperature. Figure 4-46 shows the exergetic efficiency of the absorption model against the increase in the generator's inlet hot water temperature. The exergetic efficiency reached its maximum value of 7.14% at a temperature of 88˚C; below and above this temperature value the exergetic efficiency dropped insignificantly on average by 0.03% for each 2˚C increase in the generator's inlet hot water temperature. This was mainly because of the behaviour of the exergy input curve, which is shown in the same figure.

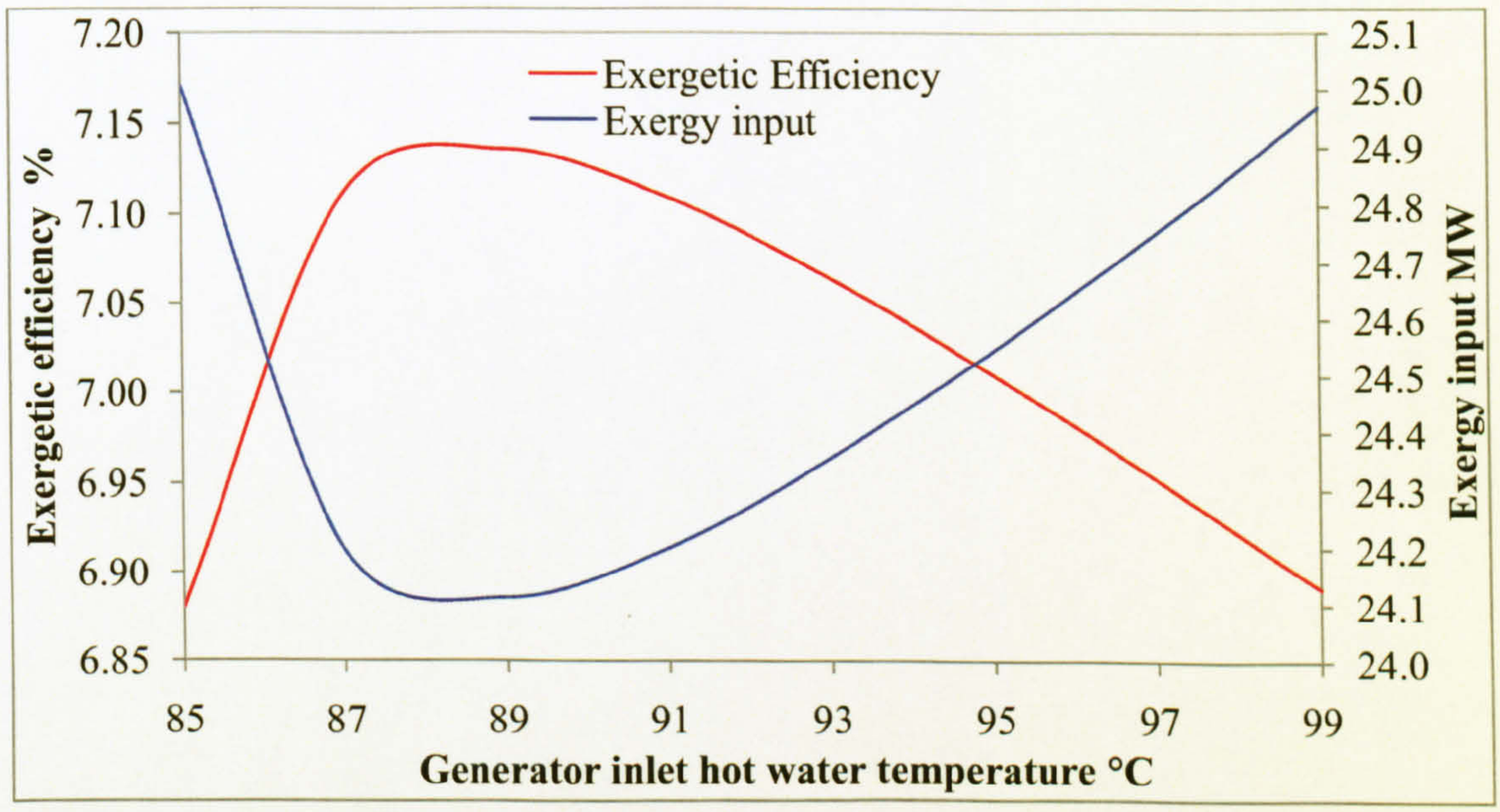

Figure 4-46 Exergetic efficiency and exergy input versus generator inlet hot water temperature

The exergy analysis results of this study suggested that the absorption chiller should be operated with a hot water stream at a temperature of 88˚C for the lowest exergy destruction and the highest exergetic efficiency; however, as indicated by the plant's real data it operated with a temperature of 97.7˚C, which is acceptable if the amount of inlet hot water and the insignificant reduction in the plant's exergetic efficiency were considered.

Chapter 5

Proposed Plants' Modelling and Results

5.1 Introduction

This chapter presents the modelling, simulation, performance assessment and off-design studies for all the proposed plants that were modelled based on the base plants introduced in the previous chapter. Firstly, the modelling configuration of each proposed plant is presented. Then, all the modelling results are introduced and compared for all proposed plants. From the result of this comparison, the optimal plant is chosen for the optimization stage. In the optimization stage the modelling configuration and results are presented and compared with those of the chosen plant before utilization. Then, the optimized plant partial load performance, operating modes and parametric studies are presented.

5.2 Proposed Plants' Modelling Configurations

The main aim of this study is to discover the optimal design that assures the minimum CO_2 emission rate, best combined cycle power plant performance and highest electricity and potable water production rates. Two different desalination technologies and coupling techniques were tested. The sequence by which these proposed plants are presented mimics the stages followed in this study to achieve the optimal proposed plant.

5.2.1 CCPP+MED

The first proposed plant (CCPP+MED) implied the maximum work hypotheses, in which the CC power plant generated its maximum nominal capacity with no changes in its structure. An MED desalination plant was connected to the power plant via a boiler that was placed after the HRSG unit to utilize a portion of the exhaust gases' heat energy emitted into the atmosphere. Figure 5-1 shows a block diagram of this proposed plant where the gas turbine consumed 8.763kg/s of natural gas to operate its generator, which generated 135.74MW of electric power and emitted 289MW of heat energy as an exhaust gas toward the HRSG unit.

The HRSG unit utilized 60.4% of that heat energy to power the steam turbine with 88-bar steam using the circulated water stream coming from the steam turbine's condenser. The steam turbine operated its generator, which generated 59.33MW of electric power. The steam turbine's condenser used a seawater stream as cooling water to condense the steam exiting the steam turbine. The MED desalination plant's boiler utilized 21.6% of the exhaust's heat energy to

generate 26kg/s of steam at a temperature of 70°C, which powered the brine heater (first effect) of the MED desalination plant.

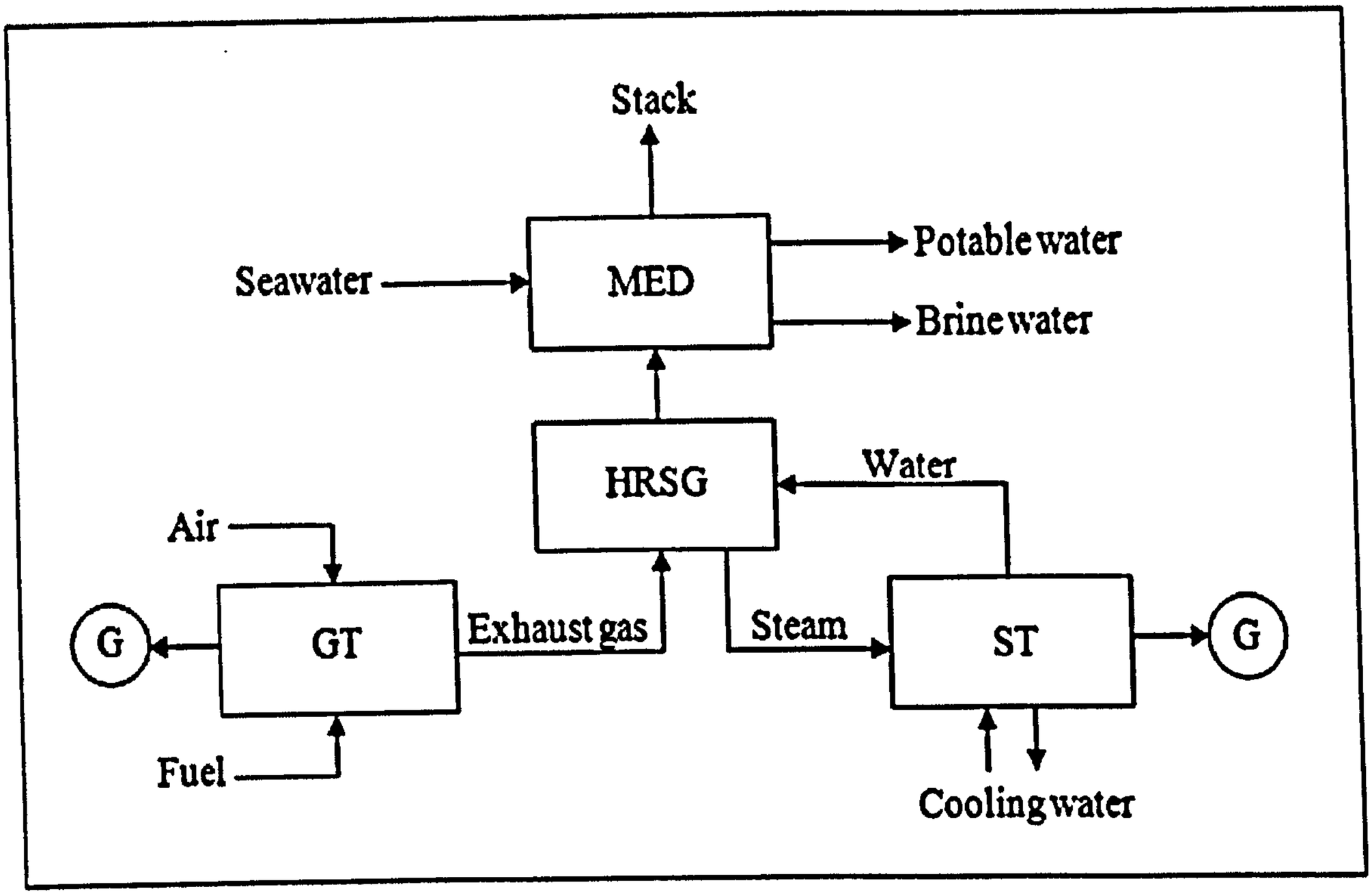

Figure 5-1 First proposed plant's (CCPP+MED) block diagram

The MED desalination plant's boiler was designed with an effectiveness of 0.80 and NTU of 1.6. On the other hand, the proposed plant emitted 51.9MW of heat energy as waste heat energy through the stack, which represented 17.9% of the total exhaust's heat energy emitted from the gas turbine.

5.2.2 CCPP+TVC-MED

The second proposed plant was similar to the first one except that the MED desalination plant was replaced by a TVC-MED desalination plant. The TVC-MED desalination plant was also connected to the power plant by a boiler that was placed after the HRSG unit as shown in Figure 5-2. The combined cycle power plant's arrangement and performance were similar to those in the first proposed plant and the base CC power plant. The TVC-MED desalination plant's boiler also recovered 21.6% of the CC power plant's waste heat energy to generate 26kg/s of steam at a temperature of 90°C, which powered the steam ejector of the TVC-MED desalination plant.

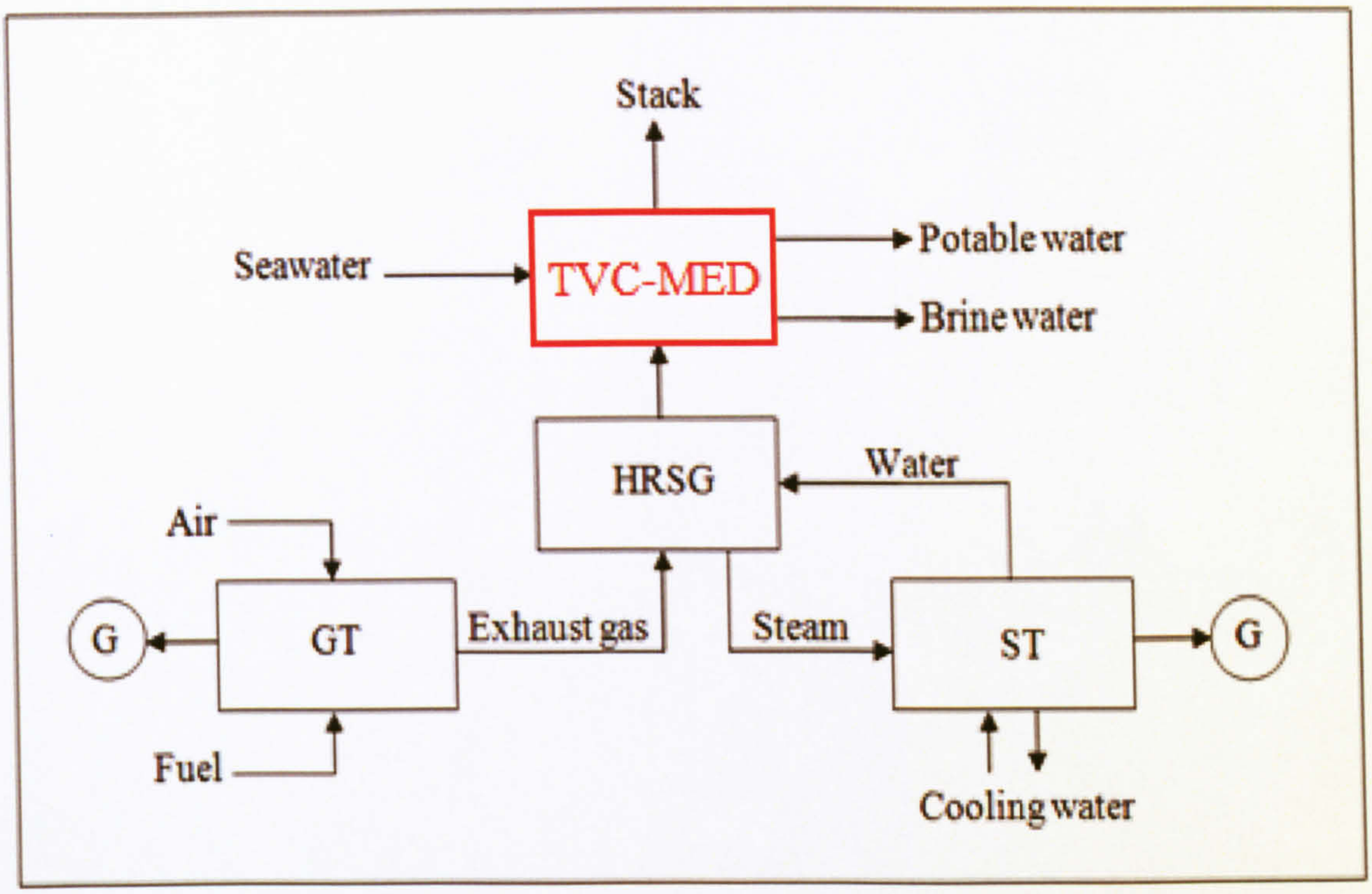

Figure 5-2 Second proposed plant's (CCPP+TVC-MED) block diagram

The TVC-MED desalination plant's boiler was designed with an effectiveness of 0.80 and NTU value of 1.75.

5.2.3 CCPP+(Boiler) TVC-MED+AC

The third proposed plant combined a combined cycle power plant, TVC-MED desalination plant and an absorption chiller. The CC power plant and the TVC-MED plant were connected by a boiler implanted between the gas turbine and the steam turbine cycle. The TVC-MED plant's boiler was placed before the steam turbine cycle to give the potable water production from the TVC-MED desalination plant priority over the electricity generated from the steam turbine.

Figure 5-3 shows the block diagram of this proposed plant, where 44.6% of the exhaust gas heat energy was recovered in the TVC-MED desalination plant's boiler. The boiler generated 55kg/s of steam at a temperature of 90°C, which powered the steam ejector of the TVC-MED desalination plant. The exhaust gas stream then proceeded to the HRSG unit, which utilized 19.5% of its heat energy to power the steam turbine. The steam turbine generated 15MW of electric power, which is only 25% of its nominal capacity. The absorption chiller's boiler then

recovered 4% of the exhaust gas heat energy to power the absorption chiller with a stream of hot water at a temperature of 97˚C.

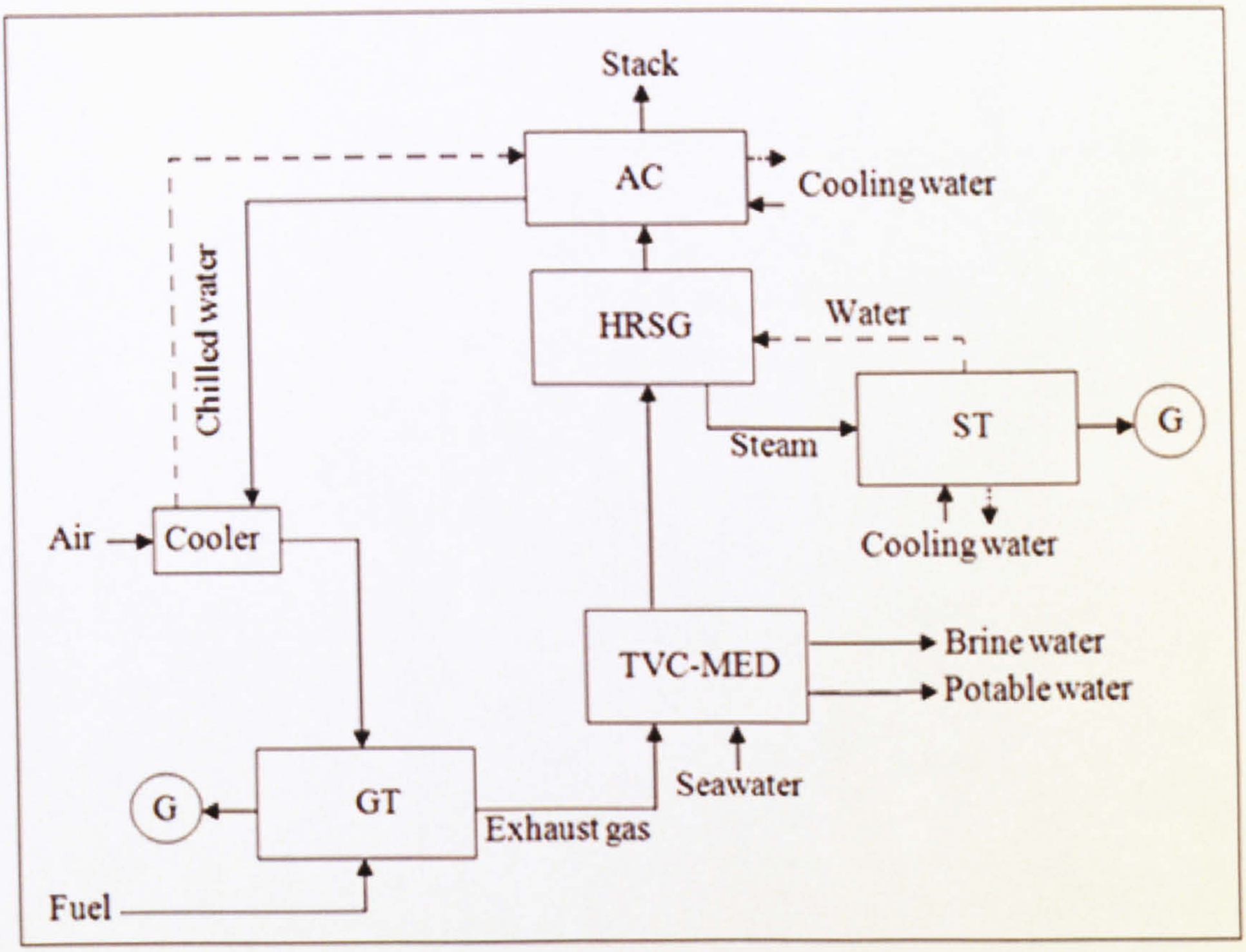

Figure 5-3 Third proposed plant block diagram

The absorption chiller produced 9304 kW of cooling effect, which was used to cool the gas turbine's compressor's inlet-air from the ambient condition to 10˚C. Two streams of seawater were used as cooling water for both the steam turbine's condenser and the absorption chiller as shown in the block diagram.

5.2.4 CCPP+(Steam extraction) TVC-MED+AC

The fourth proposed plant was similar to the previous plant (the third) and consisted of a combined cycle power plant, a TVC-MED desalination plant and an absorption chiller. However, the TVC-MED plant was powered by steam extracted from the steam turbine as shown in Figure 5-4. The CC power plant was left without modification in its construction, except that steam at 5.3 bar and at a temperature of 195˚C was extracted from the steam turbine for use as motive

steam to power the TVC-MED desalination plant. The HRSG unit recovered 63.1% of the exhaust gas heat energy to power the steam turbine with 88-bar steam.

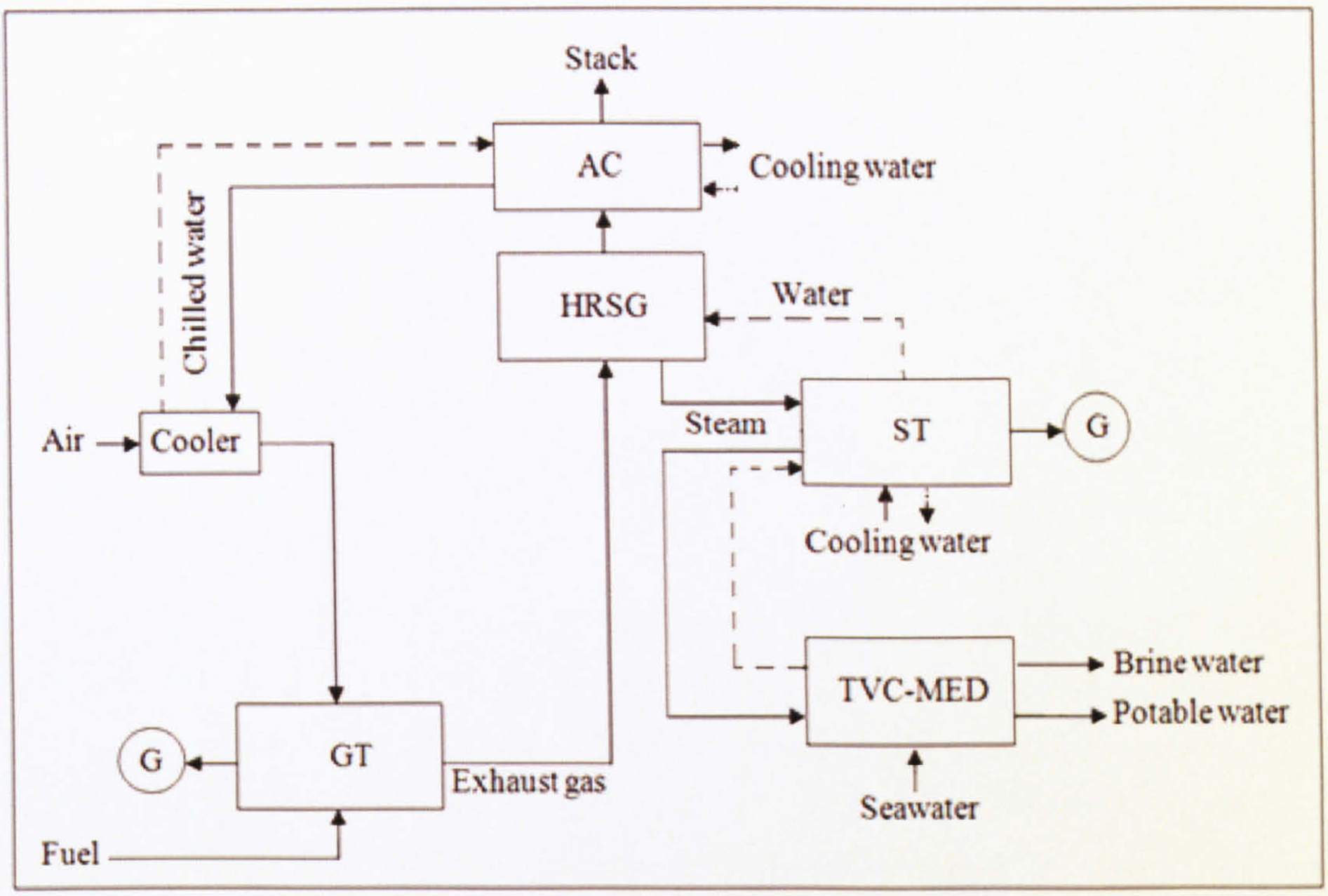

Figure 5-4 Fourth proposed plant block diagram

The steam turbine drove a generator that generated 30.64MW of electric power. The extracted steam from the steam turbine worked as a motive steam for the TVC-MED desalination plant's steam ejector, which powered the brine heater (first effect) of the desalination plant. The steam in the first effect boiled a portion of feed seawater and then exited the brine heater into the HRSG unit as make-up feed water. The exhaust gas after the HRSG unit proceeded to the absorption chiller's boiler, which recovered 4% of its heat energy to power the absorption chiller. The absorption chiller produced the cooling effect that cooled the compressor's inlet-air. The exiting water from the gas turbine's cooler then was circulated back to the absorption chiller's evaporator. From the absorption chiller's boiler the exhaust gas stream proceeded towards the stack.

5.3 Proposed Plants' Modelling Results

After the modelling stage each of the proposed plants was examined in ISO conditions. The readings for all parameters were obtained from the simulation software except the entropy and

enthalpy values of the seawater, brine water and LiBr streams, which were calculated manually as explained in Chapter 3. These reading were then used to perform full energy and exergy analyses for each plant. The results of these studies will be discussed and compared for all plants in the following sections.

5.3.1 Energy Analysis

Table 5-1 lists the energy analysis results for all the proposed plants in addition to that of the stand-alone. The CC power plant's performance in the first proposed plants was similar to the stand-alone's performance, except for the CO_2 emission rate and the energy utilization factor (EUF), which improved by 24% and 16.21% respectively. Likewise, in the second proposed plant the CO_2 emission rate and the energy utilization factor both improved by 26% and 17.51% respectively. This was mainly due to recovering about 22% of the exhaust heat energy in the desalination plant's boiler. In the second proposed plant, the TVC-MED desalination plant's production rate improved by 8.34% in comparison with that of the MED desalination plant, which improved its gain output ratio (GOR) from 7.32 to 8.14. This clearly indicated that the TVC-MED desalination process was more efficient than the MED desalination process, which is in agreement with what has been reported in a number of studies [64-68]. Therefore, in both the third and fourth proposed plants only the TVC-MED desalination process was used for the purpose of potable water production.

In the third proposed plant, the TVC-MED desalination plant produced its nominal capacity 40,000m^3/day, which improved the plant's EUF by 26.3% in comparison with the base CC power plant and by 10.09% in comparison with both the first and second proposed plants. The gas turbine electric output power was increased by 3.31MW due to cooling its compressor's inlet-air from ISO conditions to 10°C. Likewise, the plant's CO_2 emission rate in the third proposed plant dropped to 339.7kg CO_2/kW. However, the electric power generated by the steam turbine decreased by 74% because of placing the desalination boiler before the HRSG unit in order to give priority to the potable water production. This decreased the plant's net output power by 20%, which also decreased the plant's overall efficiency by 11.1%. The absorption chiller's performance was similar to its stand-alone performance.

In the fourth proposed plant, the electric power generated by the steam turbine increased to 30.64MW, which improved the overall electrical efficiency by 4.02% in comparison with the third proposed plant. Moreover, the plant's CO_2 emission rate and EUF both improved by 36.8% and 30.97% respectively in comparison with the base CC power plant. The TVC-MED desalination plant produced its nominal capacity and its GOR improved to 8.48 as a result of the increase of its motive steam pressure. Furthermore, in this proposed plant the absorption chiller's performance was similar to its stand-alone performance.

Parameters	Unit	Stand-alone	Proposed plants			
			1st	2nd	3rd	4th
Potable water production	m^3/day	40000	17688	19164	40000	40000
Evaporator cooling power	kW	9304	9304	9304	9304	9304
CO_2 emission rate	kg/kW	508.14	384.2	374.24	339.7	320.75
Net output power	MW	195.07	195.07	195.06	154.18	169.65
GT output power	MW	135.7	135.7	135.7	139.01	139.01
ST electric power	MW	59.3	59.3	59.3	15.17	30.64
Overall efficiency	%	52.79	52.79	52.79	41.68	45.70
Energy utilization factor	%	52.79	69	70.3	79.09	83.76
Desalination process GOR	-	8.13	7.32	8.14	8.14	8.48
Absorption chiller COP	-	0.79	0.79	0.79	0.79	0.79

1st: CCPP+MED
2nd: CCPP+TVC-MED
3rd: CCPP+(boiler) TVC-MED+AC
4th : CCPP+(steam extraction) TVC-MED+AC

Table 5-1 Energy analysis results of the proposed plants

Although in both the first and second proposed plants the CC power plant generated its nominal electric power capacity, both desalination plants did not produce even half of their nominal capacity, because there was no enough heat energy in the exhaust gas to fully power the desalination plant. If this were to be compensated for by the electric power generated, the third design should be considered here as it generated the lowest electricity output power, with its desalination plant producing its nominal capacity 40000m^3/day. The difference in electricity generated between both plants should be then directed towards water production through other non-thermal desalination technologies that are powered by electricity.

The third design generated 149.37MW of electricity, while the first and second plants generated the nominal capacity of the CC power plant, which is 195 MW. If this 46MW were to be used to power a reverse osmosis (RO) desalination plant with an electricity consumption of 3-10kWh/m^3, this would mean 15333m^3/day. This would increase the total potable water produced to 34497m^3/day, which is less than the desalination plant's nominal capacity, which was produced in both the third and fourth proposed plants. Considering also the initial investment cost of the RO desalination plant, and the fact that in these two designs the absorption chiller could not be integrated for the purpose of pre-cooling the gas turbine compressor's inlet-air, both the first and second proposed plants are not the optimal designs.

From the comparison between the third and fourth proposed plants based on the energy analysis, it can be concluded that the fourth proposed plant is the optimal plant, because it generated 10% more net output power and its electrical efficiency was less than the base CC power plant's efficiency by only 7% and had better CO_2 emission rate and EUF value.

5.3.2 Exergy Analysis

Table 5–2 lists the exergy analysis results for all four proposed plants in addition to that of the stand-alone. The results of the first two proposed plants show a reduction in that plant's total exergy destruction, which is mainly due to the reduction of about 82% in the exergy destroyed through the stack as a result of recovering 21.6% of the plant's waste heat energy in the desalination plant. Other than this, the CC power plant's exergetic performance was similar to its stand-alone performance. In the second proposed plant, the exergy destruction of the TVC-MED desalination plant's boiler was less than that of the MED desalination plant. Even with the addition of the steam ejector the total exergy destruction of the desalination plant was better than that of the MED desalination plant. These findings confirm the results of the energy analysis, which concluded that the TVC-MED is more efficient than the MED desalination plant.

In the third proposed plant, the desalination's boiler exergy destruction was the second largest cause of the proposed plant's exergy destruction after the gas turbine, because of its high input exergy from the exhaust gas side. Even with this increase in the desalination boiler's exergy destruction, the plant's total exergy destruction increased by only 9.44MW. This is mainly because of the reduction in the exergy destroyed through the stack and by the steam turbine

cycle's components (HRSG, steam turbine and ST condenser) by 33% and 69% respectively. However, the plant's overall exergetic efficiency dropped to 42.39% due to the reduction in the net output power.

Component	Exergy destruction in MW				
	Stand-alone	Proposed plants			
		1st	2nd	3rd	4th
Gas turbine	123.42	123.41	123.41	118.48	118.48
GT cooler	-	-	-	0.23	0.23
Desalination boiler	-	10.69	7.76	48.86	-
Desalination evaporators	9.82	4.28	5.87	9.80	10.03
Desalination steam ejector	5.1	-	2.44	5.09	19.11
Desalination condenser	4.02	2.02	1.93	3.89	3.99
HRSG	21.07	21.07	21.7	8.51	18.71
Steam turbine	12.8	12.8	12.8	3.36	6.05
ST condenser	7.27	7.27	7.27	0.98	0.15
Absorption chiller boiler	-	-	-	2.31	2.85
AC generator	0.36	-	-	0.31	0.31
AC absorber	0.30	-	-	0.30	0.30
AC evaporator	0.21	-	-	0.21	0.21
AC condenser	0.20	-	-	0.20	0.20
AC heat exchanger	0.20	-	-	0.20	0.20
AC exp. valve	0.04	-	-	0.04	0.04
Stack	25.62	4.56	4.91	17.10	24.7
Total exergy destruction	210.43	186.09	187.46	219.87	205.48
Sub-plant	Exergetic efficiency %				
Gas turbine	52.26	52.26	52.26	53.99	53.99
Steam turbine	82.25	82.25	82.25	81.85	91.58
TVC-MED desalination	31.13	-	31.14	31.43	20.73
MED desalination	39.42	39.69	-	-	-
Absorption chiller	6.9	-	-	7.06	7.06
Plant overall	-	51.6	51.36	42.39	48.16

1st: CCPP+MED
2nd: CCPP+TVC-MED
3rd: CCPP+(boiler) TVC-MED+AC
4th : CCPP+(steam extraction) TVC-MED+AC

Table 5-2 Exergy analysis results of the proposed plants

In both the third and fourth proposed plants, the gas turbine's exergy destruction decreased by 4% and its exergetic efficiency improved by 1.73% as a result of cooling the compressor's inlet-air by the absorption chiller. Moreover, in both plants the absorption chiller's exergetic performance was similar to its stand-alone performance. In the fourth proposed plant, the TVC-MED desalination components' exergy destruction increased significantly in comparison with the stand-alone model but it was still 51% less than that of the third plant. The coupling technique used in the fourth plant improved the plant's overall exergetic efficiency by 5.77% in comparison with the third proposed plant due to the increase in the plant's net output power. Furthermore, the exergy destruction of the steam turbine components decreased significantly due to the coupling technique. The exergy destroyed through the stack decreased by about 0.93MW in comparison with that of the base CC power plant, but was higher than that of the third proposed plant, which indicated the possibility of further waste heat recovery.

Although the TVC-MED produced its nominal capacity in both the third and fourth proposed plants, the TVC-MED desalination plant's exergetic efficiency in the fourth plant was 20.73% due to the higher exergy input through the motive steam that was extracted from the steam turbine at a higher pressure than that generated from the boiler in the third proposed plant. Moreover, the steam turbine's exergetic efficiency improved in the fourth proposed plant by 9% due to the steam extraction, which increased the steam turbine's exergetic product while the exergetic fuel was the same.

By comparison between all four proposed plants, the first two proposed plants had the highest exergetic efficiency and the lowest exergy destruction rates; however, neither produced the full potable water production rate and neither had the ability to power the absorption chiller. Therefore, the fourth plant must be chosen for its higher exergetic efficiency and lower exergy destruction rate in comparison with the third proposed plant.

5.4 Optimization

From the results discussed in the previous section, the exergy destroyed through the stack in the chosen proposed plant (fourth plant) in comparison with the first two proposed plant indicated the possibility of further utilization of waste heat energy. Moreover, the steam turbine condenser's cooling water, which was wasted in all the proposed plants, can be directed for

better use within the plant. This section introduces two modifications that will improve the performance of the chosen plant, and suggests number of operating modes that improves the plant flexibility.

5.4.1 Modelling Configuration

The optimization is on the structural level and this includes introducing new components to the chosen plant. Therefore, the modelling configuration is presented first.

- **Absorption chiller's cooling water**

The absorption chiller's cooling water, after exiting the absorption chiller's condenser, had a temperature averaging 35°C to 41°C depending on the intake seawater temperature. This stream of wasted water can be utilized by adding a heat exchanger to the gas turbine's exhaust system to recover a portion of the remaining heat energy for the purpose of heating up the absorption chiller's cooling water. This source of hot water (HW) can be then directed for further industrial or domestic use onsite or offsite. Figure 5-5 shows a block diagram of the chosen plant with the suggested modifications.

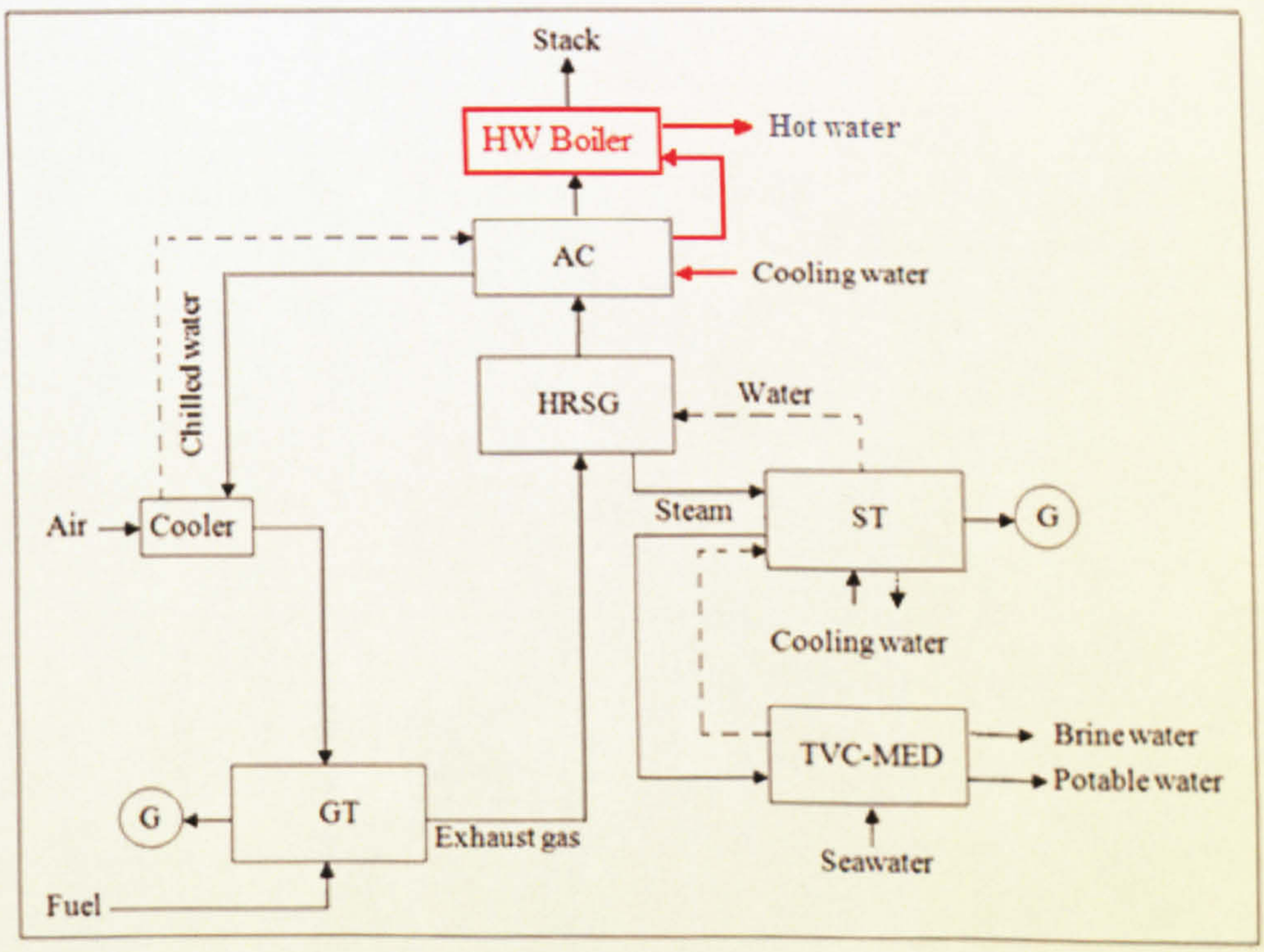

Figure 5-5 HW water optimization block diagram

The absorption chiller's cooling water will be processed into the hot water (HW) boiler, which will recover 19% of the exhaust heat energy in heating up the absorption chiller's cooling water to a temperature varying from 75°C to 81°C depending on the ambient conditions. The HW boiler was modelled with an effectiveness of 0.61 and 1.08 NTU. The steam, gas and water temperature profiles of the HRSG unit, AC boiler and HW boiler are presented in Figure 5-6.

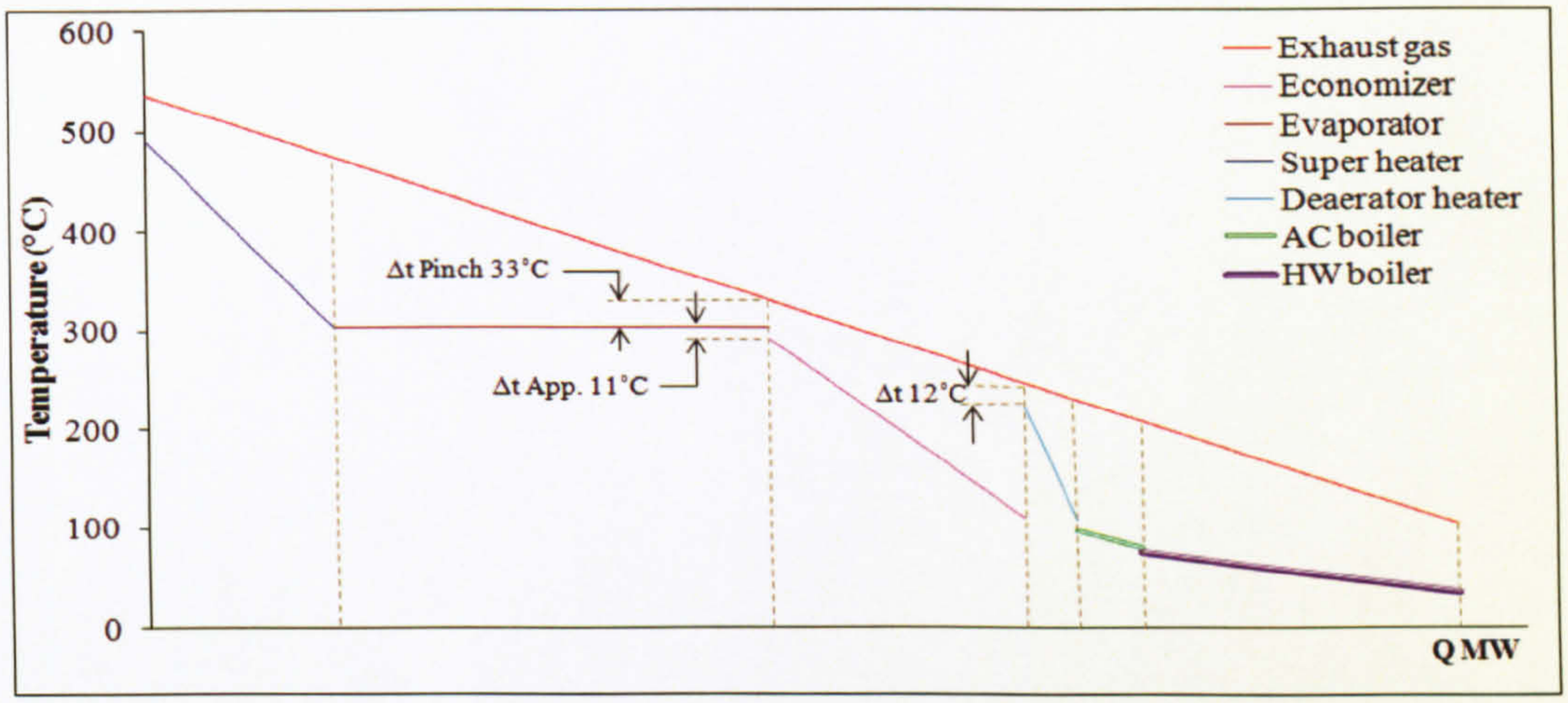

Figure 5-6 Temperature profiles of the HRSG unit, AC boiler and HW boiler

The addition of the hot water boiler reduced the waste heat energy through the stack by 51% from 112.86MW in the chosen plant to 54.93MW in the same plant after optimization. The only drawback of this modification was the back pressure caused by the HW boiler. The result of this modification was a 345kg/s stream of hot water with 108MW heat energy at a temperature of 75°C in ISO conditions.

- **Steam turbine's cooling water**

The impact of the TVC-MED desalination process due to consuming electricity is very low in comparison with other desalination processes due to its low electricity consumption. The optimized plant's environmental impact is then mainly caused by the brine that is typically rejected into the sea without treatment [133]. Although the chemical additive to the feed seawater is minimal in comparison with other desalination processes [1, 10], the salinity and temperature of the brine pose a threat to the marine environment [134]. The only post-treatment used in some desalination process plants, for example RO, is for the produced potable water to adjust its pH, add lime and remove the dissolved gases [7]. Therefore, the second suggested modification aims to utilize the wasted cooling water of the steam turbine's condenser to

minimize the salinity and temperature of the rejected brine from the TVC-MED desalination plant. Figure 5-7 shows a block diagram of the suggested modification on the chosen plant. The cooling water of the steam turbine's condenser is directed towards the desalination plant to be mixed with the brine rejected from the desalination process.

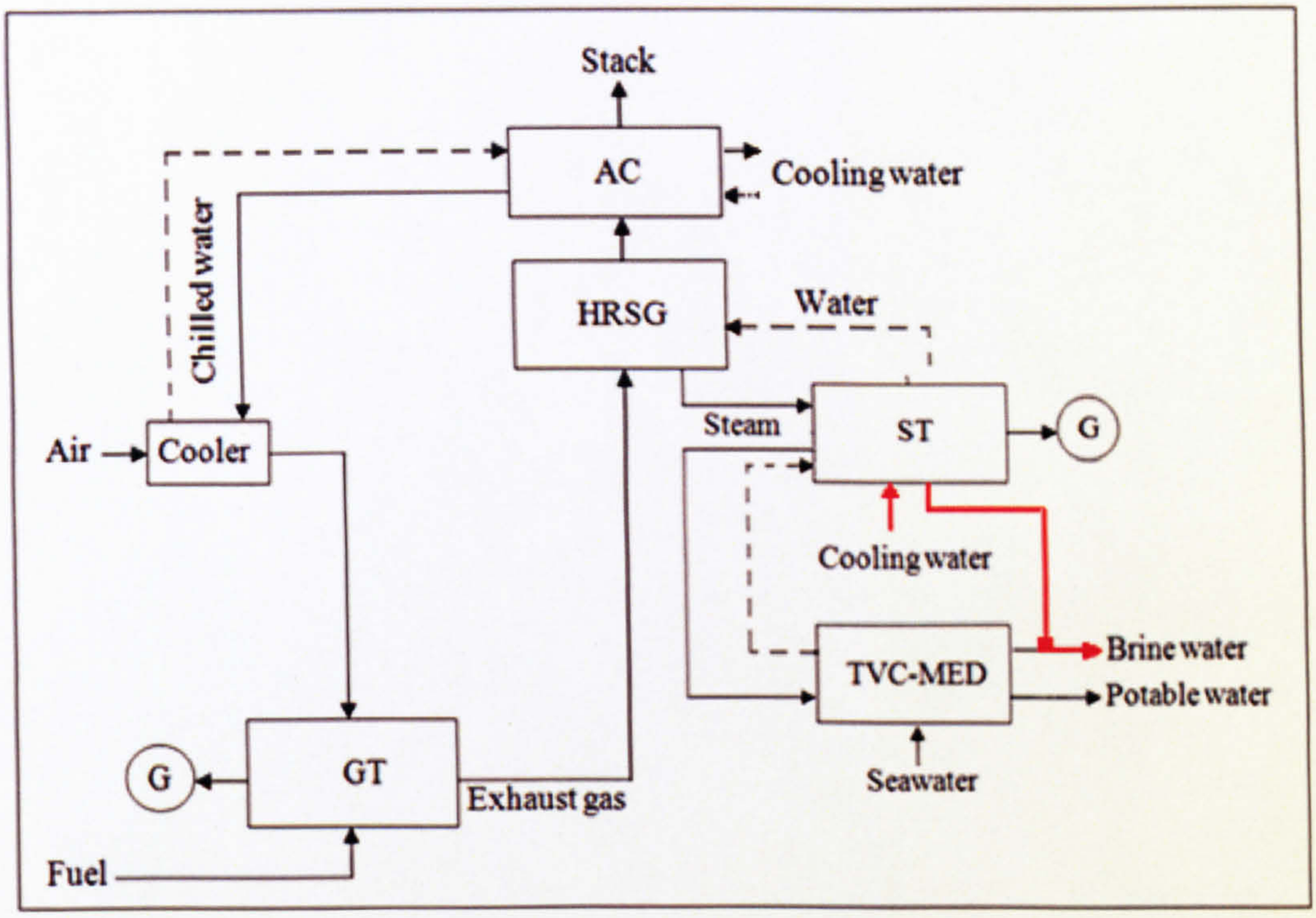

Figure 5-7 Steam turbine's cooling water optimization block diagram

This modification has no drawbacks for the proposed plant and needs no additional components other than a piping system and simple mixer. The result of this modification is a reduction in the TVC-MED desalination plant's rejected brine salinity and temperature.

5.4.2 Modelling Results

Based on the energy analysis, the plant's performance after optimization was improved by the further utilization of the exhaust gas heat energy in the hot water boiler. Table 5-3 lists the energy analysis results of the fourth proposed plant before and after optimization. In addition to the 40000m^3/day of potable water and the 169.72MW output of electric power, the plant produced a stream of hot water at a temperature varying from 75˚C to 81˚C according to the ambient conditions. The results also show that the gas turbine's output of electric power decreased insignificantly by 410kW due to the back pressure created by the HW boiler.

However, the steam turbine benefited from this back pressure where its electricity generation also improved insignificantly by 480kW, which compensated for the reduction in the gas turbine's output power, and slightly increased the optimized plant's net output power. The plant's overall electrical efficiency also improved slightly by 0.21%, as a result of the increase in the plant's output power.

Parameter	Unit	4th proposed plant	
		Before optimization	After optimization
CO_2 emission rate	Kg CO_2/kW	320.75	219.81
Net output power	MW	169.65	169.72
Gas turbine output power	MW	139.01	138.6
Steam turbine electric power	MW	30.64	31.12
EUF	%	83.76	98.87
COP	-	0.79	0.79
Overall electrical efficiency	%	45.70	45.91
Gain output ratio GOR	-	8.48	8.56
Concentration factor	-	1.87	1.42
	kg/s	-	345
Hot water production	MW	-	108.57
	°C	-	75.15
AC cooling effect	kW	9304	9304
Potable water production	m³/day	40000	40000

Table 5-3 Energy analysis results of the 4th plant before and after optimization

The plant's CO_2 emission rate decreased significantly from 320.75kg to 219.81kg CO_2/kW after optimization due to utilizing 19.7% of the exhaust heat energy in the hot water boiler. This additional product improved the plant's energy utilization factor by 15.1% reaching 98.87%. According to Horlock [135], it is possible to achieve 100% EUF in the case of continuous hot water production. Although the technique used to produce the hot water in Horlock's study was different, it gives an indication of the possibility of achieving a high EUF value. Horlock studied the steam combined cycles that produce hot water for district heating through an extraction from the steam turbine as used in this study but to power the TVC-MED desalination plant. The TVC-MED desalination plant's GOR improved insignificantly by 0.12 due to the change in the motive steam extracted from the steam turbine, which was affected by the back pressure caused by the hot water boiler. Its concentration factor (CF) improved by 22% as a result of mixing the condenser's cooling water with it. Nonetheless, the temperature of the rejected brine dropped

from 50°C to 37°C, which makes it safer to reject it back into the sea. The absorption chiller's performance was similar to its performance before optimization.

On the basis of the exergy analysis, the hot water boiler caused an exergy destruction of 19.22MW, which was compensated for by the reduction in the stack exergy destruction by the same amount. Therefore, the addition of the HW boiler did not have an effect on the plant's total exergy destruction. The plant's overall exergetic efficiency improved to 49.64% driven by the exergy content of the hot water stream, which is regarded as an additional product. Other than this, all sub-plants showed no significant responses to the new modifications and performed almost the same as before optimization. In conclusion, the modification improved the plant's overall exergetic efficiency, reduced the exergy destroyed through the stack and had no impact on the plant's overall exergy destruction.

5.4.3 Operating Modes

The proposed plant can be operated on three different modes by controlling the TVC-MED desalination plant's production rate. The TVC-MED desalination plant consists of two units each producing 20,000m^3/day; by isolating one of them the potable water production rate can be minimized to half and simply isolating both of them gives priority to the electric power generation during the sessions of high demand. Table 5-4 lists a full comparison between the three possible operating modes based on the energy analysis results. The absorption chiller's performance was not affected by changing the operating modes; it consumed the same amount of exhaust heat energy and produced the same amount of cooling effect (9304kW) at the same temperature (6.7°C). Therefore, the hot water production rate (108.57MW) and temperature (75°C) did not change either as the hot water boiler utilized the same amount of heat from the exhaust gas.

When the plant was operated to produce only 20,000m^3/day of potable water, the steam turbine electric power increased by 50% because of the reduction in the steam extracted to power the TVC-MED desalination plant. The plant's overall electrical efficiency increased to 49.81%, driven by the increase in the plant's net output power. The desalination plant's concentration factor decreased to 1.13, due to the increase in cooling water consumed by the steam turbine

condenser. The rejected brine's temperature dropped to 35°C in comparison with 50°C before optimization.

Parameter	Unit	TVC-MED operating mode		
		40000 m^3/day	20000 m^3/day	0 m^3/day
Cold water temperature	°C	6.7	6.7	6.7
Evaporator cooling power	kW	9304	9304	9304
CO_2 emission rate	Kg CO_2/kW	219.81	277.66	376.84
COP	-	0.79	0.79	0.79
Net power	MW	169.72	184.14	198.55
GT power	MW	138.6	138.6	138.6
ST power	MW	31.12	45.54	59.95
EUF	%	98.87	85	71.12
Overall electrical efficiency	%	45.91	49.81	53.7
GOR	-	8.56	8.56	-
Concentration factor	-	1.42	1.13	-
Specific heat consumption	kJ/kg	318.59	318.59	-
	kg/s	345	345	345
Hot water	MW	108.57	108.57	108.57
	°C	75.15	75.15	75.15

Table 5-4 Comparison of energy analysis results between the operating modes

In comparison with the second proposed plant, which implied the maximum work hypotheses, after optimization the fourth proposed plant was better because it included the absorption chiller, which allowed the compressor inlet-air cooling process; its CO_2 emission rate was reduced by 28%, as a result of further utilization in the absorption chiller and the HW boilers and its EUF was higher by 15%.

The TVC-MED desalination plant can also be totally turned off, when there is a higher demand for electricity. In this operating mode (0m^3/day), the steam turbine generated its nominal capacity of 59.33MW. This increased the plant's net output power to 198.55MW, which was higher than that of the base CC power plant due to cooling the compressor inlet-air. Likewise,

the plant's overall electrical efficiency improved to 53.2%, which was also higher than that of the base CC power plant. Although the plant's CO_2 emission rate increased to 376kg CO_2/kW, it was still less than that of the base power plant by 26%. The EUF also decreased to 77% as a result of isolating the TVC-MED desalination plant. However, it was still higher than that of the base CC power plant by 25%.

Based on the exergy analysis, Table 5-5 lists the most significant exergetic results for the optimized plant at the three operating modes.

	TVC-MED operating mode		
Exergy destruction MW	40000m^3/day	20000m^3/day	0m^3/day
TVC-MED evaporators	11.21	5.60	0.00
TVC-MED steam ejector	18.87	9.44	0.00
TVC-MED condenser	4.05	2.02	0.00
Steam turbine	6.16	9.57	12.97
ST condenser	0.15	1.41	2.74
HW boiler	19.22	18.38	17.50
Stack	5.53	4.42	3.41
Total exergy destruction	205.89	193.97	181.02
Overall exergetic efficiency %	49.64	51.22	54.73

Table 5-5 Operating modes' exergy analysis results

The exergy destruction of the TVC-MED desalination plant's components dropped by 50% when operating in the 20,000m^3/day mode. Although the exergy destruction of the steam turbine and its condenser increased, the plant's total exergy destruction decreased by 5.7% so that it was less than that of the base power plant. Furthermore, the plant's overall exergetic efficiency improved by 1.59 as a result of the increase in the plant's net output power.

The HW boiler's exergy destruction also decreased due to the reduction in the exergy content of its input from the exhaust gas side. In the 0m^3/day operating mode, the plant's exergetic efficiency improved to 54.73% as the power plant generated its maximum output power. The exergy destruction dropped to 181MW due to isolating the TVC-MED desalination plant totally. These results indicate that the proposal of this study can offer an improvement to any exciting

power plant, if it were to be adopted either as a whole by installing both the absorption chiller and the TVC-MED desalination plant or just one of them. In both situations the plant's electrical efficiency, EUF, CO_2 emission rate, exergy destruction and exergetic efficiency will all improve significantly.

5.4.4 Partial Load

This far, the plant's net output electric power only varied from 169.72MW to 198.55MW; further variation could have been achieved by operating the gas turbine at partial load. This is usually preferred when the plant's fuel consumption needed to be lowered or in the case of lower demands in winter months. A parametric study was performed to examine the performance of the optimized plant with different operating load patterns. The study was performed in ISO conditions, with a seawater temperature of 22˚C, and the TVC-MED plant operated at half load producing 20,000m^3/day of potable water.

All the results of this study are listed in tables 1, 2 and 3 in Appendix D, while the most significant results are plotted and discussed in this chapter. Figure 5-8 shows the plant's net output of electric power and the gas turbine's fuel consumption with the change in the gas turbine load. The plant's net electric power generation dropped by 86.6% from 184.MW at full load to 57.72MW at half load, in return for a 52% saving in fuel consumption.

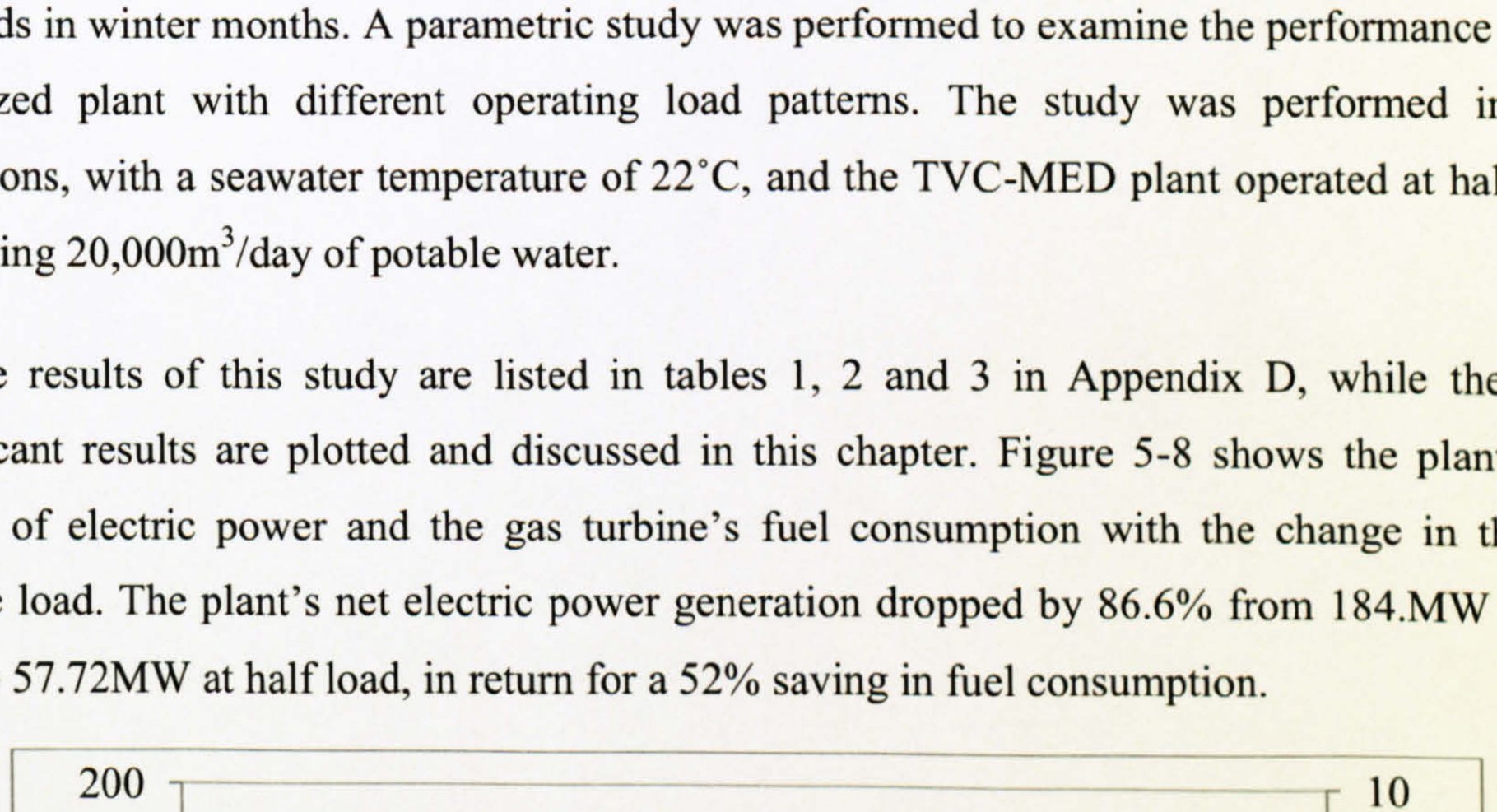

Figure 5-8 Fuel consumption and net output power performance at partial load

The gas turbine's electric power generation decreased by 62% and that of the steam turbine by 88%. This higher percentage for the steam turbine was driven by a stable rate of potable water production from the TVC-MED desalination plant and the decrease in the exhaust gas mass flow rate that was defined by the gas turbine's characteristic curves presented in the Chapter 3. Figure 5-9 shows the plant's electrical efficiency and CO_2 emission rate performance at partial load. The plant's overall electrical efficiency also dropped to 33.4% at half load, driven mainly by the 68.6% reduction in its net output of electric power, while the fuel consumption only decreased by 52%. However, the cooling effect and potable water production rates were not affected at partial load, which improved the plant's CO_2 emission rate by 5.6% at half load in comparison with full load.

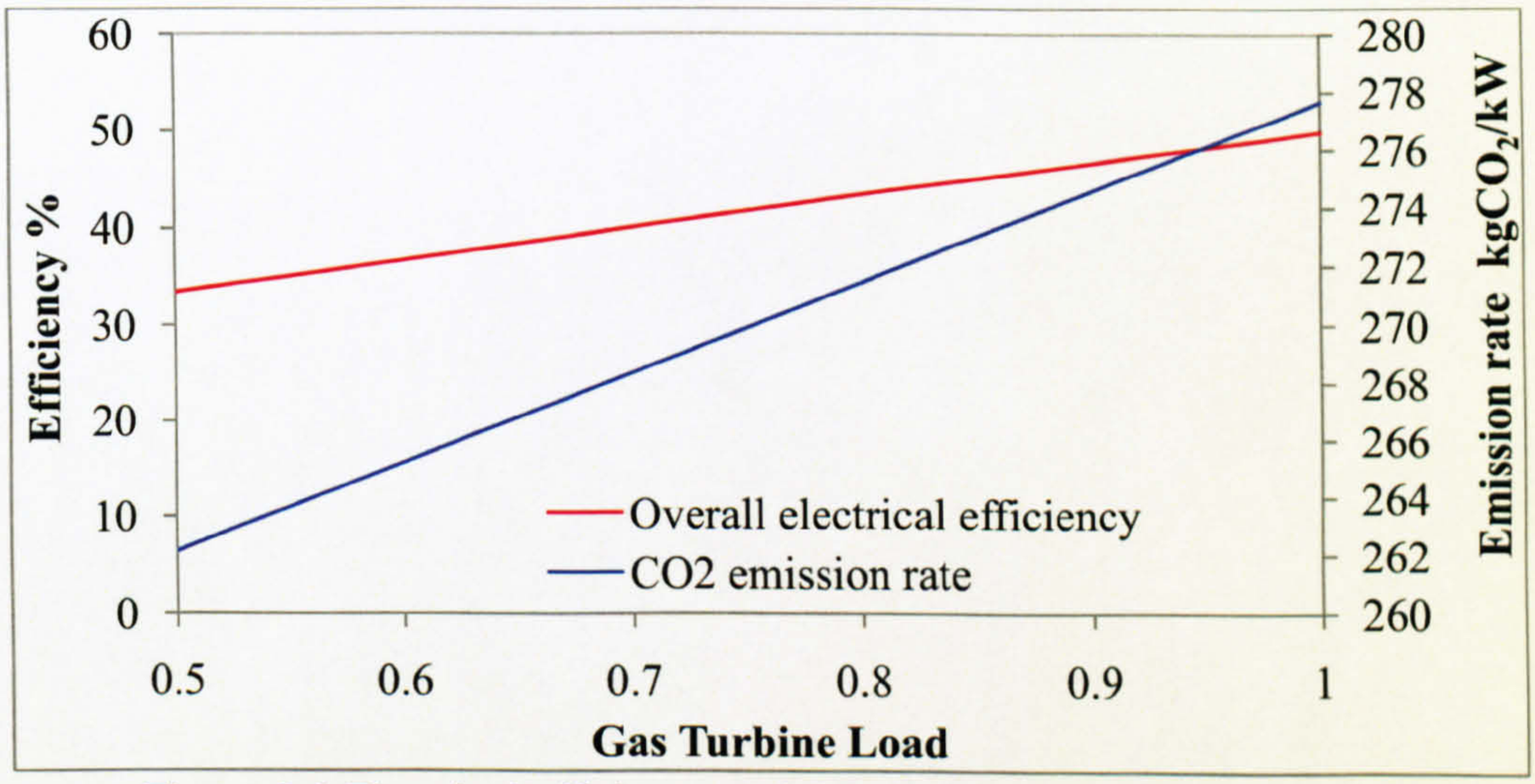

Figure 5-9 Electrical efficiency and CO_2 emission rate at partial load

On the exergy analysis basis, the exergy destruction rates of both the absorption chiller and the TVC-MED desalination plant were not affected at partial load as they maintained stable production and consumption rates. At a lower load, the exergy destruction of all other components of the plant tended to decrease, except for the HW boiler and stack, which tended to increase insignificantly as the load was lowered, as seen in Figure 5-10. This reduction is explained by the reduction in the amount of fuel, which also reduced the exhaust gas mass flow rate by 18% at half load, whereas the HW boiler still received the same amount of exergy input from the cooling water side and recovered the same amount of heat energy from the exhaust gas. Therefore, the hot water temperature increased insignificantly by 1.6°C, which insignificantly increased the exergy destruction of the HW boiler at partial load.

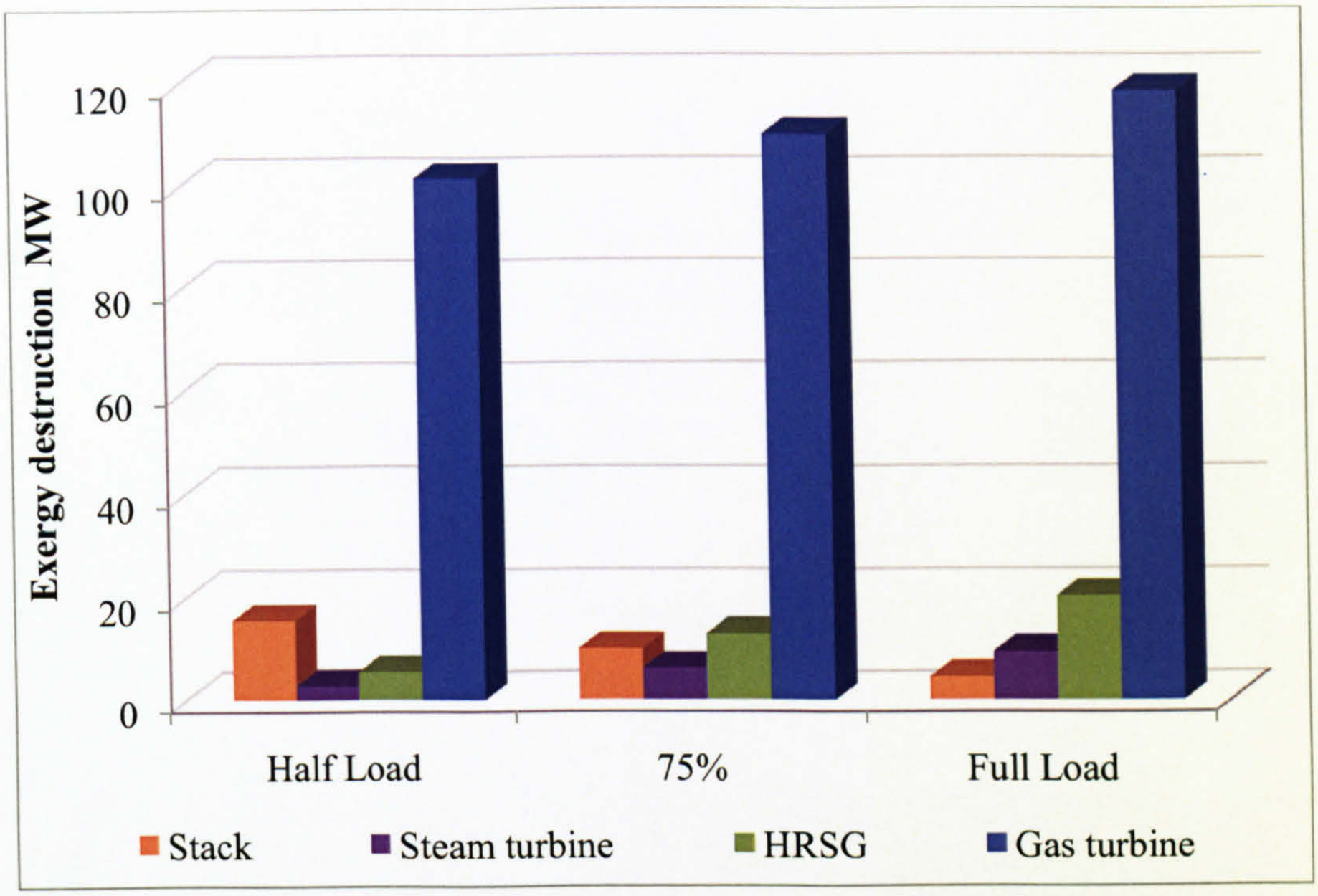

Figure 5-10 Exergy destruction results at different loads

The low grade heat energy that was not recovered in the HRSG unit was emitted through the stack causing the increase in its exergy destruction. The reduction in the gas turbine's exergy destruction by 14% at half load was the most significant, and the one driving the plant's total exergy destruction, as shown in Figure 5-11 which shows the gas turbine's and the plant's total exergy destruction at partial load. As indicated by the energy analysis results, the exergy results also confirmed that the plant performed efficiently at partial load.

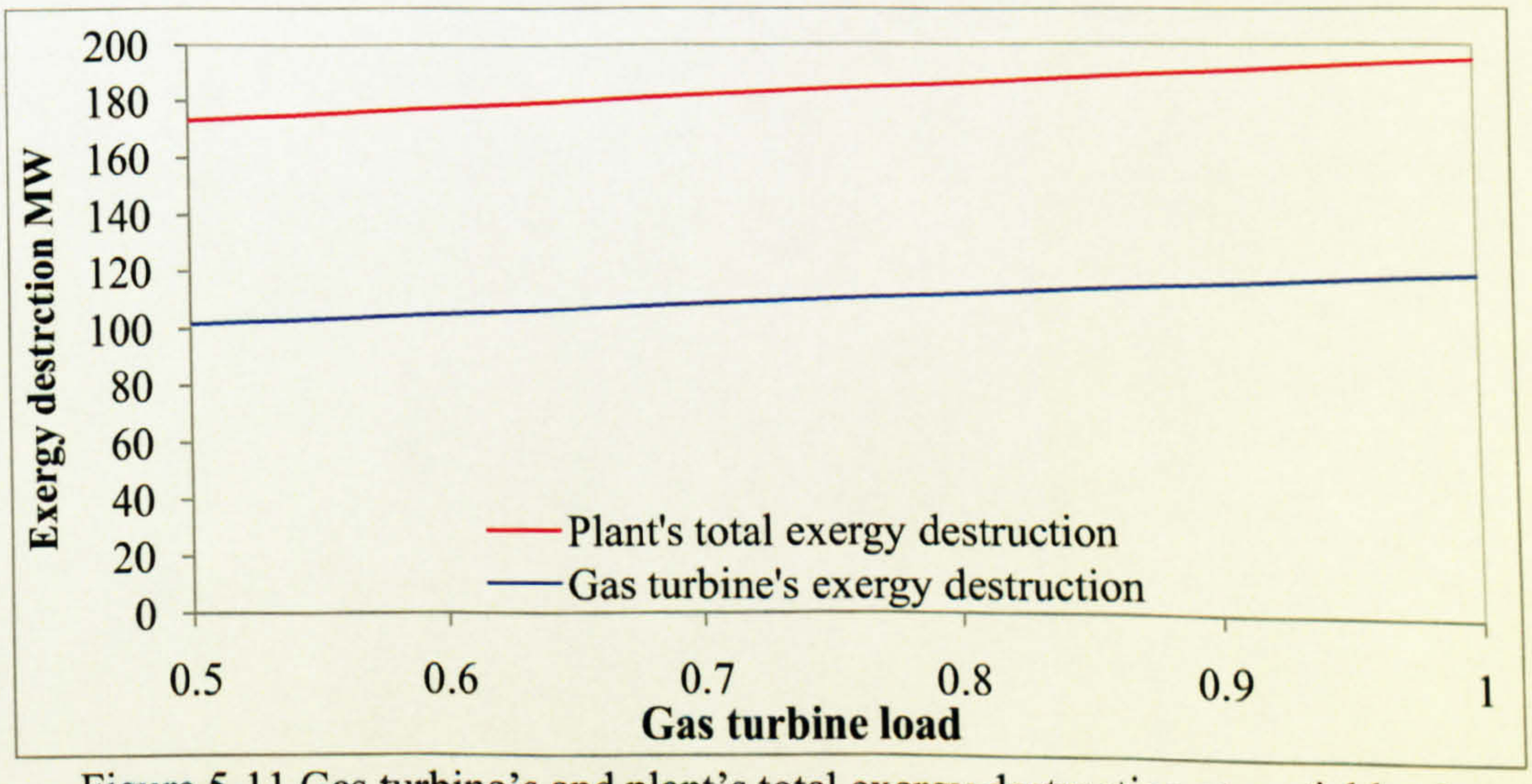

Figure 5-11 Gas turbine's and plant's total exergy destruction at partial load.

The exergetic efficiency of both the TVC-MED desalination plant and absorption chiller was not affected at partial load. The steam turbine's exergetic efficiency improved by 6.8% at half load due to the higher reduction in its fuel in comparison with its product, which was supported by the stable rate of the steam extracted into powering the TVC-MED desalination plant. For example, when operating at a load of 0.75% the steam turbine's exergetic fuel decreased by 40% while its production decreased by only 37%.

Figure 5-12 shows the gas turbine's exergetic efficiency and the plant's overall exergetic efficiency at partial load. Both efficiency rates were inversely proportional to the operating load; at half load the gas turbine's exergetic efficiency decreased by 20% while the plant's overall exergetic efficiency, affected by the reduction in the steam turbine power, decreased by 29%.

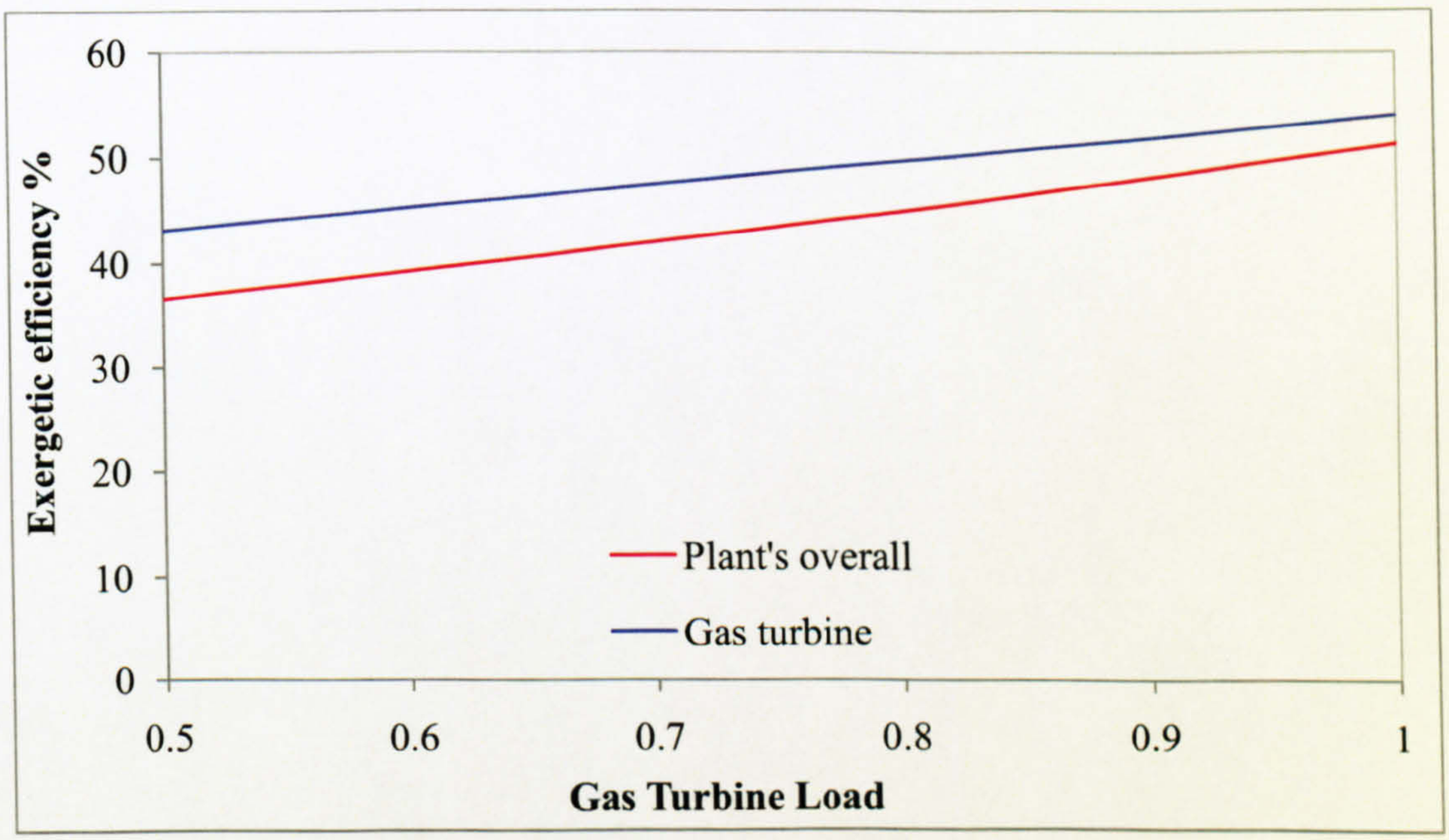

Figure 5-12 Gas turbine and overall plant exergetic efficiency at partial load

5.4.5 Parametric Studies

The effect of ambient conditions on the performance of gas turbines was established in Chapter 2 and investigated in the base power plant in Chapter 4. The results of these studies indicated that the effect of ambient humidity and seawater salinity on the power plant's performance was insignificant and could be ignored. Therefore, in this chapter only the effect of the ambient temperature and seawater temperature on the optimized plant performance is considered.

- **Ambient temperature**

The optimized plant performance at varying ambient temperatures was investigated by varying the compressor inlet-air temperature from 10°C to 50°C, in ISO conditions and with a seawater temperature of 22°C. The gas turbine and the TVC-MED desalination plant were both operated at full load. All the results of this study are listed in tables 4, 5 and 6 in Appendix D, while the most significant results are plotted and discussed in this chapter.

In the base combined cycle plant, the increase in the compressor's inlet-air temperature was found to decrease the gas turbine's electric output power by 3.8% for each 5°C increase in the ambient air temperature as seen in Figure 5-13. However, adding the absorption chiller to the proposed plant to pre-cool the compressor inlet-air temperature from the ambient condition to 10°C stabilized this effect.

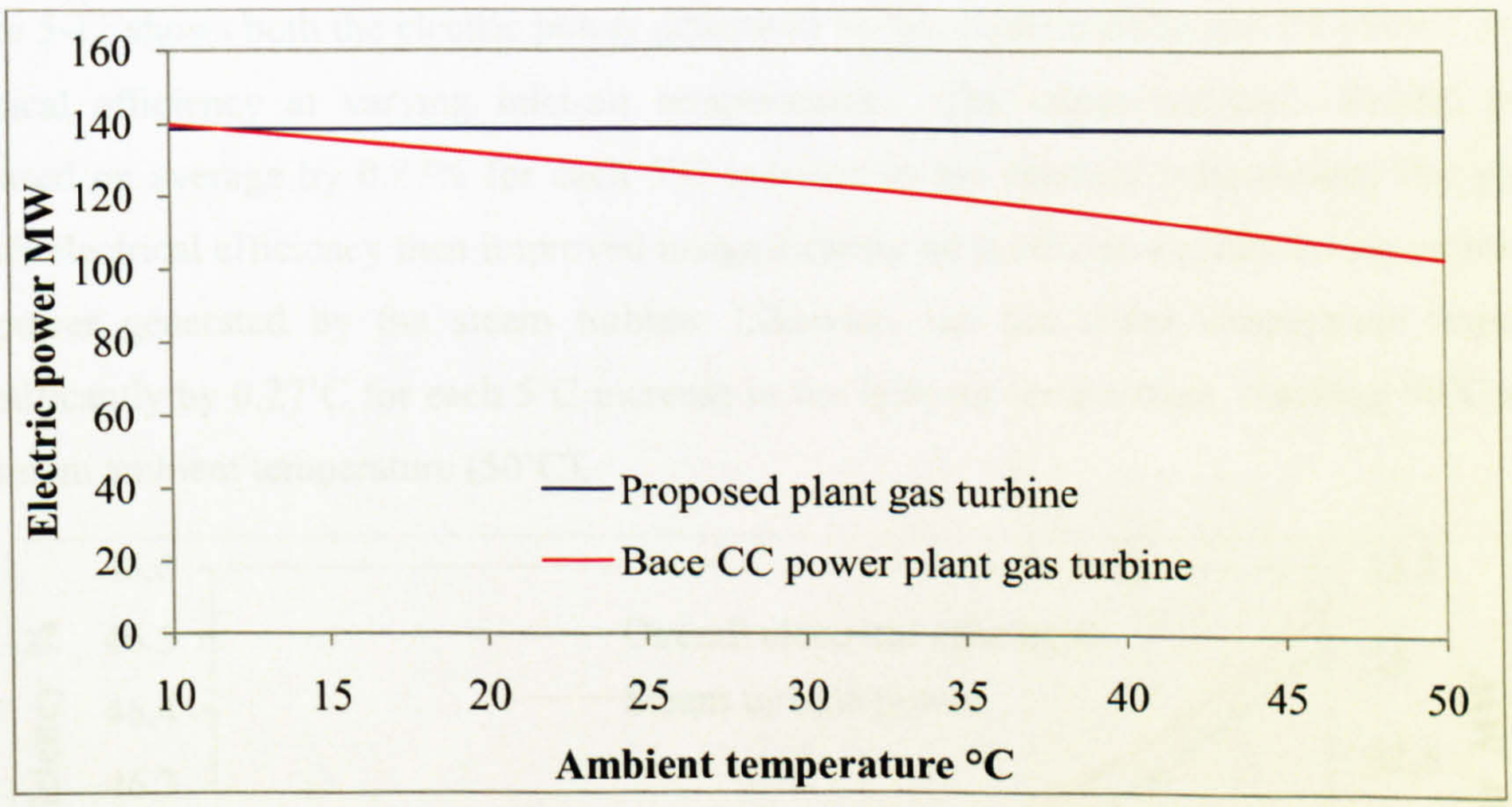

Figure 5-13 Gas turbine output power versus compressor ambient air temperature

A similar effect can be seen on the gas turbine's efficiency; in the base CC power plant the gas turbine efficiency decreased by 2.4% for each 5°C increase in the ambient air temperature. However, in the optimized plant this effect was also stabilized by stabilizing the gas turbine output power as seen in Figure 5-14. Furthermore, it was observed that the compressor's inlet-air humidity increased during the pre-cooling process. This led to an insignificant increase in the electric power generated by the steam turbine, which improved the plant's overall electrical efficiency by the same rate.

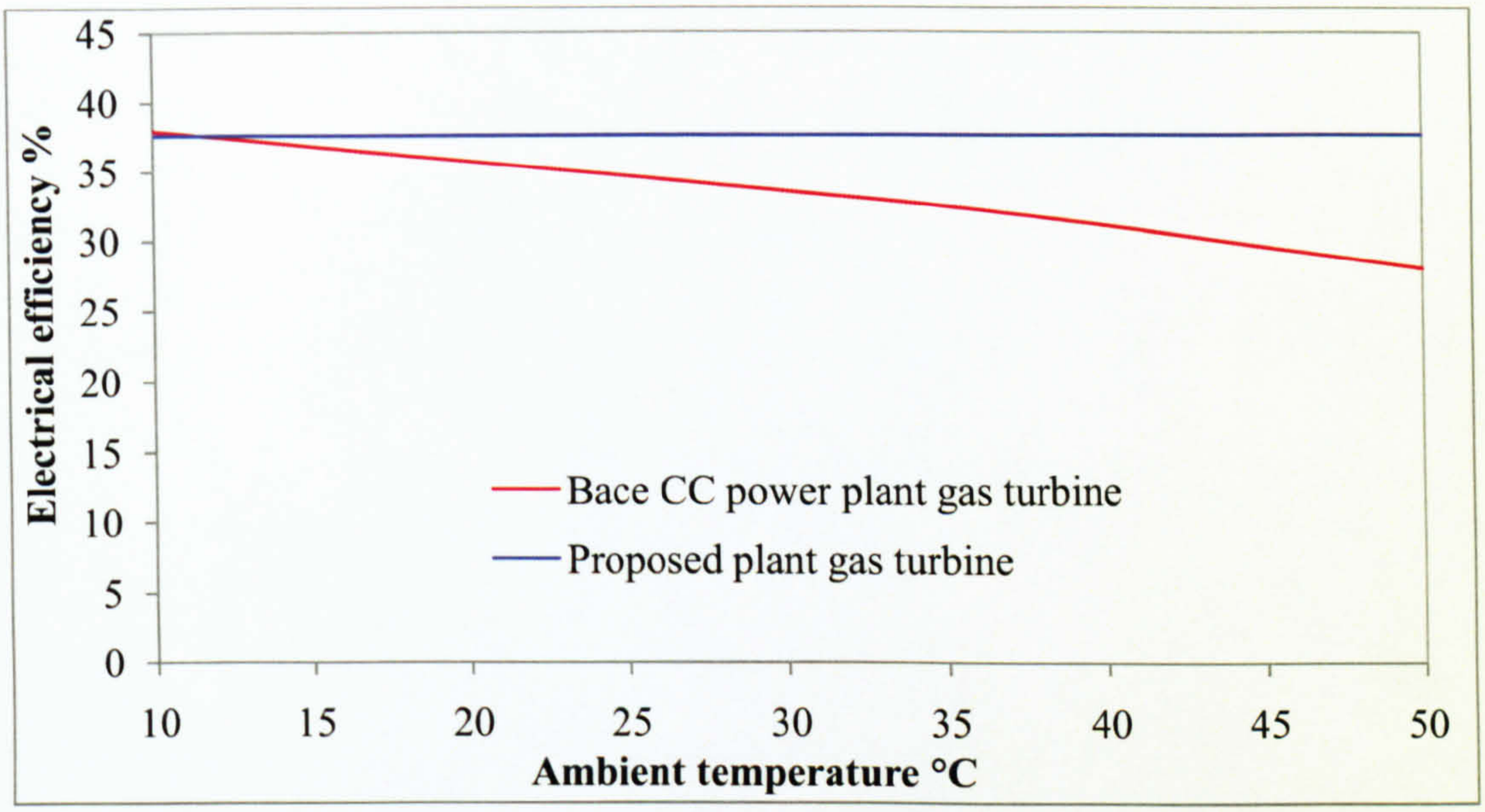

Figure 5-14 Gas turbine efficiency versus compressor ambient air temperature

Figure 5-15 shows both the electric power generated by the steam turbine and the plant's overall electrical efficiency at varying inlet-air temperatures. The steam turbine's electric power increased on average by 0.87% for each 5°C increase in the inlet-air temperature. The plant's overall electrical efficiency then improved insignificantly by 0.16% as a result of this increase in the power generated by the steam turbine. Likewise, the hot water temperature improved insignificantly by 0.27°C for each 5°C increase in the inlet-air temperature, reaching 80°C at the maximum ambient temperature (50°C).

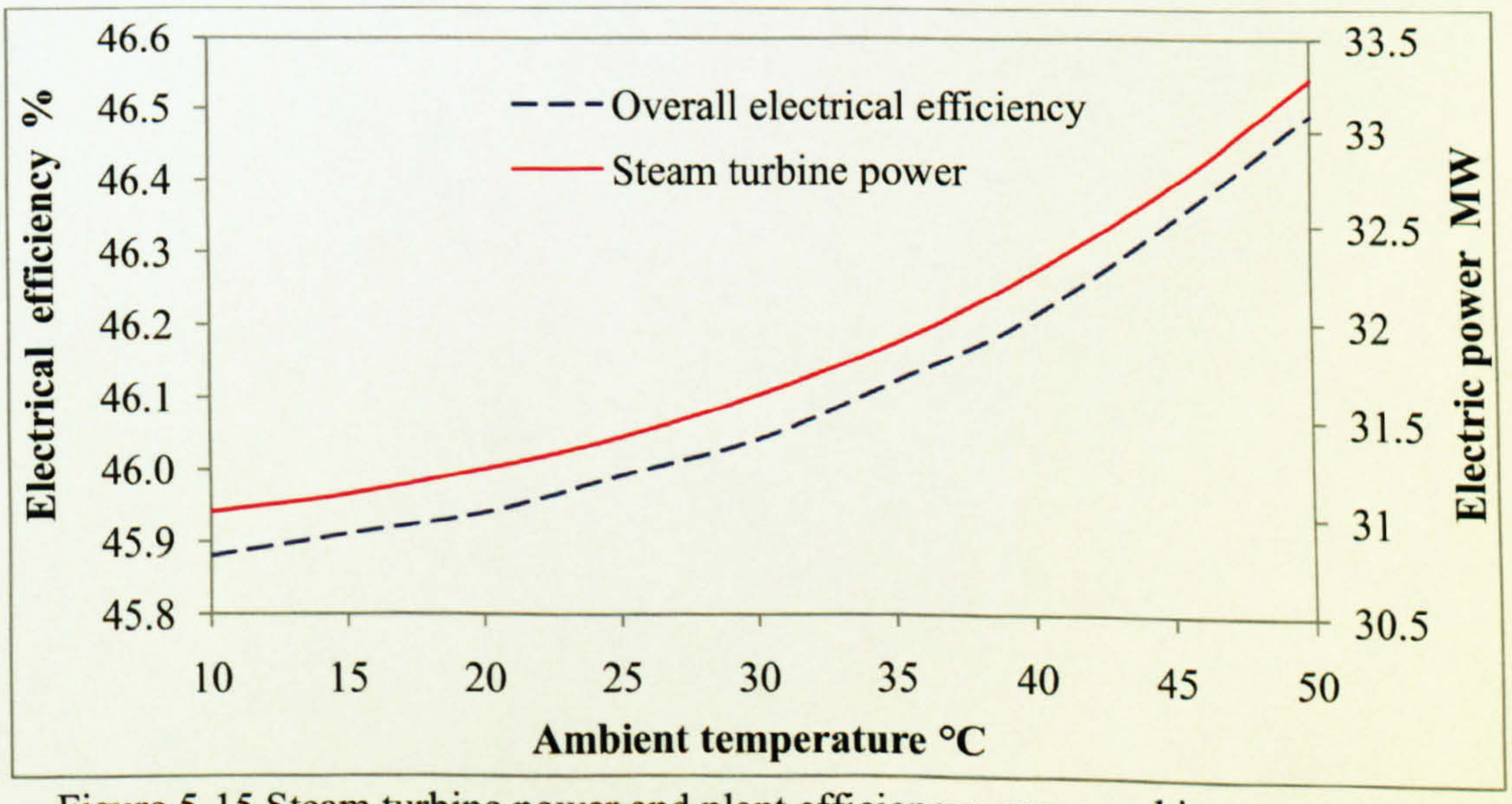

Figure 5-15 Steam turbine power and plant efficiency versus ambient temperature

The absorption chiller and the TVC-MED desalination plant were not affected by the variation in the compressor's inlet-air temperature.

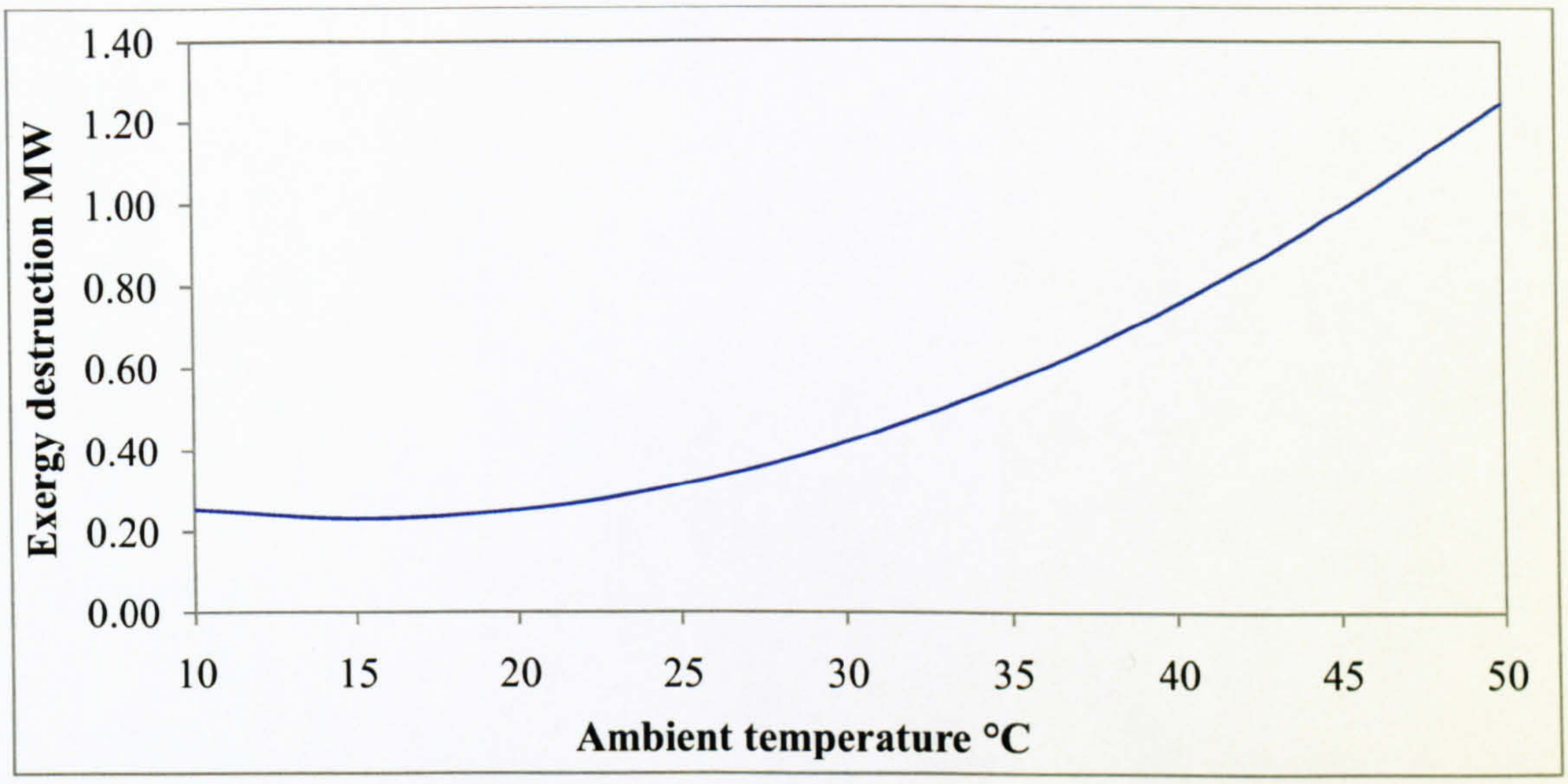

Figure 5-16 Gas turbine cooler's exergy destruction versus ambient air temperature

On the basis of exergy analysis, the most significant effect was observed in the gas turbine cooler. The gas turbine cooler's exergy destruction increased on average by 22.9% for each 5°C increase in the inlet-air temperature as shown in Figure 5-16.

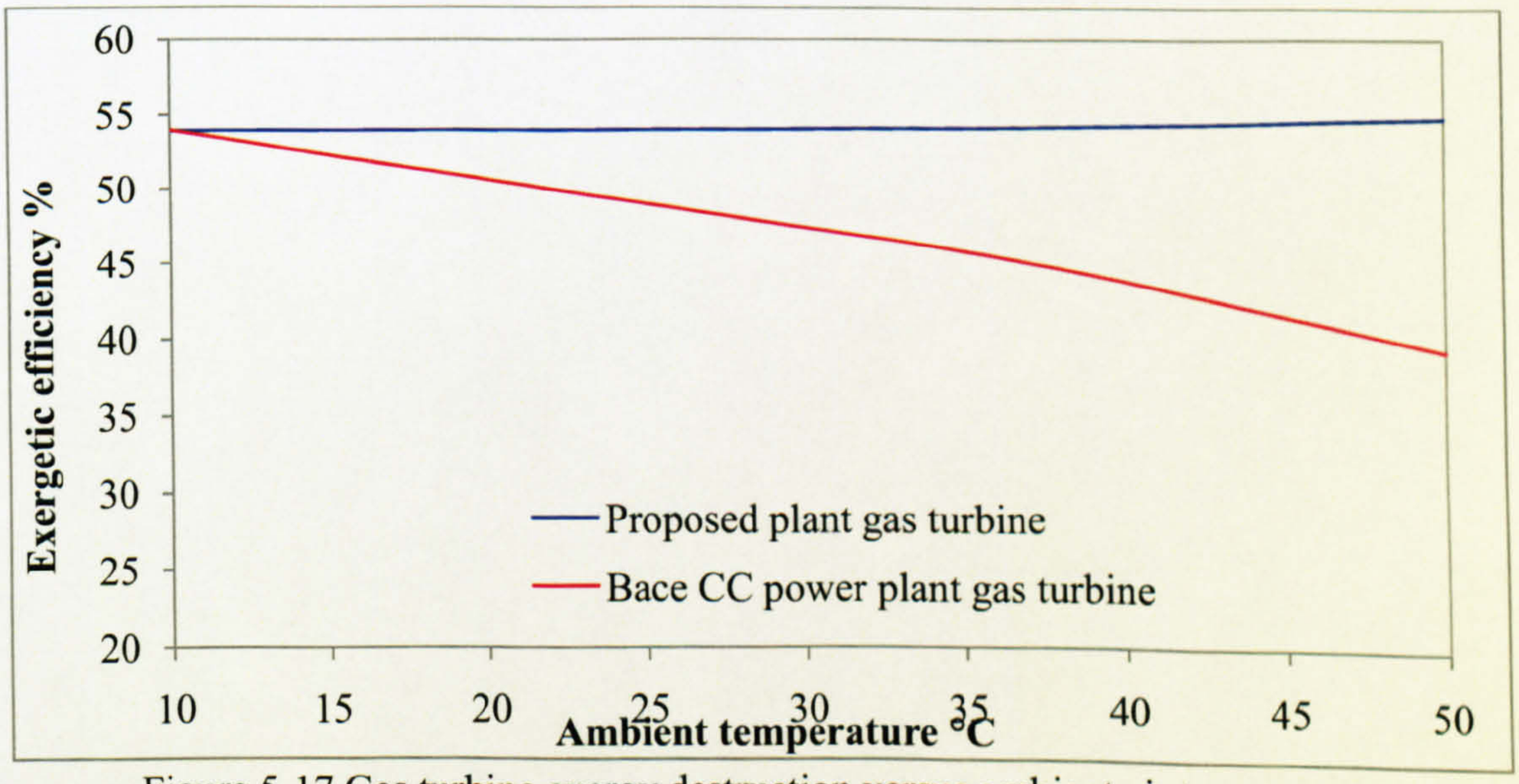

Figure 5-17 Gas turbine exergy destruction versus ambient air temperature

This increase was due to the increase in the exergy content of the inlet-air. In the base CC power plant the gas turbine's exergy destruction increased on average by 3.7% for each 5°C increase in

the inlet-air temperature; in the optimized plant this affect was stabilized by cooling the compressor's inlet-air from the ambient condition to 10°C as shown in Figure 5-17, which shows the exergetic efficiency of the gas turbine in the base power plant and in the proposed plant after installing the absorption chiller. In conclusion, the optimized plant achieved its aim of overcoming the effect of the ambient temperature on the gas turbine's performance.

- **Intake seawater temperature**

The performance of the optimized plant under varying seawater temperatures was investigated in a parametric study in ISO conditions while the plant was operated at full load. All the results of this study are listed in tables 7, 8 and 9 in Appendix D, while the most significant results are plotted and discussed in this section. Figure 5-18 shows the optimized plant CO_2 emission rate versus the change in the seawater temperature.

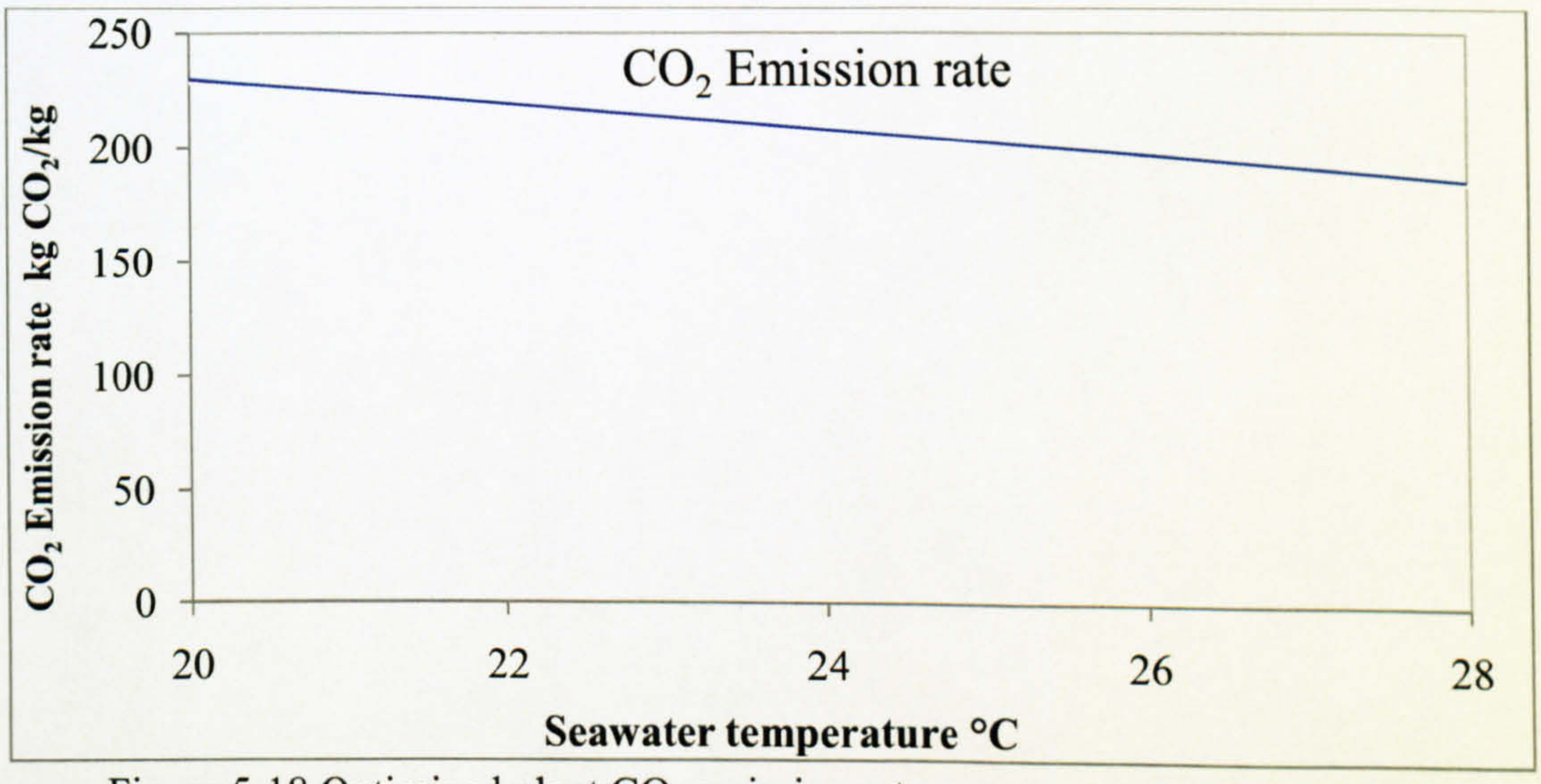

Figure 5-18 Optimized plant CO_2 emission rate versus seawater temperature

The plant's CO_2 emission rate improved on average by 5.1% for each 2°C increase in the seawater temperature as a result of the increase in the hot water production rate and temperature, which was stimulated by the higher cooling water temperature entering the absorption chiller. Figure 519 shows an improvement in the hot water production rate and temperature on average by 2.6% for each 2°C increase in the seawater temperature. This indicates that the optimized plant benefited from the increase in the seawater temperature more than the base models by utilizing the cooling water after increasing its temperature. In the base TVC-MED desalination

plant the increase in seawater temperature was found to improve the desalination process's GOR and reduce its specific heat consumption.

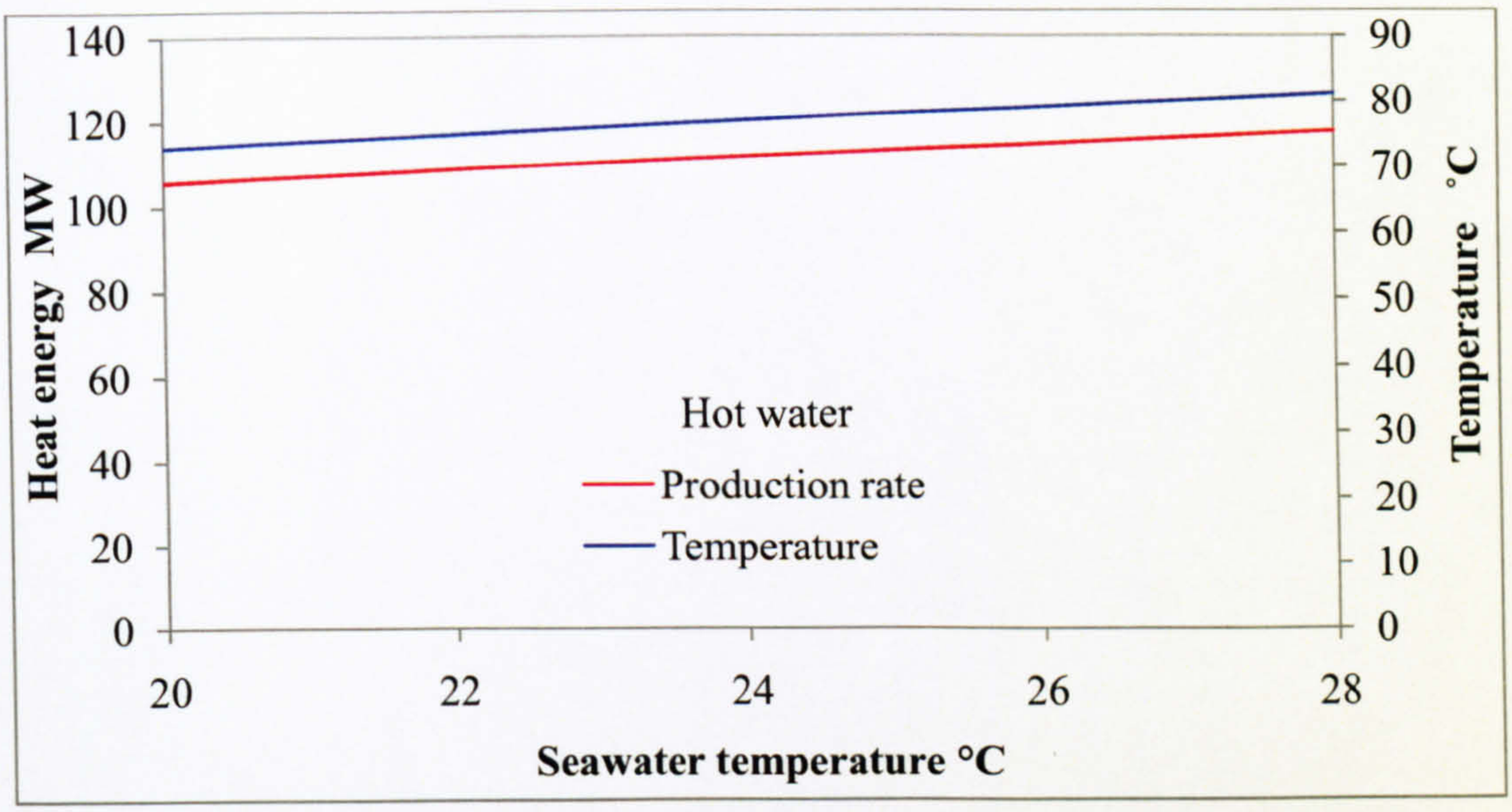

Figure 5-19 Optimized plant hot water production versus seawater temperature

This was still the case in the optimized plant as shown in Figure 5-20. For each 2°C increase in the seawater temperature the TVC-MED plant's GOR improved by 5.68%. Likewise, its specific heat consumption was reduced by 4.37% for each 2°C increase in the seawater temperature.

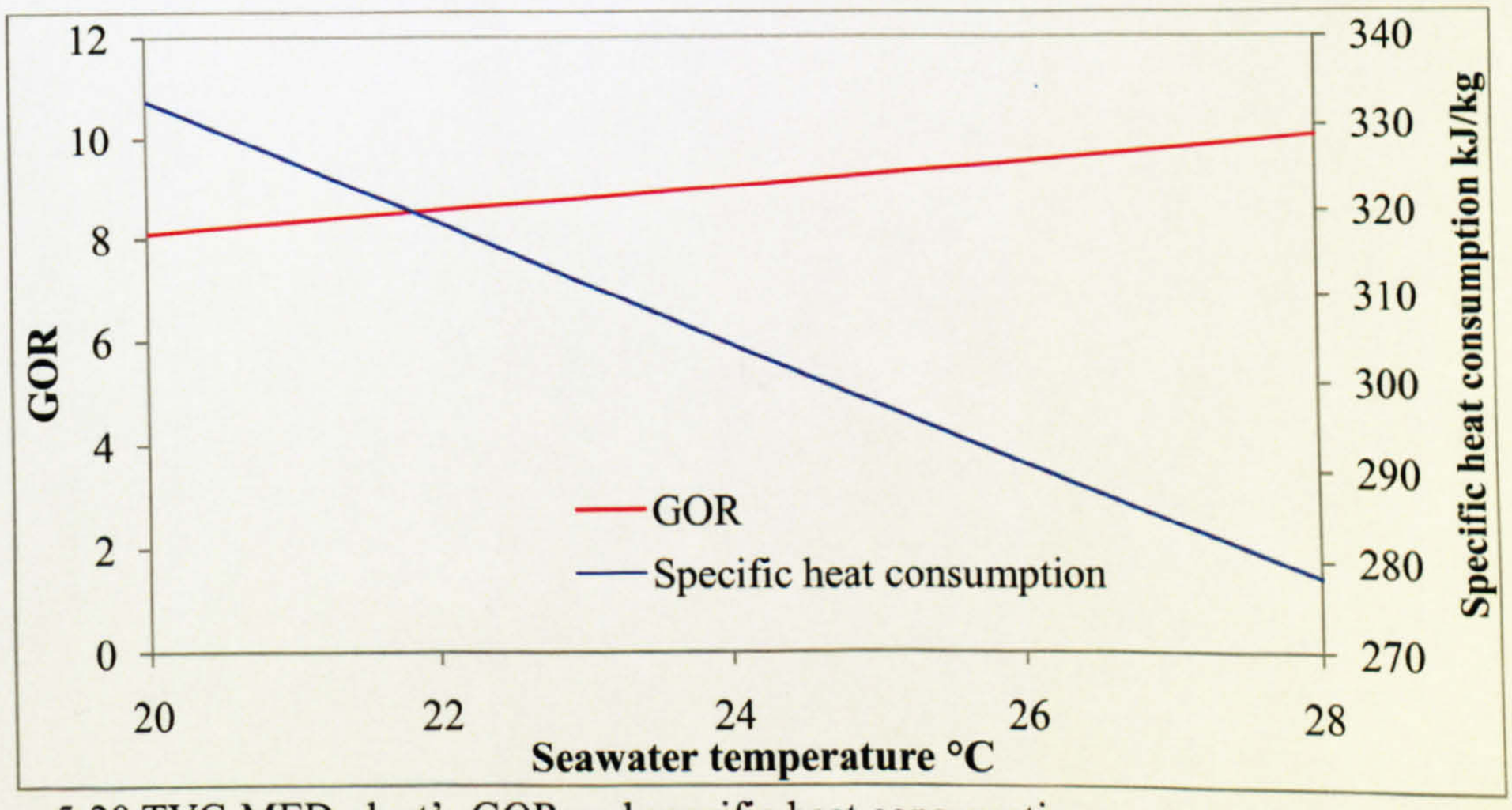

Figure 5-20 TVC-MED plant's GOR and specific heat consumption versus seawater temperature

The desalination process's concentration factor was also reduced as the seawater intake temperature increases. This was mainly because of the increase in the rejected seawater after the

TVC-MED condenser. When the feed seawater temperature increased, the condenser required a supplementary seawater mass flow rate (kg/s) in order to condense the steam exiting the last effect of the desalination process. However, the additional seawater consumed by the condenser is rejected out of the plant before getting to the evaporators and then mixed with the rejected brine, which reduced its salinity.

Figure 5-21 shows the optimized plant's concentration factor versus the variation in the seawater temperature. The concentration ratio dropped on average by 2.3% for each 2°C increase in the seawater temperature. However, this did not have an impact on the rejected brine temperature, which increased on average by 0.5°C for each 2°C increase in the seawater temperature. This was because of the increase in the temperature of the condenser cooling water, which had to be mixed with it after exiting the steam turbine's condenser.

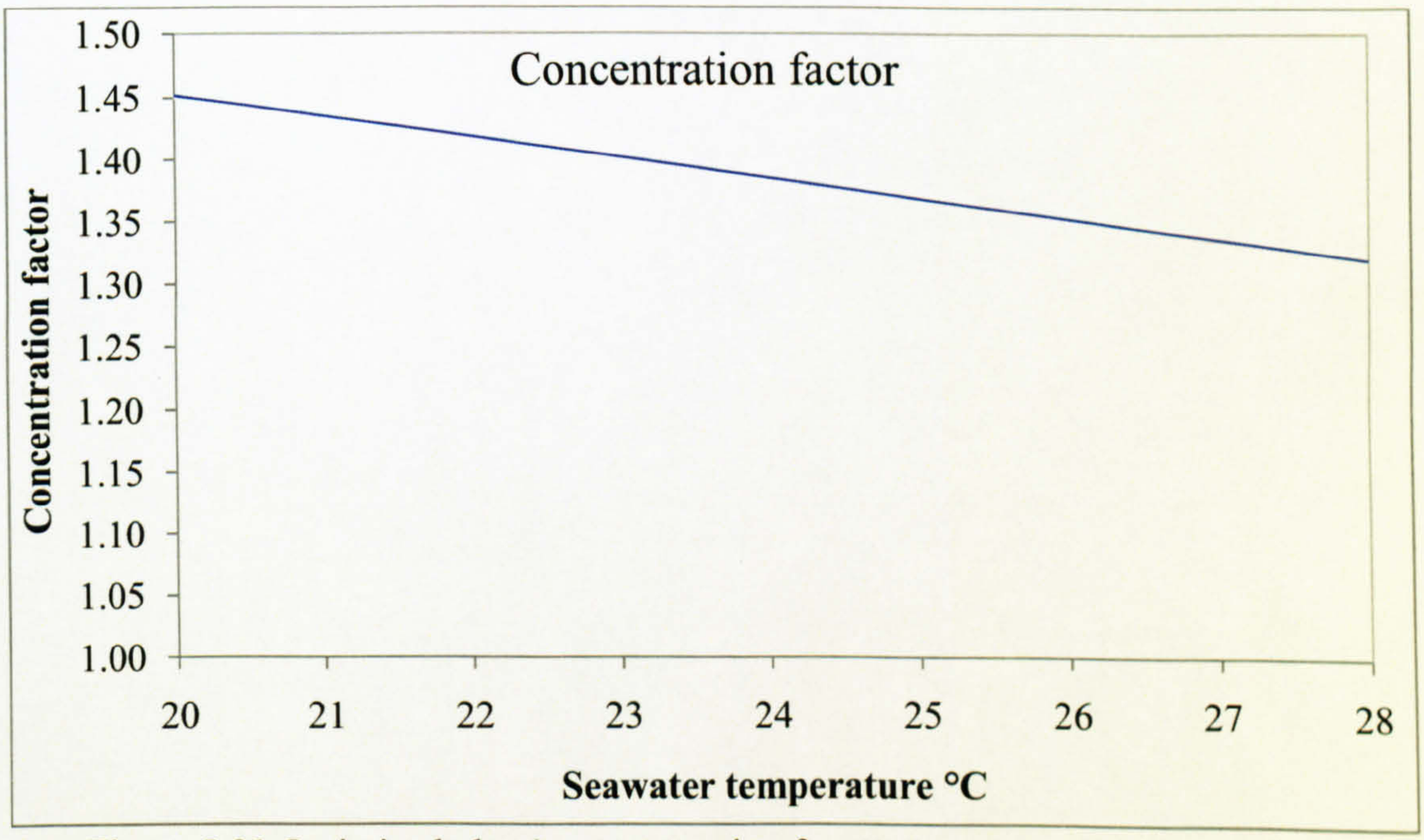

Figure 5-21 Optimized plant's concentration factor versus seawater temperature

On the basis of the exergy analysis, the most significant results can be seen in the exergy destruction of the absorption chiller's absorber and condenser. Figure 5-22 shows these components' exergy destruction values at varying seawater temperatures. The exergy destruction values of both the absorber and the condenser of the absorption chiller dropped on average by 13.5% and 6.5% respectively, which can be explained by the change in the exergy balances of each of them.

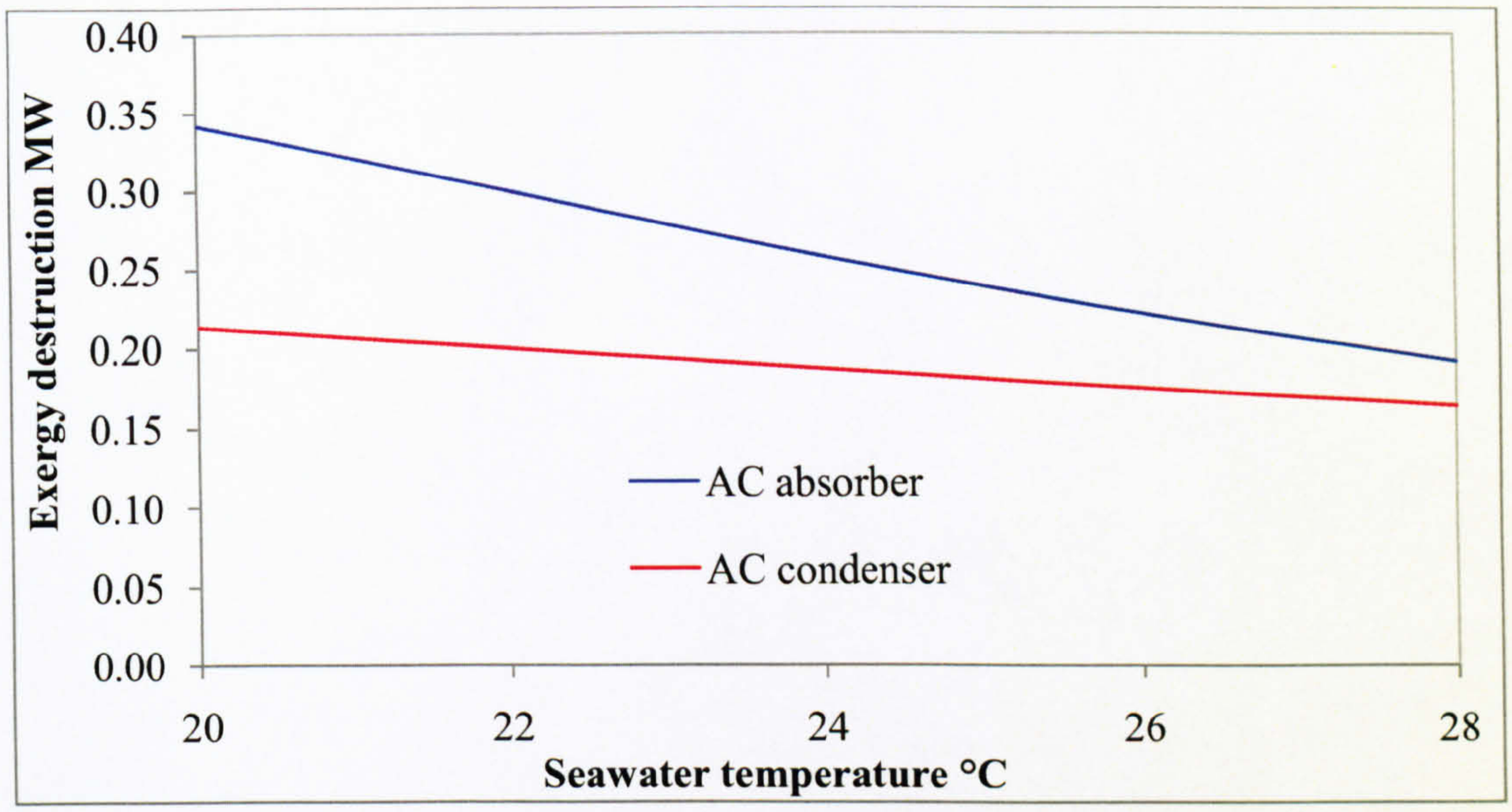

Figure 5-22 Absorption chiller's absorber and condenser exergy destruction values versus seawater temperature

The reduction in the AC's absorber and condenser insignificantly reduced the plant's total exergy destruction by 0.11% for each 2C increase in the seawater temperature, while the slight increase in the hot water temperature enhanced the plant's total exergetic efficiency on average by 0.67%. The significant improvement was in the TVC-MED desalination plant's exergetic efficiency, which followed the GOR and increased on average by 4.55% for each 2˚C increase in the seawater temperature as shown in Figure 5-23. In conclusion, this study confirmed the optimized plant's stability under changing ambient conditions, which was one of this study's aims.

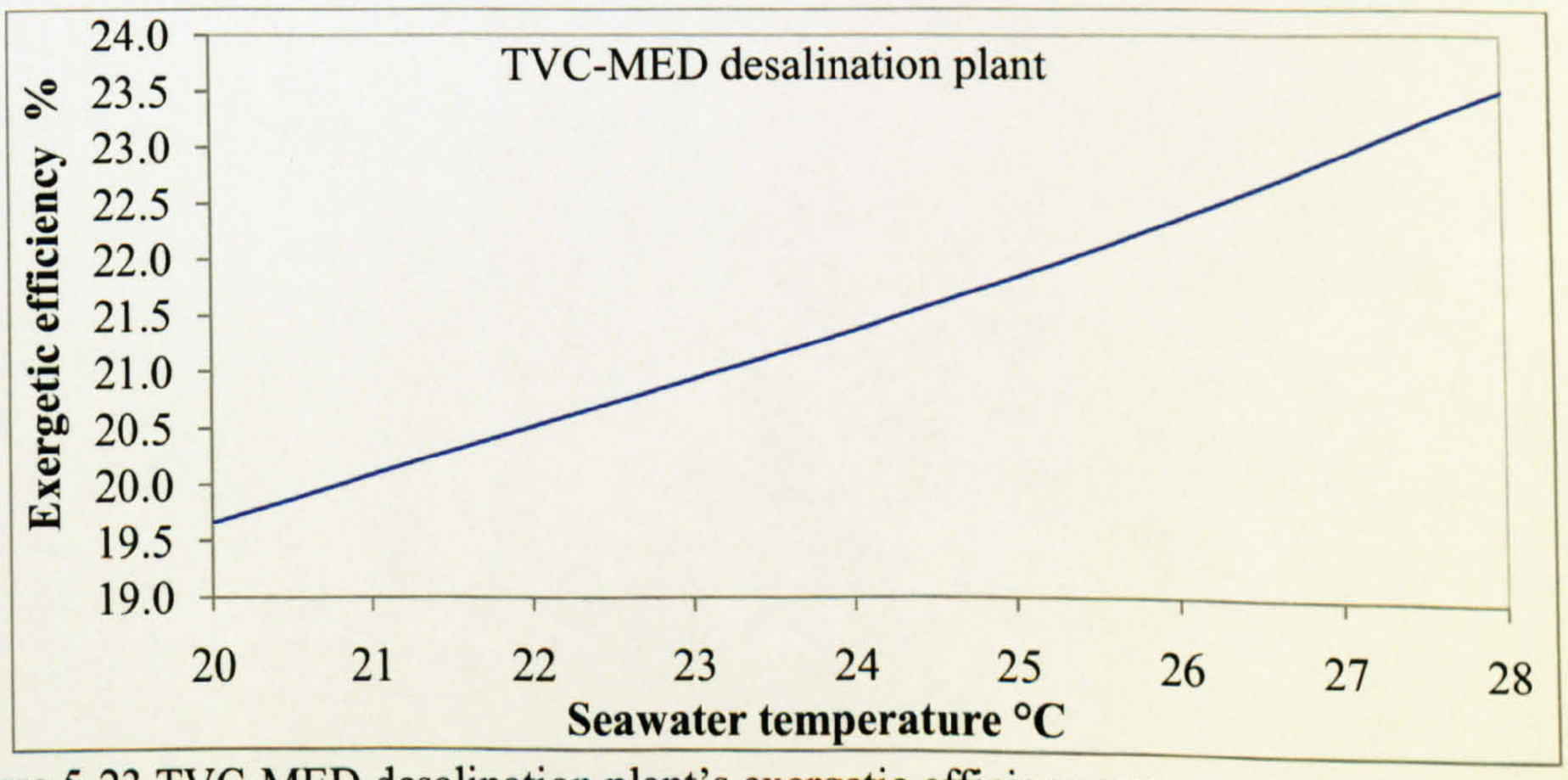

Figure 5-23 TVC-MED desalination plant's exergetic efficiency versus seawater temperature

The increase in the seawater temperature was used in improving the temperature of the produced hot water after it was just benefiting the TVC-MED desalination plant in the base model.

Lastly, these modifications were also applied to the third proposed plant, where the TVC-MED desalination plant was powered by a boiler that utilized heat energy from the exhaust gas. The results of this study can be found in tables 1, 2 and 3 in Appendix E. The heat rate of hot water produced from this plant after optimization was only 80MW with a temperature of 55°C. The CO_2 emission rate decreased by 28% and the EUF improved by only 7.8% in comparison with its performance before optimization.

5.5 Closing Remark

The modelling and simulation results of four different proposed plants have been introduced in this chapter, including two different desalination technologies, MED and TVC-MED, as well as two different techniques of coupling them with power plant. The first was by a boiler that utilized a portion of the exhaust gas stream's heat energy, while the second was through steam extracted from the steam turbine. All the plants were tested on the basis of energy and exergy analyses. From the first two proposed plants' results it was concluded that the TVC-MED desalination plant was more efficient than the MED desalination plant; hence it was chosen in the third and fourth plants. From the last two proposed plants' analysis results it was concluded that powering the desalination plant by steam extraction from the steam turbine was more efficient than powering it by a boiler; however, this coupling technique could be the only option where the power plant is not a combined cycle power plant and only has a gas turbine.

Following this, the last proposed plant was chosen for the optimization stage, in which two modifications in the plant structure were suggested to control the TVC-MED desalination plant's concentration factor and to recover extra heat energy from the exhaust heat energy. The analysis results of these two modifications were then presented and compared with the analysis results of the plant before optimization. Three different operating modes for the TVC-MED desalination plant were suggested to increase the operational flexibility of the optimized plant. In addition, the plant's performance at partial load was investigated as well as in varying ambient conditions.

Chapter 6

Economic Study

6.1 Introduction

The optimized fourth proposed plant is considered as a case study in this chapter to investigate its economic viability by evaluating its payback period (PBP), internal rate of return (IRR), profitability index (PI) and the net present value (NPV). Although fuel prices vary greatly, affecting the accuracy of any economic study's results, it is important to perform such a study in order to clarify the project's profitability and acceptability, at least at the present time. Firstly, the initial cost of each sub-plants or equipment was either calculated or obtained from official sources or past studies, and then used to calculate the capital cost. Following this the annual cash inflow was calculated according to the fuel cost and operation and maintenance costs (O&M). Then the annual cash outflow was calculated according to the products' selling prices, that is electric power, potable water and hot water. Then the four criteria for evaluating economic acceptability were employed to evaluate the plant in ISO conditions and then in accordance with the weather data presented in Chapter 3, that is off-design. Finally, a number of sensitivity studies were performed to show the effect of a number of fluctuating variables, such as fuel prices, product selling prices, interest rates and project lifetime, on the project's economic performance.

6.2 Initial Cost Estimate

The initial cost indicated the equipment purchase cost only. Although these data varied with time, the aim was to obtain them directly through vendors' quotations or by searching for the most recent one from past purchase orders or studies or, alternatively, by calculating the cost using the extensive cost databases maintained by engineering companies. In the following sections each piece of equipment and system is treated on its own, starting with the method used for estimating the initial cost of the heat exchangers and then for finding the initial costs of other systems, that is CC power plant, TVC-MED plant and absorption chiller. Furthermore, 5% of the total of all equipment purchase cost was added to represent the auxiliary equipment cost [136]. Lastly, according to Bejan, et al. [79], the purchased equipment installation cost is 33% of the purchased equipment cost, piping is 35%, instrumentation and controls are 12% and electrical equipment and materials are 13%.

The great difficulty in obtaining direct quotations through vendors for heat exchangers similar to those used in the plant enforces the calculating of their initial costs using the IHS ESDU International costing technique [137]. ESDU was assisted by the UK's major manufacturer of heat exchangers such as IMI Marston Ltd, to generate tables and curves for heat exchanger costs per unit surface area, which is used to provide the C-values required for the costing. This technique has been used to design an MS Excel model that automatically calculates the heat exchanger's final cost, when provided with the data required. Figure 6-1 shows a screenshot for this model.

Heat Exchanger Costing

Hot side		
Temperatuer In	235	°C
Temperature Out	213	°C
Cold side		
Temperature In	80	°C
Temperature Out	97.7	°C
Heat Load	11791620	W
Mean Temp. Difference	135.14	°C
(Q/ΔTm)	87256	W/°C
C1	1.40	
C2	1.40	
(Q/ΔTm)1	10000	
(Q/ΔTm)2	1000000	
C-value	**1.400**	£/W/°C
Heat Exchanger Final Cost	122,158	£

Designed By Khaled

Figure 6-1 MS Excel heat exchanger costing model screenshot

The required data for the heat load and hot- and cold-side temperatures can be extracted easily from the IPSEpro simulation software, while the other data is automatically calculated by the MS Excel model as follows: Firstly, from the input data (that is, T_h, and T_c, in and out, and the heat load$\dot{Q}$), the mean temperature difference is calculated as follows [137]:

$$\Delta T_{lm} = \frac{[(T_{h,in} - T_{c,out}) - (T_{h,out} - T_{c,in})]}{log_e[(T_{h,in} - T_{c,out})/(T_{h,out} - T_{c,in})]}$$

Then, the value of $(\dot{Q}/\Delta T_{lm})$ is calculated, which is used to read off the value of C_1 and C_2 from the ESDU tables. Then, the C-value is calculated by logarithmic interpolation as follows [137]:

$$C = exp\left\{log_e C_1 + \frac{log_e(C_1/C_2) log_e\left[(\dot{Q}/\Delta T_{lm})/(\dot{Q}/\Delta T_{lm})_1\right]}{log_e\left[(\dot{Q}/\Delta T_{lm})_1/(\dot{Q}/\Delta T_{lm})_2\right]}\right\}$$

The final cost is then calculated by multiplying the C-value by $(\dot{Q}/\Delta T_{lm})$. The model has been validated by an example from the ESDU. In the proposed plant there were three double-pipe countercurrent heat exchangers. The materials were chosen in accordance with each heat exchanger function; the hot water heat exchangers were chosen on the basis of being stainless steel E316, as they would resist corrosion. The GT air-intake cooler and AC heat exchanger materials were chosen on the basis of being stainless steel E304 in order to reduce their costs. Using the designed MS Excel model each heat exchanger's cost was calculated and the results are presented in Table 6-1.

Heat Exchanger	Cost £
Absorption chiller	122,152
Hot water heater	810,697
GT intake-air cooler	1,365,965

Table 6-1 Heat exchanger's cost estimate

The power plant's purchase cost was estimated depending on a specific cost £/kW, obtained from the Libyan General Electricity Company [138]. For a combined cycle power plant, the specific cost was £228.80 /kW. This made the purchase cost of this study's CC power plant £38,831,936.00.

The desalination plant's purchase cost was obtained as a direct quotation from IDE Technologies Ltd.[116], which specializes in research and development, as well as the design, manufacture and installation of saline water desalination processes throughout the world. For a 40,000m^3/day MED plant the equipment purchase cost is £30,626,749.02.

The absorption chiller's cost was obtained from a recently published study by Boonnasa and Namprakai [41]; for a capacity of 9304 kW a specific cost of 78.21 £/kW is obtained. Applying this to an absorption chiller with a capacity of 9304 kW gives a total cost of £727,665.84.

6.3 Annual Cash Outflow

The annual cash outflow is determined by the costs of fuel, operating and maintenance. It has been calculated as a function of the annual plant capacity factor (C_f), which defines the operating hours out of the total available 8760 hours per year. The fuel was natural gas and its cost is estimated to be £0.12/kg [41], although in Saudi Arabia the price for natural gas for industrial and petrochemical use is set by the Ministry of Water and Electricity at £0.023/kg.

The other operating and maintenance costs were considered for each system separately as a function of the plant's capacity factor. The power plant's O&M was obtained from a recently published study by Nisan and Benzarti [67] and was £3.2/MWh, while the desalination plant's O&M was taken to be £0.075/m^3 according to Methnani [66] and the absorption chiller's O&M cost was £0.39/kW according to Boonnasa and Namprakai [41].

6.4 Annual Cash Inflow

The annual cash inflow represents the income from sales that are electric power, pure water, the cooling effect and hot water. According to the Saudi Electricity Company [18], the electricity tariff in Saudi Arabia ranges according to the rate of consumption, from £0.007/kWh for consumption from 1kWh to 1MWh to £0.039/kWh for consumption more than 10MWh, in addition to other monthly fixed costs such as reading, maintenance and insurance. Likewise, the potable water tariff is £0.47/m^3 on average according to the Saline Water Conversion Corporation [19]. Although these prices are greatly subsidized by the government, an average value of £0.023/kWh for the electric power was considered, and £0.47/m^3 for the potable water in accordance with a recently published paper by Methnani [66]. On the other hand, the hot water price is considered to be £6.70/GJ, according to Oha, et al. [136].

Furthermore, Figure 6-2 shows a screenshot of another MS Excel model built in accordance with Bejan, et al.'s book [79], to calculate the final capital investment cost, annual cash inflow and outflow, and to calculate the final results of the four evaluation criteria used. The purchased equipment cost, the interest rate, project life and production and consumption data are required as input data.

Economic analysis model

Capital investment

»Purchased-equipment costs		
→ Desalination process	30,626,749	
→ Absorption chiller	727,666	
→ CC power plant	38,831,936	
→ Hot water boiler	810,697	
→ Absorption chiller boiler	122,152	
→ Gas turbine cooler	1,365,965	
→ Auxiliary equipment	3,624,258	
Total purchased-equipment costs		£76,109,423
»Purchased-equipment installation	12,301,571	
»Piping	13,047,120	
»Instrumentation and controls	4,473,298	
»Electrical equipment and materials	4,846,073	
Total capital investment		£110,777,486
→Salvage value	£11,416,413	
Total depreciable investment		£99,361,073
→Project economic life	15 years	
Annual book depreciation		£6,624,072
→ Interest rate i	5%	

Annual cash outflow

	Consumption kg/s	£/kg	CF*	
→ Fuel cost	8.76	0.12	85%	£28,178,047
	CC	AC	MED	
→ O&M cost	3,985,426	9,739	921,184	£4,916,348
	Total		£33,094,395	

Annual cash inflow

	Production/h		CF*	£/unit	
→Electricity kW	169720	kW.h	85%	0.023	£29,065,908
→Potable water m^3	1666.66	m^3.h	85%	0.47	£5,832,677
→Hot water kW	390	GJ.h	85%	6.7	£19,456,398
	Total			£54,354,982	
Total annual net cash inflow					£21,260,588
► Payback period in years			PBP		4.7
► Net present value			NPV		158,479,156
► Internal rate of return			IRR		18.6 %
► Profitability index			PI		2.44

Figure 6-2 MS Excel economic analysis model screenshot

The evaluation criteria used in this model as mentioned include the payback period (PBP), which is defined as the ratio of the total depreciable investment to the average annual profit. The net present value (NPV) is calculated as follows [79]:

$$\mathrm{NPV} = \sum_{Z=0}^{t} \frac{F_z}{(1+i)^z} - \mathrm{I_o}$$

The internal rate of return is calculated as follows [79]:

$$\mathrm{NPV} = \sum_{Z=0}^{t} \frac{F_z}{(1+\mathrm{IRR})^z} = 0$$

where (F_Z) is the net money cash flow in the year (z), (i) is the interest rate and I_0 is the initial total capital investment cost (£). Lastly, the profitability index (PI) is defined as the ratio of the present value of future net cash flows to the initial investment over its entire life [79].

$$\mathrm{PI} = \frac{\mathrm{NPV}}{I_0}$$

The model was validated using a real case study presented in Bejan, et al.'s book [79].

6.5 Case Study

The optimized plant is considered as a case study, including all the suggested operating modes. First, the plant was operated on full load and in ISO conditions with seawater at a temperature of 22°C. The plant generated 169MW of electricity, 40,000m^3/day of potable water and 108MW of hot water. Using the designed MS Excel model with an interest rate of 5%, a capacity factor of 85%, and a project life of 20 years, the results obtained indicated the economic acceptability and profitability of the proposed plant as shown in Table 6-2.

	Value
(i)	5%
(t)	20
PBP	4.7
NPV	£158,479,156
IRR	18.60%
PI	2.44

Table 6-2 Economic evaluation with a 40000m^3/day operating mode

With an internal rate of return of 18.6%, the project would pay back all the capital investment in 4.7 years. In the long run the project was also proven to be efficient, with a net present value of more than £158 million over 20 years of its life, which is even less than the usual lifetime of the normal power plant, which could be expected to extend up to 30 years or more. Nonetheless, the profitability index indicated a very promising investment with value of 2.44. Secondly, a similar study was performed on the same optimized plant where the TVC-MED desalination plant was operated to produce only half of its nominal capacity (20,000m^3/day), with the gas turbine at full

load. The assumptions made were as follows: an interest rate of 5%, a capacity factor of 85% and a project life of 20 years. The results obtained are listed in Table 6-3.

	Value
(i)	5%
(t)	20
PBP	4.7
NPV	£154,114,253
IRR	18.24%
PI	2.39

Table 6-3 Economic evaluation with a 20000m^3/day operating mode

In this operating mode the plant's economic performance will not be greatly affected as the reduced potable water production and higher O&M costs of the CC power plant will be compensated for by the higher electricity generation rate and the reduced O&M costs of the desalination plant. As mentioned previously the hot water production rate will not be affected during this operating mode, which gives the plant more economic stability. The plant achieved almost similar internal rate of return of 18.24%, payback period and profitability index value. This also applies in the long run with a net present value of £154 million over 20 years of its life. A comparison of both operating modes showed that in both modes the plant will pay back the capital investment in 4.7 years. However, the other evaluation criteria indicated that operating the TVC-MED plant on its full nominal capacity was more profitable. The total annual net cash inflow in the full operating mode was only higher by £369,513 because the electricity generated was not high enough to cancel out the effect of the extra O&M costs of the CC power plant.

When the TVC-MED desalination plant was totally shut down to investigate the base power plant's economic performance without it, assuming an interest rate of 5%, a capacity factor of 85% and a project life of 20 years, the results obtained are listed in Table 6-4.

	Value
(i)	5%
(t)	20
PBP	2.2
NPV	£193,775,149
IRR	39.65%
PI	5.00

Table 6-4 Economic evaluations without the TVC-MED desalination plant

The plant with an internal rate of return of 39.65% will pay back its capital costs in just 2.2 years. Moreover, the net present value improved to £193 million over 20 years, and the profitability index increased to 5. Although the increase in the electricity generated in this mode is only 5.4MW more than in the previous operating mode, the reason for this improvement is the subtracting of the investment capital cost and O&M costs of the desalination plant. This indicates that investing in the TVC-MED desalination plant to improve an existing CC power plant is economically acceptable and profitable. The addition of the TVC-MED desalination plant to an existing CC power plant only required 2.5 years in order to pay back the invested capital cost.

If the proposed plant was operated in accordance with electricity demand, the TVC-MED desalination plant would produce 20000m^3/day during the summer months and 40000m^3/day during the rest of the year, for more potable water production. Under the same assumption made before, the results obtained are listed in Table 6-5. The results are in between the results of the first two operating modes. The payback period was 4.7 years as the internal rate of return reached 18.55%. In the long run, the net present value was £158 million over 20 years of the plant's lifetime.

	Value
(i)	5%
(t)	20
PI	4.7
PBP	£158,051,095
NPV	18.55%
IRR	2.43

Table 6-5 Plant's economic evaluation in accordance with electricity demand.

The profitability index also decreased to 2.43. These results confirm the fact that the flexibility of the plant in varying the production rates does not affect the economic performance of the project. Moreover, it pinpoints the economical benefits of recovering the waste heat energy of the exhaust gas system, as the plant's economical performance improves as the utilization rate increases.

6.6 Sensitivity Studies

A number of sensitivity studies have been performed in order to investigate the effect of certain fluctuating economical parameters on the optimized plant economical performance. The economical parameters investigated include the fuel cost, product selling prices, interest rate, capacity factor and project lifetime.

6.6.1 Fuel Prices

The fuel cost factor typically has a great influence on the plant's economic performance because it forms 71% of the annual cash outflow as shown in Figure 6-3. In order to measure this effect, fuel prices were varied from £0.10 to £0.2/kg of NG, with steps of £0.05/kg. The study was performed while the gas turbine and TVC-MED desalination plant were at full load, in ISO conditions and with a seawater temperature of °22C. In addition, the project life and the interest rate were assumed to be 20 years and 5% respectively, and a capacity factor of 85%.

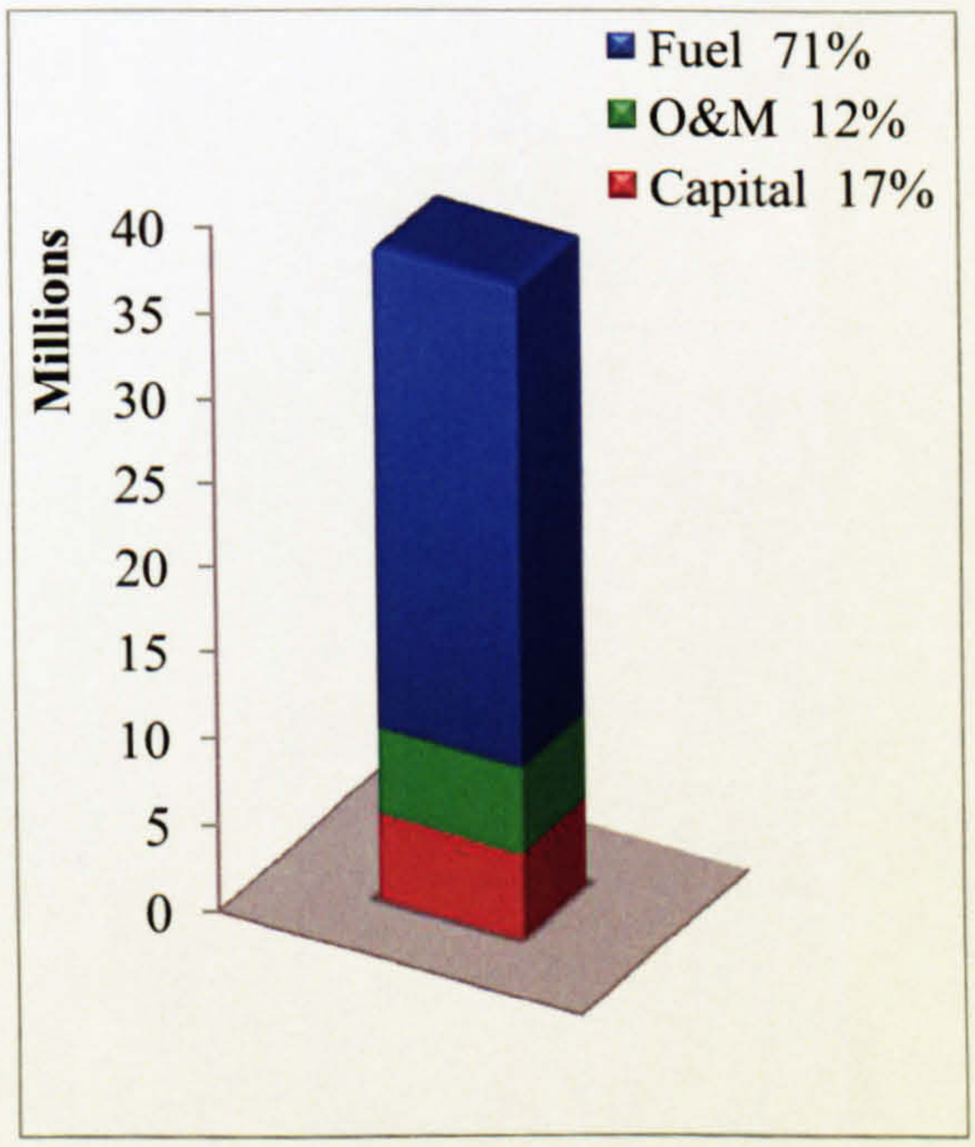

Figure 6-3 Annual cash outflow

The results indicated the great influence of fuel cost on the project's economic acceptability, as it became non-viable in the case of a fuel price higher than £0.174/kg. Figure 6-4 shows the profitability index and the project's net present value versus the variation in the fuel cost.

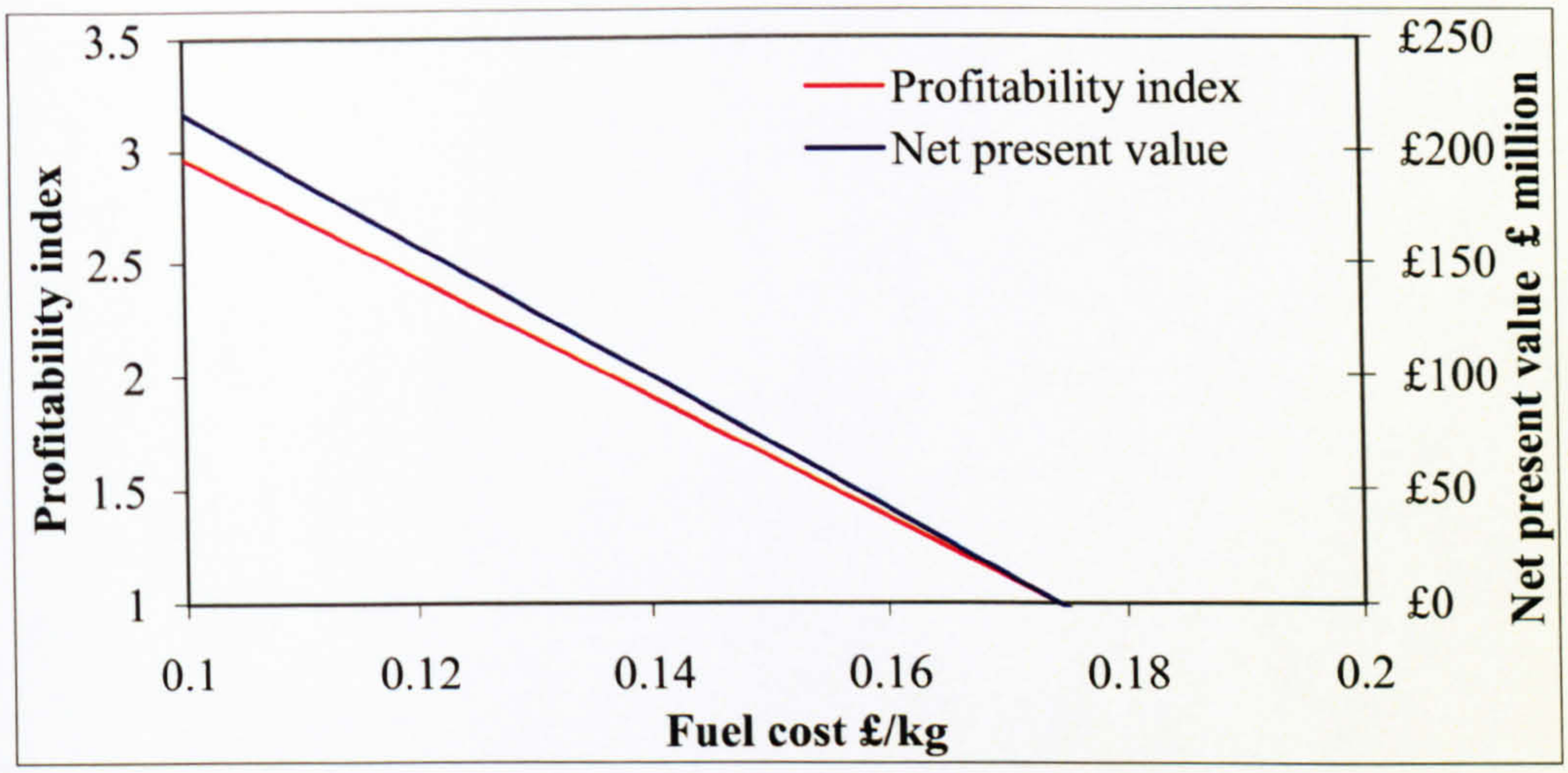

Figure 6-4 Fuel cost versus PI and NPV

The figure shows that for a fuel cost higher than £0.174 both the PI and PNV dropped lower than the minimum acceptable values. However, this scenario is not expected as the fuel prices vary from day to day up and down. If a levelized fuel cost is considered at this high rate the project will pay back its initial capital cost in 11 years. Figure 6-5 shows the payback period against the variation in the fuel prices.

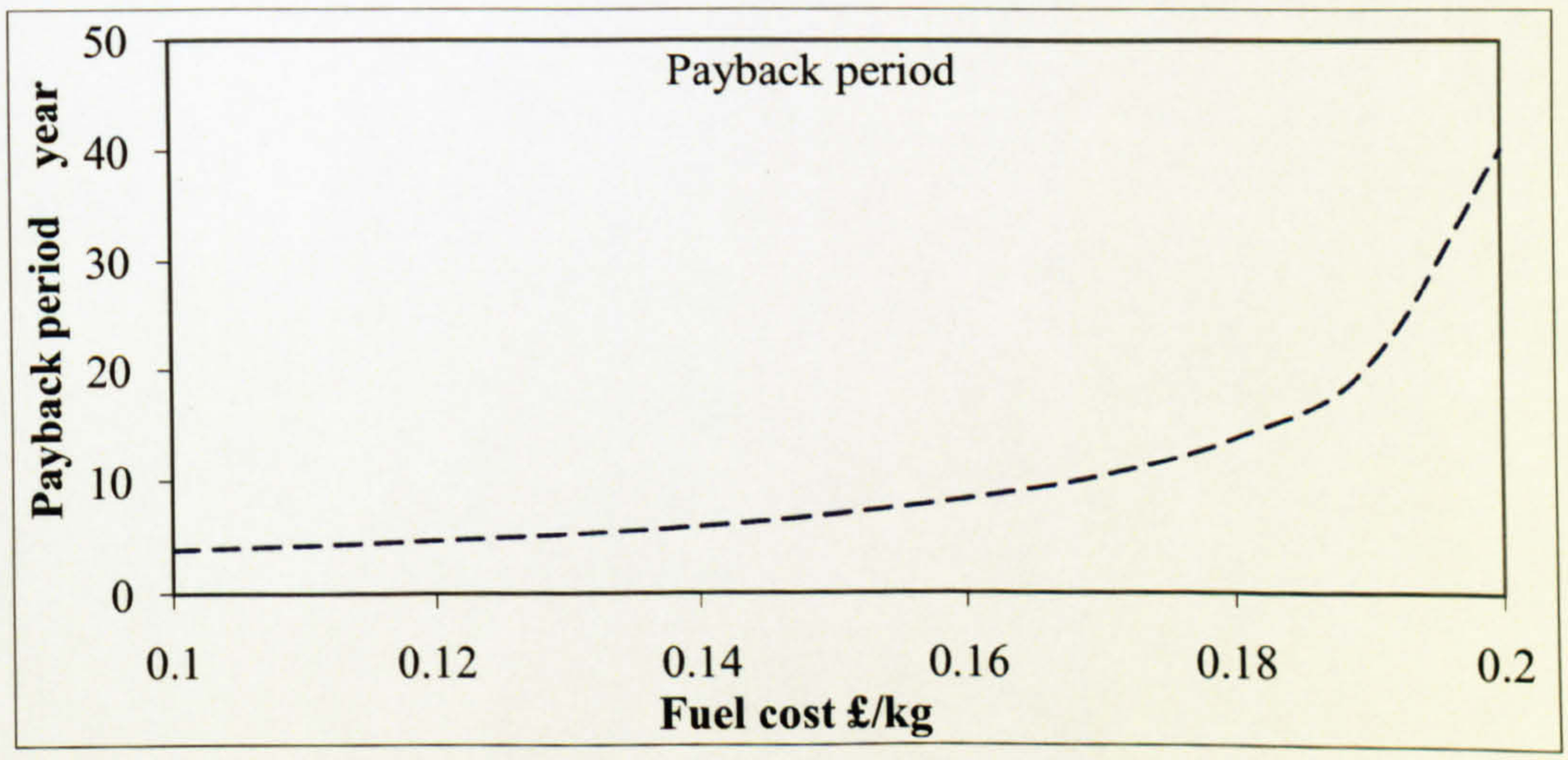

Figure 6-5 Fuel cost versus PBP

The PBP confirmed the results of the PI and the NPV where the payback period increased dramatically for fuel costs higher than £0.174 by 58% on average for each £0.05 increase in the fuel price, in comparison with an increase on average by 15% before this value. The fall in fuel prices reduced the annual cash outflow, which led to a better profitability index value and shorter payback time. Hence, an increase in some product selling prices should be considered to

reimburse the extra costs caused by the increase in the fuel prices. It is important to mention that at the time this study was performed oil prices reached their highest levels since 1860, and then started dropping. Although oil prices cannot be predicted with certainty, this can be considered as a peak.

6.6.2 Interest Rate and Project Lifetime

The second sensitivity study was performed to investigate the influence of both interest rate and project lifetime on the economic performance and acceptability of the optimized proposed plant. The study was performed while the gas turbine and TVC-MED desalination plant were at full load, in ISO conditions and with a seawater temperature of 22°C. The interest rate variation effect was noticed on the net present value and the profitability index as shown in Figure 6-6, which reveals that the project will not be economically viable and will be rejected at an interest rate of 18.7%. The profitability index dropped below 1 and the present net value below zero at an interest rate higher than this value.

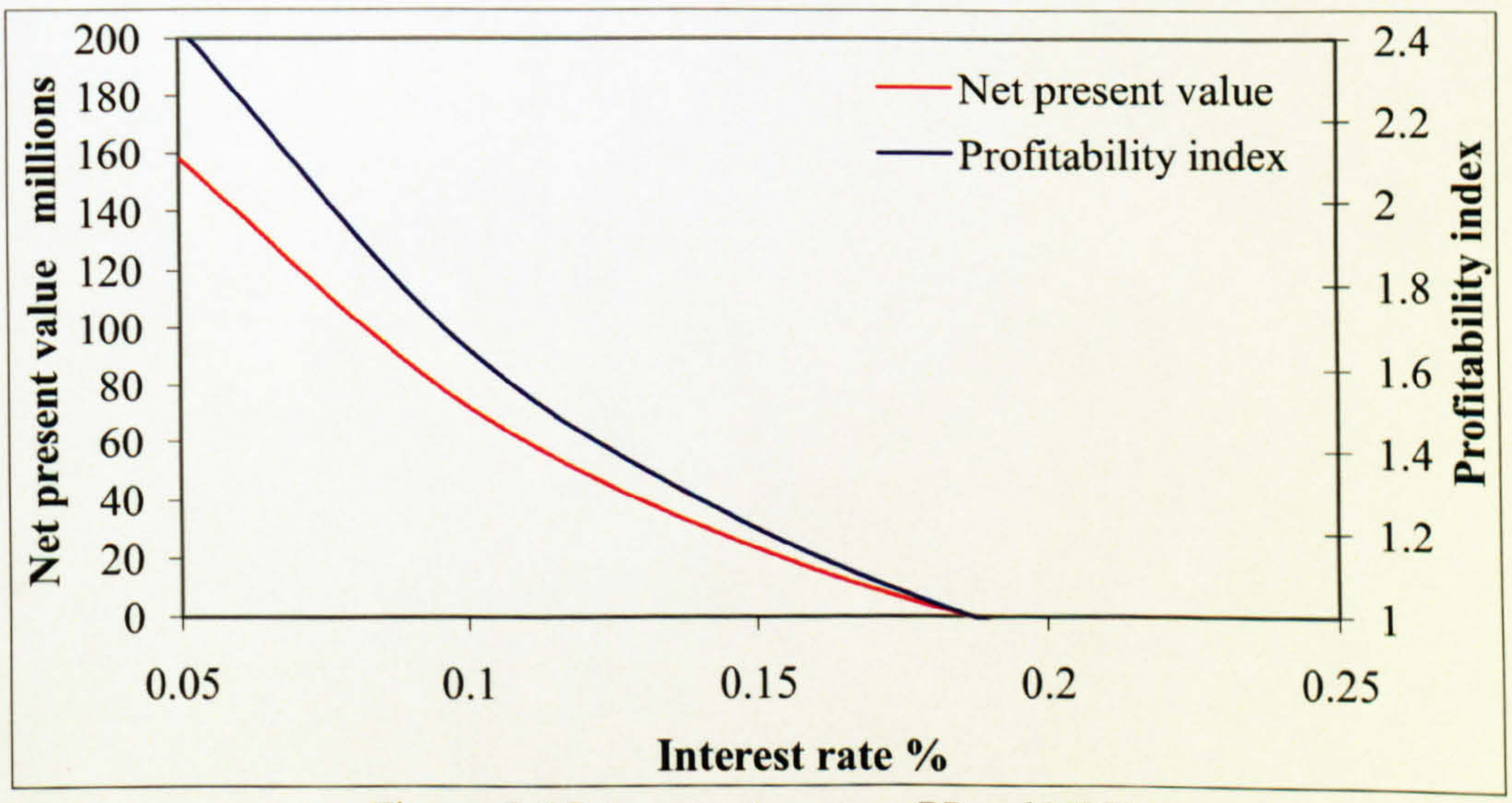

Figure 6-6 Interest rate versus PI and NPV

Furthermore, the project lifetime was observed for the same economic evaluation criteria, that is NPV and PI. As illustrated in Figure 6-7, up to a lifetime of 20 years the net present value increased on average by 57%, while the profitability index increased on average by 24% for each additional five years in the project's lifetime. On the other hand, after a lifetime of 20 years this effect reduced so that it was just on average 4.3% and 7.2% for the net present value and the

profitability index respectively for each additional five years in the project's lifetime. This is mainly due to discounting the money's future value back to its present value.

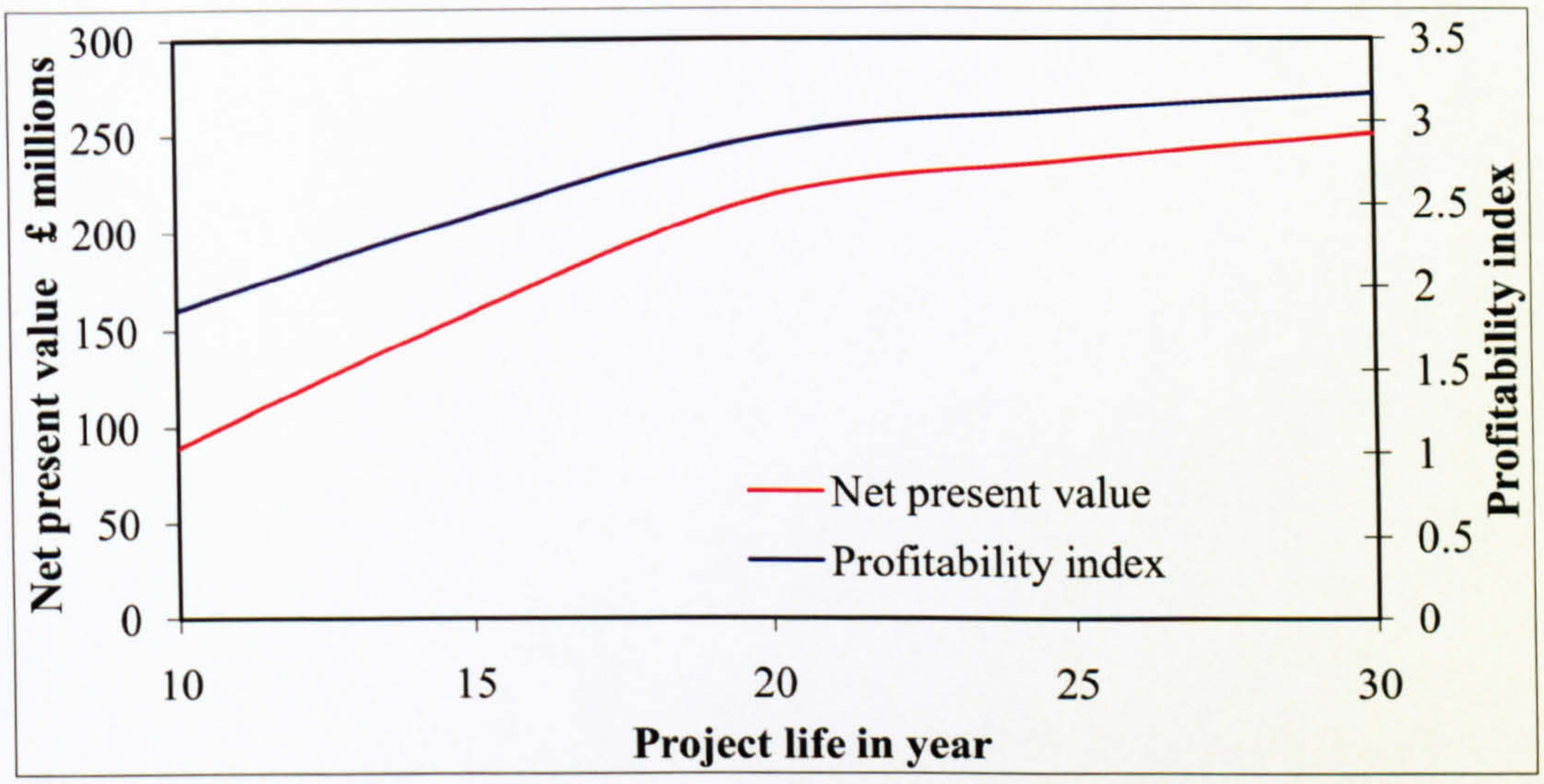

Figure 6-7 Project lifetime versus PI and NPV

In addition to this, the fuel consumption increased as the plant became less efficient with time. Nonetheless, the maintenance cost usually increased with the increase in the project's lifetime, which reduced the net present value.

6.6.3 Capacity Factor

The capacity factor for this study was taken to be 85% in accordance with the usual power plant's capacity factor [79]. However, some other studies and reports consider it to be more than that; hence a sensitivity study was carried out to investigate the influence of maximizing and minimizing the capacity factor on the chosen economic evaluation criteria. The study was performed using the designed MS Excel model to create a variation in the capacity factor from 50% to 100%, with steps of 5%, using the same economic variables: O&M costs, fuel costs and product selling prices. The study was performed with the gas turbine and TVC-MED desalination plant at full load, in ISO conditions and with a seawater temperature of °22C. In addition, the project life and the interest rate were assumed to be 20 years and 5% respectively. Although fuel consumption increased with the increase in the capacity factor, all the product production rates increased too, with an insignificant nominal increase in the O&M costs. This improved the net present value and the internal rate of return on average by 30.55% and 13.66%

respectively for each 5% rise in the capacity factor. Moreover, this improved the profitability index by 9.74% for each 5% rise in the C_f value. Furthermore, the payback period was shortened on average by 5.6 months for each 5% rise in the capacity factor, as shown in Figure 6-8.

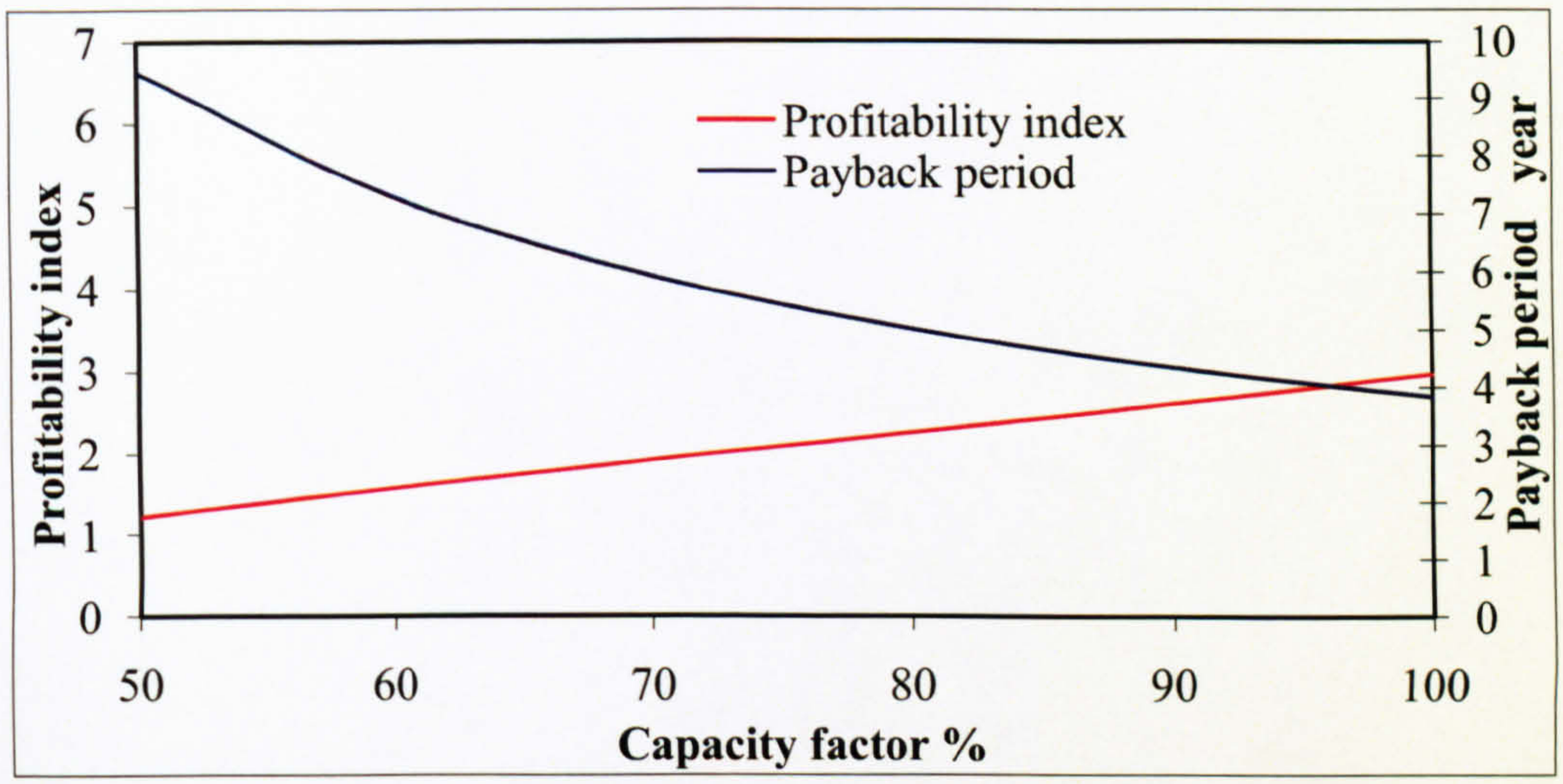

Figure 6-8 Capacity factor versus PBP and PI

The results also indicate the economic applicability of operating the proposed plant even with a capacity factor less than the design's point value.

6.6.4 Electricity Selling Prices

The electricity selling prices were chosen to be in line with the Saudi Arabian electricity prices, which are greatly subsidized by the government. Hence another sensitivity study was performed to define the minimum electricity selling prices at which the plant became economically viable, and to measure the influence of increasing this price the chosen economic evaluation criteria. Using the designed MS Excel model, a variation in the energy price from £0.01/kWh to £0.05/kWh was created with steps of £0.002/kWh, using the same economic variables: O&M costs, pure and hot water selling prices and fuel costs, while the gas turbine and TVC-MED desalination plant were at full load, in ISO conditions and with a seawater temperature of °22C. Furthermore, the project life and the interest rate were assumed to be 20 years, 85% capacity factor and 5% respectively. The results revealed that the minimum price at which the energy can be sold for was £0.013/kWh, which was very even in comparison with the subsidized Saudi tariff. With a value less than this the plant would have been economically non-viable if none of the other economical parameters changed. Figure 6-9 shows the net present value dropped below

zero at a selling price less than £0.013/kWh and the profitability index also dropped below 1 at a value less than this. Moreover, using the generated curves it is possible to estimate the plant's economic performance at a given energy selling price.

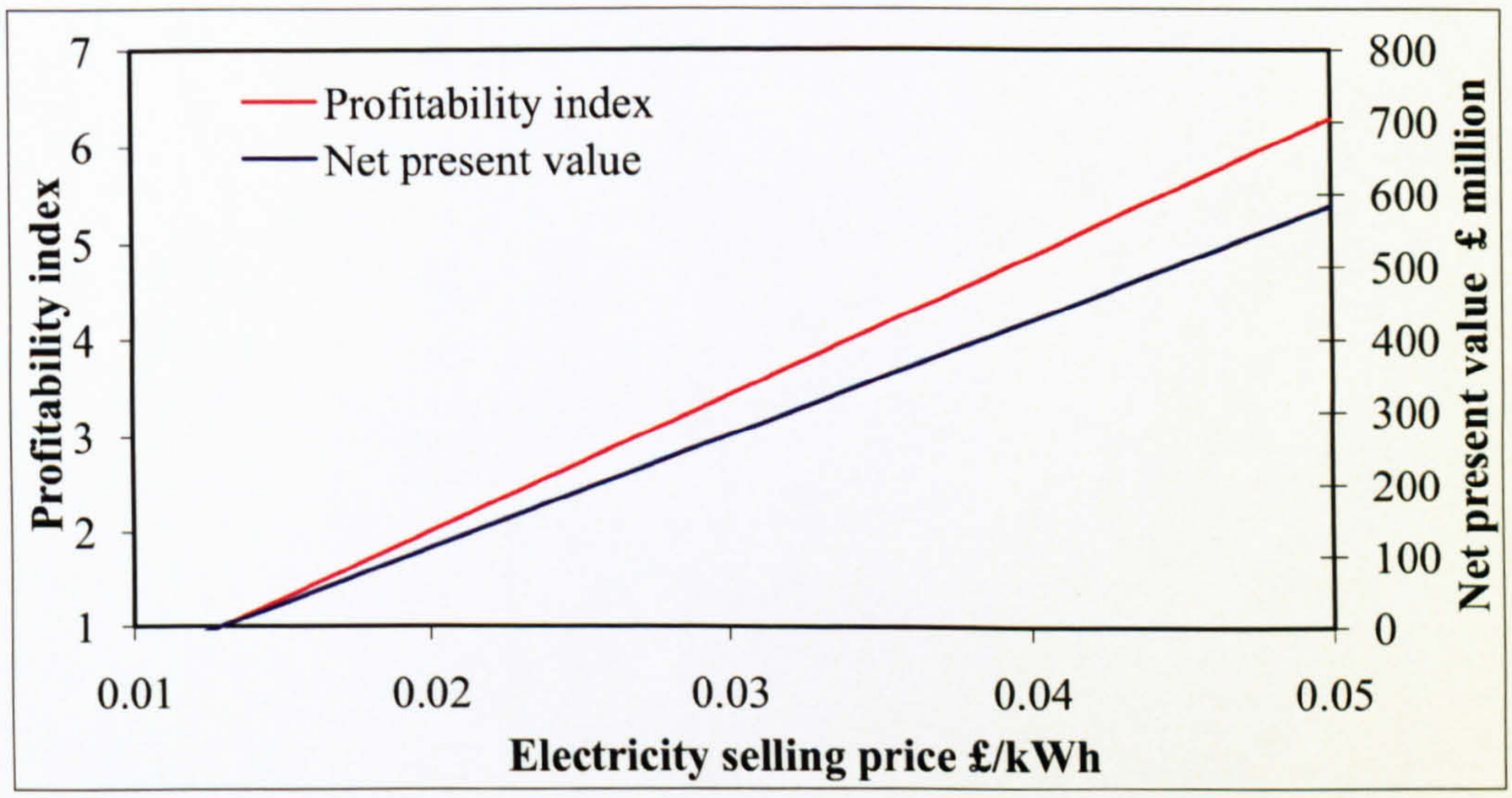

Figure 6-9 Energy selling prices versus NPV and PI

For example, if a price of £0.04/kWh was considered, the payback period was shortened to only two years and three months, simply as a result of increasing the internal rate of return to 39%. However, the results also indicated that increasing the selling price over £0.03/kWh did not seem to shorten the payback period by as much as before this value, where each £0.005/kWh rise in the energy selling price shortened the payback period by only three months on average, as shown in Figure 6-10.

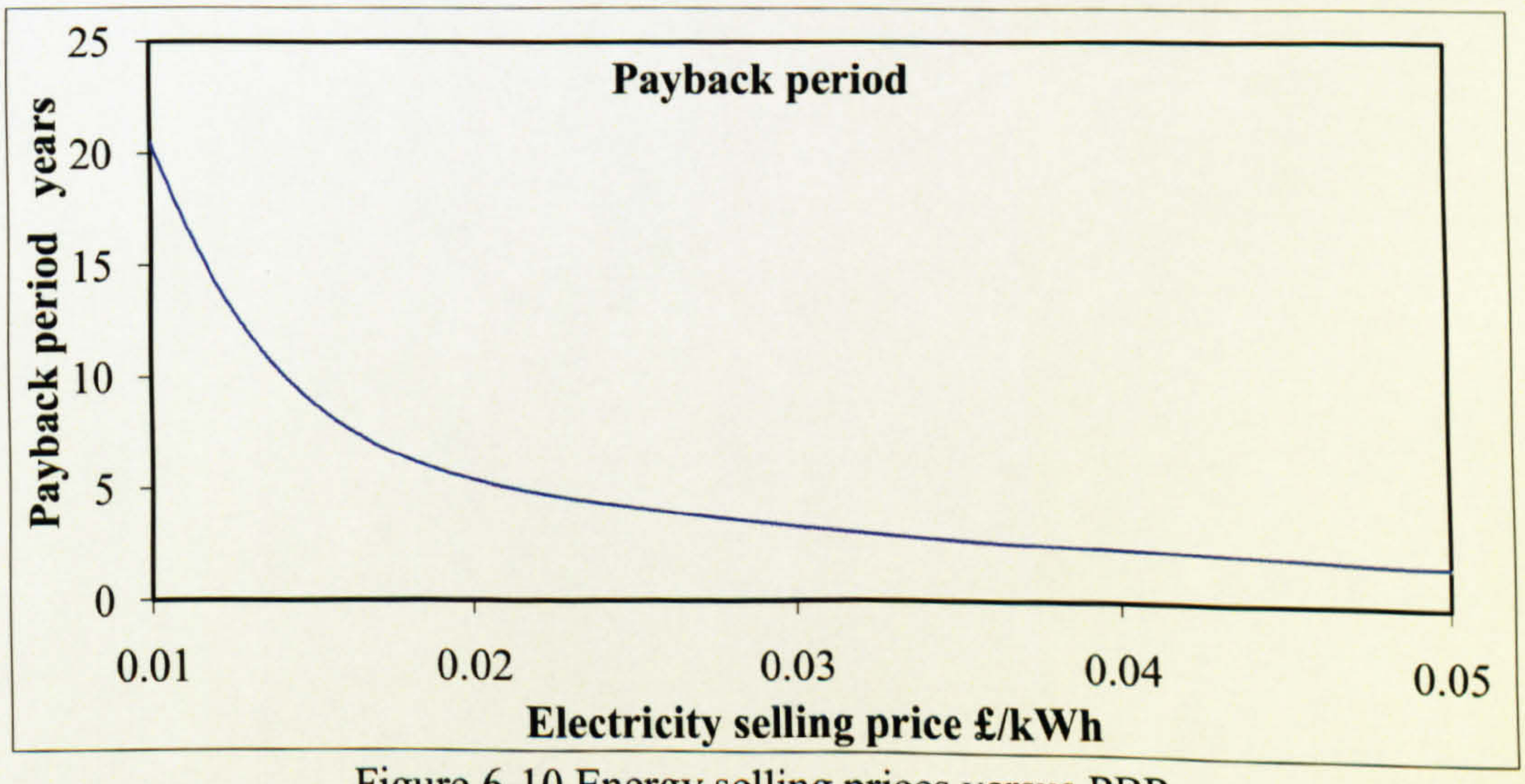

Figure 6-10 Energy selling prices versus PBP

The profitability index and internal rate of return were both directly proportional to the increase in the energy selling prices. Furthermore, for a payback period of less than 4.7 years, the electricity selling price should not have been less than £0.023/kWh, although the project was still economically acceptable at a value less than this.

6.6.5 Potable Water Selling Price

The potable water selling price was investigated in another sensitivity study to measure its influence on the plant's economic acceptability. Using the designed MS Excel model a variation in the potable water selling price was created from £0.50/m^3 to £0.80/m^3, with steps of £0.02/m^3. The study was performed under the same conditions and economic variables: O&M costs, energy and hot water selling prices and fuel costs, while the gas turbine and TVC-MED desalination plant were at full load, in ISO conditions and with a seawater temperature of °22C. The project life, capacity factor and the interest rate were also assumed to be 20 years, 85% and 5% respectively. The results showed the limited effect of adjusting the potable water selling price on the plant's economic acceptability, as the most significant influence was found to be on the payback period. Figure 6-11 shows that increasing the price from £0.4/m^3 to £0.80/m^3 would have only shortened the payback period by one year.

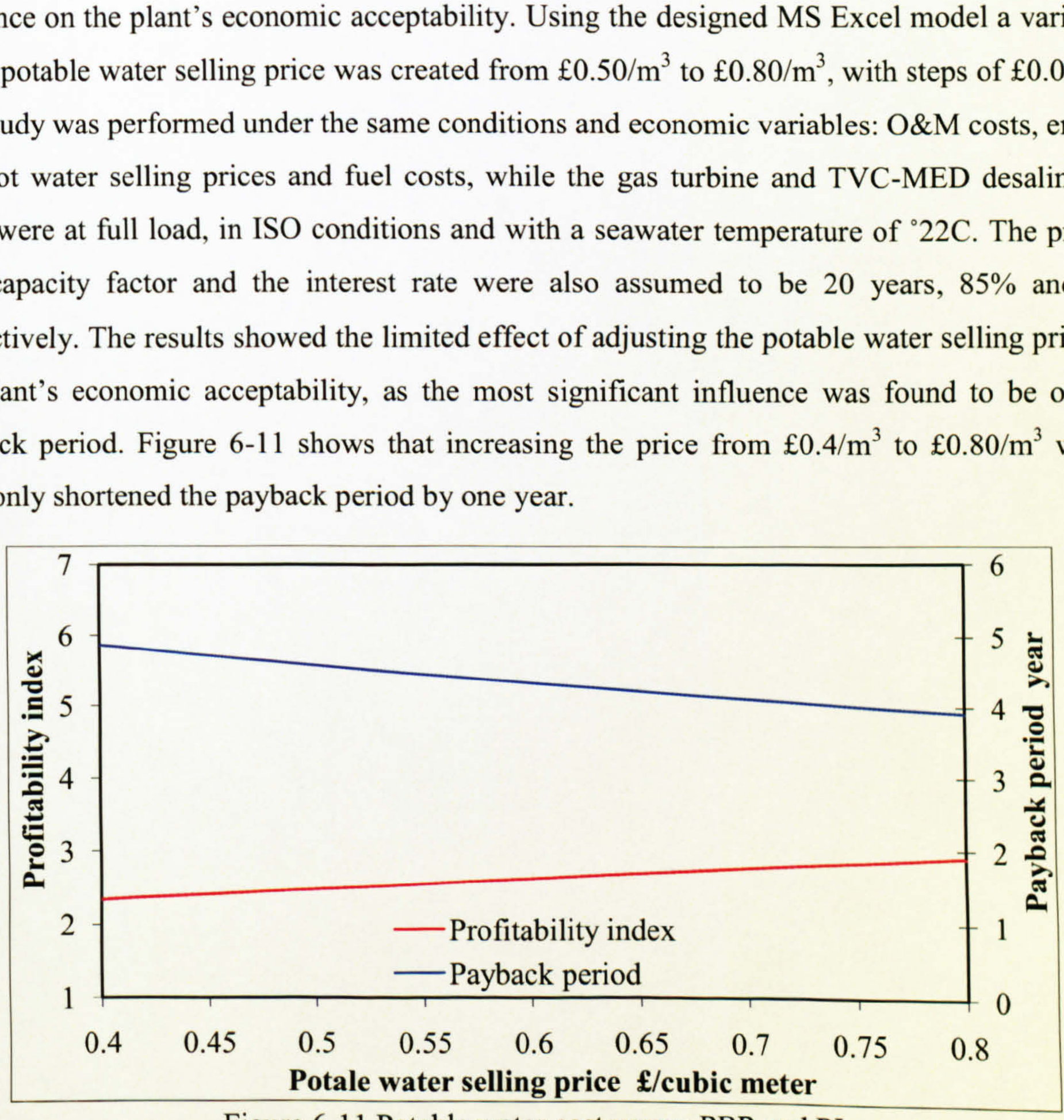

Figure 6-11 Potable water cost versus PBP and PI

This was because of the small quantity of production in comparison with the other products. Moreover, the improvement in the profitability index was limited to only 2.41% on average for

each £0.05/m^3 rise in the selling price. Likewise, the net present value and the internal rate of return were only improved by 3.9% and 2.7% respectively for each £0.05/m^3 increase in the potable water selling price. Hence, the selling price of the potable water can be discounted to compete with the subsidized Saudi tariff (£0.47/m^3) without a great effect on the plant's economic performance. If a price of 0.4/m^3 is considered the payback period will increase by only two months, while the profitability index will be as high as 2.34.

6.6.6 Hot Water Selling Price

Lastly, the hot water selling price was investigated in a sensitivity study to measure its influence on the plant's economic acceptability. Using the designed MS Excel model a variation in the potable water selling price was created from £2/GJ to £10/GJ, with steps of £1/GJ. The study was performed under the same conditions and economic variables: O&M costs, energy and hot water selling prices and fuel costs, while the gas turbine and TVC-MED desalination plant were at full load, in ISO conditions and with a seawater temperature of 22˚C. The project life, capacity factor and the interest rate were also assumed to be 20 years, 85% and 5% respectively. The results show that hot water as a product had a significant effect on the economic performance of the plant similar to that of the electricity selling price. Moreover, the results defined the minimum possible selling price of the hot water at £2.32/GJ where all other economics parameters were stable. Figure 6-12 shows both the profitability index and the payback period against the variation in the hot water selling prices.

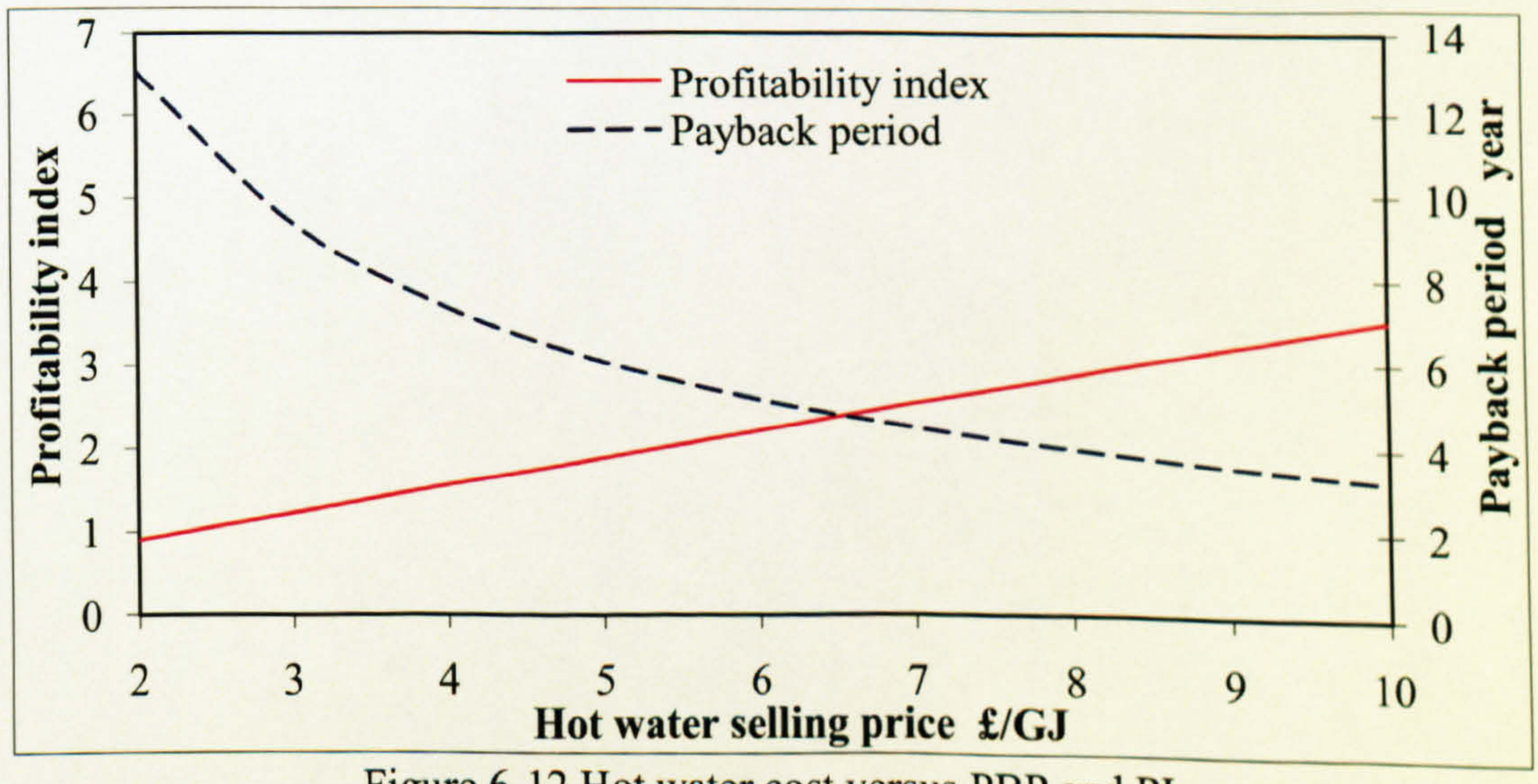

Figure 6-12 Hot water cost versus PBP and PI

The profitability index dropped below 1 at a selling price less than £2.32/GJ, and the payback period increased to more than 12 years. However, the results also indicated that raising the selling price of the hot water over £7/GJ did not seem to shorten the payback period by as much as before this value, where each £1/GJ rise in the hot water selling price shortened the payback period by only four months on average. Likewise, the net present value confirmed the same price at which it dropped below zero making the project economically unacceptable. Figure 6-13 shows both the net present value and the internal rate of return against the variation in the hot water selling prices.

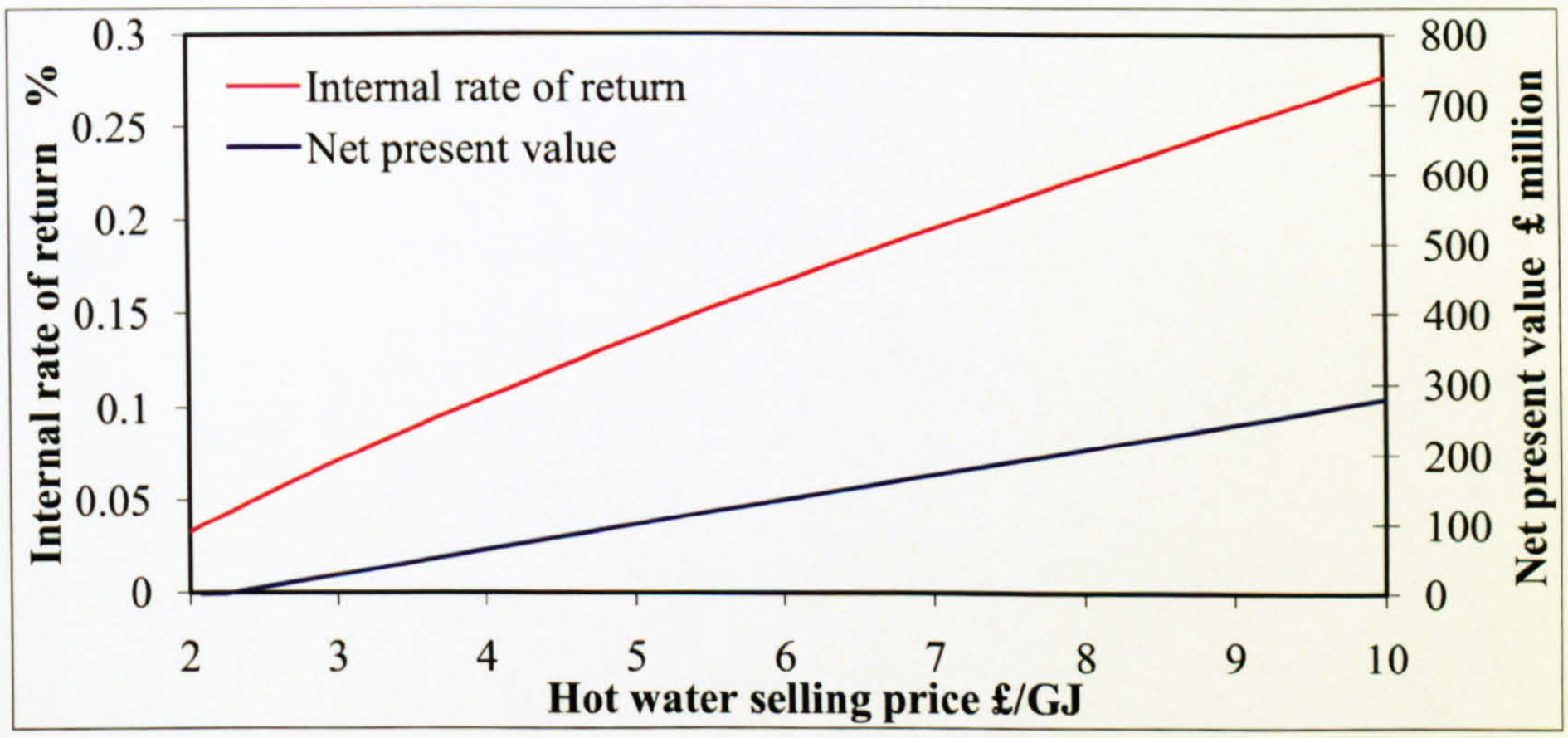

Figure 6-13 Hot water cost versus IRR and NPV

The net present value dropped below zero at a hot water selling price of less than £2.32/GJ, increasing on average by 40% for each 1/GJ increase in the hot water selling price. The internal rate of return increased on average by 19.2% for each 1/GJ increase in the hot water selling price.

In conclusion, the sensitivity studies performed indicated the economical stability of the optimized proposed plant, whilst all the plant's products selling prices can be further discounted to compete with market prices with no significant effect on the plant economical performance. Furthermore, the negative effect of increasing the other economical parameters, for example fuel cost, can be avoided by increasing these selling prices which is already discounted and competitive.

6.7 Closing Remarks

In conclusion, this chapter presented an economic impact study that employed four of the economic evaluation criteria, that is payback period (PBP), internal rate of return (IRR), profitability index (PI) and net present value (NPV), in order to assess the economic acceptability of the proposed plant. Firstly, the initial cost of each piece of equipment or sub-plant was presented or calculated using the designed economic MS Excel model, and all other capital costs were defined. Secondly, the annual cash outflow was introduced and then used in the second designed economical MS Excel model to automatically calculate the annual cash inflows and all the chosen evaluation criteria. Thirdly, a case study was performed in which the plant's economic performance was investigated in more detail in accordance with the weather data, and in the three suggested operating modes.

Lastly, a number of sensitivity studies were performed to investigate the influence of certain economic variables: fuel price, interest rate, project lifetime, capacity factor, electricity selling price, hot water selling price and potable water selling price. It was concluded that the plant was economically acceptable and profitable in all operating modes, with a payback period not greater than 4.7 years, a profitability index of up to 2.44 and a net present value reaching £158 million. On the other hand, it was found that fuel cost had the greatest effect on the plant's economic performance, while the interest rate was not economically acceptable for values higher than 18%. Furthermore, the project's life time could have been extended up to 30 years, although this did not show a great improvement in the plant's economic situation as much as in the first twenty years due to the increase in the O&M costs. The electricity selling price was found to have an important influence on the plant's economic performance and was limited to £0.013/kWh as a minimum value. The potable water selling price was not found to be as important as the hot water selling price and hence could have been discounted without a great effect on the plant's economic performance.

Chapter 7

Conclusion and Recommendations

7.1 Introduction

Technological development usually comes from research into the needs of consumers and markets that seek effective solutions to ensure the best products at the lowest prices. However, unlike other studies those deal with only one or two matters at a time, this study was intended to discover effective solutions for a number of issues and was motivated by the following factors:

- Increasing demand and the price of electrical power
- Shortage of potable water in arid and semi-arid areas
- Limited resources and increasing prices of fossil fuels
- Urgent need to reduce greenhouse gas production
- Effect of ambient conditions on power plant performance.

It was, therefore, the aim of this study to find the most effective techniques to tackle these issues. The combined cycle power plant was chosen as the electricity generator because of its large contribution to climate change. The MED desalination plant was chosen as the potable water producer because of its ability to be powered solely by thermal energy. In addition, the absorption chiller was chosen as the cooling effect generator since it is a system powered by low-grade heat energy. The aims of the study were to find the optimum way to power these systems, while consuming the same amount of fuel but producing lower amounts of CO_2 emissions. The proposed plant was able to produce electricity, potable water and hot water, while overcoming the negative effects of variations in ambient conditions on its performance as a power plant.

All plants were modelled on the basis of real data obtained from power plant site and commercially available plants. Two different technologies for the thermal desalination plant were tested: multi-effect distillation and multi-effect thermal vapour compression. Two different coupling techniques were tested to power the desalination plant: the first used a boiler to recover a portion of the heat energy of the exhaust gas stream waste heat energy, and the second extracted steam from the steam turbine. A single-effect water-cooled absorption chiller powered by the waste heat energy of the gas turbine exhaust was used to pre-cool the gas turbine's intake-air. In the optimization stage, the cooling water from the absorption chiller was utilized as a hot

water source after it had been circulated through a heat exchanger to recover a portion of the heat energy of the exhaust gases' waste heat energy. Furthermore, the steam turbine condenser's cooling water was utilized to control the salinity and temperature of the desalination plant's rejected brine. Although any of the proposed plants could have been used anywhere, Yanbu, a city in Saudi Arabia, was designated for this study. Thus, a full record of weather data for 23 years was obtained from the Presidency of Meteorology and Environment, Saudi Arabia. A software package called IPSEpro was used to simulate all the base and proposed plants, and then energy and exergy analyses, the effectiveness-NTU method, and pinch analysis were used for the HRSG unit. Using the IPSEpro modelling development kit, three of the available IPSEpro libraries — the advanced power plant, desalination and refrigeration libraries — were combined into a single library that allowed the modelling and simulation of the proposed plants.

Each of the three sub-plants was simulated and tested on a stand-alone basis under ISO conditions and off-design, and the results were presented and discussed for each model. Following this, four proposed plants were modelled and tested and their results presented, discussed and compared with each other and with stand-alone models. The optimal design was then chosen for the optimization stage. The optimization modifications were then modelled and tested, and the results were presented and discussed based on energy, exergy and pinch analyses. Three different operating modes were presented and the optimized plant was tested at each one of them, and the partial-load performance of the gas turbine was also investigated. Furthermore, a number of parametric studies were performed to investigate the optimized plant performance under varying ambient air and seawater temperatures.

In order to demonstrate the plant's economic acceptability and profitability, a full economic study was performed for all possible operating modes. Four economic evaluation criteria were chosen to perform this economic study, namely payback period, profitability index, net present value and internal rate of return. Firstly, the initial costs of all the plants and their auxiliary equipment were either calculated or obtained directly from vendors' quotations or recently published studies. Two MS Excel models were built and validated; one to calculate the initial cost of the heat exchangers and the other to calculate the annual outflow and inflow cash and the four chosen economic evaluation criteria — PBP, PI, NPV and IRR. Next, the plant was evaluated economically under all operating modes and in accordance with the monthly electricity

demand. Then the results were collected, analysed and compared with each other. A number of sensitivity studies were carried out to demonstrate the influence of certain vital economic parameters on the plant's economic performance, such as fuel prices, product selling prices, interest rate, capacity factor and project lifetime.

7.2 Conclusion

The results indicated that the optimized proposed plant was stable, efficient and economically acceptable in all conditions and under all suggested operating modes that permitted more flexibility in controlling both the electricity and the potable water production rates. The first two proposed plants, which were modelled according to the maximum work hypothesis, were not able to power the desalination plant to produce its full capacity, but did generate the nominal capacity of the combined cycle power plant. The analysis results of these two first proposed plants revealed that the thermal vapour compression MED desalination plant was more efficient than the traditional MED desalination plant as it achieved a better GOR value. From the results of the third and fourth proposed plants, it was concluded that powering the desalination plant by extracting steam from the steam turbine was better than powering it by a boiler that utilized a portion of the exhausted gas heat energy. The optimization stage offered an additional product to the plant's existing products and controlled the salinity and temperature of the desalination plant's rejected brine.

In more details, both the first and second proposed plants generated the full nominal capacity, 195MW, of the combined cycle power plant. The CO_2 emission rate decreased by 24% and 26% for the first and second proposed plants respectively in comparison with the base combined cycle power plant. The potable water production rate was greater in the TVC-MED desalination plant in the second proposed plant than in the MED desalination plant in the first proposed plant by 1476m^3/day. Furthermore, the GOR value was better by 0.82 in the TVC-MED desalination plant. However, in both proposed plants the desalination plant did not produce even half of its nominal capacity. The maximum work hypothesis was applied and discussed, and found to be not beneficial in comparison with the third and fourth proposed plants. In the third proposed plant the electricity generation decreased to 154.18MW and the CO_2 emission rate decreased to 339.7 kg CO_2/kW, in comparison with 195MW and 508 kg CO_2/kW in the base combined cycle

power plant. This drop in electricity was compensated for by the full nominal capacity production rate of the potable water from the TVC-MED desalination plant and the ability to power the absorption chiller which stabilizes the effects of ambient temperature fluctuations on the plant. The electrical efficiency of the plant decreased to 41.68% from 52% in the base combined power plant. The plant achieved an exergetic efficiency of 42.3% with a total exergy destruction rate of 219MW, and consumed 57% of the total exergy input. The main source of exergy destruction in the plant was the gas turbine followed by the TVC-MED desalination plant's boiler and then the stack.

The fourth proposed plant generated more electricity than the third plant, at 169.65MW, which was only 13%.less than that of the base combined-cycle plant. The CO_2 emission rate was 320kg CO_2/kW less than that of both the third plant and the base power plant, and the EUF reached 83.76% in comparison with 79.09% in the third proposed plant. Likewise, the drop in electricity was compensated for by the full nominal capacity production rate of the potable water from the TVC-MED desalination plant and the ability to power the absorption chiller. Moreover, the electrical efficiency improved in the fourth proposed plant to 45.7%, but it was still 6.3% less than that of the base power plant. The TVC-MED desalination plant's GOR improved to 8.48 in this proposed plant and the plant achieved an overall exergetic efficiency rate of 48.16% with a total exergy destruction rate of 205MW, consuming 54% of the total input exergy. The absorption chiller's performance in both the proposed plants (the third and fourth) was similar to its stand-alone performance. The retrofitting of the absorption chiller greatly benefited the plant in more than one way. First, it utilized about 4% of the waste heat energy, which is usually emitted into the atmosphere; this reduced the plant's CO_2 emission rate by 16%. Secondly, it stabilized the effects of ambient temperature fluctuation and assured stable production rates for all the plant's products. Thirdly, it increased the production rate and improved most of the plant's performance parameters as a direct result of cooling the compressor's intake-air to 10°C. Fourthly, it increased the gas turbine's lifetime and reduced its maintenance costs.

The fourth proposed plant was chosen for the optimization stage after a full comparison with the other proposed plants based on both energy and exergy analyses. The optimization stage offered a stream of hot water at a temperature ranging from 75°C to 81°C as an additional product. It also reduced the TVC-MED desalination plant's concentration factor to 1.4, from 1.87 before

optimization. The temperature of the rejected brine water also decreased, to 37°C from 50°C before optimization. The analysis of the results of the plant's performance after optimization showed that the plant's EUF improved to 98.87% and the exergetic efficiency rate improved to 49.64% as a result of further utilization that produced a hot water stream. The CO_2 emission rate improved to 219 $kgCO_2/kW$ from 320 $kgCO_2/kW$ before optimization. The plant's electrical efficiency was not affected by the optimization, and neither was the total exergy destruction of the plant.

The results of the parametric studies showed that the plant was stable against ambient temperature fluctuations. This was in comparison with 3.8% losses in electrical power and 1.16% losses in the overall electrical efficiency for each 5°C increase in the ambient temperature before retrofitting the absorption chiller. Moreover, the gas turbine's exergy destruction was stabilized in comparison with an average increase of 0.25MW for each 5°C increase in the ambient temperature before retrofitting the absorption chiller. The energy utilization factor was affected by the ambient temperature variation; it declined by an average of 0.61% for each 5°C increase in the ambient temperature as a result of needing a greater cooling effect to cool the compressor's intake-air against the increase in ambient temperature. The CO_2 emission rate also increased insignificantly by an average of 2.5kg CO_2/kW for each 5°C increase in the ambient temperature. The effect of ambient humidity was found to be insignificant both before and after retrofitting the absorption chiller. Likewise, the seawater temperature and salinity were found to have insignificant effects on the plant's products, except for the hot water produced. The hot water temperature increased by 0.27°C for each 5°C increase in the compressor inlet-air temperature, reaching 80°C at a maximum ambient temperature of 50°C. Likewise, it increased by 2.6% for each 2°C increase in the seawater temperature, reaching 81°C at a maximum seawater temperature of 28°C.

Economically, the optimized plant was tested at all suggested operating modes and also in the case of its being operated in accordance with the electricity demand. The results showed that the plant was economically acceptable and profitable with a payback period not greater than 4.7 years, a profitability index of up to 2.44 and a net present value reaching £158 million. The results also indicated that the flexibility of the plant did not affect its economical acceptability. Furthermore, the sensitivity studies indicated that fuel cost had the greatest effect on the plant's

economic performance, while the interest rate was found to be economically unacceptable for values higher than 18%. Moreover, the project's life time could have been extended up to 30 years, although this did not show a great improvement in the plant's economic situation as much as in the first twenty years due to the increase in the O&M costs. The electricity selling price was found to have an important influence on the plant's economic performance, and was limited to £0.013/kWh as a minimum value. The potable water selling price was not found to be as important as the hot water selling price and hence could have been discounted without having a great effect on the plant's economic performance. In conclusion, the sensitivity studies performed indicated the economical stability of the optimized proposed plant, whilst all the plant's products selling prices could have been further discounted to compete with market prices with no significant effect on the plant's economical performance. Moreover, the negative effect of increasing the other economical parameters, for example fuel cost, could have been avoided by increasing the products selling prices, which was already discounted and competitive.

Generally, the results of this study can be applied to any new or existing power plant in order to improve its EUF; gaining more products without consuming any additional fuel. Any gas turbine based power plant could be modified to power a thermal desalination plant using the techniques presented in the third proposed plant. Any MED desalination plant could be improved by applying the results of the comparison between the first two proposed plants, which showed that adding a steam ejector to the plant improves its GOR and reduces the amount of steam required by the brine heater, as well as improving the production rate. Moreover, its concentration factor can be improved by applying the technique proposed in the optimization stage in which the condenser's cooling water is mixed with the desalination plant's rejected brine. Any power plant that is located in a hot climate area could be improved, and the effects of the ambient temperature fluctuation could be avoided, by retrofitting an absorption chiller that is powered by the heat energy recovered from its exhaust system. In countries that are facing regulation to reduce carbon dioxide emissions, the techniques proposed in this study will reduce CO_2 emission rates by up to 57% once they are applied to any new or existing power plant.

7.3 Recommendations for Future Work

Based on the results of this study and the limitation imposed on it, a number of recommendations are listed in this section for future work.

- Although most of the recent published work in this research field is based on modeling and simulation software packages, the experimental research work is more precise and accurate. Therefore, it is recommended that the techniques proposed in this study be tested either on a test rig or a real power plant.
- From the results of the parametric study that investigated the effect of seawater temperature on the TVC-MED desalination plant, it was concluded that the increase in the seawater temperature improves the desalination plant's thermal performance by reducing the quantity of steam required to boil the seawater in the brine heater. Therefore, preheating the feed seawater should be investigated in future work.
- Based on the exergy analysis results, in all the proposed plants the main source of the plant irreversibility was the gas turbine. Hence, for future work it is recommended that consideration is given to improving the gas turbine cycle either by retrofitting a recuperator or preheating the fuel stream.
- Although the single absorption chiller employed in this study was adequate and beneficial, it is believed that the half-effect absorption chiller could generate double the cooling capacity of the single-effect one but with half the COP, which is not an important performance parameter as long as the heat energy source is free. Therefore, it is suggested that a half-effect water-cooled absorption chiller be installed instead of the current single-effect absorption chiller and its performance be tested thermodynamically and economically within the proposed plants..

References

1. Ophir, A. and Lokiec, F., 2005. Advanced MED process for most economical sea water desalination. *Desalination*, 182 (1/3), pp. 187198.

2. Campbell, N., 2005. *The sea shall quench. England.* Halcrow Water Services Ltd.

3. Birkett, J., 1984. A brief illustrated history of desalination: from the Bible to 1940. *Desalination*, 50, pp. 1752.

4. United Nations, 2001. Water desalination technologies in the ESCWA member countries. New York: United Nations.

5. Miller, J., 2003. *Review of water resources and desalination technologies*. California: Sandia National Laboratories.

6. Banat, F., 2007. Economical and technical assessment of desalination technology. Jordan University of Science and Technology.

7. Khawaji, A. Kutubkhanah, A, and We, J., 2008. Advances in seawater desalination technologies. *Desalination* 221 (13), pp. 47–69.

8. Al-Rawajfeh, A. Glade, H. and Ulrich, J., (2003). CO2 release in multiple-effect distillers controlled by mass transfer with chemical reaction. *Desalination*, 156 (1-3), pp.109123.

9. Semiat, R. and Galperin, Y., (2001). Effect of non-condensable gases on heat transfer in the tower MED seawater desalination plant. *Desalination*, 140 (1), pp. 2746.

10. Al-Shammiri, M. and Safar. M., (1999).Multi-effect distillation plants: state of the art. *Desalination*, 126 (13), pp. 4559.

11. Loeb, S., 1967. Sixteen months of field experience on the Coalinga pilot plant. *Desalination*, 1967. 2 (1), pp. 7580.

12. International Environmental Technology Centre, 1994. *Sourcebook of Alternative Technologies for Freshwater Augmentation in West Asia*. Geneva: United Nations Environment Program.

13. Glater, J., 1998. The early history of reverse osmosis membrane development. *Desalination*, 117 (13), pp. 297309.

14. Clayton, R., 2006. *Desalination for water supply*. UK: Foundation for Water Research.

15. Fraser, J. and Thompson, S., 1977. Preliminary design of an experimental containerized freeze desalination unit. USA: Concentration Specialists Inc..

16. Sadrzadeh, M. and Toraj, M., 2008. Sea water desalination using electro-dialysis. *Desalination*, 221 (13), pp. 440447.

17. Al-Sahlawi, M., 1999. Seawater desalination in Saudi Arabia: economic review and demand projections. *Desalination*, 123, pp. 143147.

18. Al-Zahrani, S. Al-Ajlan, A. M. and Al-Jardan, A. M., 1994. Using different types of anti-scalant at the Al-Jubail power and desalination plant in Saudi Arabia. *Desalination*, 97 (13) pp. 1728.

19. Saline Water Conversion Corporation, 2008. Projects: Working Plants, Al-Riyadh: Saline Water Conversion Corporation.

20. Saudi Electricity Company, 2008. *2020 Ambitious energy strategy*. Al-Riyadh: Saudi Electricity Company.

21. Abrahamsson, K. Gidner, A. and Jernqvist, A., 1995. Design and experimental performance evaluation of an absorption heat transformer with self-circulation. *Heat Recovery Systems and CHP*, 15 (3), pp. 257272.

22. Occhionero, A. J. Hughes, P. J. and Reid, E. A., 1991. *Absorption chillers: part of the solution*. In International CFC and Halon Alternatives Conference. 35/12/1991. *The alliance for responsible atmospheric policy*. Washington.

23. Garland, P., 1998. *A history of U.S. market share in commercial chillers*. U.S. department of energy, USA.

24. Mathews, J., 2007. Seven steps to curb global warming. *Energy Policy*, 35 (8), pp. 4247-4259.

25. The Trane Company, 2000. Air Conditioning Clinic: absorption water chillers, one of the equipment series. La Crosse: American Standard Inc.

26. Herold, K. Klein, S. and Radermacher, R., 1995. *Absorption chillers and heat pumps.* London: CRC press.

27. Senior A., 2003. *Use of ozone depleting substances in laboratories*. Copenhagan: Nordic Council of Ministers.

28. Erdem, H., and Sevilgen, S., 2006. Case study: effect of ambient temperature on the electricity production and fuel consumption of a simple cycle gas turbine in Turkey. *Applied Thermal Engineering*, 26 (23), pp. 320326.

29. Kehlhofer, R. Bachmann, R. Nielson, H. and Warner, J., 1999. *Combined-cycle gas and steam turbine power plants.* 2ed ed. Oklahoma: PennWell Publishing Company.

30. Felipe, R. Arrieta, P. Electo, E. and Lora, S., 2005. Influence of ambient temperature on combined-cycle power-plant performance. *Applied Energy*, 80 (3), pp. 261272.

31. Bassily, A., 2001. Effects of evaporative inlet and after cooling on the recuperated gas turbine cycle. *Applied Thermal Engineering*, 21 (18), pp. 18751890.

32. Hosseini, R. Beshkani, A. and Soltani, M., 2007. Performance improvement of gas turbines of Fars (Iran) combined cycle power plant by intake-air cooling using a media evaporative cooler. *Energy Conversion and Management*, 48 (4) pp. 10551064.

33. Saravanamuttoo, H. Straznicky, P. Rogers, C. and Cohen, H., 2009. *Gas turbine theory.* 6th ed. Parson Education Limited.

34. Kakaras, E. Doukelis, A. and Karellas, S., 2004. Compressor intake-air cooling in gas turbine plants. *Energy*, 29 (1215), pp. 23472358.

35. Kurz, R. and Brun K., 2009. Degradation of gas turbine performance in natural gas service. *Journal of Natural Gas Science and Engineering.* 1, pp. 95–102.

36. Ameri, M. and Hejazi, S., 2004. The study of capacity enhancement of the Chabahar gas turbine installation using an absorption chiller. *Applied Thermal Engineering*, 24 (1) pp. 5968.

37. Boyce, M., 2006. *Gas Turbine Engineering Handbook*, 3rd ed. USA Gulf Professional Publication.

38. Adel, E. Nasser, M. and El-Kalay, M., 1991. A heat-recovery cooling system to conserve energy in gas-turbine power stations in the Arabian Gulf. *Applied Energy*, 38 (2), pp. 133-142.

39. Mohanty, B. and Paloso, G., 1995. Enhancing gas turbine performance by intake-air cooling using an absorption chiller. *Heat Recovery Systems and CHP*, 15 (1), pp. 4150.

40. Boonnasa, S., Namprakai, P. and Muangnapoh, T., 2006. Performance improvement of the combined cycle power plant by intake-air cooling using an absorption chiller. *Energy*, 31 (12), pp. 20362046.

41. Boonnasa, S. and Namprakai, P., 2008. Sensitivity analysis for the capacity improvement of a combined cycle power plant (100-600 MW). *Applied Thermal Engineering*, 28 (1415), pp. 18651874.

42. Alhazmy, M. and Najjar, Y., 2004. Augmentation of gas turbine performance using air coolers. *Applied Thermal Engineering*, 24 (23), pp. 415429.

43. Wang, F. Chiou, J. and Wu, P., 2007. Economic feasibility of waste heat to power conversion. *Applied Energy*, 84 (4), pp. 442454.

44. Talbi, M. and Agnew, B., 2002. Energy recovery from diesel engine exhaust gases for performance enhancement and air conditioning. *Applied Thermal Engineering*, 22 (6), pp. 693702.

45. Salvi, D. and Pierpaoli, P., 2002. Optimization of inlet-air cooling systems for steam injected gas turbines. *International Journal of Thermal Sciences*, 41 (9), pp. 815822.

46. Yousef, S. and Najjar, H., 2001. Efficient use of energy by utilizing gas turbine combined systems. *Applied Thermal Engineering*, 21(4), pp.407438.

47. Najjar, Y., 1996. Enhancement of performance of gas turbine engines by inlet-air cooling and cogeneration system. *Applied Thermal Engineering*, 16 (2), pp. 163173.

48. Kakaras, E. Doukelis, A. Prelipceanu, A. and Karellas, S., 2006. Inlet-air cooling methods for gas turbine based power plants. *Journal of Engineering for Gas Turbines and Power*, 128 (2), pp. 312317.

49. Schwarzacher, W., 1993. *Cyclostratigraphy and the Milankovitch theory*. Amsterdam: Elsevier Science.

50. Keepin, B. and Kats, G., 1988. Greenhouse warming: comparative analysis of nuclear and efficiency abatement strategies. *Energy Policy*, 16 (6), pp. 538561.

51. Dutta, P. and Radner, K., 2009. A strategic analysis of global warming: theory and some numbers. *Journal of Economic Behaviour and Organization*, 71 (2), pp. 187209.

52. Harvey, D., 1993. A guide to global warming potentials (GWPs). *Energy Policy*, 21 (1), pp. 2434.

53. Chae, S. Kim, S. Yoon, S. and Park, S., 2010. Optimization of a waste heat utilization network in an eco-industrial park. *Applied Energy*, In Press.

54. Chaffiotte, P., 1967. The gas turbine and freshwater techno-economic aspects. *Desalination*, 3 (1), pp. 4659.

55. Rautenbach, R. Monheim, P. and Zebrowski, D., 1979. MSF-Seawater desalination plants using waste heat from electric-arc furnaces in the steel industry. *Desalination*, 31 (13), pp. 197206.

56. Tidball, R. and Kadaj, R., 1981. Waste heat powered reverse osmosis plants. *Desalination*, 39, pp. 137145.

57. Kronenberg, G., 1997. Cogeneration with the LT-MED desalination process. *Desalination*, 108 (13), pp. 287294.

58. Tay, J. Low, S. and Jeyaseelan, S., 1996. Vacuum desalination for water purification using waste heat. *Desalination*, 106 (13), pp. 131135.

59. Dajnak, D. and Lockwood, F., 2000. Use of thermal energy from waste for seawater desalination. *Desalination*, 130 (2), pp. 137146.

60. Lovato, A. Legorreta, C. and Andersson, E., 2001. Heat recovery from sulphuric acid plants for seawater desalination. *Desalination*, 136 (13), pp. 159168.

61. Maidment, Eames, I. G. Psaltas, I. Lalzad, A. and Yiakoumetti, K., 2007. Flash-type barometric desalination plant powered by waste heat from electricity power stations in Cyprus. *Applied Energy*, 84 (1), pp. 6677.

62. Cohen, M. Ianovici, I. and Breschi, D., 2003. Power plant residual heat for seawater desalination. *Desalination*, 152 (13), pp. 155165.

63. Aybar, H., 2004. Desalination system using waste heat of power plant. *Desalination*, 166, pp. 167170.

64. Henry, S. and Teresa, S., 2007. Utilization of waste heat in the desalination process. *Desalination*, 204 (13), pp. 464470.

65. Shih, H., 2005. Evaluating the technologies of thermal desalination using low-grade heat. *Desalination*, 182 (13), pp. 461469.

66. Methnani, M., 2007. Influence of fuel costs on seawater desalination options. *Desalination*, 205 (13), pp. 332339.

67. Nisan, S. and Benzarti, N., 2008. A comprehensive economic evaluation of integrated desalination systems using fossil fuelled and nuclear energies and including their environmental costs. *Desalination*, 229 (13), pp. 125146.

68. Kamali, R. and Mohebinia, S., 2008. Experience of design and optimization of multi-effects desalination systems in Iran. *Desalination*, 222 (13), pp. 639645.

69. Vlachos, G. and Kaldellis, J., 2004. Application of gas-turbine exhausts gases for brackish water desalination: a techno-economic evaluation. *Applied Thermal Engineering*, 24 (17-18), pp.24872500.

70. El-Mudir, W. El-Bousiffi, M. and Al-Hengari S., 2004. Performance evaluation of a small size TVC desalination plant. *Desalination*, 165, pp.269279.

71. Wang, Y. and Lior N., 2006. Performance analysis of combined humidified gas turbine power generation and multi-effect thermal vapour compression desalination systems. Part 1: The desalination unit and its combination with a steam-injected gas turbine power system. *Desalination*, 196 (13), pp.84104.

72. Sommariva, C., 2008. Utilization of power plant waste heat steam to enhance efficiency in thermal desalintion. *Desalination*, 222, pp.592595.

73. Dvornikov, V., 2000. Seawater multi-effect distillation energized by a combustion turbine. *Desalination*, 127 (3), pp. 261269.

74. Chacartegui, R. Sánchez, D. Gregorio, N. Jiménez-Espadafor, F. Muñoz, A. and Sánchez T., 2009. Feasibility analysis of a MED desalination plant in a combined cycle based cogeneration facility. *Applied Thermal Engineering*, 29 (23), pp. 412417.

75. Kronenberg, G. and Lokiec, F., 2001. Low-temperature distillation processes in single- and dual-purpose plants. *Desalination*, 136 (13), pp. 189197.

76. Nordell, B., 2003. Thermal pollution causes global warming. *Global and Planetary Change*, 38(34), pp. 305312.

77. Tomkiewicz, M., 2006. Global warming: science, money and self-preservation, *Competes Rendus Chimie*, 9 (2), pp. 172–179.

78. Kessel, D., 2000. Global warming: facts, assessment, countermeasures. *Journal of Petroleum Science and Engineering*, 26 (14), pp.157–168.

79. Bejan, A. Tsatsaronis, G. and Moran, M., 1995. *Thermal design and optimization*. New York: John Wiley and Sons.

80. Ameri, M. Ahmadi, P. and Hamidi, A., 2009. Energy, exergy and exergoeconomic analysis of a steam power plant: a case study. *International Journal of Energy Research*. 33 (5), pp. 499512.

81. Kopac, M. and Hilalci, A. 2007. Effect of ambient temperature on the efficiency of the regenerative and reheat Çatalağzı power plant in Turkey. *Applied Thermal Engineering*, 27 (89), pp. 13771385.

82. Rivero, R. and Garfias, M., 2006. Standard chemical exergy of elements updated. In: 17th International Conference on Efficiency, Costs, Optimization, Simulation, and Environmental Impact of Energy on Process Systems. *Energy*, 31 (15) pp. 33103326.

83. Shi, X. and Che, D., 2007. Thermodynamic analysis of an LNG fuelled combined cycle power plant with waste heat recovery and utilization system, *International Journal of Energy Research*, 31, pp. 975998.

84. Kotas, T., 1985. The exergy method of thermal plant analysis. London: Butterworths.

85. Sayyaadi, H. and Saffari, A., 2010. Thermoeconomic optimization of multi effect distillation desalination systems. *Applied Energy*, 87 (4), pp.11221133.

86. Dincer, I., Al-Muslim, H., 2002. Thermodynamic analysis of reheat cycle steam power plants. *Fuel and Energy Abstracts*, 43 (4), pp.01406701.

87. Kanoglu, M. Dincer, I. and Rosen, M., 2007. Understanding energy and exergy efficiencies for improved energy management in power plants. *Energy Policy*, 35 (7), pp.39673978.

88. Aljundi, I., 2009. Energy and exergy analysis of a steam power plant in Jordan. *Applied Thermal Engineering*, 29 (23), pp. 324328.

89. Ameri, M., Ahmadi, P. and Khanmohammadi, S., 2008. Exergy analysis of a 420 MW combined cycle power plant. *International Journal of Energy Research*, 32 (2), pp. 175-183.

90. Choi, H. Lee, T. Kim, Y. and Song, S., 2005. Performance improvement of multiple-effect distiller with thermal vapour compression system by exergy analysis. *Desalination and the Environment*, 182 (13), pp. 239249.

91. Hamed, O. Zamamiri, M. Aly S. and Lior N., 1996. Thermal performance and exergy analysis of a thermal vapour compression desalination system. *Energy Conversion and Management*, 37 (4), pp. 379387.

92. Mabrouk, A. Nafey, A. and Fathc, H., 2007. Thermo economic analysis of some existing desalination processes. *Desalination*. 205 (13), pp. 354373.

93. Kaushik, S. and Arora, A., 2009. Energy and exergy analysis of single effect and series flow double effect water–lithium bromide absorption refrigeration systems. *International Journal of Refrigeration*, 32 (6), pp. 12471258.

94. Misra, R. Sahoo, K. Sahoo, S. and Gupta, A., 2003. Thermo economic optimizations of a single-effect water/LiBr vapour absorption refrigeration system. *International Journal of Refrigeration*, 26 (2), pp. 158169.

95. Şencan, A. Yakut, K. and Kalogirou, S., 2005. Exergy analysis of lithium bromide/water absorption systems. *Renewable Energy*, 30 (5), pp.645657.

96. Talbi, M. and Agnew, B., 2000. Exergy analysis: an absorption refrigerator using lithium bromide and water as the working fluids. *Applied Thermal Engineering*, 20 (7), pp. 619-630.

97. SimTech Simulation Technology, 2003. *IPSEpro process simulator manuals: process simulation environment*. SimTech Simulation Technology.

98. SimTech Simulation Technology, 2003. *IPSEpro process simulator manuals: Model Development Kit*. SimTech Simulation Technology.

99. SimTech Simulation Technology, 2003. *IPSEpro process simulator manuals: Process Simulator*. SimTech Simulation Technology.

100. SimTech Simulation Technology, 2003. *IPSEpro process simulator manuals: Advanced Power Plant Library*. SimTech Simulation Technology.

101. SimTech Simulation Technology, 2003. *IPSEpro process simulator manuals: Desalination Process Library*. SimTech Simulation Technology.

102. SimTech Simulation Technology, 2003. *IPSEpro process simulator manuals: Refrigeration Process Library*. SimTech Simulation Technology.

103. Horlock, J. 2003. *Advanced gas turbine cycles*. Oxford: Elsevier Science Ltd..

104. Construction information Service, 2007. *Construction products industry key performance indicators handbook*. UK: Construction Products Association.

105. Kaita, Y., 2001. Thermodynamic properties of lithium bromide-water solutions at high temperatures. *International Journal of Refrigeration*, 24 (5), pp. 374390.

106. Banat, F. and Jwaied, A., 2008. Exergy analysis of desalination by solar-powered membrane distillation units. *Desalination*, 230 (13), pp. 2740.

107. Kahraman, N. and Cengel, Y., 2005. Exergy analysis of a MSF distillation plant. *Energy Conversion and Management*, 46 (1516), pp. 26252636.

108. Cerci, Y., 2002. Exergy analysis of a reverse osmosis desalination plant in California. *Desalination*, 142 (3), pp. 257266.

109. Kahramana, N. Cengelb, Y. Woodb, B. and Cercic, Y., 2005. Exergy analysis of a combined RO, NF, and EDR desalination plant. *Desalination*, 171 (3), pp. 217232.

110. Al-Sofi, A., 2001. Seawater desalination SWCC experience and vision. *Desalination*, 135 (13), pp. 121139.

111. Presidency of Meteorology and Environment, 2009. *Surface annual climatologically report*.Saudi Arabia: Ministry of Defence and Aviation.

112. China National Electric Wire and Cable Import and Export Corporation, 2009. *Technical specification of condensing steam turbines (60MW-80MW) catalogue*. China National Electric Corporation.

113. Kreith, F., 1989. *The CRC handbook of mechanical engineering*. 2ed ed. USA: CRC Press.

114. Butcher, C. and Reddy, B., 2007. Second law analysis of a waste heat recovery based power generation system. *International Journal of Heat and Mass Transfer*, 50, (1112), pp. 23552363.

115. BROAD Air Conditioning Co., Ltd, 2008. *BROAD X non-electrical chiller model selection and design manual*. China BROAD Air Conditioning Co., Ltd.

116. Inzelberg, H., henrii@ide-tech.com. 2008. *IDE Technologies Ltd*. Sent Thursday 17 April 2008, 8:48.

117. Ganapathy, V., 2003. Industrial boilers and heat recovery system generators design, applications and calculations. USA: CRC Press.

118. Cengel, Y. and Turner, R., 2001. *Fundamentals of thermal-fluid sciences*. 2ed ed. New York: McGraw-Hill Higher Education.

119. Logan, E., 1999. Thermodynamics: processes and applications. USA: CRC Press.

120. Buecker, B., 2002. *Basics of boiler and HRSG design*. Oklahoma: Penn Well Corporation.

121. Boyce, M., 2002. Handbook for cogeneration and combined cycle power plants. USA: McGraw-Hill Professional.

122. Alves, L. and, Nebra, S., 2003. Thermo-economic evaluation of a basic optimized chemically recuperated gas turbine cycle. *Thermodynamics International Journal,* 6 (1), pp.1322.

123. Dincer, I. Rosen, M. and Zamfirescu, C., 2009. Exergetic performance analysis of a gas turbine cycle integrated with solid oxide fuel cells. *Energy Resources Technology,* 31 (3), pp. 3200132012.

124. Khaliq, A., 2009. Exergy analysis of gas turbine regeneration system for combined cycle production of power heat and refrigeration. *International Journal of Refrigeration*, 32, pp. 435545.

125. X Shi, X. Agnew, B. and Che, D., 2009. Analysis of a combined cycle power plant integrated with liquid natural gas gasification and power generation system. *Journal of Power and Energy*, 223 part A.

126. Alasfour, F. Darwish, M. and Amer, A., 2005. Thermal analysis of ME TVC+MEE desalination systems. *Desalination*, 174 (1), pp. 3961.

127. Kamali, R. Abbassi, A. and Vanini, S., 2009. A simulation model and parametric study of MED–TVC process. *Desalination*, 235 (13), pp 340351.

128. El-Dessouky, H. Ettouney, H. Alatiqi, I. and Al-Nuwaibit, G., 2002. Evaluation of steam jet ejectors. *Chemical Engineering and Processing*. 41 (6), pp.551561.

129. Hegazy, A., 2007. Possible waste heat recovery in the condenser of a regenerative steam cycle. *Journal of Thermal Science and Technology*, 2 (1), pp.112.

130. Schutte and Koerting steam ejector manufacturer, 2008. *Bulletin 5E-H Catalog*. USA: Schutte and Koerting.

131. Ameri, M. Mohammadia, S. Hosseinia, M. and Seifia, M., 2009. Effect of design parameters on multi-effect desalination system specifications. *Desalination*, 245 (13), pp.266283.

132. Torío, H. Angelotti, A. and Schmidt, D., 2009. Exergy analysis of renewable energy-based climatisation systems for buildings: a critical view. *Energy and Buildings*, 41(3) pp.248-271.

133. Lattemann, S. and Höpner, T., (2008). Environmental impact and impact assessment of seawater desalination. *Desalination*, 220(13), pp. 115.

134. Sadhwani, J. Veza, J. and Santana, C., (2005). Case studies on environmental impact of seawater desalination. *Desalination*, 185, (13), pp. 18.

135. Horlock, J., 1987. Approximate analyses of feed and district heating cycles for steam combined heat and power plant. *Professional Engineering Publishing*, 201 (A3), pp.193-200.

136. Oha, S. Jungb, J. and Kwak, H., 2007. Optimal planning and economic evaluation of cogeneration system. *Energy*, 32 (5) pp. 760771.

137. Gregory, E. Lamb, B. Marsland, Johnston, R. and Summers, C., 1994. *Selection and costing of heat exchangers ESDU 92013*. London: Engineering Sciences Data Unit.

138. Libyan General Electricity Company, 2008. *Power and desalinated projects*. Libya: Libyan General Electricity Company.

Appendixes

9.1 Appendix A

Yanbu city's ambient temperature data as collected from the Presidency of Meteorology and Environment, Saudi Arabia [111].

	Mean Temperature			Extreme Temperature Readings					
Month	Max	Min	Mean	Max	Year	Day	Min	Year	Day
Jan	27.5	14.1	20.5	34.4	1985	11	4.7	2000	30
Feb	28.3	14.2	21.2	37.3	2004	29	6.5	1992	6
Mar	31.1	16.9	23.9	39.4	2001	27	8.7	1992	3
Apr	34.7	20.7	27.5	43.6	1991	26	11.5	1997	7
May	38.2	23.8	30.7	49	2003	25	15.6	2008	1
Jun	40	25	32.2	49.5	2006	6	18	1993	11
July	40.1	26.3	32.9	49.4	1989	9	21.3	2005	24
Aug	40.3	27.1	33.3	48.6	2006	18	20.4	1997	20
Sep	39.9	26.1	32.4	49	2006	10	19	2006	24
Oct	36.9	23.6	29.8	47.4	2004	1	14.3	2000	27
Nov	33.3	19.9	26.1	44.7	1991	12	12.5	1994	29
Dec	29.4	16.1	22.5	42	2004	30	7.8	2004	29
Max	40.3			49.5					
Min		14.1					4.7		
Mean			27.8						

Table 1 Yanbu city's ambient temperature data [111]

Yanbu city's relative humidity data as collected from the Presidency of Meteorology and Environment [111].

	Relative Humidity %	
Month	Mean Morning	Mean Evening
Jan	70	40
Feb	71	40
Mar	68	41
Apr	64	41
May	66	40
Jun	70	41
July	74	41
Aug	75	43
Sep	71	44
Oct	74	45
Nov	74	43
Dec	72	43
Max.	75	45
Min	64	40
Mean	70.75	41.8

Table 2 Yanbu city's relative humidity data [111]

9.2 Appendix B

The gas turbine's performance curve as collected from the Benghazi combined cycle power plant.

GT 13E1

Exhaust Temperature °C

Ambient temperature °C	Load			
	0.25	0.5	0.75	1
5	298.1	377.9	439.6	519
15	308.6	399.3	446.4	524.4
37	332.5	432	465.7	540.3
50	353.3	446.3	481.5	555

Thermal Efficiency %

Ambient temperature °C	Load			
	0.25	0.5	0.75	1
5	23.63	32.19	37.63	40.54
15	22.37	30.46	35.60	38.37
37	19.45	26.49	30.96	33.36
50	17.11	23.28	27.26	29.33

Output Power MW

Ambient temperature °C	Load			
	0.25	0.5	0.75	1
5	14.01	56.05	112.1	149.4
15	13.26	53.04	106.0	141.4
37	11.53	46.12	92.23	122.9
50	10.14	40.54	81.23	108.1

Mass Flow kg/s

Ambient temperature °C	Load			
	0.25	0.5	0.75	1
5	401.6	432.1	508.7	510.8
15	391.5	407.5	494.5	496.4
37	367.6	369.2	458	459.6
50	350.6	352	427.5	427.9

Table 1 The gas turbine's performance curve for the base power plant mode

9.3 Appendix C

Parameters	Unit	Pinch Point ΔT °C					
		15	20	25	30	35	40
UA	kW/K	1341.24	1188.09	1070.32	974.902	894.891	826.141
CO_2 emission rate	kg/kW	495.066	498.623	502.236	505.907	509.635	513.424
Net power	MW	200.216	198.787	197.357	195.926	194.492	193.057
GT power	MW	135.736	135.736	135.736	135.736	135.736	135.736
Steam turbine power	MW	64.48	63.052	61.622	60.19	58.756	57.321
Gas turbine exergy destruction	MW	123.419	123.419	123.419	123.419	123.419	123.419
HRSG exergy destruction	MW	20.25	20.532	20.772	20.969	21.127	21.245
Steam turbine exergy destruction	MW	13.911	13.603	13.295	12.986	12.676	12.367
ST condenser exergy destruction	MW	7.905	7.73	7.555	7.379	7.203	7.027
Stack exergy destruction	MW	19.588	21.206	22.869	24.576	26.325	28.117
HRSG thermal efficiency	%	65.668	64.213	62.757	61.299	59.839	58.377
Gas turbine efficiency	%	36.819	36.819	36.819	36.819	36.819	36.819
Overall plant efficiency	%	54.17	53.786	53.402	53.018	52.633	52.248
Gas turbine exergetic efficiency	%	52.262	52.262	52.262	52.262	52.262	52.262
HRSG exergetic efficiency	%	81.149	80.58	80.026	79.486	78.96	78.446
Steam turbine exergetic efficiency	%	82.254	82.254	82.254	82.254	82.254	82.254
Plant's overall exergetic efficiency	%	54.823	54.674	54.53	54.391	54.257	54.127

Table 1 Pinch point ΔT parametric study of the base power plant model

Point	Stream	e (kJ/kg)	E (MW)
1	Air	0	0
2	Fuel	43973.38	385.34
3	Gas	254.07	125.62
4	Seawater	0.48	1.33
5	Seawater	0.65	1.80
6	Water	2.44	0.13
7	Steam	126.66	6.89
8	Steam	1453.09	79.06
9	Gas	51.82	25.62

Table 2 Exergy and specific exergy of the base power plant streams

		Load		
Parameter	Unit	0.5	0.75	1
CO_2 emission rate	kg/kW	681.587	591.192	508.14
Net power	MW	69.95	135.216	195.07
GT power	MW	51.58	101.806	135.74
ST power	MW	18.373	33.41	59.33
Gas turbine exergy destruction	MW	66.753	114.501	123.42
HRSG exergy destruction	MW	8.786	13.92	21.068
Steam turbine exergy destruction	MW	4.041	7.333	12.8
ST condenser exergy destruction	MW	2.426	4.318	7.274
Stack exergy destruction	MW	33.092	35.199	25.621
Gas turbine efficiency	%	29.087	34.241	36.819
Plant's overall efficiency	%	39.377	45.395	52.787
Gas turbine exergetic efficiency	%	43.418	46.943	52.262
HRSG exergetic efficiency	%	73.998	76.537	79.169
Steam turbine exergetic efficiency	%	81.97	82.002	82.254
Plant's overall plant exergetic efficiency	%	46.107	49.165	54.31
Fuel consumption	kg/s	4.215	7.06	8.763

Table 3 Parametric study of the base power plant model's partial load

Parameter	Unit	Ambient Temperature °C									
		5	10	15	20	25	30	35	40	45	50
Air intake mass flow rate	**kg/s**	500.49	493.07	485.66	477.79	469.93	462.06	454.20	443.06	429.75	416.44
Gas turbine temperature ratio	**°C**	7.61	7.23	6.88	6.58	6.30	6.05	5.82	5.61	5.41	5.23
Exhaust gas temperature	**°C**	531.76	534.46	537.16	540.77	544.38	548.00	551.61	556.45	562.10	567.76
CO_2 emission rate	**kg/kW**	488.04	497.89	508.14	518.04	528.32	538.95	549.93	564.79	582.95	602.22
Net power	**MW**	203.10	199.08	195.07	191.34	187.62	183.91	180.24	175.50	170.03	164.59
GT power	**MW**	143.88	139.81	135.74	131.73	127.72	123.71	119.69	114.64	108.90	103.16
ST power	**MW**	59.22	59.27	59.33	59.61	59.90	60.21	60.55	60.85	61.13	61.43
Gas turbine exergy destruction	**MW**	114.10	118.75	123.42	127.82	132.21	136.58	140.91	146.62	153.26	159.83
HRSG exergy destruction	**MW**	21.19	21.13	21.07	21.06	21.06	21.06	21.08	21.05	20.99	20.94
Steam turbine exergy destruction	**MW**	12.80	12.80	12.80	12.85	12.90	12.95	13.01	13.06	13.10	13.15
ST condenser exergy destruction	**MW**	7.29	7.28	7.27	7.29	7.31	7.33	7.36	7.37	7.38	7.39
Stack exergy destruction	**MW**	26.85	26.23	25.62	24.92	24.25	23.61	23.00	22.16	21.20	20.29
HRSG utilization	**%**	59.53	59.98	60.42	61.01	61.58	62.14	62.70	63.44	64.27	65.10
Gas turbine efficiency	**%**	39.03	37.92	36.82	35.73	34.64	33.56	32.47	31.10	29.54	27.98
Plant's overall efficiency	**%**	54.96	53.87	52.79	51.78	50.77	49.77	48.78	47.49	46.01	44.54
Gas turbine exergetic efficiency	**%**	55.67	53.96	52.26	50.65	49.05	47.46	45.89	43.87	41.56	39.28
HRSG exergetic efficiency	**%**	79.05	79.11	79.17	79.25	79.32	79.40	79.47	79.57	79.68	79.79
Steam turbine exergetic efficiency	**%**	82.23	82.24	82.25	82.27	82.28	82.30	82.31	82.33	82.35	82.37
Plant's overall exergetic efficiency	**%**	56.74	55.52	54.31	53.17	52.04	50.92	49.82	48.40	46.76	45.16

Table 4 Ambient temperature parametric study of the base power plant model

		Relative Humidity %										
Parameter	**Unit**	**1**	**10**	**20**	**30**	**40**	**50**	**60**	**70**	**80**	**90**	**100**
Exhaust gas enthalpy	kJ/kg	581.770	582.250	582.780	583.310	583.840	584.38	584.91	585.45	585.98	586.52	587.05
Exhaust gas entropy	kJ/kg k	8.0625	8.0679	8.0740	8.0800	8.0860	8.0920	8.0981	8.1041	8.1101	8.1161	8.1221
CO_2 emission rate	kg/kW	508.993	508.863	508.718	508.573	508.427	508.28	508.14	507.99	507.85	507.70	507.55
Net power	MW	194.738	194.787	194.843	194.899	194.954	195.01	195.07	195.12	195.18	195.23	195.29
GT power	MW	135.736	135.736	135.736	135.736	135.736	135.74	135.74	135.74	135.74	135.74	135.74
ST power	MW	59.002	59.052	59.107	59.163	59.219	59.27	59.33	59.39	59.44	59.50	59.55
Gas turbine exergy destruction	MW	124.098	123.995	123.880	123.765	123.650	123.54	123.42	123.30	123.19	123.07	122.96
HRSG exergy destruction	MW	20.959	20.976	20.994	21.013	21.031	21.05	21.07	21.09	21.11	21.12	21.14
Steam turbine exergy destruction	MW	12.729	12.740	12.752	12.764	12.776	12.79	12.80	12.81	12.82	12.84	12.85
ST condenser exergy destruction	MW	7.233	7.240	7.246	7.253	7.260	7.27	7.27	7.28	7.29	7.29	7.30
Stack exergy destruction	MW	25.490	25.509	25.532	25.554	25.576	25.60	25.62	25.64	25.67	25.69	25.71
HRSG utilization	%	60.413	60.414	60.416	60.418	60.419	60.42	60.42	60.43	60.43	60.43	60.43
Gas turbine efficiency	%	36.819	36.819	36.819	36.819	36.819	36.82	36.82	36.82	36.82	36.82	36.82
Plant's overall efficiency	%	52.699	52.712	52.727	52.742	52.757	52.77	52.79	52.80	52.82	52.83	52.85
Gas turbine exergetic efficiency	%	52.126	52.147	52.170	52.193	52.216	52.24	52.26	52.29	52.31	52.33	52.36
HRSG exergetic efficiency	%	79.163	79.164	79.165	79.166	79.167	79.17	79.17	79.17	79.17	79.17	79.17
Steam turbine exergetic efficiency	%	82.254	82.254	82.254	82.254	82.254	82.25	82.25	82.25	82.25	82.25	82.25
Plant's overall exergetic efficiency	%	54.199	54.216	54.234	54.253	54.272	54.29	54.31	54.33	54.35	54.37	54.39

Table 5 Relative humidity parametric study of the base power plant model

Thermodynamic Properties	Unit	2	3	4	5	6	7	8	9	10
Potable water production	m^3/day	40000	40000	40000	40000	40000	40000	40000	40000	40000
GOR		1.89	2.77	3.61	4.38	5.1	5.75	6.33	6.86	7.32
Specific heat consumption	kJ/kg	1235.49	840.95	646.55	532.09	457.54	405.76	368.19	340.08	318.59
Input energy	MW	563.76	383.73	295.02	242.79	208.78	185.15	168.01	155.18	145.37
Seawater intake mass	kg/s	5978.05	3954.51	2943.8	2338.43	1935.91	1649.48	1435.75	1270.62	1139.62
Rejected brine water	kg/s	544.49	541.64	538.98	536.47	534.08	531.8	529.61	527.5	525.47
Rejected seawater	kg/s	4977.260	2956.560	1948.520	1345.660	945.530	661.380	449.840	286.810	157.850
Concentration factor		1.838	1.842	1.847	1.851	1.854	1.858	1.862	1.865	1.868

Table 6 Parametric study for the number of effects of the base MED model

Point	w_s	w_w	M	x_S	x_w	Temp.	S_{salt}	S_{water}	$S_{seawater}$	h_{salt}	h_{water}	$h_{seawater}$
R_c	0.04	0.960	18.513	0.013	0.987	288.15	0.0447	0.224761	**0.23269**	12.552	63.079008	**61.058**
3.11	0.04	0.960	18.513	0.013	0.987	317.841	0.1268	0.634668	**0.62948**	37.397	187.266635	**181.272**
5	0.074735	0.925	18.982	0.024	0.976	323.524	0.1416	0.708661	**0.69440**	42.153	211.060294	**198.437**
9	0.066538	0.933	18.869	0.021	0.979	322.173	0.1381	0.691205	**0.67944**	41.022	205.370454	**194.435**
10	0.04	0.960	18.513	0.013	0.987	295.15	0.0648	0.325262	**0.32997**	18.410	92.381942	**89.423**

Table 7 Enthalpy and entropy calculations for the base MED desalination plant model

Component	Unit	Intake Seawater Temperature °C				
		20	22	24	26	28
MED evaporators exergy destruction	MW	12.79	11.67	10.65	9.72	8.79
MED condenser exergy destruction	MW	10.22	9.17	8.23	7.38	5.86
Plant's overall exergetic efficiency	%	11.26	13.14	15.33	17.89	19.83
GOR		7.28	7.32	7.36	7.40	7.44
Specific heat consumption	kJ/kg	320.51	318.75	317.00	315.25	313.51
Pumps power	MW	0.31	0.29	0.28	0.26	0.24
Heat transfer in first effect	MW	157357.97	145040.83	132950.81	121084.91	109440.14
Heat energy source mass flow rate	kg/s	67.47	62.19	57.01	51.92	46.93

Table 8 Parametric study for the intake seawater temperature for the MED desalination plant

Component	Unit	Input Heat Energy Temperature °C										
		50	60	70	80	90	100	110	120	130	140	150
MED evaporators	MW	2.77	6.21	9.65	13.09	16.34	19.41	22.33	25.1	27.73	30.24	32.62
MED condenser	MW	4.57	4.57	4.57	4.57	4.57	4.57	4.57	4.57	4.57	4.57	4.57
Plant's overall exergetic Efficiency	%	49.26	44.34	39.42	34.5	30.86	28.05	25.83	24.02	22.52	21.26	20.18
GOR		7.475	7.396	7.317	7.238	7.157	7.075	6.991	6.905	6.815	6.722	6.626
Specific heat Consumption	kJ/kg	318.7	318.7	318.7	318.7	318.7	318.7	318.7	318.7	318.7	318.7	318.7
Concentration factor		1.663	1.663	1.663	1.663	1.663	1.663	1.663	1.663	1.663	1.663	1.663
Pump power	MW	0.2918	0.2918	0.2918	0.2918	0.2918	0.2918	0.2918	0.2918	0.2918	0.2918	0.2918
Heat transfer in first effect	MW	145	145	145	145	145	145	145	145	145	145	145
Feed seawater mass flow rate	kg/s	1140.89	1140.89	1140.89	1140.89	1140.89	1140.89	1140.89	1140.89	1140.89	1140.89	1140.89
Heat energy mass flow rate	kg/s	60.83	61.51	62.19	62.87	63.57	64.31	65.09	65.9	66.77	67.69	68.67

Table 9 Parametric study for the MED's input heat energy temperature

Component	Unit	Intake Seawater Salinity kg/kg					
		0.036	0.038	0.04	0.042	0.044	0.045
MED evaporators	MW	9.2	9.42	9.65	9.88	10.11	10.21
MED condenser	MW	4.61	4.59	4.57	4.55	4.53	4.52
Overall plant exergetic Efficiency	%	41.51	40.52	39.42	38.32	37.22	37.08
Capacity	m^3/day	40000	40000	40000	40000	40000	40000
GOR		7.319	7.318	7.317	7.316	7.315	7.3145
Specific heat consumption	kJ/kg	318.662	318.706	318.755	318.81	318.871	318.903
Concentration factor		1.667	1.665	1.663	1.662	1.66	1.66
Pump power	MW	0.2927	0.2921	0.2918	0.2916	0.2913	0.2912
Heat transfer in first effect	MW	145000.85	145020.61	145043.05	145068.11	145095.79	145110.61
Feed seawater mass flow rate	kg/s	1137.52	1139.22	1140.89	1142.54	1144.17	1144.98
Heat energy source mass flow rate	kg/s	62.17	62.18	62.19	62.20	62.21	62.22

Table 10 Parametric study of the intake seawater temperature of the base MED model

Thermodynamic Properties	Unit	2	3	4	5	6	7	8	9	10	11	12	13	14	15
GOR		2.25	3.28	4.23	5.09	5.87	6.57	7.16	7.70	8.14	7.97	7.83	7.68	7.55	7.42
Specific heat consumption	kJ/kg	1236	841.3	646.7	532.3	456.8	405.0	368.3	339.4	318.6	319.4	320.4	322.3	324.4	326.8
Energy input	MW	532.8	366.0	284.0	236.0	204.4	182.8	167.7	155.	147.4	149.8	152.4	155.5	158.1	160.9
Seawater intake mass	kg/s	5121	3390	2525	2006	1659	1419	1237	1090	979.7	974.9	972.6	970.3	968.2	966.1
Motive steam mass flow	kg/s	202.4	139.0	107.9	89.68	77.68	69.48	63.74	59.24	56.05	56.96	57.98	59.16	60.16	61.22
Suction mass flow rate	kg/s	33.05	21.87	16.28	12.92	10.68	9.09	7.93	7.01	6.29	5.41	4.75	4.21	3.79	3.44
Concentration factor		1.84	1.84	1.85	1.85	1.85	1.86	1.86	1.87	1.87	1.87	1.88	1.88	1.88	1.89

Table 11 Number of effects for the TVC-MED parametric study

Point	w_s	w_w	M	x_S	x_w	Temp.	S salt	S water	**S seawater**	h salt	h water	**h seawater**
Rc	0.04	0.960	18.513	0.013	0.987	288.15	0.0447	0.224761	**0.23269**	12.552	63.079008	**61.058**
12, 13	0.04	0.960	18.513	0.013	0.987	317.87	0.1269	0.635053	**0.62986**	37.422	187.389068	**181.390**
7	0.074735	0.925	18.982	0.024	0.976	323.524	0.1416	0.708672	**0.69441**	42.153	211.064055	**198.440**
10	0.07445	0.926	18.978	0.024	0.976	323.49	0.1415	0.708224	**0.69404**	42.125	210.91903	**198.352**
11	0.04	0.960	18.513	0.013	0.987	295.15	0.0648	0.325262	**0.32997**	18.410	92.381942	**89.423**

Table 12 Entropy and enthalpy calculations for the TVC-MED plant model

Component	Unit	Intake Seawater Temperature °C				
		20	22	24	26	28
TVC-MED steam ejector's exergy destruction	MW	5.06	5.09	5.13	5.18	5.24
TVC-MED evaporators' exergy destruction	MW	9.75	9.82	10.00	10.07	10.13
TVC-MED condenser's exergy destruction	MW	4.28	4.02	3.66	3.51	3.27
Plant's overall exergetic efficiency	%	30.22	31.75	33.45	35.36	37.58
GOR		7.67	8.14	8.61	9.08	9.55
Specific heat consumption	kJ/kg	332.21	318.59	304.81	291.03	277.25
Concentration factor		1.87	1.87	1.87	1.57	1.45
Pump power	MW	0.28	0.28	0.28	0.3	0.32
Heat transfer in first effect	MW	151.17	144.97	138.7	132.38	126
Feed seawater mass flow rate	kg/s	973.48	980.18	986.92	993.82	1000.84
Motive steam mass flow rate	kg/s	58.84	55.89	52.89	49.84	46.75

Table 13 Parametric study of the seawater temperature for the TVC-MED plant model

		Evaporator Inlet Temperature °C						
Parameter	Unit	10	12	14	16	18	20	22
Generator exergy destruction	kW	234.36	316.52	367.28	385.93	371.72	323.86	241.53
Absorber exergy destruction	kW	143.21	229.85	316.44	402.98	489.48	575.95	662.39
Evaporator exergy destruction	kW	67.88	134.39	220.86	326.79	451.70	595.21	756.94
Condenser exergy destruction	kW	70.80	113.63	156.44	199.22	241.99	284.73	327.47
Heat exchanger exergy destruction	kW	92.41	148.31	204.18	260.03	315.84	371.64	427.41
Exp. valve exergy destruction	kW	19.64	31.53	43.41	55.28	67.14	79.00	90.86
Exergy input	kW	1233.36	1919.94	2574.73	3197.09	3786.32	4341.66	4862.33
Absorption chiller exergetic efficiency	%	8.95	7.91	6.73	5.47	4.17	2.81	1.40
COP	%	0.79	0.79	0.79	0.79	0.79	0.79	0.79
Evaporator heat transfer	MW	4.39	7.05	9.70	12.36	15.01	17.66	20.31
Generator heat transfer	MW	5.57	8.93	12.30	15.66	19.03	22.39	25.75
Absorber heat transfer	MW	4.26	6.83	9.41	11.98	14.56	17.30	19.70
Condenser heat transfer	MW	4.76	7.65	10.53	13.41	16.28	19.16	22.04
Heat exchanger heat transfer	MW	1.87	3.00	4.13	5.26	6.39	7.52	8.65
Cooling seawater mass flow rate	kg/s	113.63	182.38	251.09	319.76	388.40	457.01	525.60
Chilled water temperature	°C	6.70	6.70	6.70	6.70	6.70	6.70	6.70
Refrigerant mass flow rate	kg/s	1.93	3.10	4.27	5.44	6.61	7.77	8.94
$LiBr/H_2O$ solution mass flow rate	kg/s	22.03	35.37	48.69	62.00	75.31	88.62	101.92
Relative generator ΔT (T_2/T_3)	°C	114.779	109.456	104.133	98.8075	93.481	88.1532	82.8242

Table 14 Parametric study for the inlet temperature of the absorption chiller evaporator

AC Generator	Unit	Cooling Water Temperature °C				
		20	22	24	26	28
Generator exergy destruction	kW	362.08	361.69	362.08	362.08	362.08
Absorber exergy destruction	kW	338.21	296.42	253.00	209.51	165.75
AC evaporator exergy destruction	kW	206.85	206.64	206.85	206.85	206.85
Condenser exergy destruction	kW	218.49	204.78	188.10	177.71	162.44
AC heat exchanger exergy des.	kW	196.35	195.81	196.35	196.35	196.35
AC exp. valve exergy destruction	kW	41.74	41.62	41.74	41.74	41.74
Exergy input	kW	2484.86	2478.57	2484.86	2484.86	2484.86
Absorption chiller exergetic efficiency	%	6.92	6.92	6.92	6.92	6.92
COP	%	0.79	0.79	0.79	0.79	0.79
Evaporator heat transfer	MW	9.33	9.33	9.33	9.33	9.33
Generator heat transfer	MW	11.83	11.83	11.83	11.83	11.83
Absorber	MW	9.05	9.05	9.05	9.05	9.05
Condenser heat transfer	MW	10.12	10.12	10.12	10.12	10.12
Heat exchanger heat transfer	MW	3.97	3.97	3.97	3.97	3.97
Cooling seawater mass flow rate	kg/s	216.59	240.40	270.50	309.91	363.97
Refrigerant	kg/s	4.11	4.11	4.11	4.11	4.11
$LiBr/H_2O$	kg/s	46.82	46.82	46.82	46.82	46.82
Generator outlet temperature	°C	104.88	104.88	104.88	104.88	104.88
Chilled water temperature	°C	6.69	6.69	6.69	6.69	6.69

Table 15 Parametric study for the cooling water temperature

Parameter	Unit	Generator Inlet Temperature °C							
		85	87	89	91	93	95	97	99
Generator exergy destruction	kW	377.90	296.84	288.40	297.30	312.92	331.79	352.42	374.10
Absorber exergy destruction	kW	298.19	298.19	298.19	298.19	298.19	298.19	298.19	298.19
Evaporator exergy destruction	kW	206.85	206.85	206.85	206.85	206.85	206.85	206.85	206.85
Condenser exergy destruction	kW	207.20	207.20	207.20	207.20	207.20	207.20	207.20	207.20
Heat exchanger exergy des.	kW	196.35	196.35	196.35	196.35	196.35	196.35	196.35	196.35
Exp. valve exergy destruction	kW	41.74	41.74	41.74	41.74	41.74	41.74	41.74	41.74
Exergy input	kW	2500.67	2419.62	2411.18	2420.08	2435.70	2454.56	2475.20	2496.88
Exergetic efficiency	%	6.88	7.11	7.14	7.11	7.06	7.01	6.95	6.89
COP	%	0.79	0.79	0.79	0.79	0.79	0.79	0.79	0.79
Evaporator heat transfer	MW	9.33	9.33	9.33	9.33	9.33	9.33	9.33	9.33
Generator heat transfer	MW	11.83	11.83	11.83	11.83	11.83	11.83	11.83	11.83
Absorber heat transfer	MW	9.05	9.05	9.05	9.05	9.05	9.05	9.05	9.05
Condenser heat transfer	MW	10.12	10.12	10.12	10.12	10.12	10.12	10.12	10.12
Heat exchanger heat transfer	MW	3.97	3.97	3.97	3.97	3.97	3.97	3.97	3.97
Cooling water mass flow rate	kg/s	240.4	240.4	240.4	240.4	240.4	240.4	240.4	240.4
Refrigerant mass flow rate	kg/s	4.11	4.11	4.11	4.11	4.11	4.11	4.11	4.11
$LiBr/H_2O$ mass flow rate	kg/s	46.82	46.82	46.82	46.82	46.82	46.82	46.82	46.82
Generator outlet temperature	°C	104.88	104.88	104.88	104.88	104.88	104.88	104.88	104.88
Chilled water temperature	°C	6.69	6.69	6.69	6.69	6.69	6.69	6.69	6.69
Hot water mass flow rate	kg/s	1481.06	721.74	477.05	356.22	284.20	236.38	202.32	176.83

Table 16 Parametric study for the generator's inlet hot water temperature

9.4 Appendix D

9.4.1 Study Results for Optimized Plant's Partial Load

Components	Unit	Gas Turbine Load		
		1	0.75	0.5
GT cooler	MW	0.23	0.23	0.22
Gas turbine	MW	118.48	110.01	64.91
TVC-MED boiler	MW	26.72	23.51	20.50
TVC-MED evaporators	MW	4.90	4.90	4.90
TVC-MED steam ejector	MW	2.55	2.55	2.55
TVC-MED condenser	MW	1.95	1.95	1.95
HRSG	MW	18.11	10.63	4.58
Steam turbine	MW	8.68	4.64	1.13
ST condenser	MW	2.86	1.60	0.40
HW boiler	MW	19.91	19.147	18.38
AC boiler	MW	1.70	2.15	2.47
AC generator	MW	0.31	0.31	0.31
AC absorber	MW	0.31	0.31	0.31
AC evaporator	MW	0.21	0.21	0.21
AC condenser	MW	0.19	0.19	0.19
AC heat exchanger	MW	0.20	0.20	0.20
AC exp. valve	MW	0.04	0.04	0.04
Stack	MW	10.82	15.00	15.80
Total exergy destruction	MW	198.24	178.41	120.65

Table 1 Optimized plant's components' exergy destruction rates at partial load

Exergetic Efficiency %	Gas Turbine Load		
	1	0.75	0.5
Gas turbine	53.99	48.58	44.78
Steam turbine	81.89	81.86	81.84
TVC-MED desalination plant	31.43	31.43	31.43
Absorption chiller	7.06	7.06	7.06
Plant overall	47.53	41.74	33.88

Table 2 Optimized plant's exergetic efficiency at partial load

		Gas Turbine Load		
	Unit	0.5	0.75	1
Fuel consumption	kg/s	4.193	7.065	8.763
Evaporator cooling power	kW	9304	9304	9304
CO_2 emission rate	kg/kW	262.10	269.88	277.66
COP	-	0.79	0.79	0.79
Net electric power	MW	57.72	124.15	184.14
GT power	MW	52.64	103.66	138.6
ST power	MW	5.08	20.48	45.54
GT efficiency	%	32.12	34.86	37.6
EUF	%	85.14	85.07	85
Overall electrical efficiency	%	33.39	41.6	49.81
GOR	-	8.08	8.11	8.56
Concentration factor	-	1.59	1.36	1.13
Specific heat consumption	kJ/kg	318.54	318.59	318.59
	kg/s	345	345	345
Hot water production	MW	108.57	108.57	108.57
	°C	75.15	75.15	75.15
Potable water production	m^3/day	20000	20000	20000

Table 3 Optimized plant's energy analysis results at partial load

9.4.2 Parametric Study for Optimized Plant's Ambient Temperature

		Ambient Temperature °C								
Components	Unit	10	15	20	25	30	35	40	45	50
GT cooler	MW	0.25	0.23	0.25	0.32	0.42	0.57	0.75	0.98	1.25
Gas turbine	MW	118.61	118.42	118.15	117.81	117.36	116.78	116.04	115.10	113.92
TVC-MED evaporators	MW	11.21	11.21	11.21	11.21	11.21	11.21	11.21	11.21	11.21
TVC-MED steam ejector	MW	18.87	18.87	18.87	18.87	18.87	18.87	18.87	18.87	18.87
TVC-MED condenser	MW	4.05	4.05	4.05	4.05	4.05	4.05	4.05	4.05	4.05
HRSG	MW	18.76	18.79	18.83	18.89	18.96	19.06	19.18	19.34	19.53
Steam turbine	MW	6.14	6.16	6.19	6.22	6.27	6.33	6.41	6.50	6.63
ST condenser	MW	0.14	0.148	0.16	0.18	0.21	0.24	0.29	0.34	0.41
HW boiler	MW	19.20	19.223	19.26	19.32	19.38	19.47	19.58	19.71	19.89
AC boiler	MW	2.85	2.85	2.85	2.85	2.85	2.85	2.85	2.85	2.85
AC generator	MW	0.31	0.31	0.31	0.31	0.31	0.31	0.31	0.31	0.31
AC absorber	MW	0.33	0.33	0.33	0.33	0.33	0.33	0.33	0.33	0.33
AC evaporator	MW	0.21	0.21	0.21	0.21	0.21	0.21	0.21	0.21	0.21
AC condenser	MW	0.33	0.33	0.33	0.33	0.33	0.33	0.33	0.33	0.33
AC heat exchanger	MW	0.20	0.20	0.20	0.20	0.20	0.20	0.20	0.20	0.20
AC exp. valve	MW	0.04	0.04	0.04	0.04	0.04	0.04	0.04	0.04	0.04
Stack	MW	5.52	5.53	5.54	5.55	5.57	5.60	5.63	5.67	5.72
Total exergy destruction	MW	207.01	206.89	206.78	206.68	206.57	206.44	206.27	206.04	205.73

Table 4 Optimized plant's components' exergy destruction rates at varying inlet-air temperatures

	Ambient Temperature °C								
Exergetic Efficiency %	10	15	20	25	30	35	40	45	50
Gas turbine	53.89	53.93	53.98	54.05	54.15	54.27	54.43	54.63	54.89
Steam turbine	92.28	92.27	92.25	92.22	92.19	92.15	92.1	92.03	91.95
TVC-MED plant	20.51	20.51	20.51	20.51	20.51	20.51	20.51	20.51	20.51
Absorption chiller	7.06	7.06	7.06	7.06	7.06	7.06	7.06	7.06	7.06
Plant overall	50.26	49.64	49.03	48.42	47.82	47.23	46.65	46.08	45.52

Table 5. Optimized plant's exergetic efficiency at varying inlet-air temperatures

		Ambient Temperature °C								
Components	Unit	10	15	20	25	30	35	40	45	50
Cold water temperature	°C	6.7	6.7	6.7	6.7	6.7	6.7	6.7	6.7	6.7
Evaporator cooling power	kW	9304	9304	9304	9304	9304	9304	9304	9304	9304
CO_2 emission rate	kg/kW	218.69	219.81	220.91	221.99	223.05	224.08	225.06	225.98	226.83
COP	-	0.79	0.79	0.79	0.79	0.79	0.79	0.79	0.79	0.79
Net power	MW	169.63	169.72	169.85	170.01	170.23	170.5	170.86	171.31	171.88
GT power	MW	138.6	138.6	138.6	138.6	138.6	138.6	138.6	138.6	138.6
ST power	MW	31.03	31.12	31.25	31.41	31.63	31.9	32.26	32.71	33.28
GT efficiency	%	37.6	37.6	37.6	37.6	37.6	37.6	37.6	37.6	37.6
EUF	%	99.49	98.87	98.26	97.67	97.09	96.54	96.02	95.54	95.09
Overall electrical efficiency	%	45.88	45.91	45.94	45.99	46.04	46.12	46.21	46.34	46.49
GOR	-	8.56	8.56	8.56	8.56	8.56	8.56	8.56	8.56	8.56
Concentration factor	-	1.42	1.42	1.42	1.42	1.42	1.42	1.42	1.42	1.42
Specific heat consumption	kJ/kg	318.59	318.59	318.59	318.59	318.59	318.59	318.59	318.59	318.59
	kg/s	345	345	345	345	345	345	345	345	345
Hot water production	MW	108.49	108.57	108.69	108.84	109.04	109.3	109.62	110.04	110.56
	°C	75.1	75.15	75.24	75.35	75.48	75.66	75.89	76.17	76.54
Potable water production	m^3/day	40000	40000	40000	40000	40000	40000	40000	40000	40000

Table 6 Optimized plant's energy analysis at varying inlet-air temperatures

9.4.3 Parametric Study for Optimized Plant's Seawater

Components' Exergy Destruction in MW	Seawater Temperature °C				
	20	22	24	26	28
GT cooler	0.23	0.23	0.23	0.23	0.23
Gas turbine	118.42	118.41	118.42	118.42	118.42
TVC-MED evaporators	11.21	11.20	11.21	11.21	11.21
TVC-MED steam ejector	18.87	18.87	18.87	18.87	18.87
TVC-MED condenser	4.32	4.04	3.76	3.47	3.18
HRSG	18.79	18.79	18.79	18.79	18.79
Steam turbine	6.16	6.16	6.16	6.16	6.16
ST condenser	0.136	0.140	0.143	0.147	0.151
Hot water boiler	19.05	19.22	19.28	19.36	19.45
AC boiler	2.85	2.84	2.85	2.85	2.85
AC generator	0.31	0.31	0.31	0.31	0.31
AC absorber	0.342	0.30	0.25	0.22	0.19
AC evaporator	0.21	0.21	0.21	0.21	0.21
AC condenser	0.21	0.20	0.18	0.17	0.16
AC heat exchanger	0.20	0.20	0.20	0.20	0.20
AC exp. valve	0.04	0.04	0.04	0.04	0.04
Stack	5.53	5.52	5.53	5.53	5.53
Total exergy destruction	206.87	206.68	206.44	206.18	205.95

Table 7 Optimized plant's exergy analysis at varying seawater temperatures

Exergetic Efficiency %	Seawater Temperature °C				
	20	22	24	26	28
Gas turbine	53.93	53.93	53.93	53.93	53.93
Steam turbine	92.27	92.27	92.27	92.27	92.27
TVC-MED desalination	19.66	20.51	21.36	22.34	23.49
Absorption chiller	7.06	7.06	7.06	7.06	7.06
Plant Overall	49.30	49.64	49.98	50.3	50.64

Table 8 Optimized plant's exergetic efficiencies at varying seawater temperatures

Exergetic Efficiency %	Unit	Seawater Temperature °C				
		20	22	24	26	28
Cold water temperature	°C	6.7	6.7	6.7	6.7	6.7
Evaporator cooling power	kW	9304	9304	9304	9304	9304
CO_2 emission rate	kg CO_2/kW	229.19	219.81	209.46	197.99	185.21
COP	-	0.79	0.79	0.79	0.79	0.79
Net power	MW	169.72	169.72	169.72	169.72	169.72
GT power	MW	138.6	138.6	138.6	138.6	138.6
Steam turbine electric power	MW	31.12	31.12	31.12	31.12	31.12
GT efficiency	%	37.6	37.6	37.6	37.6	37.6
EUF	%	98.87	98.87	98.87	98.87	98.88
Overall electrical efficiency	%	45.91	45.91	45.91	45.91	45.91
GOR	-	8.08	8.56	9.03	9.54	10.08
Concentration factor	-	1.45	1.42	1.39	1.35	1.32
Specific heat consumption	kJ/kg	332.672	318.59	304.508	291.049	278.185
Hot water production	Kg/s	345	345	345	345	345
	MW	105.68	108.57	111.45	114.34	117.22
	°C	73.16	75.15	77.15	79.14	81.14
Potable water production	m^3/day	40000	40000	40000	40000	40000

Table 9 Optimized plant's energy analysis at varying seawater temperatures

9.5 Appendix E

Third proposed plant (CCPP + (Boiler) TVC-MED + AC) optimization results

Components	Exergy Destruction in MW	
	Before Optimized	After Optimized
GT cooler	0.23	0.23
Gas turbine	118.48	118.39
TVC-MED boiler	48.86	35.09
TVC-MED evaporators	9.80	14.54
TVC-MED steam ejector	5.09	18.08
TVC-MED condenser	3.89	0.32
HRSG	8.51	9.34
Steam turbine	3.36	3.45
ST condenser	0.98	1.69
HW boiler	-	6.02
AC boiler	2.31	2.03
AC generator	0.31	0.31
AC absorber	0.30	0.33
AC evaporator	0.21	0.21
AC condenser	0.20	0.33
AC heat exchanger	0.20	0.20
AC exp. valve	0.04	0.04
Stack	17.10	5.46
Total exergy destruction	219.87	216.06

Table 1 Third plant's exergy analysis results after optimization

Components	Exergetic Efficiency %	
	Before Optimized	After Optimized
Gas turbine	53.99	53.9
Steam turbine	81.85	81.98
MED exergetic	31.43	31.39
Absorption chiller	7.06	7.06
Plant overall	42.39	45.63

Table 2 Third plant's exergy analysis results after optimization

Parameters	Unit	Before Optimized	After Optimized
Cold water temperature	°C	6.7	6.7
Evaporator cooling power	kW	9304	9304
CO_2 emission rate	kg CO_2/kW	339.7	244.08
COP	-	0.79	0.79
Net power	MW	154.18	154.12
GT power	MW	139.01	138.4
ST power	MW	15.17	15.72
GT efficiency	%	37.71	37.54
EUF	%	79.09	86.98
Overall electrical efficiency	%	41.68	41.69
GOR	-	8.14	8.14
Concentration factor	-	1.87	1.42
Specific heat consumption	kJ/kg	318.59	365.56
Hot water production	kg/s	-	345
	MW	-	80.18
	°C	-	55.51
Potable water production	m^3/day	40000	40000

Table 3 Third plant's energy analysis results after optimization